HAL open science

Divergence of exploratory locomotion and the underlying neuronal circuitry in two closely related vertebrate species

Gokul Rajan

To cite this version:

Gokul Rajan. Divergence of exploratory locomotion and the underlying neuronal circuitry in two closely related vertebrate species. Neurons and Cognition [q-bio.NC]. Université Paris sciences et lettres, 2020. English. NNT : 2020UPSLT010 . tel-03505902

HAL Id: tel-03505902

https://theses.hal.science/tel-03505902v1

Submitted on 1 Jan 2022

HAL is a multi-disciplinary open access archive for the deposit and dissemination of scientific research documents, whether they are published or not. The documents may come from teaching and research institutions in France or abroad, or from public or private research centers.

L'archive ouverte pluridisciplinaire **HAL**, est destinée au dépôt et à la diffusion de documents scientifiques de niveau recherche, publiés ou non, émanant des établissements d'enseignement et de recherche français ou étrangers, des laboratoires publics ou privés.

PSL UNIVERSITÉ PARIS

THÈSE DE DOCTORAT
DE L'UNIVERSITÉ PSL

Préparée à l'Institut Curie

Divergence of exploratory locomotion and the underlying neuronal circuitry in two closely related vertebrate species

Divergence de la locomotion exploratoire et des circuits neuronaux sous-jacents chez deux espèces de vertébrés étroitement apparentées

Soutenue par

Gokul RAJAN

Le 17 Septembre 2020

Ecole doctorale n° 158

Cerveau, cognition, comportement

Spécialité

Neuroscience

Composition du jury :

Jean-Francois, BRUNET Directeur de recherche, Ecole Normale Superieure – CNRS	*Président*
Nadine, PEYRIERAS Directeur de recherche, Paris-Saclay – CNRS	*Rapporteur*
Sylvie, RETAUX Directeur de recherche, Paris-Saclay – CNRS	*Rapporteur*
Volker, BORMUTH Maitre de conferences, Laboratoire Jean Perrin, SU	*Examinateur*
Filippo, DEL BENE Directeur de recherche, Institut de la Vision, SU - INSERM	*Directeur de thèse*

institutCurie | PSL

"When you change the way you look at things, the things you look at change."

— Max Planck

Table of Contents

List of Figures viii

List of Tables xi

Abbreviations xi

Acknowledgements xiii

Chapter 1: Introduction 1

1.1 The model systems: *Danionella translucida* and *Danio rerio* 2

1.2 Behavioral neuroscience and the comparative method 5

1.3 Evolution of locomotor circuits 7

1.4 Locomotor signatures of larval zebrafish 9

1.5 Supraspinal neuronal correlates of locomotion 11

1.6 Summary and objectives of the current study 14

Chapter 2: Materials and Methods 15

2.1 Animal maintenance 16

2.1.1 *Danio rerio* (zebrafish) 16

2.1.2 *Danionella translucida* 16

2.2 Behavior 17
2.2.1 Free-swimming behavioral acquisition, fish tracking and tail segmentation .. 17
2.2.2 Analysis pipeline for free-swim data 18
2.2.3 Clustering of free-swim half tail beats 21
2.2.4 Head-embedded swimming behavior set-up 21
2.2.5 Analysis pipeline for head-embedded data 22
2.2.6 Assay to study tap-induced escape behavior 22
2.2.7 Analysis pipeline for tap-induced escape data 23
2.2.8 Mean squared displacement (MSD) and reorientation analysis 24
2.2.9 Energetics and swimming speed 24
2.2.10 Quantification of depth preference 25
2.2.11 Quantification of body length and swim bladder inflation 25

2.3 Anatomy 26
2.3.1 Fluorescence *In-situ* hybridization and Immuno-histochemistry 26
2.3.2 Confocal imaging of the whole brain FISH/IHC samples 29
2.3.3 Retrograde labelling of reticulospinal (RS) neurons 30

2.4 Physiology 31
2.4.1 Generation of pan-neuronal calcium sensor *Tg(HuC-H2B:GCaMP6s)* line ... 31
2.4.2 Light-sheet imaging 32
2.4.3 Image processing and analysis pipeline for whole-brain light-sheet data 32

2.5 Statistical methods 33

Chapter 3: Characterization of exploratory locomotion in Danionella translucida (DT) and Danio rerio (ZF) 35

3.1 Length of larval DT and ZF is in a similar range 37

3.2 DT execute swim events with a continuous tail-burst activity 38

3.3 Duration of swim events are much longer in DT 39

3.4 DT swim slower with a lower half beat frequency and tail angle 41

3.5 DT has lower mean escape velocity than ZF but tends to show a lower latency to achieve peak escape velocity 43

3.6 Exploratory swimming in DT has a longer ballistic phase 45

3.7 The continuous swimming in DT can be divided into at least two types, slow and fast swims 47

3.8 DT's instantaneous energy requirement during activity appears lower than ZF 49

3.9 A lower oxygen availability and delayed swim bladder inflation might have contributed to the differences in swimming style at the micro scale 51

Chapter 4: Anatomy and physiology underlying locomotion in *Danionella translucida* and *Danio rerio* 54

4.1 Anatomy 56

4.1.1. Distribution of glutamatergic, glycinergic and GABAergic neurons in the hindbrain of DT 56

4.1.2. Reticulospinal (RS) neurons in DT and ZF 57

4.2 Physiology 60

4.2.1 Generation of pan-neuronal *Tg(HuC:H2B-GCaMP6s)* DT fish and whole-brain imaging 60

4.2.2 Similar brain nuclei are correlated with swimming in DT and ZF 62

4.2.3 Neurons in the identified nuclei of DT constitute a functionally heterogenous population 64
4.2.4 Onset neurons form a continuum between onset and swim maintenance components 69

Chapter 5: Discussion 71
5.1 General experimental approach 72
5.2 Kinematics of spontaneous swimming and escapes 73
5.3 Exploration and organismal biology 75
5.4 Anatomy 80
5.5 Physiology 82
5.6 Conclusions and future directions 91

Chapter 6: Appendix 93

Bibliography 103

Annex #1 117

Annex #2 133

Annex #3 158

Author contributions 206

Résumé 207

List of Figures

Figure 1. 1: 11 months old adult female and male *Danionella translucida* 2

Figure 1.2 : Distribution of ZF and DT in south and South-East Asia..... 3

Figure 1.3: Mounting of adult DT for non-invasive in-vivo brain imaging 6

Figure 1.4: Illustration of convergent and divergent evolution..... 8

Figure 1.5: Emergence of various behaviors in ZF larvae during development. 10

Figure 1.6: Illustration showing descending control of locomotion in vertebrates..... 12

Figure 2.1: An illustration of the free-swimming behavioral analysis set-up. 17

Figure 2.2: Illustration of half beat identification in a swim bout of zebrafish 20

Figure 2.3: Illustration of the 140 ms window selected for the analysis of tap-induced escape kinematics 23

Figure 2.4: The Tol2-elavl3-H2B-GCaMP6s plasmid used for creating the *Tg(HuC:H2B-GCaMP6s) Danionella translucida*..... 31

Figure 3.1: DT and ZF measure similar in size at 5 dpf..... 37

Figure 3.2: Representative swimming pattern of DT and ZF 38

Figure 3.3: Duration of swim events in DT is longer than in ZF..... 40

Figure 3.4 : Swimming kinematics of DT and ZF in a spontaneous free-swimming assay 41

Figure 3.5: Escape response in DT and ZF in a tap-induced escape assay..... 44

Figure 3.6: Exploratory swimming in DT has a longer ballistic phase 46

Figure 3.7: Slow and fast swims in DT. 47

Figure 3.8: Slow and fast half beats in DT. 48

Figure 3.9: Oxygen consumption in DT and ZF 50

Figure 3.10: Depth preference in DT and ZF..... 51

Figure 3.11: Swim bladder inflation in ZF occurs earlier than in DT. 52

Figure 4.1: Distribution of (A) glutamatergic (B) glycinergic and (C) GABAergic neurons in the hindbrain of DT using *in-situ* hybridization (ISH) and immunohistochemistry (IHC)..... 56

Figure 4.2: Distribution of reticulospinal (RS) neurons in the brainstem of DT 58

Figure 4.3: Comparison of reticulospinal (RS) neurons in DT and ZF 59

Figure 4.4: *Tg(HuC:H2B-GCaMP6s)* fish in DT and ZF..... 60

Figure 4.5: Whole brain imaging using light sheet microscopy 61

Figure 4.6: Neuronal correlates of swimming in DT and ZF..... 62

Figure 4.7: Activity of neuronal correlates of swimming temporally scale with the long swim events of DT 63

Figure 4.8: Neuronal correlates of swimming onset in DT 64

Figure 4.9: Neuronal activity of onset neurons 65

Figure 4.10: Neuronal correlates of swimming offset in DT. 66

Figure 4.11: Neuronal activity of offset neurons 67

Figure 4.12: A lateral view of a segmented and analyzed DT brain 68

Figure 4.13: The onset neurons are a functionally diverse group which form a continuum between onset and swimming 69

Figure 6.1: Bout-wise kinematics of ZF 94

Figure 6.2: Mean speed in DT and ZF was comparable over long time scale 95

Figure 6.3: Swimming in 1-week and 2-week old DT larvae. 95

Figure 6.4: *in-situ* hybridization performed on ZF and DT 96

Figure 6.5: Distribution of glutamatergic, glycinergic and GABAergic neurons in the hindbrain of ZF obtained from Z-brain atlas (Randlett *et al*., 2015) 97

Figure 6.6: Distribution of (A) glutamatergic (B) glycinergic and (C) GABAergic neurons in the DT brain is shown in red along with distribution of HuC:H2B-GCaMP6s expressing neurons in green 97

Figure 6.7: Neuronal correlates of swimming in ZF and DT 98

Figure 6.8: Identification of maintenance neurons and diversity of onset neurons in DT 99

Figure 6.9: DT brains showing a continuum between onset and swimming components in the onset neurons..... 100

Figure 6.10: DT shows negative phototaxis..... 101

Figure 6.11: Analytical model showing lower availability of dissolved oxygen (DO) in the surrounding can lead to a shorter inactivity time (based on Weihs, 1980)..... 101

List of Tables

Table 2.1: Primers (5'->3') used for generating anti-sense probes..... 27

Table 2.2: Age and species dependent time period for proteinase-K treatment 28

Abbreviations

CPG: Central pattern generator

CRISPR: Clustered Regularly Interspaced Short Palindromic Repeats

DA: Dopaminergic

dpf: days post fertilization

DT: *Danionella translucida*

GECI: Genetically encoded calcium indicator

GFP: Green fluorescent protein

GLYT: Neuronal glycine transporter

I_{CAN}: Calcium-activated non-selective cationic current

IHC: Immunohistochemistry

DO: Dissolved oxygen

IR: infra-red

ISH: *in-situ* hybridization

LED: Light-emitting diode

LLC: Long latency C-bend

LPGi: Lateral paragigantocellular nucleus

LSM: Laser scanning microscope

MAD: Median absolute deviations

MLR: Mesencephalic locomotor region

MSD: Mean squared displacement

NaN: Not a Number

nucMLF/nMLF: Nucleus of the medial longitudinal fascicle

nucRE: Nucleus of reticular formation

nucVE: Vestibular nucleus

PBS: Phosphate Buffered Saline

ROI: Region of interest

RS: Reticulospinal

SLC: Short latency C-bend

SSC: saline-sodium citrate

TBF: Tail-beat frequency

TNT: Tris-NaCl-Tween buffer

TRD: Texas Red dextran

usAHP: Minute-long afterhyperpolarization

UV: Ultra-violet

VGLUT: Vesicular glutamate transporter

ZF: Zebrafish

Acknowledgements

"If I have seen further it is by standing on the shoulders of Giants."
— Isaac Newton's letter to Robert Hooke, 1675

I would firstly like to thank my supervisor, Filippo Del Bene, for providing me with the opportunity to work with him. In the summer of 2016, he had to select one candidate from the many international applicants to his lab and I had to choose one of the four PhD positions that were available to me. Although numerically my decision seemed easier, a lot of thought went into it as it meant a long commitment away from home. In retrospect, while I can only hope that Filippo believes that he made the right choice, I definitely had made the right choice by joining his troop at Institut Curie. If I've to go back in time and make the decision again, I would make the same choice all over again. Filippo has been a great mentor and provided me with many opportunities to fail, learn and succeed. He is always available to talk and provide guidance on science and beyond. All in all, his attitude towards science and mentoring is really what made my PhD work a cherishing experience, both scientifically and personally. Inadvertently, he has also set my expectations from a future supervisor pretty high! My sincere thanks to you for all the support and guidance that you have extended to me.

All the members of the lab have played an important role: Karine, Marion, Shahad, Fanny and Giulia. Working with a new species is demanding, and it would not have been possible without Karine's support. Karine's help in tackling the French bureau-crazy(!) needs appreciation of its own. A shout-out to all the ex-members of the lab: Chris, Celine, Flavia, Giulia, Vincenzo, Juliette and Valerie. As a new member in the lab, Chris's guidance was important and appreciated. Celine, along with Marion and Shahad also helped me to navigate the French system and numerous French translations. And the Italian crew kept the morale high. I would extend my thanks to the staff at Institut Curie. Especially Oliviers' from the microscopy platform and the staff from the animal facility.

It would not be justified if I do not thank the IC-3i family as they were the only people I knew when 12 of us first arrived in Paris in 2016 to join the IC-3i PhD programme at Institut Curie. Special thanks to Zeina, Melanie and Anemone. And the good friends with whom I lived in the beautiful Cite Universitaire at both, College Franco-Britannique and Maison du Cambodge over the years, thank you all!

During my thesis, I've collaborated and shared science with some interesting people, thanks to all of you: Mycola Kadobianskyi and Benjamin Judkewitz (Charite, Berlin); Martin Carbo-Tano and Claire Wyart (ICM, Salpetriere); Julie Lafaye, Georges Debregeas, Thomas Panier and Raphael Candelier (LJP, Sorbonne).

Like any scientific work, this work has benefitted from many past works, and thanks to the internet, I've also been able to interact with some of the authors who published their works 20 or 40 years ago! Apart from that, the thesis work has directly benefited from my interactions with the following people: Adrien Jouary and Mike Orger (Champalimaud, Lisbon), Roshan Jain (Haverford, USA) and Tim Dunn (Harvard, USA). Especially, interactions with Mike on the behavioral analysis was very much appreciated and during the time Roshan spent in Paris, I have had many fruitful discussions with him.

Outside books and the internet, I think some of my teachers have had an influence on my thinking in science and philosophy. I would like to extend my gratitude to them: Joby Joseph (University of Hyderabad), Narayan Punekar (IIT Bombay), Swati Patankar (IIT Bombay), Seyed Hasnain (IIT Delhi), and KMR Nambiar (Osmania University).

Above all, any success that I have achieved wouldn't be possible without the unconditional support of my family. To write a thesis amidst a pandemic is not easy; my partner, Anu motivated me through this to focus on the writing, and supported to keep the COVID-19 analysis and information dissemination still active. Apart from our stimulating discussions in science, our shared interests in art and literature (and more!) have definitely played a big role in keeping the work/life balance in check (to some extent at least!). She also served as an editor and illustrator during my thesis writing! My mom, Prasanna and dad, Rajan are two of the most amazing people. Whether it was science or athletics, they have equally encouraged me to follow all my interests and are always an infinite source of emotional support. My big brother, Rahul deserves a special mention. I believe that I got a head start in most things because he would patiently guide me through them. From fishing with him in the Indian monsoons as an 8-year old to doing a PhD, so much has changed but he has always been the constant person I look up to when things go south. And it is all so unconditional that a thank you would neither ever suffice nor ever be expected, nevertheless a big thanks to you all for everything!

Chapter 1

Introduction

"There is no scientific study more vital to man than the study of his own brain. Our entire view of the universe depends on it." — Francis Crick

"To move things is all that mankind can do, and for this the sole executant is a muscle, whether it be whispering a syllable or felling a forest." — Charles Sherrington

† Sections 1.1 and 1.2 are used to prepare a book chapter on *Danionella translucida* (see Annex #1).

1.1 The model systems: *Danionella translucida* and *Danio rerio*

Danionella translucida (DT) is an emerging model organism in neuroscience (Schulze et al., 2018). I used DT and the more popular model system *Danio rerio* / zebrafish (ZF) in this study. DT are cyprinid fish belonging to the Danioninae subfamily, the same group of fishes to which the popular model organism zebrafish (ZF) belongs. The adults of DT measure only 10-12 mm in length as seen in Figure 1.1. DT was first reported by Roberts (1986) from the roots of floating aquatic plants in Myanmar. They were found in shallow (maximum 1 m deep), slow flowing streams in the Pegu Division of Myanmar. Some other fishes collected from this site included other cyprinids – *Danio* and *Microrasbora*, and other fishes like *Hara* and *Oryzias.*

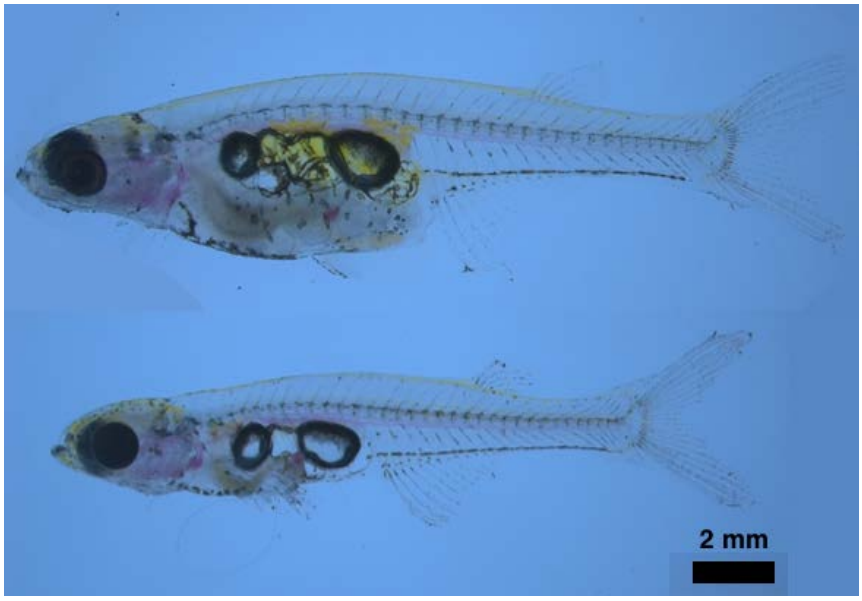

Figure 1.1: 11 months old adult female and male *Danionella translucida.*

Figure 1.2 : Distribution of *Danio rerio* and *Danionella translucida* in South and South-East Asia (Parichy, 2015 and Roberts, 1986).

Both DT and ZF are found in the freshwaters of the tropical regions in South-East Asia. A comparison of recent reported sightings of ZF and DT based on Parichy (2015) and Roberts (1986) respectively is shown in Figure 1.2. DT share the unique features of danionins which include a large indentation in the medial margin of mandibles (Howes 1979, as cited in Roberts, 1986), longer anal fin and a higher number of caudal vertebrae when compared to abdominal vertebrae. Their reduced adult size makes them an interesting candidate model organism. This reduction in size is a result of miniaturization, a developmental phenomenon observed in at

least 36 species of Cyprinidae (Rüber et al., 2007). It is suggested that this phenomenon might have evolved independently several times in the cyprinid family. Some of these miniature fish show developmental truncation and DT is one of them. Among these, *D. translucida* along with *Danionella mirifa* and *Paedocypris* are some of the most truncated fish (Britz & Conway, 2009). They have a two chambered swim bladder with the anterior and posterior chambers widely separated. Wild-type DT has very little pigmentation except in the eyes. More melanophores are present on the ventral side compared to the dorsal side where the few melanophores are mostly limited to the head.

On the other hand, the biology, natural history and research applications of ZF has been well reviewed (Parichy (2015) and the textbook by Cartner et al. (2020) provide a good documentation). ZF has particularly become an exciting model system to understand the genetics and development of a vertebrate system. However, not much is known about their natural history. Adult ZF are found to occupy waters with other larger *Danio* species and some competition among the larvae of different species can be expected (Parichy, 2015). Behavioral studies on ZF from the wild have specifically focused on the adults and their complex behaviors such as shoaling (Spence et al., 2008). It is difficult to follow the behavior of the larval form in the wild, given their small size. Even from what is observed among the various strains of adult ZF, it appears that adult ZF can show a range of variation in their behaviors which can be interesting to compare to develop an understanding of the evolution of behavioral traits (Robison & Rowland, 2005, Oswald et al., 2013 and Martins & Bhat, 2014). However, the larval fish provides many advantages to this comparative approach with respect to genetics, imaging and behavioral tracking. Another feature that is widely studied among the various strains of ZF is pigmentation – while this varies widely among the adults, the larval fish seem to have a very conserved pigmentation pattern (Parichy, 2015). An explanation to this conserved pattern of pigmentation that covers the central nervous system in larval ZF is hypothesized to be a mechanism of protection against UV exposure in larvae dwelling in shallow waters (Mueller & Neuhauss, 2014). If true, this might indicate that the DT larvae with less amount of pigmentation might actually live in deeper waters with less exposure to UV.

1.2 Behavioral neuroscience and the comparative method

Larval ZF has become a very popular model organism in behavioral neuroscience. The popularity can be ascribed to their small size, transparency and development of tools over the years to perform genetic manipulations. One of the major advantages is the ability to image whole brain activity at single cell resolution using genetically encoded calcium indicators (GECI) (Ahrens et al., 2013). By virtue of the close evolutionary relationship between ZF and DT, a lot of these genetic tools are easily transferable from the former to the latter. To create a mutant lacking any pigmentation, including in the eye -- based on the fact that *tyr* gene encoding tyrosinase is involved in melanin synthesis pathway in ZF -- Schulze, Henninger et al., (2018) successfully used CRISPR-Cas9 genome editing technique to target *tyr* gene in DT. They have also been successful in generating a stable *Tg(NeuroD:GCaMP6f)* transgenic line using Tol2 mediated transgenesis technique. Moreover, Kadobianskyi et al. (2019) have recently published an assembled and annotated genome sequence of DT. This will aid all the future work on targeted genetic manipulations in DT.

In ZF, most studies have focused on simple behavioral questions pertaining to perception, locomotion or sensorimotor transformations of reflexive nature. This is mainly due to the fact that most complex behaviors appear in the later stages of larval development. ZF larvae start to show reliable learning at 3 weeks (Valente et al., 2012). Similarly, social preference starts to appear in 3 weeks old larvae (Dreosti et al., 2015). This is where the advantages of DT become more obvious. While the adults of DT are small in size and transparent, they also show a rich repertoire of behaviors. They perform visually mediated shoaling and schooling. The males also exhibit vocalization which is likely related to male-male aggression (Schulze, Henninger et al., 2008). Penalva et al. (2018) also showed socially reinforced learning in adult DT. As shown in Figure 1.3, imaging of adult fish can be carried out non-invasively in moderately sedated fish embedded in agar where the gills are still free to move. This rich behavioral repertoire in adult DT combined with its small size, lack of pigmentation and the ease of transfer of genetic tools from ZF to DT makes adult DT a very favorable system to understand neuronal underpinnings of complex behaviors.

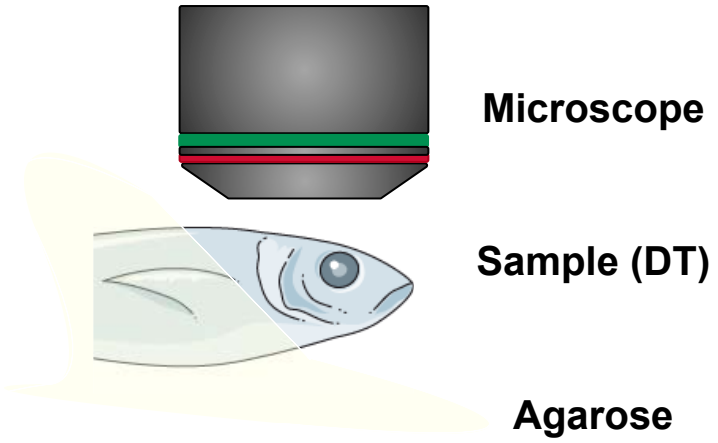

Figure 1.3: Mounting of adult *Danionella translucida* for non-invasive *in-vivo* brain imaging.

In addition to the aforementioned direct neurobehavioral applications in adult DT, there can be at least two other interesting applications of DT in neuroscience: 1) To study ontogeny of behaviors. In a vertebrate organism, it can be often challenging to closely follow the development of a behavior and its underlying neuronal circuit over various developmental stages in life. DT fares well here due to its small size and transparency throughout the life cycle. We can track the changes in neuronal networks as they mature. 2) To identify general principles and evolution of neuronal circuits. Given the high degree of evolutionary closeness between DT and ZF (and possibly other danionins), they can be used to understand functional divergence of neuronal circuit if divergent behaviors can be identified between the species. It is this second approach that I will use in this study.

Studies on ossification in *Danionella dracula* and *Paedocypris* show that most bones affected by truncation are those which appear late in the development of ZF. This suggests that the developmental truncation occurs later in the ontogeny of these fish species. Hence, developmentally the two species are very much comparable in early stages. This should come as an advantage for comparative studies of DT and ZF which look at the larval and juvenile stages of the two fish species. Comparatives studies following this methodology can be seen in invertebrates like Nudipleura (Newcomb et al., 2012 and Sakurai & Katz, 2017), but such studies at the level of neuronal circuits are not common in vertebrates due to the inherent difficulty of working with organisms of higher biological complexity.

1.3 Evolution of locomotor circuits

Most studies on neuronal circuits try to characterize a functional circuit in a single organism at a given timepoint. Within an animal, the functional circuits change over the ontogenic time course. Changes can also be observed across different animal species due to differences that emerged over the evolutionary time course. As highlighted in the previous section, the first question on ontology is also well answered in a species like DT where the optical accessibility is well maintained from larval stages to adulthood. However, in this study, I focused on the second question using two animal species, DT and ZF. More studies looking at such comparisons would increase the scope of the discipline of evolutionary-development to include neuroscience in its purview (Raff, 2000). Here, I will briefly look at motor control from an evolutionary perspective. Katz & Hale (2017) provide a comprehensive review.

Two important concepts are homology and homoplasy. Homologous entities have same origin but can slightly diverge in form and/or function over time, whereas homoplasy is the independent evolution of two entities to attain a similar form and/or function. In the current context of the two closely related species, we are more interested in homology and expect to see very conserved structures to behave differently. The concept of homology can, of course, be extended to genes, proteins, cells, networks and behaviors. A good example of a homologous neuron identified among many different fish and amphibian species is the Mauthner neuron which is implicated in the conserved escape response at the behavioral level.

Homoplasy can arise from convergent evolution of two different systems to give rise to a similar system or from parallel evolution of similar systems to produce similar systems without much divergence from each other in form and function. Convergence is an important phenomenon in evolution which points to specific conserved ways of laying out an optimal system. A good example is the ribbon fin found in *Apternotus albifrons* and African *Gymnarchus niloticus* -- although they appear very similar and both generate counter-propagating travelling waves, the fins originate from anal fin and dorsal fin respectively (Katz & Hale, 2017). In contrast, homologous systems can show divergence over time and acquire new functions. A very good example of this is seen in the decapod Crustacea. Telson and uropods, the structural parts of the tail-fan at the end of the stomach, are used together in lobsters and crayfish (Edwards et al., 1999). However, in sand crab, the telson and uropod become uncoupled and the animal swims

with only its uropods beating back-and-forth dorsally (Paul, 1991). An illustration of how convergent and divergent evolution occur is shown in Figure 1.4.

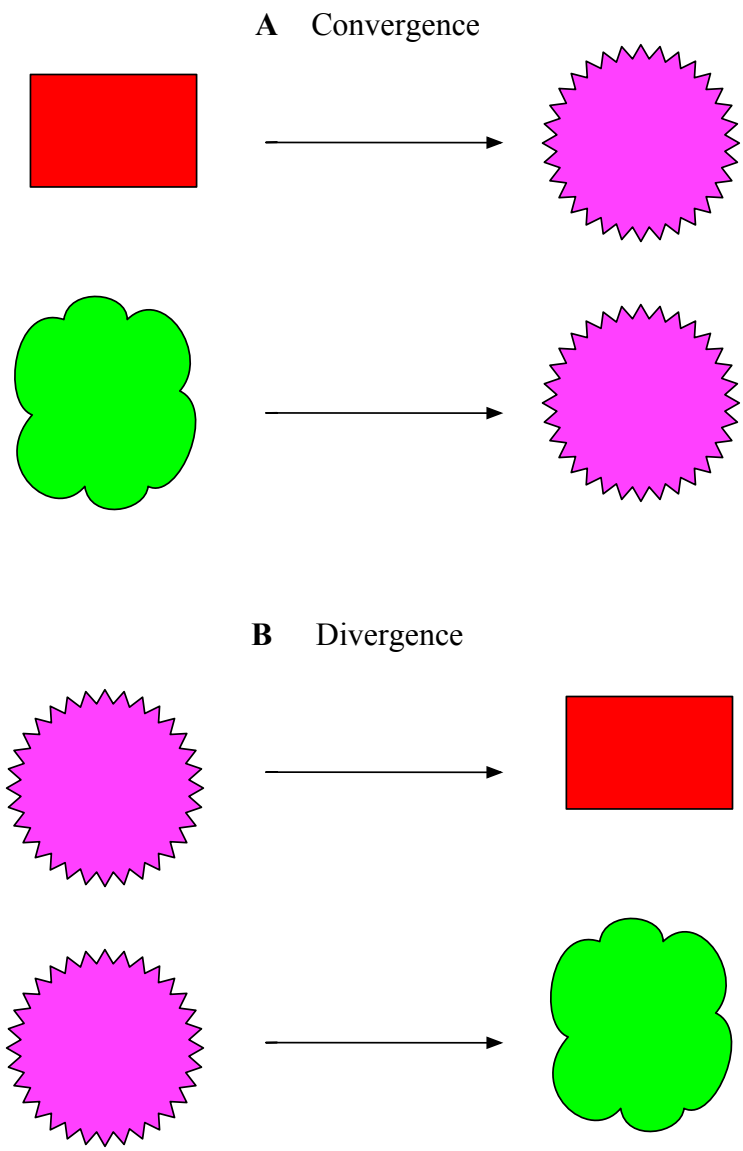

Figure 1.4: Illustration of convergent and divergent evolution. (A) shows two systems starting in two different states and later arriving at a similar comparable state by convergence. (B) shows divergence of two comparable systems into widely different systems. The structure and color of the illustration can be considered as the form and function of the system respectively.

For a new behavior to emerge, it can broadly happen in three ways from a neuronal circuit viewpoint (Katz & Hale, 2017): (1) Changes in peripheral systems without major changes to the central neuronal networks. For instance, in a sensory-mediated response, a difference in response can easily emerge due to an underlying difference in the sensitivity of the sensory modalities. (2) Rewiring of functional neuronal circuits involved in the behavior. At first, it might seem like an unrealistic approach or one that can only be seen in evolutionarily distant animals. However, an impressive example of this can be found within mammals. During trotting in horse, the legs on the side move in the opposite direction whereas while pacing, the legs move in the same direction. Interestingly, Icelandic horse harboring a nonsense mutation in the *DMRT3* gene, naturally exhibit pacing instead of trotting (Andersson et al., 2012). *DMRT3* is normally expressed in ipsilaterally and contralaterally projecting spinal interneurons. Mice with this copy of the allele have uncoordinated locomotion. In another mice model where Ephrin receptor A4 (EphA4), an axon guidance molecule is knocked out in the spinal cord, excitatory interneurons cross the midline and the mice show a hopping gait instead of a regular alternating gait (Kullander et al., 2003). (3) Changes in neuronal network activity without any changes in the hardwiring. This can be due to the cellular and network properties of the neurons involved, or due to neuromodulatory inputs. For example, in fictive preparations of *Xenopus* and *Rana* larvae, noradrenaline (NA) and nitric oxide (NO) slow down the swimming rhythm in *Xenopus* larvae but does not show this effect in *Rana* larvae. Such modulatory effects can alone change the behavior of a network. It is important to keep in mind that these mechanisms are not mutually exclusive and can in fact occur in parallel.

1.4 Locomotor signatures of larval zebrafish

A lot has been characterized about behaviors and underlying stereotypical locomotion in larval zebrafish (ZF). ZF exhibits swimming in temporally distinct events called bouts. Each bout consists of a tail burst followed by a glide. This distinct pattern has helped in characterizing the behaviors in terms of the underlying pattern of the bouts. Larval ZF show a variety of behaviors. The emergence of these behaviors during development is shown in Figure 1.4. During the thesis work, I focused on spontaneous exploratory swimming and acoustic startle behaviors in DT and ZF. Additionally, I also looked at prey capture (see Annex #1), opto-motor response and loom-induced escape (unpublished collaborative work) behaviors in ZF. In this section, I will

briefly review some of the widely described ZF locomotor patterns underlying some of the behaviors outlined in Figure 1.4. For a thorough review of ZF behaviors, see Fero et al. (2011) and Orger & De Polavieja (2017).

Kinematic analysis of swim bouts has produced information on different movement patterns produced by larval ZF. During exploration, forward propulsion is achieved by low-angle slow-swim movements or scoots, along with faster swims called burst swims where the large tail amplitudes are used (Budick & O'Malley, 2000). Change in orientation is achieved by what is called a 'routine turn' and produces a change in orientation of around 45 degrees.

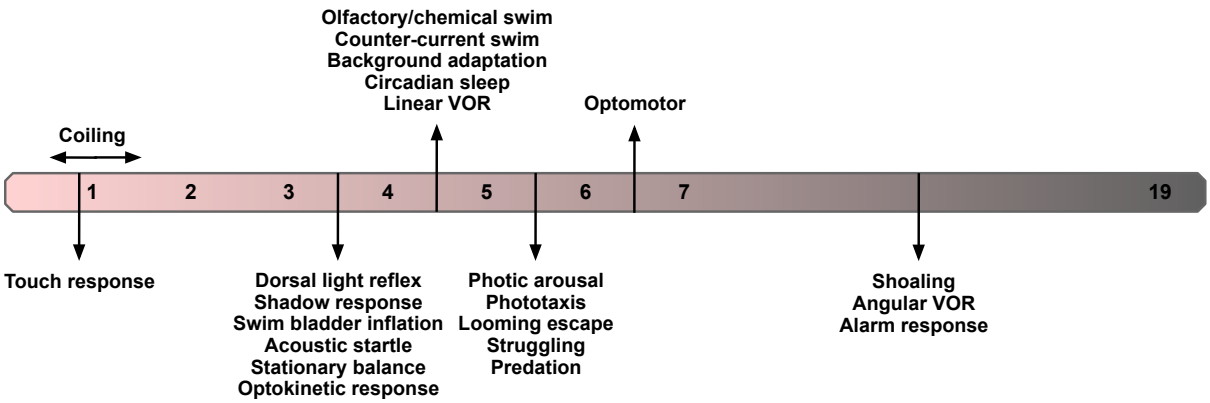

Figure 1.5: Emergence of various behaviors in zebrafish larvae during development (adapted from Fero et al., 2011). The numbers indicate the days post fertilization (dpf).

A widely characterized behavior in ZF is the escape response. Escape induced by acoustic stimulus develops around 3 dpf whereas escape mediated by looming stimulus develops around 5 dpf. During both, the fish execute a 'C-startle' response which is basically a C-shaped turn to one side, followed by a counterturn. A short latency C-startle and a long latency C-startle is noted in ZF which arise from a high-intensity and low-intensity stimulus respectively (Burgess & Granato, 2007).

The above two behaviors, exploratory swimming and escape induced by acoustic stimulus are directly investigated in this thesis work using both DT and ZF.

Another well studied behavior in ZF is predation. Predation or hunting behavior develops in ZF around 5 dpf when the yolk sac is used up. During prey capture, ZF executes a very stereotypical

swim pattern. The so called 'J-turns' with small angle flexion at the tail end are first used by the fish to orient itself with respect to the fish. This is followed by a 'capture swim' to strike at the prey (McElligott & O'Malley, 2005 and Borla et al., 2002).

More recently, using unsupervised clustering, Marques et al. (2018) have identified 13 basic swim types that are used in various combinations across different behavioral contexts in ZF. The idea, going forward, would be to dissect these swim types into their respective neuronal correlates and to investigate how these swim types and their usage across behaviors have diverged over evolution among other danionin larvae with respect to the underlying neuronal correlates.

1.5 Supraspinal neuronal correlates of locomotion

An advantage of directly investigating the locomotor circuits is its reliably quantifiable motor readout. Despite this, we still have many gaps in our understanding of the sophisticated network which controls locomotion. It partly arises from the fact that locomotion is controlled at many levels as shown in Figure 1.5. Central pattern generators in the spinal cord, for instance, are known to be able to produce movements independent of any supraspinal inputs. However, in this thesis work, I have primarily focused on the supraspinal control of locomotion. Hence, I will review our current understanding of the supraspinal control of locomotion with a special emphasis on ZF.

At the top of this control hierarchy is the basal ganglion, which is involved in selection of the motor programs. The direct GABAergic projection from the globus pallidus interna (GPi) and substantia nigra pars reticulata (SNr) of basal ganglion can provide continuous inhibition to the downstream locomotor command regions like the mesencephalic locomotor region (MLR) and diencephalic locomotor region (DLR). Input from striatum can cause a disinhibition of this inhibition, leading to release of specific motor programs (Hikosaka & Wurtz (1985) and Ménard & Grillner (2008)) Much of our understanding on this is based on works on cat, monkey, mouse and lamprey; the equivalent structures are yet to be described in larval ZF.

The MLR region provides a graded control over the intensity of locomotion. The mammalian MLR is found to be composed of a variety of cell types – cholinergic, glutamatergic and GABAergic (Ryczko & Dubuc, 2013). In mouse, glutamatergic cells of MLR were found to be necessary for locomotion and locally projecting GABAergic cells inhibited the glutamatergic cells (Roseberry et al., 2016). In a rather unexpected result in lamprey, it was observed that stimulation of the same glutamatergic MLR cells can either start or stop locomotion (Grätsch et al., 2019). The MLR region, again, is not well characterized in ZF. The neurons of the MLR activate downstream neurons called the reticulospinal (RS) neurons.

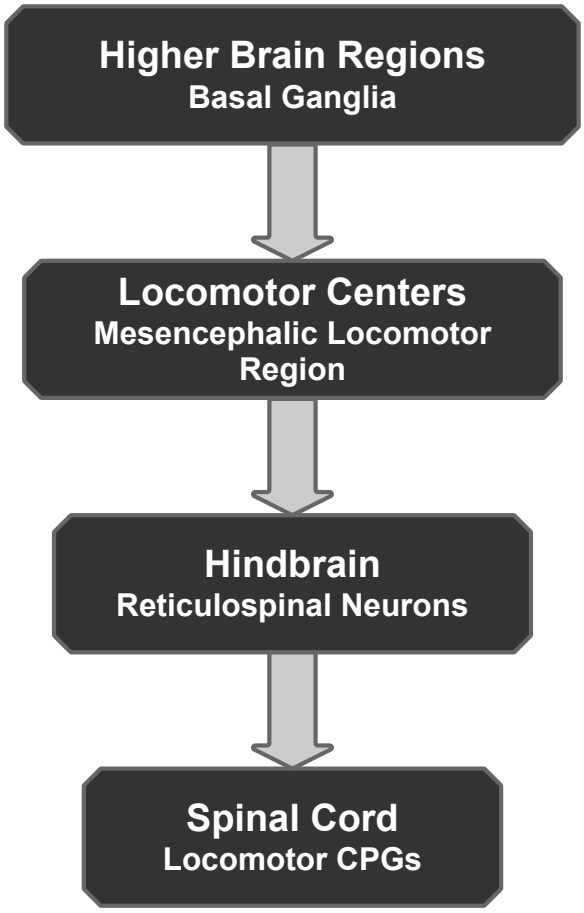

Figure 1.6: Illustration showing descending control of locomotion in vertebrates.

The RS neurons project from the brainstem to the spinal cord and play a crucial role in controlling the activity of the CPGs. Although, they had been first identified in cats, a lot about the RS neurons is known from work on lampreys. In lamprey, a functionally heterogenous

group of neurons associated with initiation, maintenance and end of locomotion have been identified (Bouvier et al., 2015). Moreover, RS neurons in lamprey have been shown to consist of both, excitatory and inhibitory types (Buchanan et al., 1987). Much progress in the understanding of supraspinal control of locomotion in ZF has been made at the level of RS neurons in the brainstem. Calcium imaging of the nucleus of the medial longitudinal fasciculus (nMLF), a small group of reticulospinal neurons in the zebrafish midbrain has shown nMLF to be correlated with duration of swim bouts (Severi et al., 2014). Another brain region in ZF known to be involved in spontaneous swimming is the anterior rhombencephalic turning region which is implicated in turning behavior (Dunn et al., 2016). A glutamatergic V2a neuron population in ZF were identified in the hindbrain and their optogenetic activation led to initiation of locomotion (Kimura et al., 2013). In contrast, activation of similar V2a neurons in mice were shown to lead to a termination of locomotion (Bouvier et al., 2015). The RS neurons can, in turn, have a direct influence in controlling the activity of the CPGs.

There are many ways to cluster neurons of an identified nucleus into defined sub-groups. One of the approaches is to identify the excitatory and inhibitory neurons in the population. Functionally, a more useful way to do this is by assigning neurons to different phases of the behavior under study. In lamprey, RS neurons correlated to initiation, maintenance and termination of swimming are identified (Juvin et al., 2016). Specifically, 'stop' cells have been identified which reliably fire during the termination of swimming (Grätsch et al., 2019). Similar neurons responsible for termination have been noted in *Xenopus* and mouse (Perrins et al., 2002 and Bouvier et al., 2015).

Identification of such neurons in ZF is difficult with the existing calcium imaging techniques as the temporal resolution is not appropriate to resolve the ZF swim events into different phases. However, given the long duration of swimming in DT, it is possible to achieve this in DT. This will be another advantage of the comparative approach where neuronal circuits can be examined in related species at different scales and the obtained information can be translated between organisms to hypothesize previously unidentified mechanisms.

1.6 Summary and objectives of the current study

DT is a new, emerging danionin model system. ZF, a related danionin species on the other hand, is a well characterized classical model system in developmental biology. By virtue of the high degree of conservation between DT and ZF, I developed an approach to compare the two species in a behavior which is executed differently in the two species. The behavior in focus is spontaneous exploratory swimming in the fish. The idea is to understand how the difference in behavior is implemented by using very similar circuitry.

In this study, I thoroughly characterize the swimming behavior in DT and ZF in Chapter 3. At the cellular and physiological level, I begin from a purely descriptive anatomical characterization of the hindbrain and later incorporate findings from functional imaging to comment on the differences in the operation of the supraspinal control centers in the brain of DT and ZF. The difference in swimming behavior is also exploited to find functionally diverse group of neurons in DT brain which were not reported in ZF before. The cellular and physiological findings are reported in Chapter 4. Following this, Chapter 5 provides a comprehensive discussion of the results in Chapters 3 and 4. A collection of supplementary data is provided in Chapter 6 which supports the results and discussion.

The findings, I believe, will also serve as a foundation for future works looking at comparative neurophysiology underlying vertebrate behavior. Danionins are a good candidate for carrying this out as there are many related species which can be grown and experimented on, using the same resources as used in DT/ZF. By incorporating many related species in the study, eventually, a better understanding of the functional divergence of neuronal circuits can be developed.

Chapter 2

Materials and Methods

"You know my method. It is founded upon the observation of trifles."
— Arthur Conan Doyle, The Boscombe Valley Mystery

2.1 Animal maintenance

2.1.1 *Danio rerio* (zebrafish)

6 days post-fertilization (dpf) zebrafish (ZF) larvae of TL/mitfa-/- (nacre) strain were used for behavioral experiments. For imaging experiments, 5 dpf nacre fish were used as they lack pigment in the skin. The two strains do not show any apparent differences in their swimming behavior.

2.1.2 † *Danionella translucida*

6 days post-fertilization (dpf) wild-type *Danionella translucida* (DT) were used for behavioral experiments. For imaging experiments, 5dpf wild-type fish were used. The pigmentation on skin is very scarce. DT adults were grown at a water temperature of 25 to 28° C, pH of 6.3 to 8.3 and a conductivity of 250 to 450 uS. These conditions are very similar to the requirements of ZF. Indeed, we had some ZF colonies growing in the same system. Adult DT are fed with Gemma Micro 150 (Skretting, USA) (twice a day) and live *Artemia* (once a day). They are also known to spawn in crevices. Hence, 2 to 4 silicone tubes (~ 5 cm long) were added in the adult tanks to aid spawning.
† For a more thorough information on the husbandry and breeding of *Danionella translucida* (DT) used in this study, refer to annex # 1.

The larvae were grown at a density of <50 larvae per 90 cm Petri plate in E3 egg medium (without methylene blue). For behavioral experiments, at 5 dpf, both larval ZF and DT were transferred to a 250 ml beaker with 100 ml E3 egg medium (without methylene blue) and fed with rotifers. They were maintained at 28°C in an incubator until the experiment.

All animal procedures (zebrafish and *D. translucida*) were performed in accordance with the animal welfare guidelines of France and the European Union. Animal experimentations were approved by the committee on ethics of animal experimentation at Institut Curie and Institut de la Vision, Paris.

2.2 Behavior

2.2.1 Free-swimming behavioral acquisition, fish tracking and tail segmentation

A high-speed camera with a high quantum efficiency in the infrared range (MC1362, Mikrotron-GmbH, Germany) and a Schneider apo-Xenoplan 2.0/35 objective (Jos. Schneider Optische Werke GmbH, Germany) were used to carry out the free-swimming acquisitions. The resolution of the images were 800 x 800 pixels with 17 pixels /mm and the temporal resolution of the acquisition was 700 Hz. The fish were illuminated with an infrared LED array placed below the swimming arena. An 850 nm infrared bandpass filter (BP850-35.5, Midwest Optical Systems, Inc.) was used on the objective to block all the visible light. Figure 2.1 illustrates the set-up.

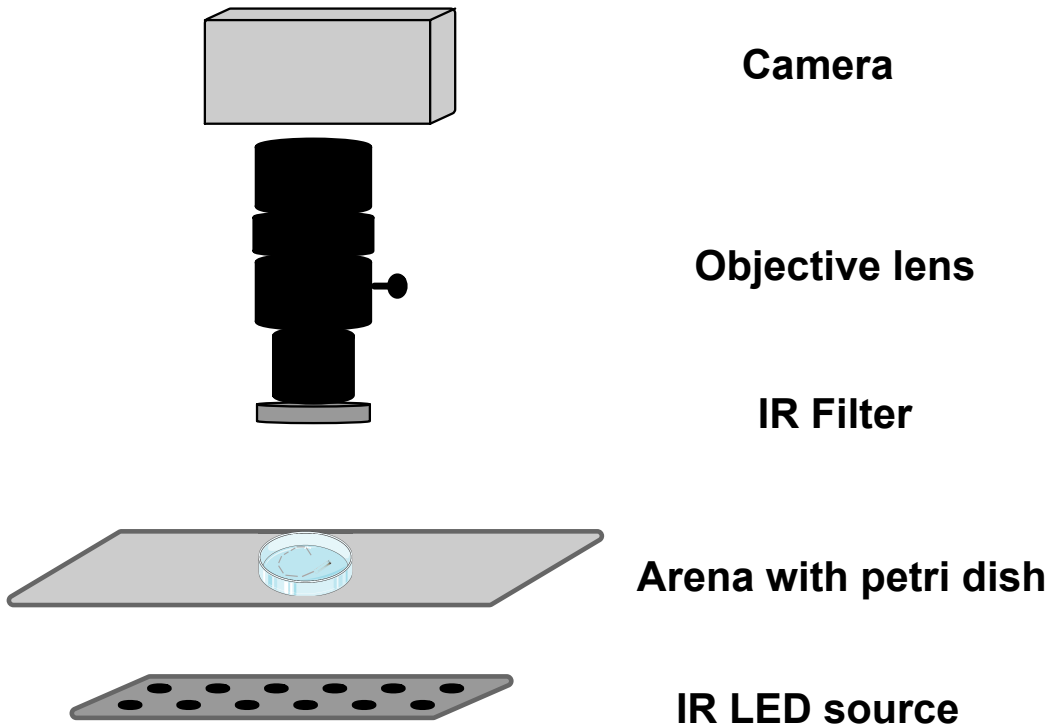

Figure 2.1: An illustration of the free-swimming behavioral analysis set-up.

The behavioral arena was illuminated at 220 lux which was similar to the light intensity in the home incubator. Both DT and ZF were fed at 5 dpf with filtered rotifers and 6 dpf fish were used for the experiment. The fish were transferred to 35 mm Petri plates and acclimatized for > 2 hours before the behavioral acquisitions. 23 DT and 37 ZF were tested with the acquisition lasting for ~ 20 - 30 mins.

Image acquisition, fish tracking and tail segmentation were performed using a custom-written C# (Microsoft, USA) program. The online tracking of the fish and tail segmentation was carried out as described in (Marques et al., 2018). Briefly, the following method was performed. A background was calculated by taking the mode of a set of frames which are separated in time so that the fish occupies a different position in each frame. This background image was subtracted from each acquired frame. The subtracted image was smoothened using a pixel boxcar filter. A manually selected threshold was used to separate the fish from the background. The fish blob was selected by performing a flood fill starting at the maximum intensity point. The center of mass of this shape was considered the position of the larva. The middle point on a line joining the center of mass of each eye was defined as the larva's head position. The direction of the tail was identified by finding the maximum pixel value on a 0.7 mm diameter circle around the head position. Then, a center of mass was calculated on an arc centered along this direction. The angles of ~10 tail segments measuring 0.3 mm were calculated. To do this, successive tail segments were identified by analyzing the pixel values along a 120-degree arc from the previous segment. This same algorithm was used for both DT and ZF. The empirically selected threshold to separate the fish from background was different in the two fish.

2.2.2 Analysis pipeline for free-swim data

Data cleaning

Poor tracking was identified using pixel intensities of the tail segments. Data entries with sum of the absolute pixel intensities of the tail segments lower than 100 were flagged as non-reliable (8-bit images are used) and replaced with NaN. The threshold of 100 was empirically decided after inspecting the distribution of sum of the pixel intensities of the tail segments for many fish. Despite the slight differences in pigmentation between the two fish, this threshold did hold well for both the fish.

The lost frames, if any, were identified based on a 32-bit time stamp encoded in the first 4 pixels of all the images. These lost frames are then interpolated and filled with NaN values for the recorded parameters.

Pre-processing

Discontinuities in turning when the fish turns from 0 to 360 degree or vice versa were corrected. The raw X and Y coordinates were smoothened using the savitzky golay digital filter: in MATLAB (MathWorks, USA), sgolayfilt function is used to implement this. A 2nd order polynomial fit was employed on a window size of 21 units (30 ms). Displacement was calculated using these X and Y coordinates of the centroid of the fish.

Bout detection using tail curvature

I used a measure of tail curvature to identify the bouts as described in (Marques et al., 2018). The first 8 tail segments were incorporated in the analysis based on the reliability of the tracking as assessed by the raw pixel intensities. The change in the curvature of the tail was emphasized over local fluctuations by taking a cumulative sum of the values along the tail. The differences in tail angles were calculated as we want to detect movements. The tail movements were then smoothened using a boxcar filter of size equivalent to ~14.30 ms. The absolute of the segment angles were then convolved into a single curvature measure. A maxima/minima filter of 28.6 ms/ 572 ms was specifically applied to this tail curvature dataset of zebrafish based on the knowledge of bout and inter-bout durations available to us. An empirically validated cut-off was used on the convolved and smoothened tail curvature measure to identify the starts and ends of swim bouts. It is important to note that in the analysis, I identify only the 'burst' phase of 'burst-and-glide' swims in ZF.

The 7th tail segment was used for calculating tail beat frequency and maximum tail angle. The trace of the tail segment is smoothened and small gaps (less than 7 ms) in the swim events due to tracking were interpolated. Swim events with larger gaps were eliminated from the analysis. Any identified event shorter than 71.5 ms in length, if present, were discarded as well to avoid artefacts. On the bout-based kinematics, the bout distance, inter-bout duration, mean and maximum speed, maximum tail angle and tail beat frequency were calculated.

Half beat based kinematics in Zebrafish and *Danionella translucida*

I defined a peak-to-peak half cycle as a half tail beat cycle and this was used for the kinematic calculations to be able to compare a similar unit of locomotion between the two fish.

In zebrafish: to identify the half-beats, on every swim bout, the absolute of the tail angles was calculated from the 8th segment of the tail and the peaks of tail angle were identified using the findpeaks function in MATLAB. Figure 2.2 shows this for a swim bout in zebrafish.

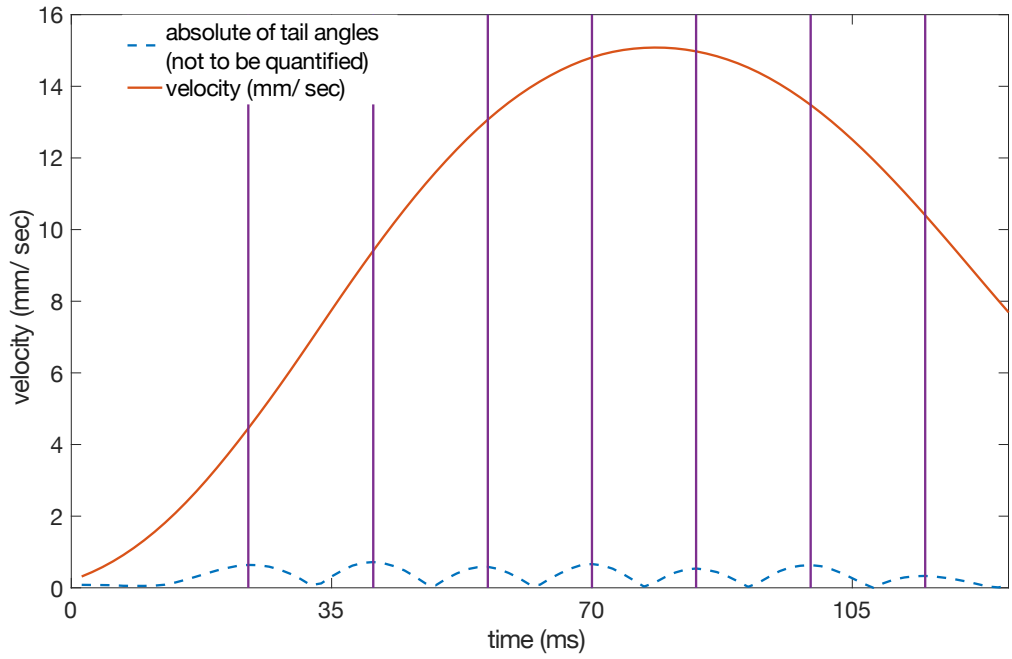

Figure 2.2: Illustration of half beat identification in a swim bout of zebrafish. The vertical lines show the peak of tail bend which considered as the start and/or end of a half beat.

In *Danionella translucida*: the trace of the tail segment is smoothened using sgolayfilt function of 3rd order with a window size of 50 ms. Small gaps (less than 7 ms) in the tracking are interpolated.

Using bwlabel function in MATLAB on the binary matrix of good/ bad tracking, all continuous stretches of good tracking are labelled. From this, I selected only the stretches longer than 35 frames (or 50ms) for further analysis to avoid small tracking artefacts if any. On these identified stretches, we identify half beats as mentioned above for zebrafish.

On every half beat in both the fishes, I calculated the following kinematics parameters: duration, distance, mean and maximum speed, maximum tail angle and half beat frequency. The 8th tail segment is again used for calculating tail beat frequency and max tail angle.

2.2.3 Clustering of free-swim half tail beats

A total of over 200,000 half beats from 14 DT: ~18,000 half beats per fish were used and the three variables - mean speed, half beat frequency and maximum tail angle - were considered as the predictors for performing k-means clustering. Outliers and missing values were identified and the respective data entries were discarded. An outlier is defined as a value that is more than three scaled median absolute deviations (MAD) away.

I tested cluster sizes of 2 to 5 and optimal clustering was detected at k=2 with a silhouette coefficient >0.50. The silhouette coefficient gives a measure of the similarity between the points of the same cluster by measuring how close the points of a given cluster lie when compared to their distance to the points in the other clusters. It ranges from -1 to 1. A higher silhouette value indicates a better clustering. Once we identified the cluster size to be 2, the clustering was then performed with k=2 clusters and n=100 repetitions to obtain a reliable clustering.

The representative trajectory with slow/fast tracks was plotted by first filtering the raw velocity traces from 700 Hz acquisition with a 100 ms moving mean filter and then down sampling the signal into 70 Hz. The velocity was normalized between 0 and 1. Every step is 100 ms in time.

2.2.4 Head-embedded swimming behavior set-up

I used a high-speed camera (MC4082, Mikrotron-GmbH, Germany) with a Navitar Zoom 7000 macro lens to carry out the head-embedded acquisitions. The resolution of the images were 400 x 400 pixels with 75 pixels /mm and the temporal resolution of the acquisition was 250 Hz. The fish were illuminated with an infrared LED array placed below the swimming

arena. An 850 nm infrared bandpass filter (BP850-35.5, Midwest Optical Systems, Inc.) was used on the objective to block all the visible light.

6 dpf DT and ZF were embedded in 0.5ml of 1.5% agarose. For ZF, nacre incross were used. The agarose covered the head up to the pectoral fins. Each fish was acclimatized for at least 90 minutes before acquisition. Recordings lasted for 10-20 mins per fish. 4 DT / 5 ZF were used in this experiment.

2.2.5 Analysis pipeline for head-embedded data

The head-embedded videos were primarily used to determine the amount of time spent in swimming. I wrote a custom program on MATLAB to achieve this. Briefly, the following approach was used. An ROI was drawn around the tail. A threshold was selected empirically for every video to binarize the image to segment the tail. The image was divided into 12 vertical bocks perpendicular the tail segment. A mask was used to run through the image block-by-block to determine the center of mass of the largest blob (tail segment) per block. This center of mass information was used to calculate the angle between two consecutive tail spots. Of the 11 tail segment angles, the first nine were used to determine a curvature of the tail throughout the video. A cut-off value on the curvature was used to determine regions of active swimming. The results from the obtained from script were manually verified. 6 dpf ZF (n=6) and DT (n=5) were used for the experiment. The duration of swimming was normalized to the total length of the acquisition and reported as a percentage of the total duration of acquisition.

2.2.6 Assay to study tap-induced escape behavior

The same set-up as described in 2.2.1 was used for this assay. In addition to the free-swimming acquisition system, I added an Arduino controlled solenoid to the behavioral arena. The Arduino was triggered from the aforementioned acquisition program written in C# (Microsoft, USA). When triggered, the solenoid would hit the surface of the arena from the bottom and cause the fish to escape in response to this stimulus. The trigger was only initiated if the fish was not at the edges of the Petri dish and there was an inter-stimulus interval of at least 50 seconds between the trials. The delay between the trigger onset and the delivery of

the solenoid on the arena was estimated and incorporated in the analysis to calculate an accurate reaction time. 19 DT (n=141 trials) and 15 ZF (n=159 trials) were tested in the assay.

2.2.7 Analysis pipeline for tap-induced escape data

To analyze the escape kinematics, the peak escape velocities were identified in a window of approx. 450 ms after the stimulus delivery. A peak speed was considered as at least 2 times the peak speed during free-swimming (9.25mm/s and 42.5 mm/s for DT and ZF respectively). In case of multiple peak escape velocities in the window, only the first one was considered. Now, I selected a 140 ms region of interest around the peak speed to consider 40 ms before the peak and 100 ms after the peak as shown in Figure 2.3 for a zebrafish. The region of interest was empirically decided after exploring many trials across both the fish species. Mean and maximum velocities, total distance covered and the delay to reach the peak speed after the stimulus delivery – these parameters were computed for all the trials in each fish.

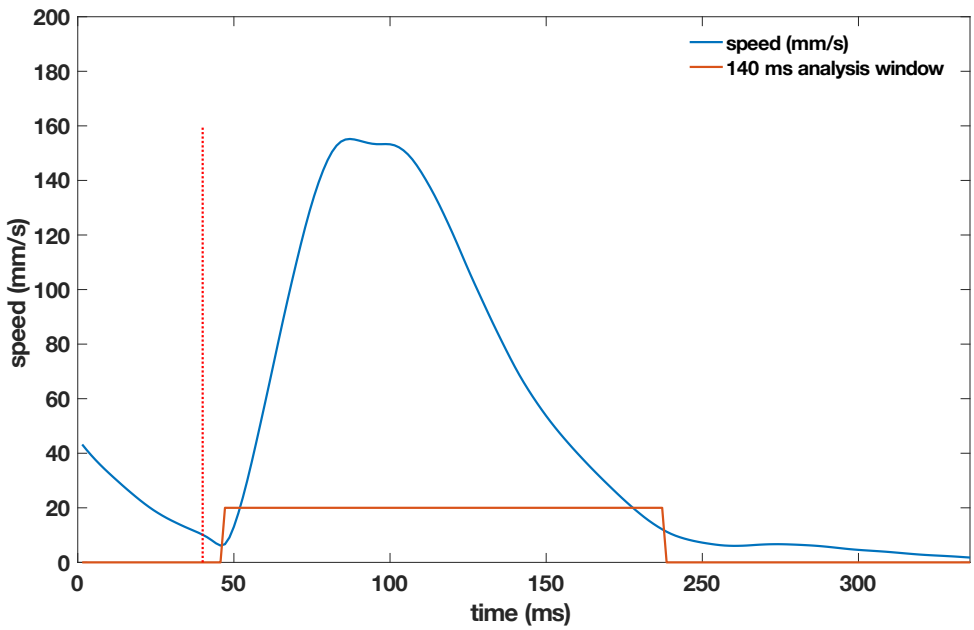

Figure 2.3: Illustration of the 140 ms window selected for the analysis of tap-induced escape kinematics. The vertical line shows the time of stimulus delivery.

The major differences in the processing pipeline from the free-swimming analysis pipeline were as follows. The X/Y displacement vectors were further filtered using zero-phase digital filtering (*filtfilt* function in MATLAB) with a filter size of 11 ms to identify the peak escape velocities. Kinematics were neither calculated on half beats nor bouts, but on the custom

defined 140 ms window for a better comparison of the escape events in the two species of fish.

2.2.8 Mean squared displacement (MSD) and reorientation analysis

Information on X/Y- coordinates was used to compute the Mean squared displacement (MSD) and decorrelation in heading orientation (R) over time. A Savitsky-Golay filter was applied on the X and Y to fit a 2nd order polynomial on a 200 ms window. The filtered trajectories were then downsampled to 70 Hz. For each fish, discrete continuous trajectories were identified in a circular region of interest of radius of 300 pixels (18mm) to mitigate border-induced bias. These trajectories were used for the computation. Some of the raw trajectories are also illustrated.

The time-evolution of MSD and R were calculated at every 100 ms time-step and averaged over all trajectories for each animal. To compute R, we extracted at each time t a unit vector $\mathbf{u}(t)$ aligned along the fish displacement [dx,dy] calculated over a 1s time window. Notice that this vector was only calculated if the fish had moved by at least 0.5 mm in this time period. The heading decorrelation over a period Δt was then computed as $R(\Delta t)=\langle \mathbf{u}(t).\mathbf{u}(t+\Delta t)\rangle_t$. This function R quantifies the heading persistence over a given period: R=1 corresponds to a perfect maintenance of the heading orientation, whereas R=0 corresponds to a complete randomization of the orientations. The MSD and R values were plotted over time for DT (n=23 fish) and ZF (n=37 fish).

2.2.9 Energetics and swimming speed

A relation between oxygen consumption and swimming speed in 3-weeks old larval zebrafish (ZF) was obtained from (Bagatto et al., 2001): Log C = 2.103 + 0.309 x V, where C is a measure of oxygen consumed per mg of the animal per hour and V is the speed.

Instantaneous speed obtained from kinematic analysis (2.2.2) of DT and ZF was used to calculate the consumption of oxygen in DT and ZF. By virtue of their similar age and size, we approximated the metabolic demands to be similar and used the above equation with the

experimentally calculated speeds to determine an approximate value for oxygen consumption in both the fish.

2.2.10 Quantification of depth preference

Two sets of 3 vertical glass cylinders with 36 cm water height were used in this experiment. 6 dpf zebrafish larvae (n=30 per cylinder) were added to three cylinders. 6 dpf *Danionella translucida* (DT) larvae (n=30 per cylinder) were added to the other three cylinders.

The cylinders were considered as consisting of three sections and marked accordingly: the bottom 12 cm, middle 12 cm and the top 12 cm sections. The number of fish in each section of the column was manually counted once every hour for 10 hours. This was used to calculate the average normalized fish density in every section of the water column.

2.2.11 Quantification of body length and swim bladder inflation

Body length was measured in 5 dpf larvae of the two species (n = 10 for DT and n = 9 for ZF). Pictures of the larvae were captured using AxioCam MR3 camera. The magnification of the optics was noted and the physical dimension of camera pixel was used to calculate the pixel size in µm as follows: pixel size = (260/magnification) x binning factor.

To quantify swim bladder inflation, from a population of growing larvae (3 dpf to 15 dpf), five or more larvae were sampled for each age and the proportion of larvae with inflated swim bladder was quantified. A moving averaging was performed using a window size of two units to smoothen the curve and the swim bladder inflation results were reported from 3.5 to 14.5 days.

2.3 Anatomy

2.3.1 Fluorescence In-situ hybridization (FISH) and Immuno-histochemistry (IHC)

Probe synthesis:

To generate anti-sense probes, DNA fragments were obtained by PCR using Phusion™ High-Fidelity DNA Polymerase (Thermo Scientific™) and the following primers (5'->3') as shown in Table 2.1. Total cDNA for ZF and DT were used as a template.

	Zebrafish (T_m= 60°C)		*Danionella* (T_m= 58°C)	
Gene	Forward primer (5' ➔ 3')	Reverse Primer (5' ➔ 3')	Forward primer (5' ➔ 3')	Reverse Primer (5' ➔ 3')
dbx1a	GCATTCACCCTTTCCAGCTCAC	AGACAGAAATGCGATGGAGCG	AAGCAACATCTCCACCCTCG	TGAATACTGACGCGATCCGG
en1b	GCGCGATGTATTGTCTGACA	AATTTTCGTGTCCTTGGGCC	TGTCTGCCATGAAGAACGCT	CCTGGAACTCGGCTTTCAGT
evx2	CGATCAAGGGCCGACTCTAT	CATCGCTGTTCATGTCGGAG	GGCTTCCAGCTCGTAAAGGT	TTCATCCGCCGGTTCTGAAA
gad2/ gad65	ACGGGCTGACAAAACATTGC	GGCGTTCCAAGACTACCACA	NA	NA
gad1b/ gad67	CTGTTCGCGCGAGATCTACT	ATCCAAGAACAGCTCCTGCC	NA	NA
slc6a9/ glyt1	CAATGCCACTTTCGCCAACA	CCAGAGTCTCCAACAGGCAG	NA	NA
slc6a5/ glyt2	**AAAATGGATGCATCGACCGG**	**TACACGTGTCCAAAAGCAGC**	**TGGAAGGATGCTGCTACACA**	**TGACCATAAGCCAGCCAAGA**
pax2a	AATGTTCGCCTGGGAGATCA	CTGAACCGCCAAGCTTCATT	GTGTTTGTGAACGGCAGACC	CTCCAGCTGCTGTTGAGTGA
slc17a7a/ vglut1	GAGGAGGTGTTCGGCTTTGA	TTGTCCCAACCGGTTGAACA	NA	NA
slc17a6a/	**GGTCGGCACACTT**	**TAGCGTCCATTGG**	**GCAATCATCGTAG**	**ACTCCTCTGTTTT**

vglut2b	**TCTGGTA**	**ATGTGCA**	**CCAACTTC**	**CTCCCATC**
slc17a6b/ vglut2a	**CAGGGTGATAGAA AAGCGGC**	**TCCCAAAGCAGCC ATAGACA**	**AGTCGTCTAGCCA CAACCTC**	**CACACCATCCCTG ACAGAGT**
vsx2/chx10	GGACCGACTCGAA AGCAAAG	GGGCAGAGGGATA GAGTGAC	AATAGTCTCAGCG GCACCAT	GCAAGCATTTCTC TGGCGTA

Table 2.1: Primers (5'->3') used for generating anti-sense probes. The genes highlighted in bold were used for fluorescence *in-situ*.

PCR fragments were cloned into the pCRII-TOPO vector (Invitrogen) according to manufacturer's instructions. All plasmids used were sequenced for confirmation.

***in-situ* hybridisation:**

Digoxigenin RNA-labeled or Fluorescein RNA-labeled probes were transcribed *in vitro* using the RNA Labeling Kit (Roche Diagnostics Corporation) according to manufacturer's instructions. Dechorionated embryos at the appropriate developmental stages were fixed in fresh 4% paraformaldehyde (PFA) in 1X phosphate buffered saline (pH 7.4) and 0.1% Tween 20 (PBST) for at least 4 hours at room temperature or overnight at 4° C. Following this, the samples were preserved in methanol at -20° C until the *in-situ* experiments described below.

Whole-mount digoxigenin (DIG) *in-situ* hybridization was performed according to standard protocols (Thisse & Thisse, 2008). Briefly, the fixed samples were then rehydrated in a decreasing series of methanol/PBST solution. A protease-K (10 µg/mL) treatment was performed depending on the age and species of the sample. This differential treatment is summarized in Table 2.2. The fish were again incubated in 4% PFA and added to HY4 buffer for 1 hour at 68° C. The samples were then incubated overnight at 68°C in a solution of DIG-labeled probe at a dilution of 1:50 in HY4 buffer. Excess probes were removed by several washes. The samples were blocked using 2% blocking solution (Roche) for at least 1 hour before adding the Fab fragments of the alkaline phosphatase-conjugated anti-DIG-AP antibody (Roche) to detect DIG. This reaction mixture was kept overnight at 4° C. A chromogenic NBT-BCIP substrate (Roche) was used to detect the hybridization.

Imaging of DIG labelled samples:

After staining, the whole-mount DIG labeled embryos were washed twice in PBST. The embryos/larvae were again fixed overnight in 4% PFA/PBST. Glycerol was added to the samples before imaging on a stereoscope with AxioCam MR3 camera.

Whole-mount Fluorescence *in-situ* hybridizations were performed as follows: the embryos stored in methanol at -20ºC from above were rehydrated by two baths of 50% methanol/PBST followed by two baths of PBST. This was incubated for 10 min in a 3% H_2O_2, 0.5% KOH solution, then rinsed in 50% methanol/ 50% water and again dehydrated for 2 hours in 100% methanol at -20°C. Embryos were rehydrated again by a series of methanol baths from 100% to 25% in PBST, and washed two times in PBST. This was followed by an age and species dependent treatment of proteinase-K (10 µg/mL) at room temperature as described in Table 2.2. Following this, the samples were again fixed in 4% PFA/PBST.

Age	ZF	DT
24 hpf	8 mins	4 mins
48 hpf	20 mins	10 mins
72 hpf	70 mins	35 mins
96 hpf	96 mins	48 mins
120 hpf	120 mins	90 mins

Table 2.2: Age and species dependent time period for proteinase-K treatment.

After 2 hours of pre-hybridization in HY4 buffer at 68° C, hybridization with fluorescein-labelled probes (40ng probes in 200 µl HY4 buffer) was performed overnight at 68°C with gentle shaking. Embryos were rinsed and blocked in TNB solution (2% blocking solution (Roche) in TNT) for 2 hours at room temperature. This was then incubated overnight with Fab fragments of anti-Fluo-POD (Roche) diluted 1:50 in TNB. For signal revelation, embryos were washed with 100 µl Tyramide Signal Amplification (TSA, PerkinElmer) solution and incubated in the dark with Fluorescein (FITC) Fluorophore Tyramide diluted 1:50 in TSA. The signal was then followed for 30 minutes for *glyt* and 1 hour for *vgult2b* until a strong

signal was observed. After which, the reactions were stopped by 5 washes with TNT, and incubated for 20 minutes with 1% H_2O_2 in TNT. All the steps after Fluorescein (FITC) incubation were processed in the dark.

Antibody staining:

Following fluorescent *in situ* hybridisation staining, whole mount embryos were washed twice in TNT solution. Subsequently, they were blocked for 1 hour at room temperature in 10% Normal Goat Serum (Invitrogen) and 1% DMSO in TNT solution. Rabbit GAD65/67 primary antibody (AbCam) diluted 1/5000 in 0.1% blocking solution was incubated overnight at 4°C. The Alexa Fluor 635 secondary antibody goat anti-rabbit IgG (1/500) (Life Technologies) was added in 0.1% blocking solution and incubated overnight at 4°C. After 5 washes in PBST buffer, microscopic analysis was performed. For labelling cells expressing H2B-GCaMP6s in *Tg(HuC:H2B-GCaMP6s)* DT, a similar protocol with an anti-GFP primary antibody was used.

The composition of the buffers used are noted below:

HY4 buffer: 50% formamide, 5x saline-sodium citrate (SSC), 50 μg/ml heparin, 0.1% Tween 20, 5mg/ml Torula RNA.

1x Phosphate Buffered Saline (PBS): 137 mM NaCl, Na_2HPO_4, 10 mM KH_2PO_4, 1.8 mM, 2.7 mM KCl, pH 7.4.

PBST: 0.1% Tween 20 in 1x PBS.

Tris-NaCl-Tween buffer (TNT): 0.1 M Tris pH7.5, 0.15 M NaCl, 0.1% Tween 20.

2.3.2 Confocal imaging of the whole brain FISH/IHC samples

To image the whole brain *in-situ* hybridization and immunohistochemistry samples, we used Zeiss LSM 780, LSM 800 and LSM 880 confocal microscopes with a 10x or 40x objective using appropriate lasers and detection schemes suitable to the labelled sample. Whole brain images were acquired in tiles and stitched together using the stitching algorithm available in Zeiss ZEN blue and ZEN black (on LSM 800). The images are shown as maximum intensity projections created on imageJ. In GAD65/67, non-specific blobs of signal likely originating from residual dye left on the skin after the washing step was removed using image processing in the representative image.

2.3.3 Retrograde labelling of reticulospinal (RS) neurons

A solution containing 10% w/v Texas Red dextran (TRD, 3,000 MW, Invitrogen) in water was pressure injected in the spinal cord (between body segment 7 to 14) of 4dpf ZF and DT. In DT, this method resulted less efficient in labeling the whole RS neurons. The best results were obtained by cutting the tail beyond segment 14th with fine scissors and pressure injecting the TRD in the exposed spinal cord. After the labeling, the fish were allowed to recover in E3 egg medium for 24 hours at 28° C.

At 5dpf, the surviving injected larvae were anaesthetized with 0.02% Tricaine (MS-222, Sigma), mounted in 1.5% low melting point agarose and imaged under a VIVO 2-photon microscope (3I, Intelligent Imaging Innovations Ltd). Labelling was often sparse and varied among the injected fish which survived to 5dpf (n=4 fish per species). Maximum intensity projection images of the reticulospinal neurons in ZF and DT is shown from the animals where almost all the RS neurons were labelled. RS neurons in DT brain were annotated based on their anatomical similarity to the ones in zebrafish (Kimmel et al., 1982).

2.4 Physiology

2.4.1 Generation of pan-neuronal calcium sensor *Tg(HuC-H2B:GCaMP6s)* line

To create *Tg(HuC:H2B-GCaMP6s)* DT fish, 6 ng/µl of the plasmid and 25 ng/µl of Tol2 was used. Injections were performed in embryos which were less than or equal to 4-cell stage. The injection was performed free-hand and the egg was targeted directly. Tol2-elavl3-H2B-GCaMP6s plasmid was a gift from Misha Ahrens (Addgene plasmid # 59530; http://n2t.net/addgene:59530; RRID: Addgene_59530). It was published in Freeman et al. (2014) .

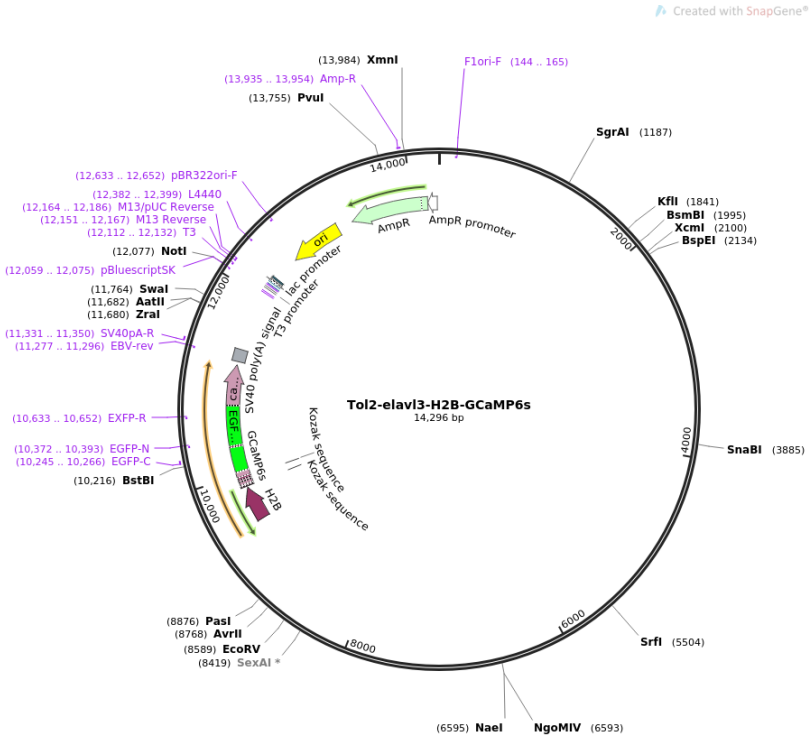

Figure 2.4: The Tol2-elavl3-H2B-GCaMP6s plasmid used for creating the *Tg(HuC:H2B-GCaMP6s) Danionella translucida*.

2.4.2 Light-sheet imaging

I used transgenic DT and ZF expressing H2B-GCaMP6s under the HuC promoter. The GCaMP is nuclear tagged, so its expression is limited to the nucleus which makes it easier for segmentation of the neurons. The fishes were embedded in a capillary with 2.5% agar. The tail was freed and recorded simultaneously to extract a readout of the spontaneous swimming behavior. Before each recording, the embedded fish were acclimatized to the recording chamber with the blue laser switched on for at least 10 minutes. The scanning objective was lateral and the beam entered from the left side of the fish and the detection objective was placed upright on the top. Both the objectives were moved with a piezo so that the light sheets were always in the focal plane of the detection objective. Average laser power was at 0.05 mW. Approximately 280 µm of the brain volume was imaged in each fish. Brain imaging was carried out at approximately 1 Hz (1 whole brain volume / sec) and the tail movement was acquired at ~ 40-80 Hz. Each acquisition lasted for ~ 20 minutes.

2.4.3 Image processing and analysis pipeline for whole-brain light-sheet data

For ZF and DT, image processing was performed offline using MATLAB. Based on visual inspection, if needed, image drift was corrected by calculating the cross-correlation on a manually selected region of interest (ROI). The dx and dy values employed to correct the drift in this ROI were extrapolated to the whole stack. Brain contour was manually outlined on mean graystack images for each layer. Background value for each layer was estimated from the average intensity of pixels outside the brain contour. The segmentation procedure consisted of a regression with a gaussian regressor convolved with the same gaussian regressor. The result was regressed a second time with the same regressor. Baseline and fluorescence were calculated for each neuron identified by the segmentation. The fluorescence $F(t)$ signal was extracted by evaluating the mean intensity across the pixels within each neuron. For ZF, the baseline was calculated by the running average of the 10th percentile of the raw data in sliding windows of 50 sec. For DT, the baseline for identifying "swim" neurons was calculated as the 10th percentile of the raw data within each inactive period defined as the time period between 5 sec after the end of a swim event and 3 sec before the beginning of the next swim event (from tail acquisition data). The baseline values for the active periods were interpolated using the values in the inactive periods. For both ZF and DT,

the relative variation of fluorescence intensity *dF/F* was calculated as *dF/F* = (*F(t)* – baseline) / (baseline-background).

2.5 Statistical methods

Behavior data:

All the averaged values per fish were prepared in Matlab 2017b (Mathworks) and statistical tests between the populations were carried out in Prism 8 (GraphPad). Kruskal-Wallis test by ranks was performed in all cases where the dataset did not follow a normal distribution.

Light-Sheet imaging data:

For both ZF and DT, neurons from the more rostral part of the brain were removed (y coordinates between y_{max} – 10 um and y_{max}) because of dF/F artefact due to image border. A multi-linear regression was performed using the classical normal equations. In DT, this was performed on dF/F for the whole duration of the experiment and in ZF, on dF/F for a manually selected time period with many well isolated swim bouts. The analysis determines the best-fit coefficient β to explain the neuronal data (y) by the linear combination $y = \sum \beta_j * x_j + \beta_o$, where x_j is the regressor. For ZF, a constant regressor and a swim maintenance regressor (based on the tail acquisition data) were used. For DT, four regressors were used: constant, swim maintenance, swim onset and swim offset. The onset and offset regressors were obtained from the initiation and termination of swim events (based on the tail acquisition data) with a time window of -3 sec to +1 sec around the event. Swim maintenance, onset and offset regressors were convolved with a single exponential of 3.5 sec decay time which approximates the H2B-GCaMP6s response kernel in ZF (Migault et al., 2018). T-scores were computed for every neuron/regressor combination.

To characterize highly responsive neurons for a specific regressor, the regression coefficient and t-score distributions were first fitted with a gaussian model (μ_{dist}, σ_{dist}) to estimate a sub-distribution responsible for noise (neurons that are not correlated well with the regressor). These sub-distributions, defined as the maximum distribution ± σ_{dist}, were then fitted again with a gaussian model (μ_{nosie}, σ_{noise}). The highly responsive neurons were defined as neurons with both, a regression coefficient higher than regression threshold $_{coefficient}$ = $\mu_{noise\ coefficient}$ + 3

$\sigma_{noise\ coefficient}$ (or threshold $_{coefficient}$ = $\mu_{noise\ coefficient}$ + 4 $\sigma_{noise\ coefficient}$) and a t-score higher than t-score threshold $_{t\text{-}score}$ = $\mu_{noise\ t\text{-}score}$ + 3 $\sigma_{noise\ t\text{-}score}$ (or threshold $_{coefficient}$ = $\mu_{noise\ t\text{-}score}$ + 4 $\sigma_{noise\ t\text{-}score}$).

To quantify the responsiveness of highly correlated neurons, a score was created for each neuron based on the sum of the regression coefficient normalized by the regression threshold$_{coefficient}$ (a_1) and the t-score normalized by the t-score threshold$_{t\text{-}score}$ (a_2). The higher the score, the more responsive is the neuron.

For characterization of the swim onset and maintenance components of the onset neurons, the distribution of all the onset neurons was first visualized on a $[a_1+a_2]_{swim\ regressor}$ versus $[a_1+a_2]_{onset\ regressor}$ plot (see Figure 6.8-B). The angle of a vector from the point of intersection of the normalized thresholds of $[a_1+a_2]_{swim\ regressor}$ and $[a_1+a_2]_{onset\ regressor}$ (at [2,2]) to an individual neuron's position was calculated for every onset neuron. An onset neuron with an angle between pi and pi/2 was considered to possess only a swim onset component (green) whereas an onset neuron with an angle between pi/2 and zero was considered to possess both, strong onset and maintenance components.

† Chapters 3 and 4 are compiled together as a manuscript for a peer-reviewed publication (see annex #3).

Chapter 3

Characterization of exploratory locomotion in *Danionella translucida* (DT) and *Danio rerio* (ZF)

"We see in order to move; we move in order to see." — William Gibson

A thorough understanding of the behavior, from both mechanistic and organismal perspective, is critical to probe the underlying neuronal circuitry or its divergence among animals. In this context, the aims of the current chapter are to:

- Understand the fine structure of locomotion in spontaneously swimming DT and compare it to ZF.

- Quantify the duration of swim events in a head-embedded preparation.

- Compare the escape kinematics of DT and ZF in a tap-induced escape assay.

- Compare exploration and energy consumption in spontaneously swimming DT and ZF.

- Suggest selective pressures based on empirical evidence which might have caused the divergence in swimming pattern.

3.1 Length of larval DT and ZF is in a similar range

DT undergo a developmental truncation which leads to a small body size in adults with a partially developed cranium. This is indeed what makes them interesting for functional neuroscience studies. However, studies on ossification in *Danionella dracula* demonstrate that most bones affected by truncation are formed later in the development of zebrafish (Britz et al., 2009). Hence, developmentally the two species should be very much comparable in the early stages of development. This is an advantage to comparative studies of DT and ZF which look at the larval and early juvenile stages of the two fish species.

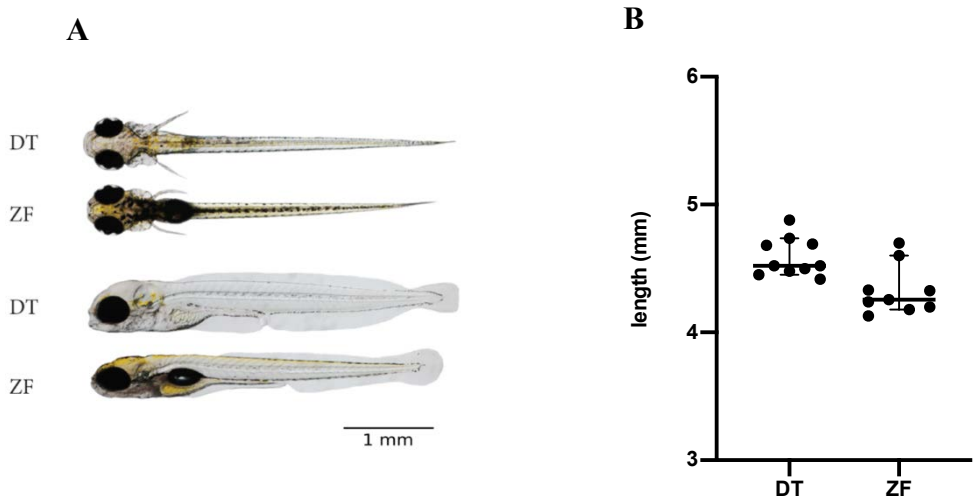

Figure 3.1: DT and ZF measure similar in size at 5 dpf. (A) shows a dorsal and lateral view of DT and ZF at 5dpf. (B) shows the measurement of body length in 5 dpf DT and ZF (N= 10 DT; N= 9 ZF).

During undulatory swimming, propulsive forces result from the fluid-body interaction. The resulting thrust and hydrodynamic resistance strongly depend on the animal body size (Muller, 2004 and Van Leeuwen et al., 2015). Here, in Figure 3.1, I provide an overview of the size of the two larvae at 5 dpf. Although there is a subtle difference in their length, they fall in a similar range. In our small dataset, the length of DT ranges from 4.4 to 4.9 mm and the length of ZF ranges from 4.1 to 4.7 mm. With this comparable range in size, they would be expected to develop similar propulsive forces and hydrodynamic resistance during swimming.

3.2 DT execute swim events with a continuous tail-burst activity

ZF are known to swim in a beat-and-glide pattern wherein a burst of tail activity lasting ~140 ms is followed by a small glide phase (Budick & O'Malley, 2000). In contrast to this, in DT, I observe sequences of continuous tail activity lasting for hundreds or thousands of seconds.

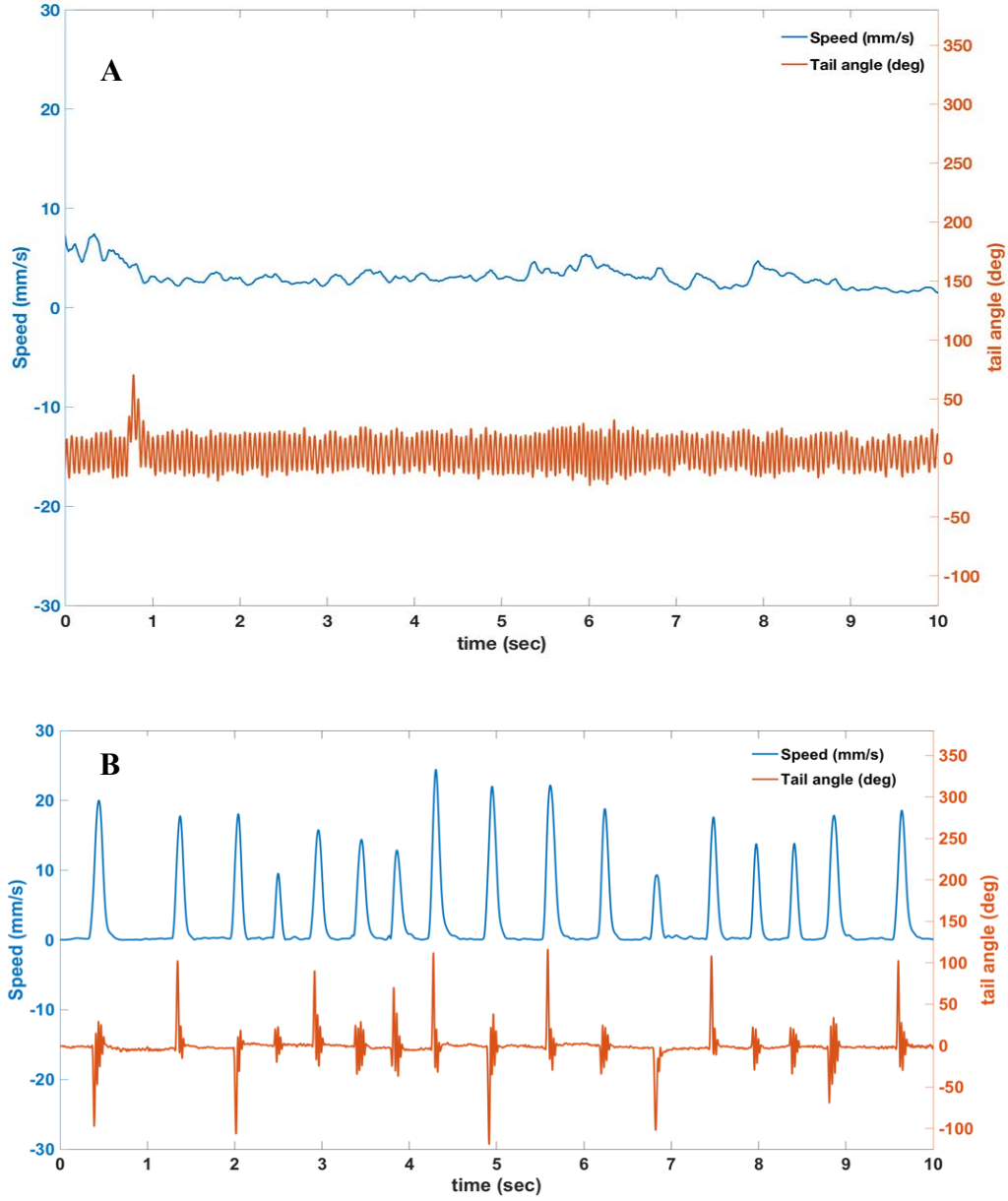

Figure 3.2: Representative swimming pattern of DT and ZF. (A) shows swimming in DT for 10 seconds and (B) shows swimming in ZF for 10 seconds. Both graphs represent translational speed (blue) and tail angle (orange) over time

I used a high speed (700 Hz) imaging system to record spontaneous swimming in fish. The swimming speed of the fish was determined based on the X/Y coordinates of the fish and the tail angle can be considered as the angle of the farthest tail segment from the body with respect to the body axis. Figure 3.2 shows the behavioral difference in a time window of 10 seconds for a representative fish from both the fish species. In Figure 3.2(A), the swimming of DT is illustrated. Here, one can note the continuous activity throughout the 10 s window. In contrast, the swimming in ZF, represented in Figure 3.2(B), is clearly intermittent with longer pauses as compared to the period of activity.

Differences in the kinematics are also readily apparent from the Figure 3.2. However, I will examine these kinematic differences thoroughly in section 3.4.

A drawback of this spontaneous free-swimming assay (described thoroughly in 2.2.1) is that the long continuous stretches of swim events in DT are often split into smaller fragments of tracks by the edges of the arena where background illumination causes a problem with reliable identification and tracking of the fish. This can lead to an underestimation of the length of the swim events in DT.

3.3 Duration of swim events are much longer in DT

To overcome the aforementioned caveat, I used a head-embedded preparation of DT and ZF. This gives the ability to confine the animal with its tail-free to continuously monitor the maximum duration of the swim events. The animal was acclimatized to the recording conditions for >90 minutes. The recordings lasted for 10-20 minutes.

In Figure 3.3 (A) and (B), the difference in the length of swimming is strikingly clear. The black regions indicate swimming, while the white regions indicate the periods of rest. Figure 3.3 (A) represents 4 DT fish which swim for most part of the recording. On the contrary, Figure 3.3 (B) shows 4 ZF which swim in small bursts of activity, interspersed with long pauses. Figure 3.3 (C), quantifies this result. The median percentage of the total time spent swimming by DT is 98.5 % whereas for ZF, it is only at 2%. Additionally, the absolute duration of the swims was found to be very variable for DT, ranging from a minimum of 106 sec to a maximum of 1289

sec (theoretically infinite as 1289 sec was the maximum duration of the acquisition). For ZF, this range was between 460 ms and 938 ms. This is higher than what we see in a free-swimming ZF and this difference is already reported in the literature (Severi et al., 2014).

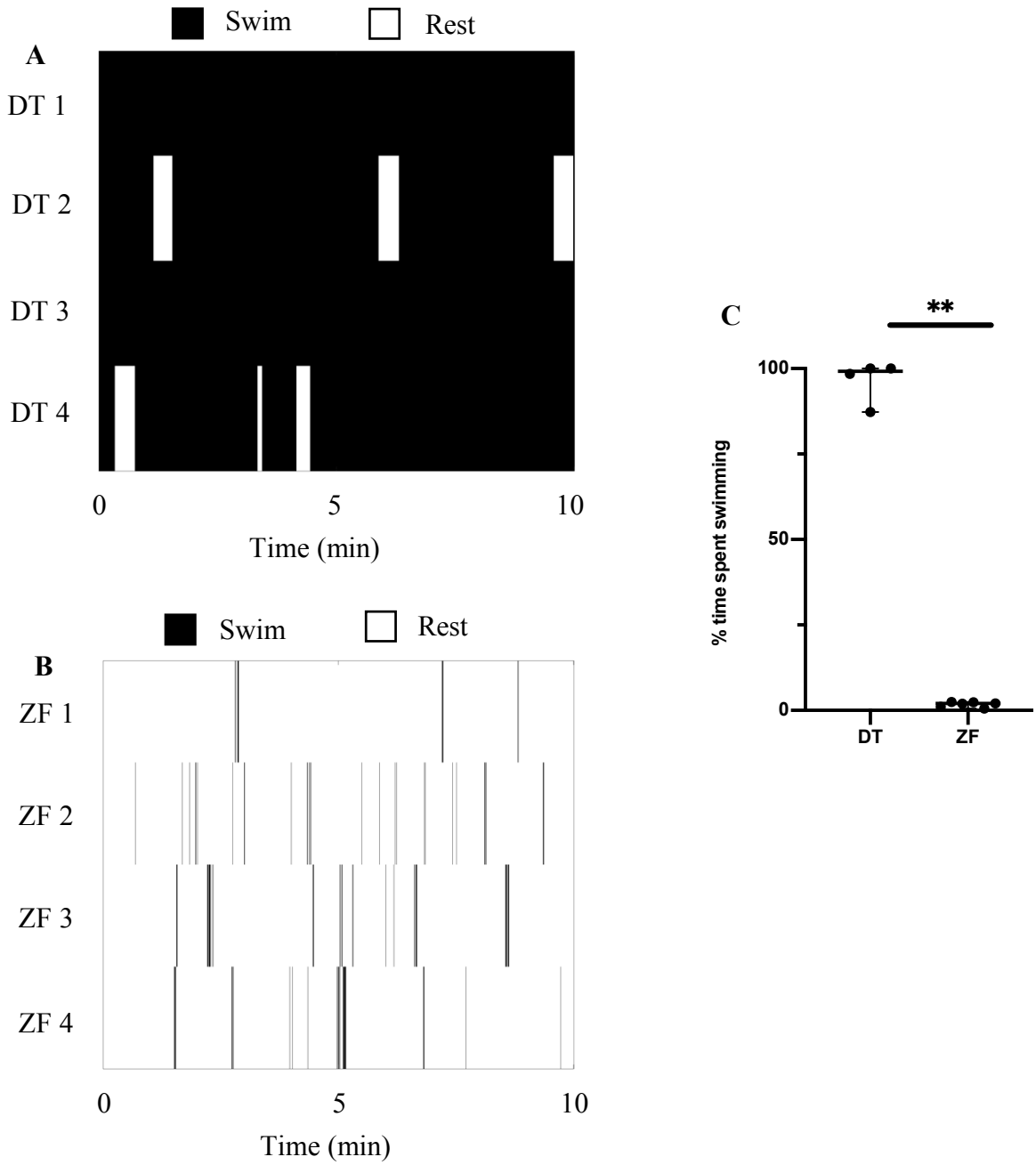

Figure 3.3: Duration of swim events in DT is longer than in ZF. (A) and (B) illustrate the duration of swim periods (sec) in DT and ZF respectively. (C) shows the normalized time spent actively swimming (% of total acquisition time) in ~20 mins long acquisitions (n=5 DT and n= 6 ZF; ** $p<0.01$, Mann-Whitney test).

When I compare the median length of swim events between the two fish species, DT's swim events are more than 1180 folds longer than that of ZF. For DT, this is still an underestimation given that some of the fish swim for the entire duration of the acquisition.

3.4 DT swim slower with a lower half beat frequency and tail angle

Now that we have seen the differences at the macro-level in terms of the global swimming pattern and the duration of swim events, I will examine the finer kinematics of the swimming behavior in the two fish species.

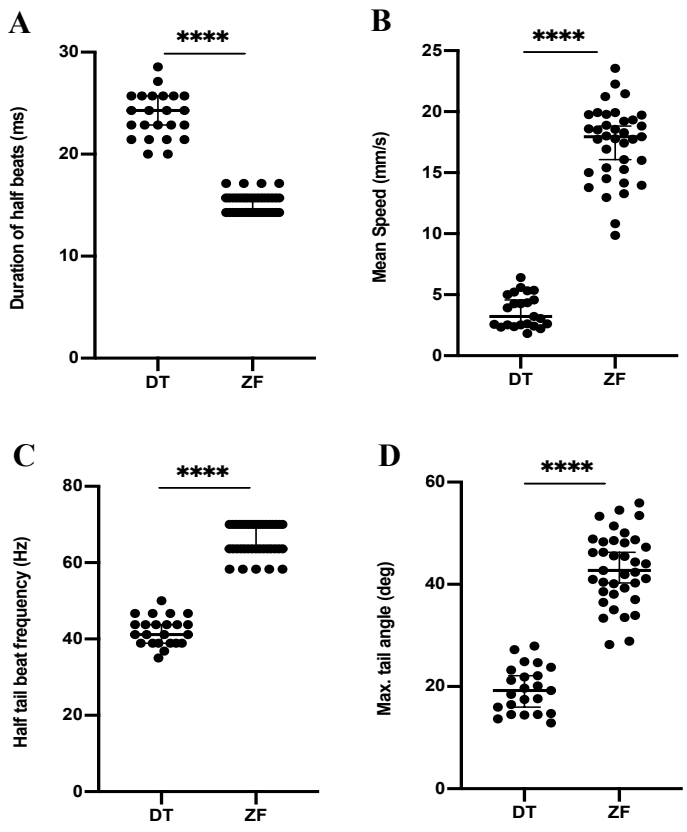

Figure 3.4 : Swimming kinematics of DT and ZF in a spontaneous free-swimming assay. (A) shows the duration of half tail beat (ms). (B) shows the mean speed (mm/s) of half tail beats. (C) represents the half tail beat frequency (Hz) in the two fish species. (D) represents the distribution of maximum tail angles (degree) attained during the half tail beats. (N= 23 DT, n = 494628 half tail beats and N= 37 ZF, n = 202176 half tail beats; **** $p<0.0001$, Mann-Whitney test).

To achieve this, I defined half tail beats using the tail angle signal as described in section 2.2.1 and illustrated in Figure 2.2. Approximately thousands of these half beats per fish were used in the analysis to calculate the kinematic parameters such as duration of half beats (ms), mean instantaneous speed (mm/s), half tail beat frequency (Hz) and maximum tail angle (degree). This is shown below in Figure 3.4.

Figure 3.4 (A) shows that the half beats in DT last for a longer duration, indicating that the half tail beats are executed slower. This will also become apparent in the half tail beat frequency. The median duration of half beats in DT and ZF are 24.29 ms and 15.71 ms respectively. This is the duration of the unit of locomotion over which the kinematic parameters are calculated for each species. The difference in the population median of the mean speed can be seen from Figure 3.4(B): ZF's mean speed is 16.93 mm/s whereas the mean speed of DT is 3.07 mm/s. The frequency of half beats is shown in Figure 3.4(C). In DT, the median half beat frequency is 41.18 Hz and in ZF, it is 63.64 Hz. In terms of tail angle, the maximum tail angle lies at 19.23 degree and 42.73 degree for DT and ZF respectively. This lower half beat frequency combined with lower tail angle in DT would lead to generation of a lower thrust when compared to ZF. In conclusion, the slower swimming observed in DT can be explained by the lower thrust generated by its lower half beat frequency and tail angle.

The above results are based on the half beat analysis, specifically ~460,000 half beats from 23 DT and 190,000 half beats from 37 ZF. It was important to formulate the analysis based on half-beats to be able to work with two comparable units of locomotion. It is important to note that although the half beat based analysis would lead to slightly different kinematic results in ZF when compared to the classical bout-based analysis, this would not change the conclusions in terms of the large differences that I note in the kinematics of DT and ZF. The bout-wise analysis was also performed on the same dataset and is presented in Figure 6.1 in Appendix (Chapter 6).

3.5 DT has lower mean escape velocity than ZF but tends to show a lower latency to achieve peak escape velocity

After analyzing the spontaneous explorative swimming, I looked at the escape response in the two fish to compare their escape kinematics. As the auditory escape response is very conserved among various fish species and is known to follow a very stereotypical pattern in ZF, it was interesting to test how this might differ in DT by virtue of its differing spontaneous swimming pattern. I built a tap-induced escape assay to study this. Briefly, a tap is delivered to the behavioral arena platform when the fish swims in the center region of the arena. The stimulation events are, of course, spaced in time by at least 50 secs to avoid any habituation. The results are summarized in Figure 3.5.

Figure 3.5(A) and (B) show the striking similarity in the escape response between DT and ZF. Both fish species initiate a fast escape response with a C-turn followed by a counter bend. This highly conserved escape response was expected to be similar between the two fish. Based on this, it would also be expected that the underlying neuronal circuitry for escapes comprising of Mauthner cells is also conserved.

However, there are minor differences in the kinematics. The analysis of the kinematics was carried out in a window of 140 ms around the escape maneuver. This window was empirically selected based on exploratory analysis of escape events in both the fish species. I used the time window around peak speed of the escape maneuver which was comparable in the two fish. As can be seen in Figure 3.5(C), DT swims with a lower mean speed and covers a smaller distance during this period compared to ZF. Despite that, the mean escape speed of DT at 30.5 mm/s is as much as a 10-fold increase from its free-swimming speed. In ZF, this increase is only ~3 folds at 42.9 mm/s. This has to be interpreted cautiously though as the free-swimming velocity and escape velocities are not directly comparable since the time windows used for their estimation are very different. DT seems to undergo a larger change in speed during the escape. The distance covered by DT (4.3 mm) is less when compared to ZF (6.0 mm). This alone does not quantify the efficiency of the escape very well though. Another important parameter would have been the variability in the directionality of the escapes but this parameter is not suitable to the tap-induced escape assay being tested here.

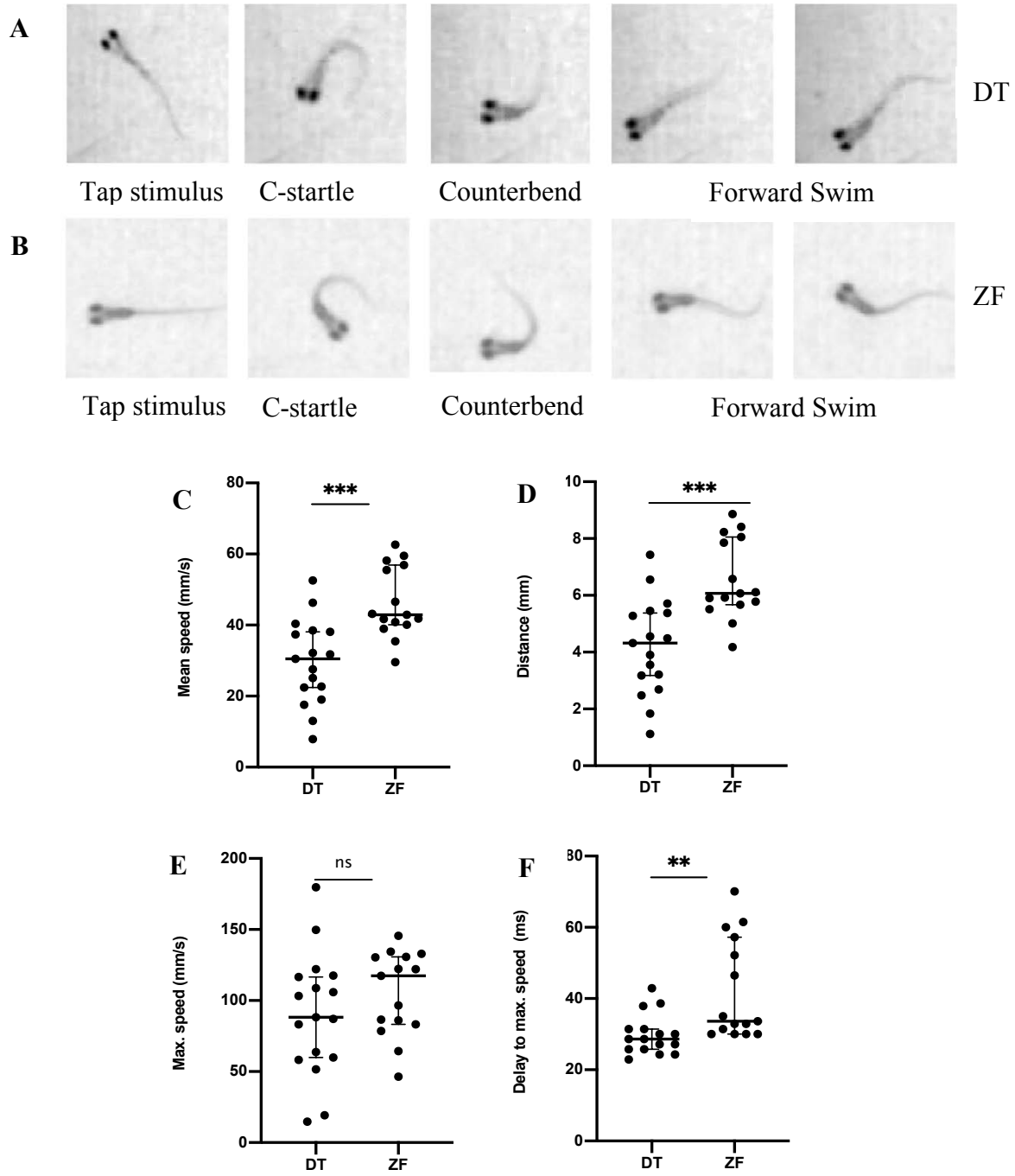

Figure 3.5: Escape response in DT and ZF in a tap-induced escape assay. The kinematics are calculated on a 140 ms window around the escape swim after stimulus delivery. (A) and (B) show the sequence of escape response immediately after the tap stimulus in DT and ZF respectively. The images in the two sequences are ~10 ms apart from each other. (C) represents the mean speed in a 140 ms time window after the tap stimulus. (D) represents the distance travelled in this time period. (E) is the distribution of maximum escape speed (mm/s). (F) is the time delay (ms) to achieve the maximum escape speed. (DT: N=19 fish, n=141 events; ZF: N=15 fish, n=159 events. ** $p<0.01$, *** $p=0.001$, Mann-Whitney test.)

On the other hand, interestingly, both the fishes attain a similar maximum speed during the escape but the delay in achieving the maximum speed is different in the two fish. This delay is surprisingly found to be smaller in DT at 28.6 ms when compared to 33.6 ms in ZF. It can have interesting implications which I will explore in Chapter 5.

3.6 Exploratory swimming in DT has a longer ballistic phase

Mean squared displacement (MSD) can be thought of as a measure of the space explored by a motile agent over a given time. This quantity can help us to get an idea of the extent of spatial spread of an animal's trajectory over time. The MSD obviously depends on the instantaneous speed as examined earlier, but it also depends on the dynamics of reorientation. To quantify the latter, the decorrelation in heading angle (R) was calculated, from which we extracted the time-scale over which the motion of the fish can be considered to be ballistic.

Although ZF's instantaneous velocity is larger than DT as shown in section 3.4, the MSD of both species are comparable over our experimental range as shown in Figure 3.6 (A). This is due to a faster randomization of orientation in ZF compared to DT, as evidenced by the comparison of the heading decorrelation dynamics in Figure 3.6 (B). For ZF, the decorrelation function R(t) decays in about 1 second down to 0.3, then reaches zero in 6-7 seconds. By comparison, for DT, R(t) shows a small initial drop (down to 0.8) then reaches 0 exponentially over ~8 seconds. For DT, this randomization can be understood by describing the fish navigation as a series of straight ballistic periods interspersed by discrete reorientation events, akin to the classical run-and-tumble mechanisms of motile bacteria (Berg & Brown, 1972, Watari & Larson, 2010 and Darnton et al., 2007). The small initial decay can be interpreted as a short time-scale fluctuation in heading direction during run periods. The subsequent slow exponential decay has a decay time of ~6 seconds that corresponds to the mean duration of the straight segments. This slower decay in heading decorrelation of DT is expected to yield a longer ballistic regime compared to ZF. To illustrate this fact, we estimated the ballistic component of the MSD as:

$$MSD_{bal}(t) = \langle \left[\int_{t_0}^{t_0+t} v * R(t' - t_0).dt' \right]^2 \rangle_{t_0}$$

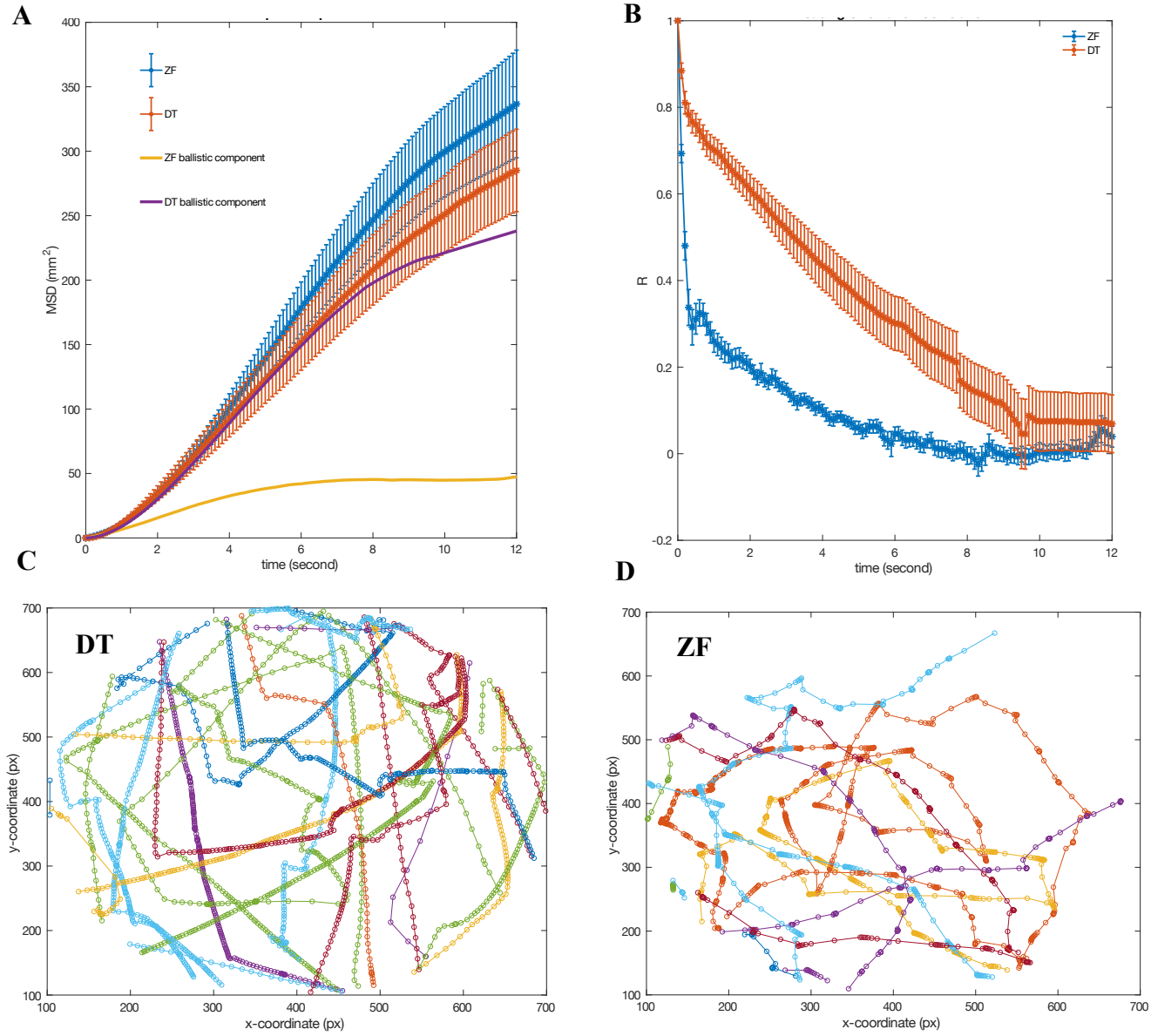

Figure 3.6: Exploratory swimming in DT has a longer ballistic phase. (A) Mean squared displacement (MSD) in DT and ZF over time. The MSD over time for the ballistic component of DT and ZF is also overlapped on the plot. The ballistic component of the MSD was estimated as: $\boldsymbol{MSD_{bal}(t)} = \langle\left[\int_{t_0}^{t_0+t} \boldsymbol{v} * \boldsymbol{R}(t' - t_0).\, dt'\right]^2\rangle_{t_0}$. (B) shows the change in heading persistence over time. At R=1, the animal is moving in a straight trajectory and at R=0, it is completely random. (C) and (D) represent a few tens of trajectories (each trajectory with a different color) picked from a single DT and ZF respectively to visualize the heading decorrelation result on actual trajectories of DT. This illustrates the more frequent reorientation in zebrafish when compared to a longer ballistic regime in DT.

As shown in Figure 3.6 (A), for DT, this quantity correctly captures the MSD of the ballistic regime up to ~6 seconds. In contrast, for ZF, the MSD departs from the ballistic component from 1 second (or approximately 2 bouts) onwards, indicating that beyond this threshold the diffusive component becomes dominant. Figure 3.6 (C) and (D) represent a few continuous trajectories of a DT and ZF to provide a visual representation of the longer ballistic regime in the swimming of DT.

In conclusion, although ZF is significantly faster at short-time scales, the longer ballistic regime of DT leads to a comparable exploratory kinematics at long time-scale (beyond 10 seconds).

3.7 The continuous swimming in DT can be divided into at least two types, slow and fast swims

In ZF, the swimming is broadly composed of two types of swim bouts, slow swims and faster burst swims, as highlighted in Budick & O'Malley, 2000. In DT, on the other hand, the fish is able to continuously modulate its swimming speed. This is illustrated in Figure 3.7 (A) where a swim track of DT is color-coded with its normalized speed. Stretches of slow and fast swims can be observed in a single continuous swim event.

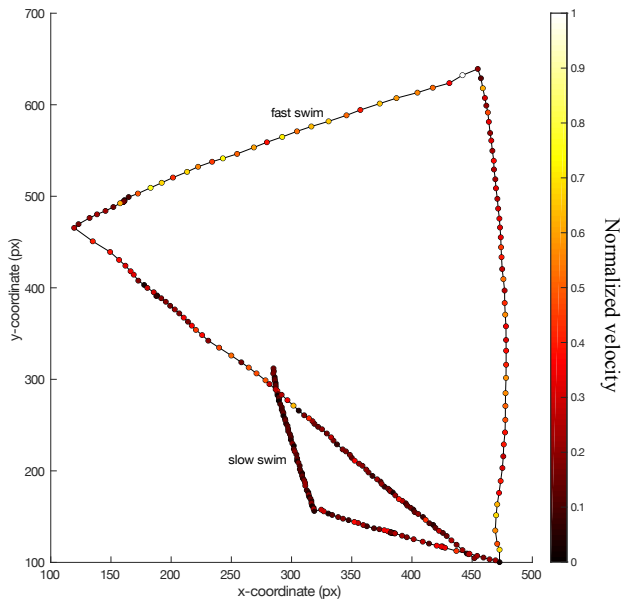

Figure 3.7: Slow and fast swims in DT. A ~25s long trajectory of a DT representing a slow and fast track of swimming. Each step is 100 ms apart.

All the earlier kinematic analysis was performed on half tail beats. Given this slow and fast swims that I observe at a macro time scale, I performed a simple K-means clustering on the half tail beats to evaluate if the half tail beats can be divided into sub-types which might underlie the slow and fast swim types noted in Figure 3.7 and if so, which parameters would best explain the slow and fast swims.

A K-means clustering performed on 200,000 half beats from 14 DT using mean speed, half beat frequency and tail angle as predictors identified two clusters. The number of clusters was not forced, instead a range of clusters from 2 to 5 were tested. K=2 clusters performed the best clustering based on a silhouette coefficient of >0.5. The silhouette coefficient gives a measure between -1 and 1 and indicates the similarity between the points of the same cluster by measuring how close the points of a given cluster lie when compared to their distance to the points in the other clusters. A higher silhouette value indicates a better clustering. The clustering is shown in Figure 3.8 (A).

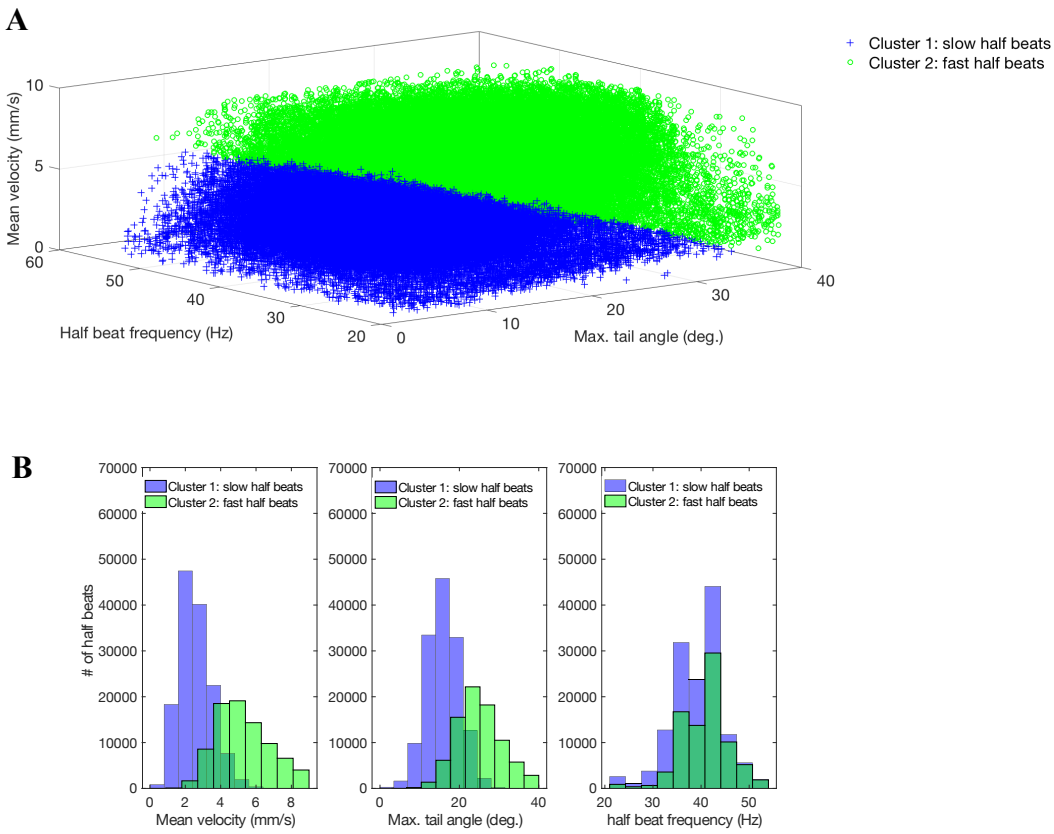

Figure 3.8: Slow and fast half beats in DT. (A) shows a clustering of half beats into slow and fast type based on three predictors, mean velocity, half-beat frequency and max. tail angle (200,000 half beats from 14 DT). (B) shows the distribution of these three predictors in the fast and slow beats clusters.

The distribution of the kinematics of half beats in the two clusters are plotted in Figure 3.7 (B). The tail angle and mean velocity appear to be the strongest predictors of the clusters; while tail beat frequency is also significantly different in the two groups. Based on the kinematics of the two clusters, they can be labeled as slow half beats and fast half beats. Based on Figures 3.7 and 3.8, it appears that the half beats of a certain type would be used for a period of time before switching over to another type to modulate the swim speed. This opens up another exciting opportunity in DT to investigate the neuronal circuit mechanisms controlling the continuous modulation of swimming speed.

3.8 DT's instantaneous energy requirement during activity appears lower than ZF

A natural question that arises from an organismal and evolutionary perspective is: why would such different swimming patterns emerge in two closely related organisms? This can be evaluated from at least two aspects: 1) Whether one of the swimming patterns is energetically more efficient? 2) What selective forces would have led to the divergence in the swimming patterns?

With the mechanistic understanding of the swimming patterns that we have developed in the previous sections, I can now try to address these questions. I will focus on the energetics in this section and look at plausible selective forces in the next section.

Many studies in different fish species have looked at the relationship between swimming speed and oxygen consumption. Classically, this has been studied in trouts (Webb, 1971). More recently, Bagatto et al., 2001 have obtained such a relationship for a 3-week old ZF larvae:

$$\text{Log } C = 2.103 + 0.309 \times V$$

where C is a measure of oxygen consumed per mg of the animal per hour and V is the speed. It is important to note that the oxygen consumption is used as a proxy for energy consumption and hence, any role of anaerobic metabolism is ignored. An advantage, again, of working with

two similar larvae during the same stage of development is that I can approximate their baseline metabolic demands to be similar. This lets us directly compare the energy consumption of the two larvae.

From Figure 3.9, it is clear that during activity DT expends less energy based on its lower instantaneous speed. It is to be noted that the average swimming speed of the two fish species over long time-range can be similar as shown in Figure 6.2 in Chapter 6. In such a case, the global energy expenditure during swimming might be comparable in the two fish species. In conclusion, the instantaneous energy requirement in DT would be clearly low during activity. However, based on the difference in the spontaneous swimming pattern between DT and ZF, the energy requirement over larger time-scale tends to be more similar.

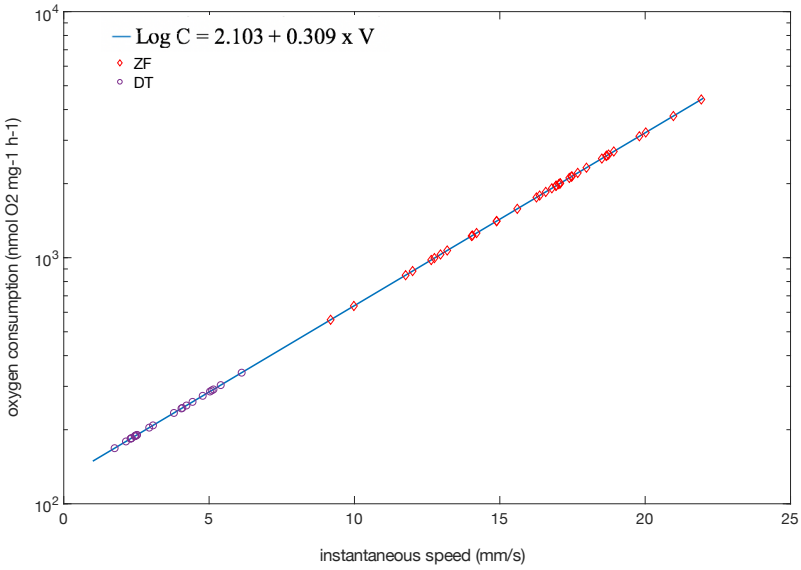

Figure 3.9: Oxygen consumption in DT and ZF. Instantaneous oxygen consumption of the animals estimated using instantaneous speeds. Log C = 2.103 + 0.309 x V, where C is a measure of oxygen consumed per mg of the animal per hour and V is the speed (Bagatto et al., 2001).

3.9 A lower oxygen availability and delayed swim bladder inflation might have contributed to the differences in swimming style at the micro scale

A pertinent question is what selective forces, physiological or environmental if any, would have led to the differing pattern of swimming at the smaller time-scale. Considering the generation time of the animal models used in the study, these are not best suited for an experimental evolution approach unlike prokaryotic and some unicellular eukaryotic models, so my proposals are based on quantitative empirical evidence as described below.

Fish were tested in a long column (36 cm) of water for their preference of depth. For analysis, the column was divided into three zones - upper, middle and lower. As can be seen in Figure 3.10, larval DT show a preference for the bottom of the water column and larval ZF prefer the top zone of the water column. Upper layers of a water column are richer in dissolved oxygen (DO) when compared to the bottom layers (Boehrer & Schultze, 2008 and Davis, 1975). Hence, the difference in depth preference of the fish would result in a difference in availability of DO for the fish. Moreover, DT is found in waters which can be as deep as 1m (Roberts, 1986).

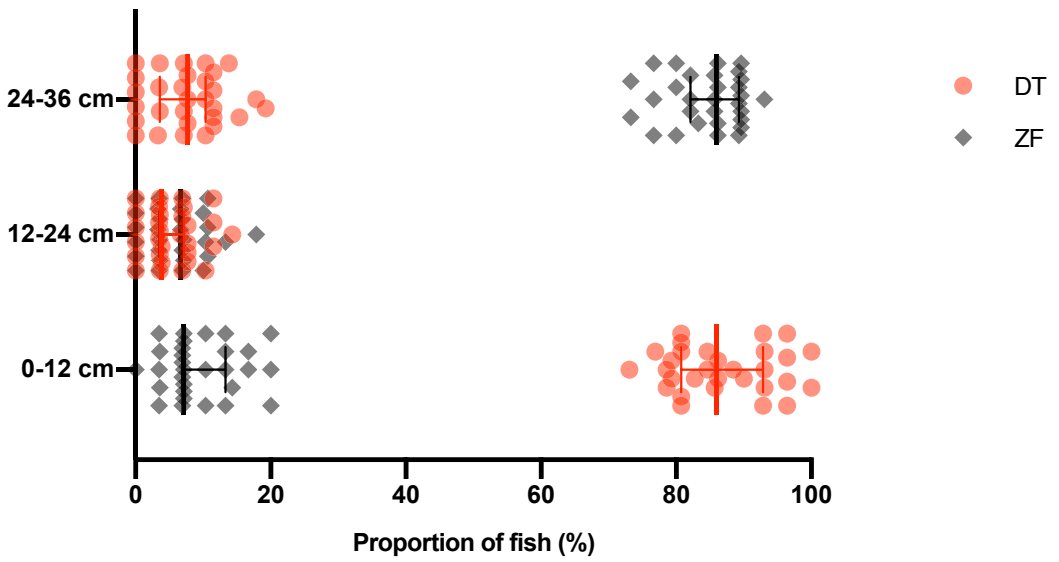

Figure 3.10: Depth preference in DT and ZF. DT larvae prefer the bottom of the water column whereas ZF larvae prefer the top. (N= ~30 ZF; n = 10 readings) x 3 replicates and (N = ~30 DT; n=10 readings) x 3 replicates.

A lower availability of oxygen (from depth preference shown in Figure 3.10) would prevent the animal from executing high speed swims which would demand a higher consumption of oxygen as shown earlier in Figure 3.9. This will favor a slow swimming. Further to energetically optimize for displacement, a slow swimmer would have to swim for a longer duration. Also, a continuous movement would allow the animal to replenish the DO in its surrounding by either displacing itself to a new location or by locally mixing the DO in its immediate surrounding with motion (Weihs, 1980). I will discuss this in more detail in Chapter 5.

Another observation of plausible consequence is the delayed inflation of swim bladder in DT. A complete inflation of swim bladder in DT has been observed at ~15 dpf as shown in Figure 3.11.

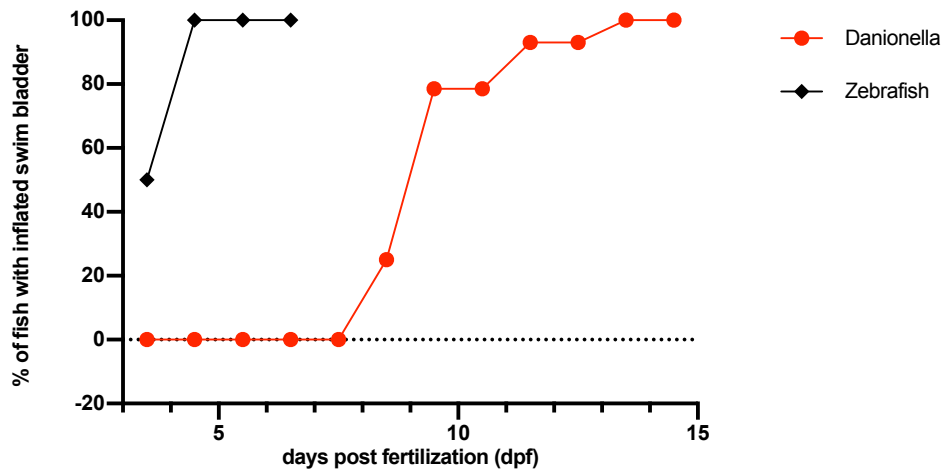

Figure 3.11: Swim bladder inflation in ZF occurs earlier than in DT. A complete inflation of swim bladder in ZF occurs at ~ 4dpf whereas the DT population undergoes a complete inflation of its swim bladder at around 15 dpf. N = 10 DT and 9 ZF.

In ZF, the inflation of swim bladder already occurs at ~4dpf, which is around the same time (~5dpf) when the animal has to start actively feeding as the yolk is used up. The yolk disappears at ~4 dpf in DT as well but the swim bladder inflation is delayed. It would imply that DT has to actively swim without a swim bladder and explore its environment to be able to feed and survive. A fish without swim bladder would have to exert a continuous downward force which is estimated to be 5-8% of its body weight in air to be able to maintain its position in water

column and this is readily seen in mackerels which have to swim vigorously to maintain their level in the water (Denton & Marshall, 1958).

However, it is important to note that the delayed inflation of swim bladder alone would not explain the difference in swimming. A small population of 15 dpf DT larvae with inflated swim bladder were also tested. This is shown in Figure 6.3 (A) and (B) in Appendix (Chapter 6). Although, a decrease is seen in the proportion of time spent swimming (Figure 6.3 A), it is still continuous swimming with long swim events (Figure 6.3 B) and very different from the burst-and-glide swims of ZF. This would suggest that the resultant swimming pattern of DT may be a result of a combination of a few factors which likely include lower availability of DO and delayed inflation of swim bladder.

† Chapters 3 and 4 are compiled together as a manuscript for a peer-reviewed publication (see annex #3).

Chapter 4

Anatomy and physiology underlying locomotion in *Danionella translucida* and *Danio rerio*

"Anatomy is to physiology as geography is to history; it describes the theatre of events."
— Jean Fernel

"It is this potential for plasticity of the relatively stereotyped units of the nervous system that endows each of us with our individuality." — Eric Kandel, Principles of Neural Science

With the understanding of the swimming behavior that we have developed in Chapter 3, we will now explore the anatomy and physiology underlying the swimming behavior in DT and ZF. Briefly, the objectives of the chapter are to:

- Visualize distribution of major excitatory (glutamatergic) and inhibitory (glycinergic and GABAergic) neurons in the hindbrain.

- Visualize reticulospinal (RS) neurons in the brainstem which project to the spinal cord.

- Create a transgenic DT with a near pan-neuronal expression of genetically encoded calcium indicator (GECI) to be able to carry out whole-brain calcium imaging.

- Identify neurons correlated with swimming.

- Resolve swimming correlated neurons into onset, maintenance and offset neurons in DT.

4.1 Anatomy

4.1.1. Distribution of glutamatergic, glycinergic and GABAergic neurons in the hindbrain of DT

Determining the anatomy was the first step to understand the cellular underpinnings of the change in swimming. I first looked at the distribution of excitatory (glutamatergic) and inhibitory (glycinergic and GABAergic) neurons in the hindbrain as this has been already well characterized in the ZF brain. For labelling glutamatergic and glycinergic cells, I used *in-situ* hybridization and for GABAergic cells, immunohistochemistry was used.

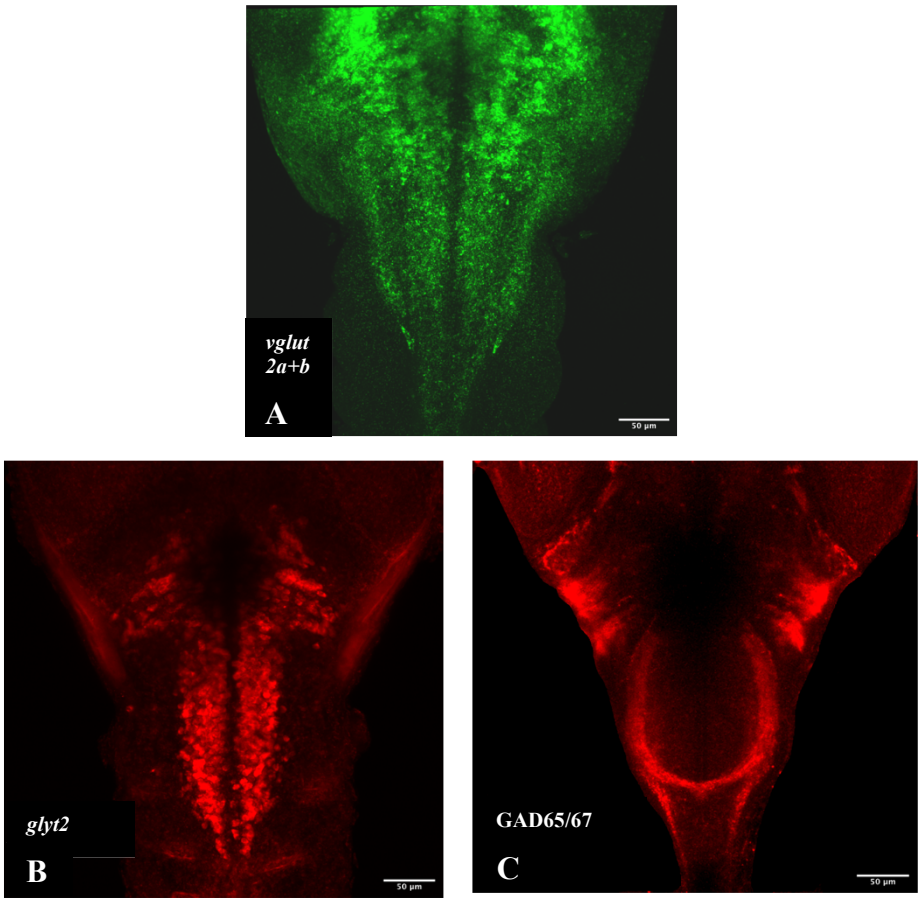

Figure 4.1: Distribution of (A) glutamatergic (B) glycinergic and (C) GABAergic neurons in the hindbrain of DT using *in-situ* hybridization (ISH) and immunohistochemistry (IHC). Anti-*vglut2a* + -*vglut2b* ISH and anti-*glyt2* ISH in (A) and (B) respectively. Anti-GAD65/67 IHC in (C). All images are a maximum intensity projection. Scale bar is 50 µm.

As can be seen from Figure 4.1, the distribution of the excitatory and inhibitory neurons forms roustro-caudally running stripes in the hindbrain. This has been reported widely in ZF and is represented in Figure 6.5.

There are developmental and functional implications of this patterned distribution which will be discussed in Chapter 5. The conserved pattern in DT indicates that these developmental and functional consequences might also be conserved in the two species. In addition, an anti-GFP immunohistochemistry against GCaMP6s was carried out in *Tg(HuC:H2B-GCaMP6s)* fish along with the aforementioned *in-situ* hybridization/ immunohistochemistry. The results of this are represented in Figure 6.6 and can be useful to identify cell type of the identified cell population from whole brain imaging of *Tg(HuC:H2B-GCaMP6s)* DT.

4.1.2. Reticulospinal (RS) neurons in DT and ZF

After characterizing the global architecture of hindbrain in terms of distribution of excitatory and inhibitory neurons, next I looked at the distribution of reticulospinal (RS) neurons. Since the RS neurons project directly from the brainstem to the spinal cord, as command neurons, they are good candidates for controlling the pattern of locomotion.

To visualize these neurons, I carried out backfill experiments using Texas Red in DT and ZF. Figure 4.2 shows the labelling of reticulospinal (RS) neurons in DT. In both DT and ZF, a similar experimental protocol was used to label the RS neurons to be able to directly compare them. A representative example is shown in Figure 4.3.

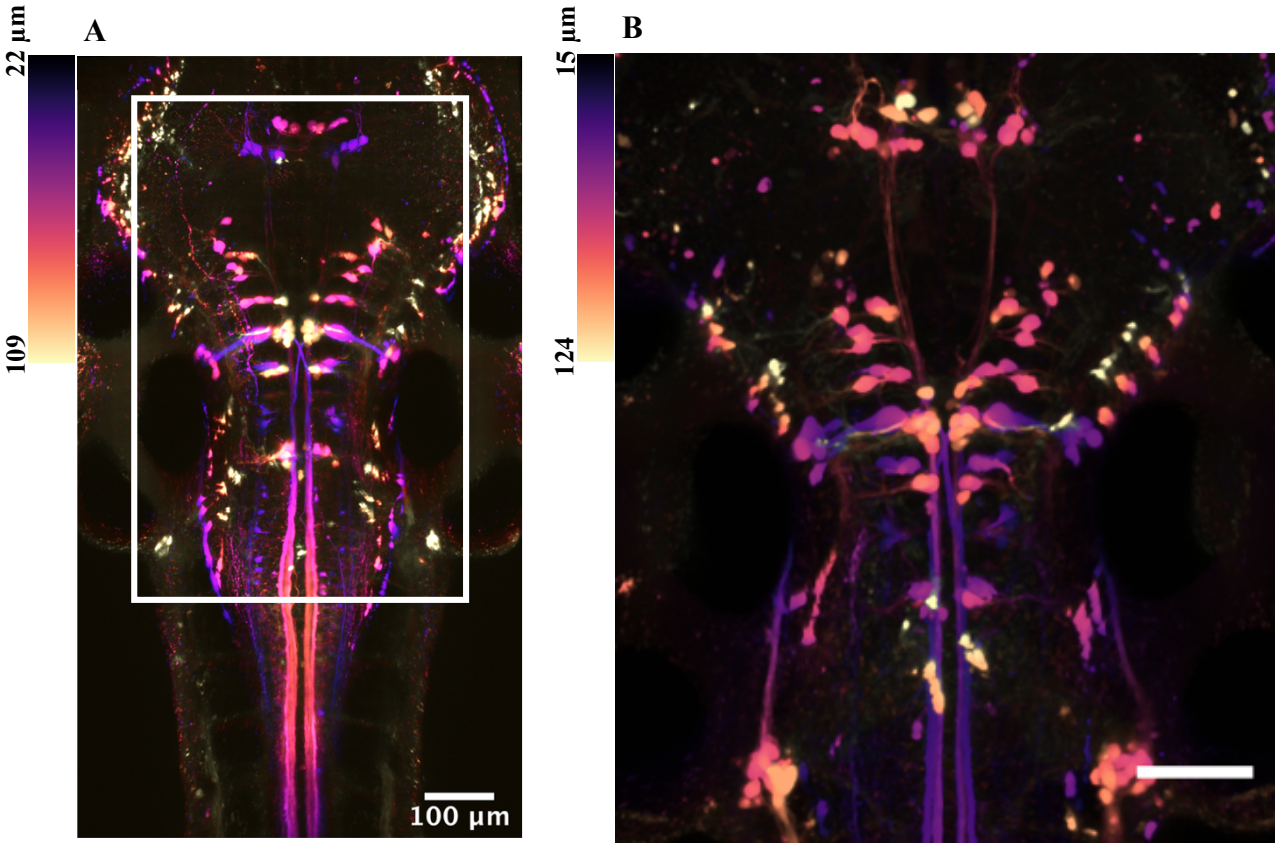

Figure 4.2: Distribution of reticulospinal (RS) neurons in the brainstem of DT. (A) The distribution of RS neurons in a DT fish. (B) a closer look at the ROI from (A) in another DT fish. Scale bar is 100 µm. Maximum intensity is color coded for the depth.

I could identify cells of the mesencephalic nucleus of the medial longitudinal fascicle (nucMLF/nMLF), the rhombocephalic reticular formation (nucRE) and the rhombocephalic vestibular nucleus (nucVE) that are described in ZF. Specifically, the various cells from the rostral (RoL, RoM, RoV), middle (Mauthner neuron, MiR, MiM, MiV, MiD) and caudal (CaD, CaV) RE nucleus were identified. In the nMLF, MeM and MeL cells were identified. Dendrites crossing the midline from MeM cells were identified in DT as described in ZF earlier (Figure 4.3B). The annotations are based on the cell descriptions in ZF (Kimmel et al., 1982 and Orger et al., 2008).

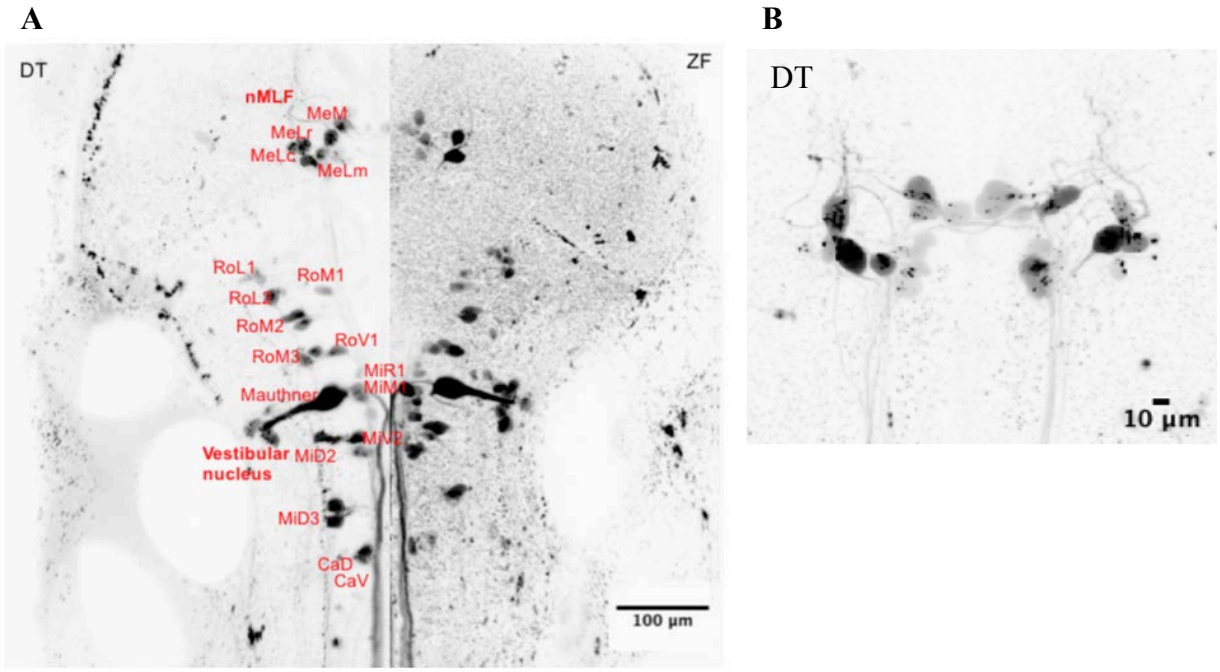

Figure 4.3: Comparison of reticulospinal (RS) neurons in DT and ZF. (A) A cell-to-cell comparison of RS neurons in a maximum intensity projection of RS neurons in DT and ZF. The RS neurons in DT are annotated based on the description of RS neurons in ZF as described in Kimmel et al., 1982 and Orger et al., 2008. (B) A closer look at the nucleus of the medial longitudinal fasciculus (nMLF) in another DT fish showing maximum intensity projection.

4.2 Physiology

4.2.1 Generation of pan-neuronal *Tg(HuC:H2B-GCaMP6s)* DT fish and whole-brain imaging

To identify functionally relevant nuclei in the brain corresponding to swimming activity, I created a transgenic line, *Tg(HuC:H2B-GCaMP6s)* expressing a near pan-neuronal nuclear-localized GCaMP6s indicator. It is shown in Figure 4.4. A comparison with an equivalent transgenic in ZF is shown. The expression of the indicator was found to be stable at 21 dpf DT.

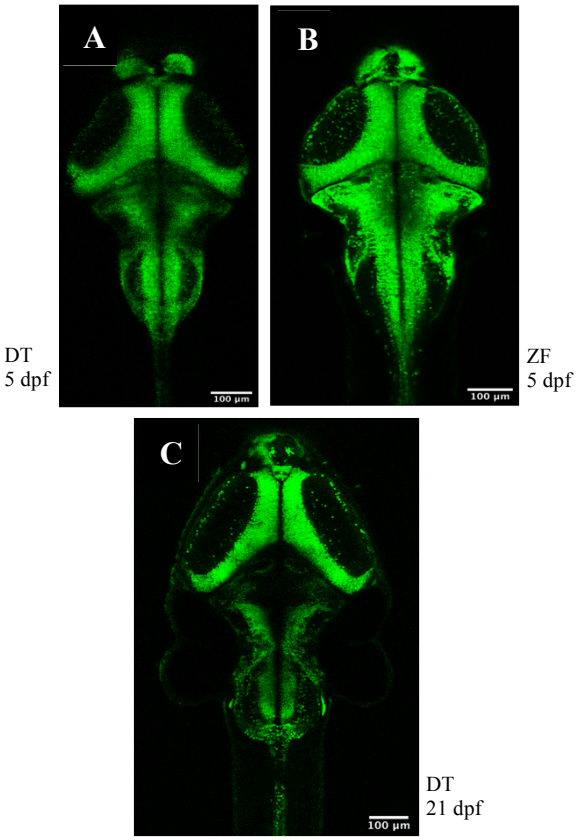

Figure 4.4: Tg(HuC:H2B-GCaMP6s) fish in DT and ZF. (A) A maximum intensity projection of 5dpf *Tg(HuC:H2B-GCaMP6s)* DT fish. (B) A maximum intensity projection of 5 dpf *Tg(HuC:H2B-GCaMP6s)* fish. (C) A maximum intensity projection of 21 dpf *Tg(HuC:H2B-GCaMP6s)* DT fish. Scale bar is 100 µm.

For the whole-brain imaging experiments, I used 5dpf DT and ZF and acquired a brain volume of ~200 µm at ~1 Hz while the tail of the fish was freed to record the swimming movements simultaneously. Few of the layers of brain acquisition in DT is represented in Figure 4.5.

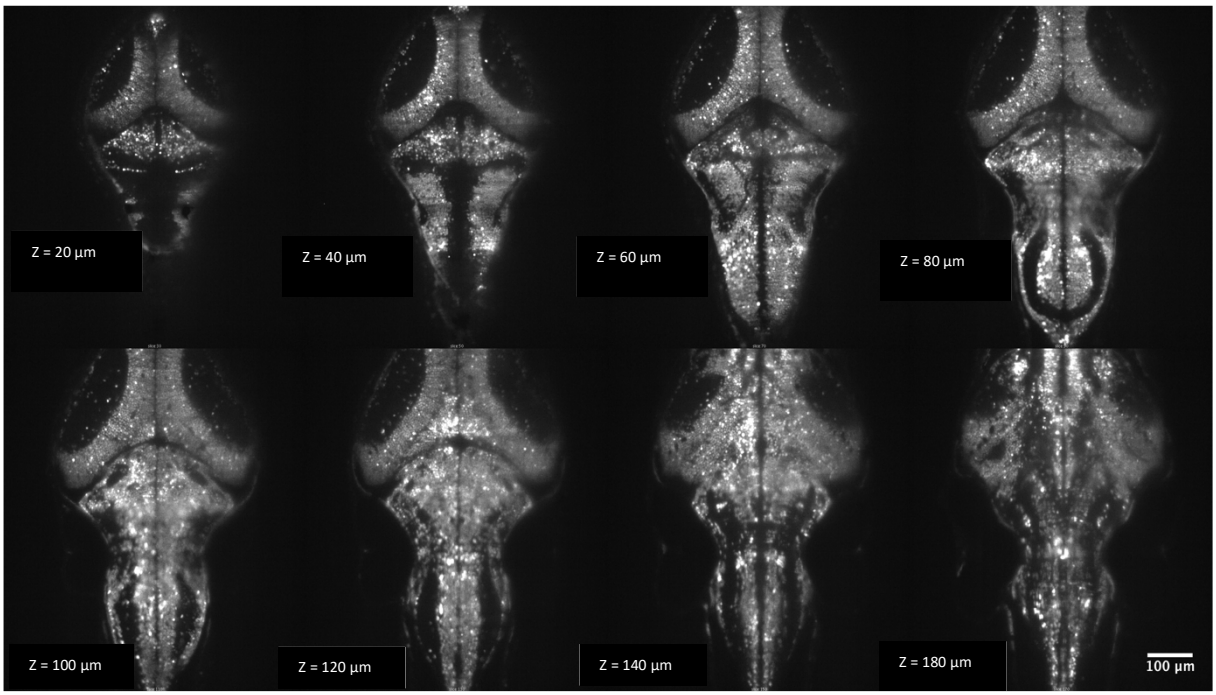

Figure 4.5: Whole brain imaging using light sheet microscopy. A 5dpf DT brain at various depths represented by Z (0 µm being most dorsal). Approximately 200 µm of brain (in 8 µm steps) in DT and ZF was acquired at 1 Hz during simultaneous recording of tail activity to identify and compare the activity of neuronal correlates of locomotion in the two species. Scale bar is 100 µm.

4.2.2 Similar brain nuclei are correlated with swimming in DT and ZF

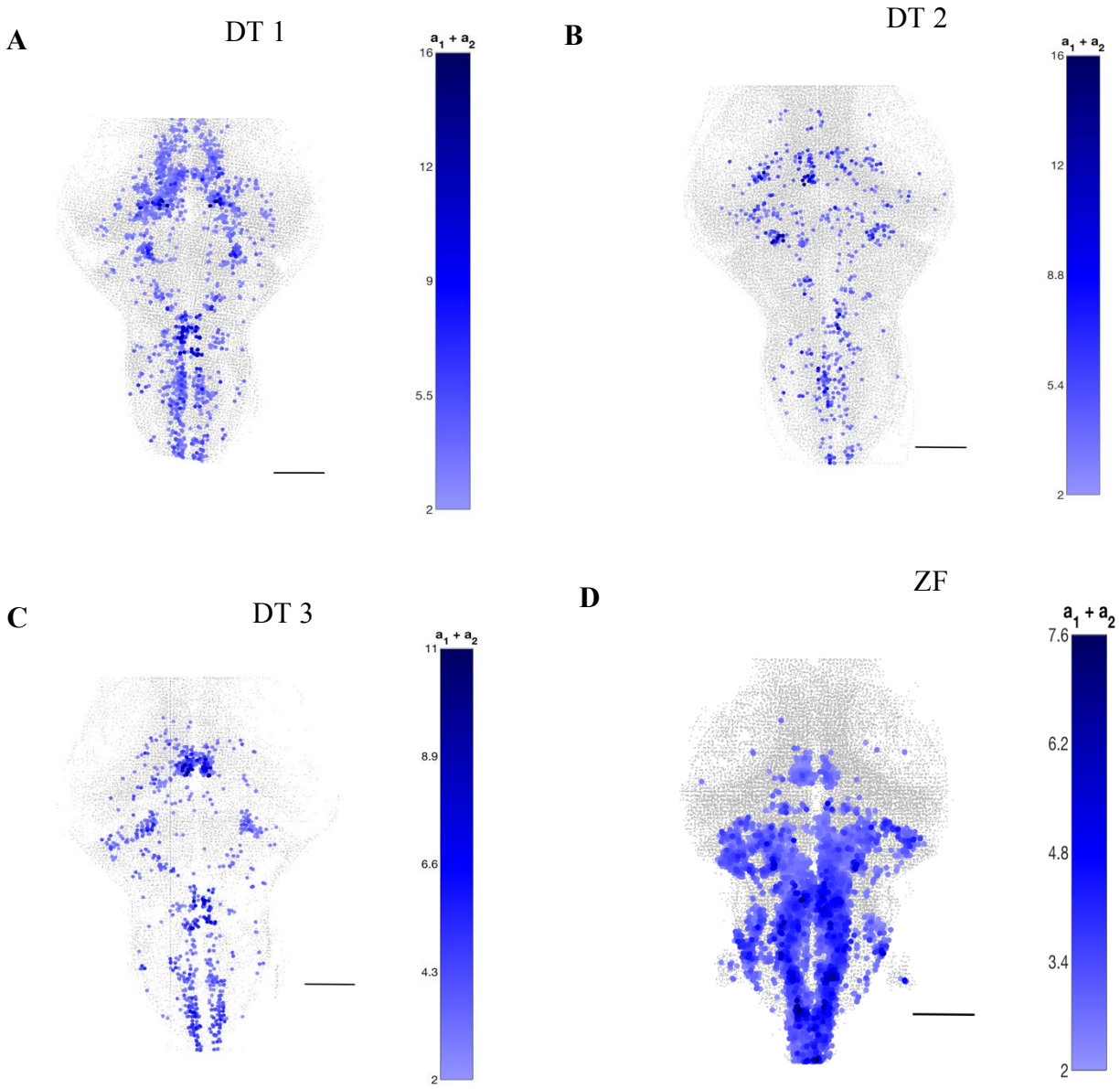

Figure 4.6: Neuronal correlates of swimming in DT and ZF. (A), (B) and (C) show neuronal correlates of swimming in three different DT. (D) shows a representative figure of neuronal correlates of swimming in ZF. More examples of ZF brains and another DT brain is in Figure 6.7. Highly correlated neurons of DT are color-coded according to their identification confidence based on the regression coefficient (a_1) and t-score (a_2). See Figure 6.8 (A) for an example of the selection process. The nuclei correlated with swimming are located in the medial mid-brain, lateral midbrain and the hindbrain, and are conserved in DT and ZF. N=3 DT; n=34 swim events. Scale bar is 100 µm.

The foremost goal of this analysis was to identify the supraspinal centers of locomotion in the brain and to compare their activity between the two species. The whole brain acquisitions were segmented into thousands of regions of interest (ROIs) representing individual neurons. The behavior of the fish was extracted from the tail acquisitions and converted into a binary on/off signal. A regression analysis was performed between the neuronal fluorescence signal and the regressors representing the swim events, and their onset and offset. Firstly, we will look at the analysis based on the swim regressor. A set of nuclei were obtained in DT and ZF brains that were highly correlated with the swimming behavior – these neurons will be referred to as swim neurons or swim "maintenance" neurons. The distribution of the nuclei in the medial mid-brain, lateral mid-brain and hindbrain is very conserved between the two species. This is shown in Figure 4.6. More representative brains for ZF/DT are shown in Figure 6.7. An illustration on the methodology for selecting swim cells with a confidence value (a_1+a_2) is shown in Figure 6.8 (A).

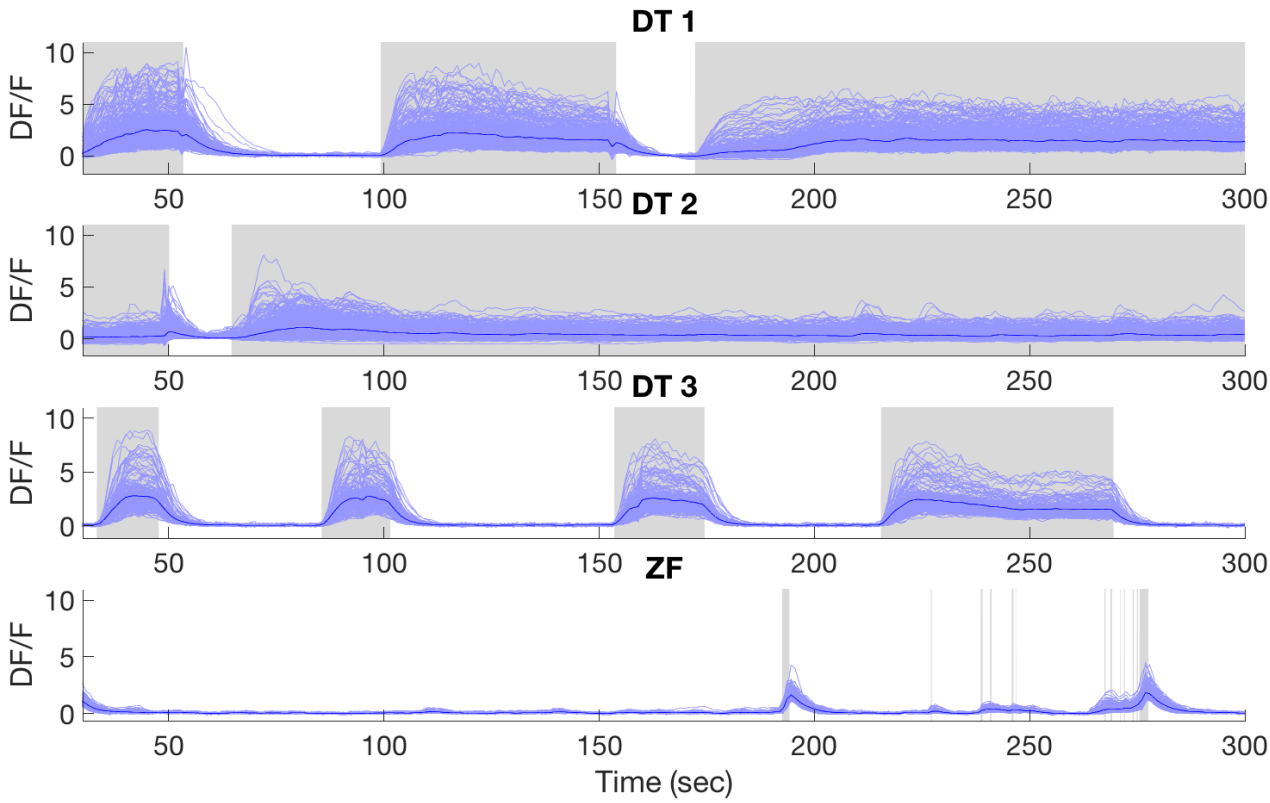

Figure 4.7: Activity of neuronal correlates of swimming temporally scale with the long swim events of DT. Neuronal activity of swim maintenance neurons in three DT compared to their activity in ZF for a duration of 300 secs. The activity of the conserved nuclei in DT is sustained for long durations, scaling with their long swim events. The grey shaded regions represent active swimming. N= 3 DT and 1 ZF.

In Figure 4.7, the mean neuronal activity of the identified neurons is plotted with swim events (in grey). As can be seen in the figure, the activity in these identified nuclei scale with the long swim events of DT. This points to a role of these nuclei in the maintenance of the long swim events.

4.2.3 Neurons in the identified nuclei of DT constitute a functionally heterogenous population

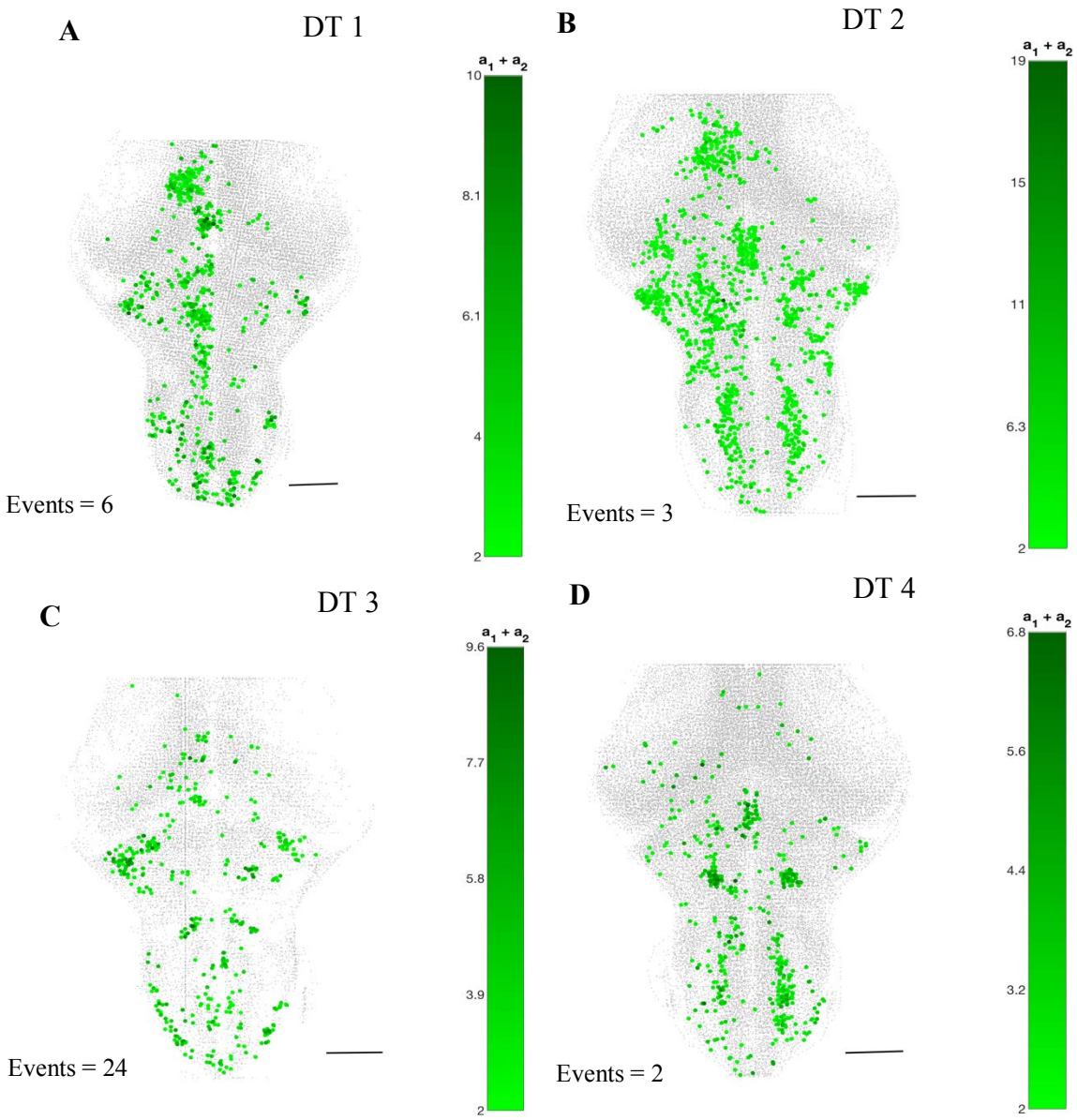

Figure 4.8: Neuronal correlates of swimming onset in DT. (A), (B), (C) and (D) show neuronal correlates of swimming onset in four different DT brains. Highly correlated neurons of DT are color-coded according to their identification confidence based on the regression coefficient (a_1) and t-score (a_2). The swim maintenance and onset

neurons seem to be heterogeneously distributed in the various nuclei located in the medial mid-brain, lateral midbrain and hindbrain of DT. N=4 DT; n= 35 onset events. Scale bar is 100 µm.

In addition to identifying the swimming maintenance neurons as shown above, I can dissect the neuronal population into functionally distinct sub-types such as swimming onset or offset based on whether they are active during the initiation or termination of swimming. Using GECIs, this analysis cannot be directly done on ZF at a brain-wide scale, given the short swim events and the slow kinetics of the calcium indicator.

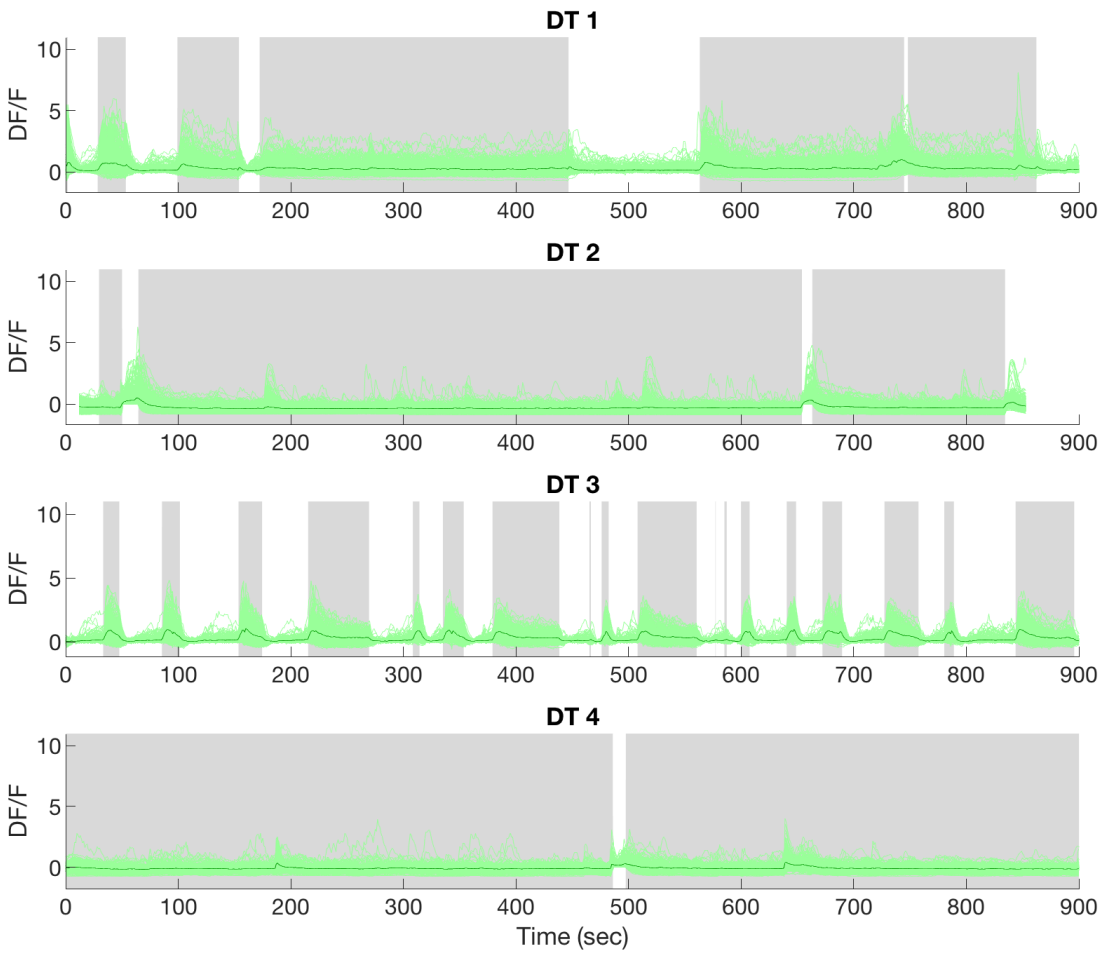

Figure 4.9: Neuronal activity of onset neurons. Neuronal activity of onset neurons in DT during 900 secs of acquisition. An increase in mean activity is observed during the initiation of a swim event. The grey shaded regions represent active swimming. N=4 DT.

Taking advantage of this, we first identified neurons active during the onset of swim events. Figure 4.8 shows the distribution of the identified "onset" neurons. It appears to be

heterogeneously distributed among the nuclei earlier identified for swim maintenance. Figure 4.9 shows the mean neuronal activity of onset neurons against swimming events (in grey). As can be seen, the onset neurons reliably peak in their activity during the initial phase of the swimming. However, the activity does not die down to baseline immediately, but follows the swimming event until the end. This will be explored in a later section.

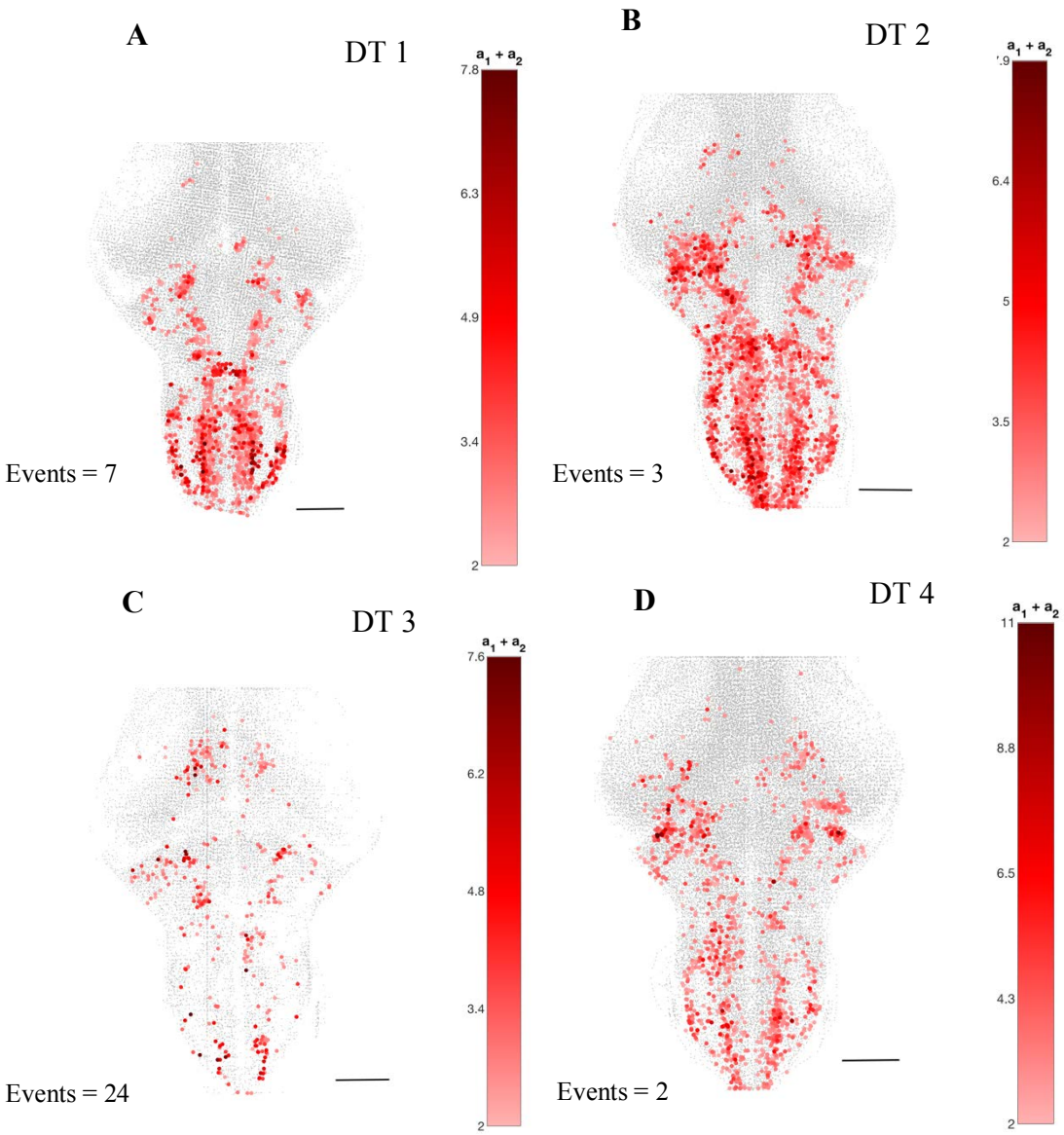

Figure 4.10: Neuronal correlates of swimming offset in DT. (A), (B), (C) and (D) show neuronal correlates of swimming offset in four different DT brains. Highly correlated neurons of DT are color-coded according to the identification confidence based on the regression coefficient (a_1) and t-score (a_2). The highly correlated swim offset neurons are mostly located in the hindbrain and lateral mid-brain of DT. N=4 DT; n= 36 offset events. Scale bar is 100 µm.

Next, we looked for offset neurons which would be active at the termination of swim events. While such neurons are reported in lamprey and mice, they are not yet reported in ZF. The result of the regression analysis is shown in Figure 4.10 as DT brain maps. The "offset" neurons seem to be majorly distributed in the hindbrain and lateral midbrain. The mean neuronal activity of the identified offset neurons is plotted in Figure 4.11. The neurons are seen to reliably fire at the termination of swimming in the majority of the swim events.

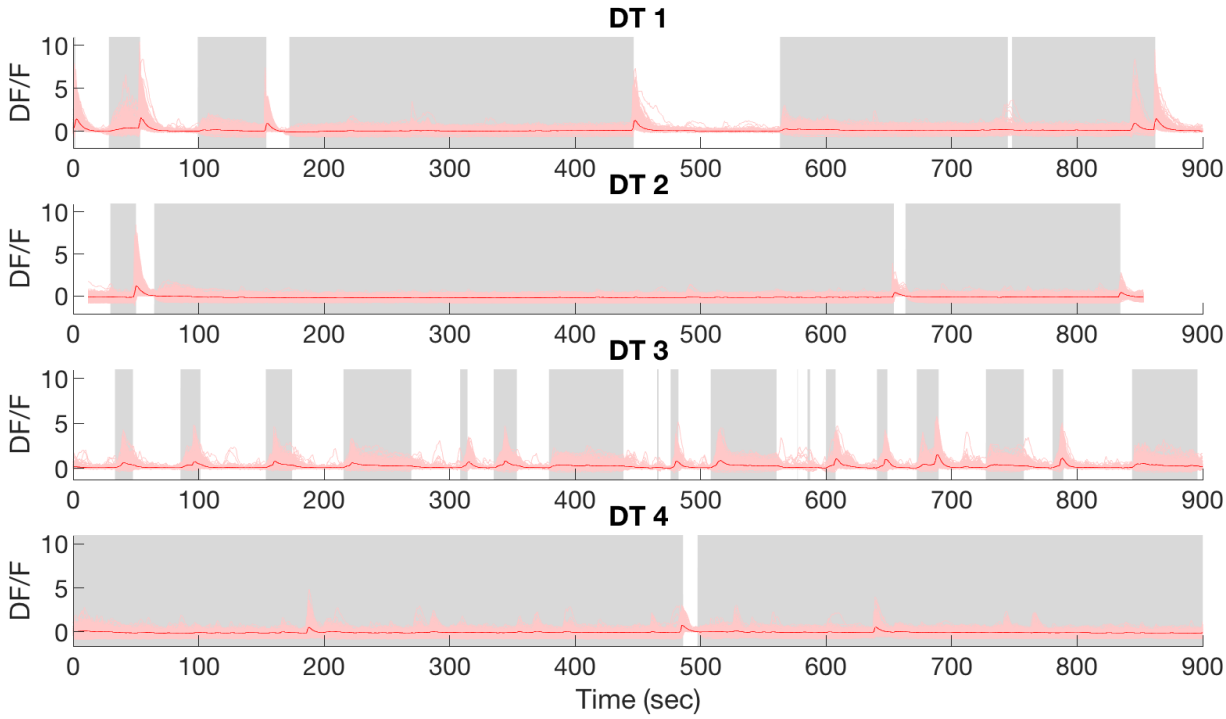

Figure 4.11: Neuronal activity of offset neurons. Neuronal activity of offset neurons in DT during 900 secs of acquisition. An increase in mean activity is observed during the termination of a swim event. The grey shaded regions represent active swimming. N=4 DT.

The variability in the swim/onset/offset maps across different DT can be attributed to the fact that the number of trials (swim/ onset/ offset events) were variable, ranging from 2 to 24 events per fish, and a low number of trials can negatively influence the outcome of the regression analysis. This is a caveat of the method as DT executes few numbers of long swim events when compared to the many small swim events executed by ZF. One way to overcome this disadvantage would be register the individual brain maps on a single brain with a weighted average based on number-of-events per DT. Similar brain registrations are routinely carried out in ZF (Randlett et al., 2015).

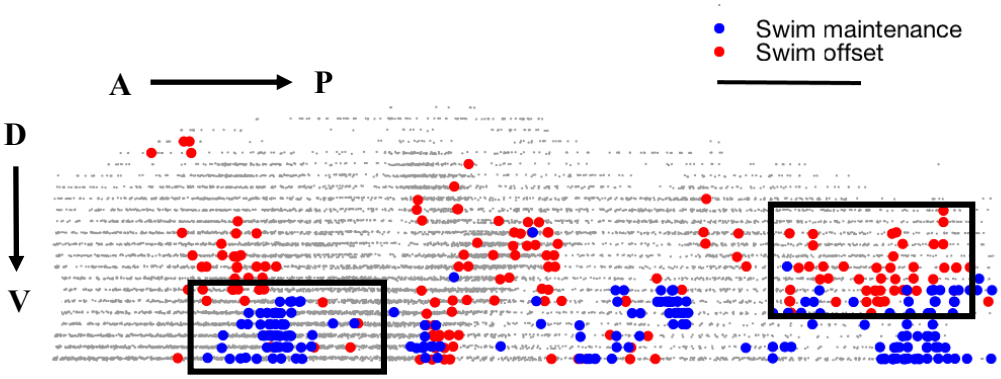

Figure 4.12: A lateral view of a segmented and analyzed DT brain. A single DT brain with swim maintenance (blue) and offset (red) neurons is shown. Ventral mid-brain nucleus and dorsal hindbrain nucleus constitute majority of swim maintenance and offset neurons respectively. The rectangle highlights the two areas with high density of swim maintenance and offset neurons. n= 30 swim and offset events. A: anterior, P: posterior, D: dorsal and V: ventral. Scale bar is 100 µm. Number of layers = 23. Step size between layers is 8 µm.

Taking a closer look at the distribution of swim maintenance and offset neurons, a dense cluster of maintenance neurons are found in the ventral mid-brain whereas a dense cluster of offset neurons are found in the dorsal hindbrain. These two clusters are highlighted in Figure 4.12. It is possible that the hindbrain cluster is composed of GABAergic neurons producing inhibition. Such a functional class of swim offset neurons have not been reported in ZF. On the other hand, the ventral mid-brain population identified as swim maintenance neurons appear to constitute the midbrain neuronal populations that have been implicated in swimming in ZF (Dunn et al., 2016 and Abdelfattah et al., 2018). This conserved swim maintenance nuclei with its upstream location in the midbrain is a good candidate for driving the downstream reticulospinal neurons to keep the CPGs active for the long swim events.

4.2.4 Onset neurons form a continuum between onset and swim maintenance components

As noted earlier, the mean activity of the onset neurons does not die down to its baseline after the peak during initial phase of the swimming. Given this, their activity was further explored closely.

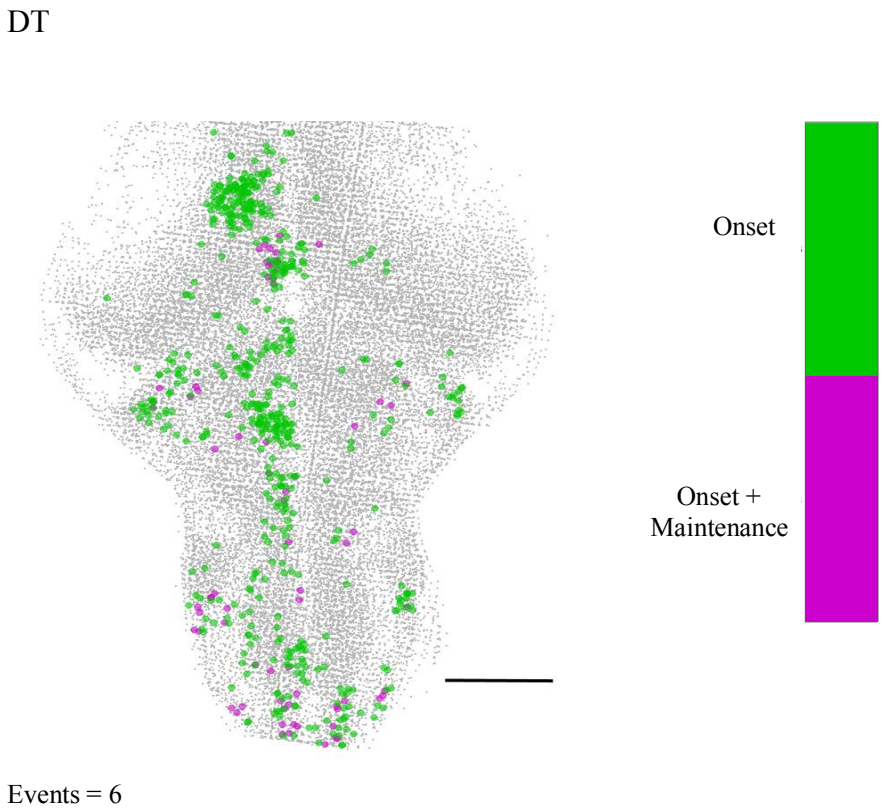

Figure 4.13: The onset neurons are a functionally diverse group which form a continuum between onset and swimming. The distribution of identification confidence (a_1+a_2) for onset and swim maintenance was used to identify the onset/swim maintenance contribution of the onset neurons. The neurons are accordingly color-coded for their contribution to onset (green) / onset + maintenance (magenta) in DT. See Figure 6.8 (B) for an example of the selection procedure. N= 4 DT: see Figure 6.9 for other DT brains. Scale bar is 100 µm.

The correlation of onset neurons with swim onset and maintenance regressors was evaluated based on their regression coefficient and t-score as indicated in Figure 6.8 (B). A cluster of cells was found to possess an above-threshold value for both swimming and onset of swimming,

indicating their dual contribution in swimming maintenance as well swimming onset. In Figure 4.13, such cells appear in magenta. Similar breakdown of onset neurons according to their contribution to swimming maintenance/onset in other DT brains is shown Figure 6.9.

Chapter 5

Discussion

"The problems are solved, not by giving new information, but by arranging what we have known since long." — Ludwig Wittgenstein, Philosophical Investigations

5.1 General experimental approach

The similar morphology and evolutionary closeness of the larvae of the two species provide a unique opportunity to understand how differences in behaviors can arise from relatively conserved neuronal circuits. I carried out a behavioral characterization of DT and found differences in visual (see Figure 6.10) and motor behaviors. Given the striking differences in motor behavior – I primarily looked at spontaneous free-swimming behavior in this study in the absence of any locomotion-inducing stimulation.

It can be convoluted to decipher which stage of the two fish species is directly comparable. No single marker or even a combination of markers can be assumed to have an effective readout of the relative age of the two fish species. To overcome this, I used fish of the same age based on their absolute developmental stage. This, I argue, is more effective here as the behaviors under study do not change by a matter of seven or less days in either of the fish species. Moreover, this approach does not assume anything about the developmental stage of the fish based on a few physiological/morphological markers. I carry out all the experiments in the range of 4 to 6 dpf to maintain consistency. Within this range, again, within an experiment, animals of the same age were used in the two fish species. This experimental approach will incorporate lower variability as compared to say, an ontological study of behavior within the same species, as there would be more morphological, physiological and metabolic changes in a species as it develops (Webb & Weihs, 1986). The comparable size of the two larvae and their presence in similar environments is another advantage. By virtue of this, they would experience similar hydrodynamic resistance during swimming.

With this methodological framework, I carried out the behavioral, anatomical and physiological experiments that I will discuss in the following sections.

5.2 Kinematics of spontaneous swimming and escapes

In the analysis of fine kinematics, I found differences in swimming speed along with half tail beat frequency and maximum tail angle as noted before in Chapter 3. ZF with its high half-beat frequency and maximum tail angle, can generate more propulsive force generating a higher swimming speed (Van Leeuwen et al., 2015).

An important difference in the analysis of spontaneous swimming that I introduce is, instead of analyzing the swimming based on bouts as is classically done in ZF (Severi et al., 2014), I use half tail beats which are defined as a peak-to-peak tail beat cycles. This was important to be able to evaluate swimming in the two species at a level that is comparable to each other. Half tail beats were the most basic unit of locomotion. This did lead to a slight difference in the kinematic parameters noted in ZF in this study when compared to the values obtained from bout-wise analysis. A particular example is the maximum tail angle. In bout-wise analysis, there are two types of bouts noted in ZF: slow swims and burst swims with a lower and higher maximum tail angle respectively (Budick & O'Malley, 2000). An underlying skewness in the distribution of maximum tail angles in slow and burst swimming in a fish can introduce a large variance in the recorded maximum tail angles of a swimming ZF. In contrast, half tail beats with lower maximum angle are always the proportionately dominant category in any bout type. The bout-wise analysis of the same dataset from ZF is shown in Figure 6.1. Although this explains the higher variance that is seen in bout-based analysis, these subtle differences would not change the conclusions of the study as the differences I note between the two fish species are very striking.

In the behavioral acquisition set-up that I developed, the arena size was 30 mm in diameter. With the long swim durations in DT, it would often reach the edge of the arena where the tracking is less reliable due to artefacts caused by illumination. This is a major caveat as I was interested in the duration of swimming events in DT. To overcome this, I carried out head-embedded experiment to quantify the duration of swim events. The results of this were striking: DT could swim continuously for hundreds of seconds to tens of minutes; this was limited to less than 1 sec in ZF. This is a very striking difference at the smaller time scale. However, given the slow and continuous swimming in DT, as shown in Figure 6.2, the mean speed over longer time scales was found to be comparable. This is interesting from a broader perspective - the

animals seem to be executing a similar swimming pattern over longer time scales, whereas the pattern at a shorter time scale is very different.

Given the differences in spontaneous swimming pattern in ZF and DT, next I asked if this would cause a difference in the escape swim executed in the two fish species. In ZF, this has been widely studied and is a very conserved response involving the Mauthner cell network (Budick & O'Malley, 2000 and Dunn et al., 2016). Qualitatively, I observed a similar C-bend mediated escape as would be associated in a Mauthner induced escape response. DT also increased its swimming speed many folds; although the mean escape speed remained lower in DT than that in ZF. The degree of variance observed in latency to attain the maximum escape velocity could be a result of differing escape modes, such as short latency C-bend (SLC) and long latency C-bend (LLC), employed during the escape as has been previously noted in ZF (Burgess & Granato, 2007). This is plausible as the distance of the fish from the tap-stimulus is not maintained constant and can vary depending on the position of the fish in the arena, leading to a difference in the perceived intensity of the stimulus. Interestingly, DT showed a lower latency than ZF. This could be a result of a trade-off between escape speed and response time. The speed of escape alone doesn't suggest much about the success of an escape response. Directionality or variability in directionality of escape could be another important parameter in escape response (Bhattacharyya et al., 2017). To test this, one would have to use a different assay than the tap-induced escape assay that is used in this study. A visual looming stimulus is a good candidate assay to study directionality of escape.

However, a recent study in ZF has suggested that neither speed or directionality can be a good predictor of the efficiency of an escape response (Nair et al., 2017). The authors found that the ability to locate the predatory stimulus from a distance was the best predictor of a successful escape response. This makes the sensory systems a more important factor in an escape response. In DT, a decrease is observed in the delay to achieve the maximum swim velocity during escape. This quick response can be mediated at the level of the motor system or the sensory system. At the motor level, due to the fact that DT is swimming when it receives the threatening stimulus, it is possible that switching the motor program into an escape mode might be easier than initiating a swim from rest which is often what a ZF has to do. At the same time, at the sensory-level, there might be a faster sensory integration or a sensory-motor transformation that happens when the animal is in an active state of locomotion as opposed to at rest. In mice, locomotion is shown to enhance the firing rate of neurons in the visual cortex without altering the sensory

tuning and also produced an enhancement in stimulus specific enhancement in the visual cortex (Niell & Stryker, 2010, Dadarlat & Stryker, 2017, Kaneko, Fu, & Stryker, 2017).

5.3 Exploration and organismal biology

After the aforementioned analysis of the fine structure of swimming pattern, I compared the influence of this swimming pattern on explorative swimming in DT and ZF. I compared the mean squared displacement (MSD) which depends on both, instantaneous speed which I've already reviewed above and the reorientation in heading angle. Although ZF's instantaneous velocity is higher than DT, the MSD is comparable in the two fish. This can be explained by studying the heading decorrelation curve. ZF is seen to show a rapid drop in heading decorrelation, reaching R=0.3 in 1 sec. In DT, on the contrary, although an initial small decline of R=0.8 is seen – it later drops to R=0 slowly over a period of over 8 seconds. This delay in decay of heading decorrelation indicates a longer ballistic regime in DT compared ZF. It is to be noted that the length of ballistic swims in DT can still be an underestimation as swimming in the confined space of the arena in my experimental set-up can alter its reorientation frequency.

During these long ballistic swims in DT, I show that DT alternates between slow and fast swimming. Such a modulation must be essential for a continuously swimming animal to constantly adapt to its surrounding. I also propose that two different kinds of half tail beats might underlie the slow and fast swimming in DT. In ZF, slow movements with low tail beat amplitude and fast movements with large tail beat amplitude constitute the bout types during explorative swimming (Budick & O'Malley, 2000). The above finding indicates that a similar structure with tail beat amplitude might be also present in the explorative swimming of DT, but arranged in a continuum instead.

Briefly, I also looked at characteristics at organismal level which might be able to explain the observed differences in swimming behavior. Firstly, the instantaneous requirement for oxygen is estimated be higher in ZF during swimming, when compared to DT. This is based on the relationship obtained between speed and oxygen consumption in larval ZF obtained by Bagatto et al., 2001. It is to be noted that as the swimming pattern in ZF is not continuous, the high

expenditure of energy in the shorter timescale is likely balanced by the periods of rests to produce a swimming pattern that is overall energetically comparable to that of the continuous swimming in DT. To study efficiency of swimming, many authors have used oxygen consumption as readout for energy input. For instance, it has been shown in trout, goldfish and *Euphausia pacifica* that oxygen consumption increases with increase in swim speed (Webb, 1971, Smit et al., 1971, Torres & Childress, 1983). A similar dependency of speed on oxygen consumption has been noted in *Oncorhynclws nerka* (sockeye salmon) and *Melanogrammus aeglefinus* (Brett, 1964). Although oxygen consumption is a good measure of energy input, it ignores the contribution of anaerobic energy.

I note two plausible factors that can contribute to this observed difference in swimming pattern. The long generation time of DT and ZF prevents the use of experimental evolution approach to demonstrate link between differences at organismal level and its role in the development of the swimming pattern. Hence, I demonstrate my quantified observations with existing analytical and experimental evidence to theoretically establish the link.

The first of these observations is the difference in preference of depth that I observed in ZF and DT. The difference in preference was first noted in DT adults in their home tanks where they occupied the bottom layer of the tank – and then I quantified this behavior in larval DT. This was found to be conserved in larval DT. On the contrary, ZF larvae show a complete opposite preference - for the top layers of the water column as shown in the results. Considering that DT are reported in waters as deep as ~1 meter, this might cause a low availability of dissolved oxygen for DT at such depths. Specifically, ZF adults are known to spawn in the shallow water pools created in the monsoons (Parichy, 2015) and if DT adults spawn in its reported 1 meter deep waters, this will create a difference in the exposure of the two larvae to dissolved oxygen. Lower oxygen availability in DT would limit the maximum oxygen consumption and thus lead to a lower swim speed. Of course, many animals thrive in deep sea environments with extremely low oxygen levels but this might be dependent on a large number of adaptations which might have promoted lower oxygen consumption (Childress & Seibel, 1997). In closely related freshwater species, more subtle adaptation such as a difference in swimming can be expected.

However, in bonnethead shark*, Sphyrna tiburo,* it has been reported that as the DO levels decrease, there is an increase in swimming activity and speed (Parsons & Carlson, 1998). I argue that while for an acute shortage of oxygen that might be an appropriate response, this will

not be energetically optimal for an organism in an environment with consistently lower DO. For instance, a study in herrings showed how an initial increase in swimming speed in response to hypoxic conditions is followed by a decrease in swim speed (Domenici et al., 2000). At a shorter time-scale, such a behavior - increased swim speed in response to hypoxia - can indeed be rewarding as it provides an opportunity to find more oxygen-rich waters. But eventually, there would be a physiological exhaustion leading to a switch to slower swim speed. However, at an evolutionary time-scale, a system that is selected to swim in an environment with lower dissolved oxygen would find it energetically more optimal to swim at a lower swim speed to reduce oxygen consumption.

Although I did not quantify the recruitment of pectoral fins in swimming, in ZF it has been observed that pectoral fins are recruited more during slow swims compared to fast swims. Additionally, it has been shown that pectoral fin recruitment might be useful in low DO conditions to increase fluid transport along the body (Green et al., 2011, Green et al., 2013).

In an analytical model, Weihs (1979) also shows how a more continuous swimming would be recruited in low DO conditions. The author does it based on an analytical model (see Figure 6.11) to explain long swim events in anchovy larva. The larva is considered to be an oxygen sink which would arrive at a new location in the water and start depleting the oxygen in its surrounding by diffusive uptake of oxygen along its body surface. To replenish the oxygen in its surrounding, the larva has to move again - to either displace itself to a new location where it will again encounter oxygen rich waters or to displace the used water to replace it with new oxygen rich water. Hence, the time of rest of the larva at a location in the water is limited by the rate of oxygen uptake in this model. This rate of oxygen uptake is represented as:

$$J= 4\prod\partial DC_o a^2 ((1/a) * (1/2\sqrt{D*t}))$$

Where J is rate of uptake of oxygen,
∂ is density of water, 1 gm/cm^3,
D is diffusion constant for dissolved oxygen at 22°C, 2.22E-5
C_o is initial concentration of dissolved oxygen,
a is the radius of an equivalent sphere, the surface area of which is equal to the surface area of

larval body 4∏a2 = 4∏r2 + 2*l*b, where r, l and b represent the radius of head, length and width of tail segment respectively. Since both ZF and DT larvae measure similar in size, we can approximate them to have the same surface area.
t is the time elapsed from the point when the fish arrives and rests at a new position

We can then evaluate the oxygen flux in a stationary larva at different initial concentrations (C_o) of oxygen in the water. The rate of oxygen transport drops rapidly as discussed below and it is a function of the initial DO concentration (C_o) and the time (t) spent by the larvae at a given position.

Assuming that the free-swimming inter-bout interval of ~0.6 sec of a larval ZF is observed in waters of DO content in the maximum of the range used here (6E-6 g/ cub. cm), we can take the corresponding J at this point to be the critical J (Jc, represented with red dotted line in Figure 6.8). At this point, a larva would have to move again to replenish the DO in its local surrounding. As can be seen from Figure 6.8, the time taken to reach the Jc decreases with decreasing initial concentration of DO in the waters. According to this, a decreasing initial DO concentration of the water can indeed favor a more continuous movement in animals irrespective of the higher oxygen demand that it may incur. This higher demand could be compensated by the organism by moving slower, which although is not explicitly shown in the model, it is clearly observed in my experimental results.

There are, however, points to be cautious of while extending this model to freshwater fishes like DT and ZF for comparison. The oxygen diffusion is a temperature dependent property and can be more variable in these freshwater systems. Also in nature, ZF spawn in the shallower ephemeral pools created in the monsoons (Parichy, 2015). Shallow waters can experience more mixing in oxygen due to convection which would be less so in a deeper freshwater body like the river where DT are found in Myanmar (Roberts, 1986). This might, in fact, make the differences more pronounced by making more oxygen rich waters available to ZF, but limits the direct extension of the model to the two species.

Based on the available literature and evidence presented in this work, I propose that in addition to slow swimming in low-DO environments, a continuous movement can also be useful to sustain reasonable DO levels in such environments.

The second characteristic that I observed which seemed to offer an explanation to the difference in swimming pattern was the delayed swim bladder inflation as noted in the results (Chapter 3). At first, the preference to the bottom might seem to be associated with the delayed inflation of the swim bladder but this might not be necessarily be true as the preference seems to be also conserved in adult DT with inflated swim bladder. A swim bladder provides the ability to swim at various levels of the water columns without expending significant amount of energy to stay afloat. A fish without swim bladder would have to continuously exert a downward force equivalent to 5% of its weight in air to maintain a level in the water (Denton & Marshall, 1958). For instance, as noted earlier in Chapter 3, mackerels (*Scomber scombrus*) do not possess a swim bladder and are observed to swim vigorously, likely to maintain their height in water column. An interesting observation from the fish species lacking swim bladder is that many of them possess lightly ossified skeletons and thin muscle layers of the trunk and tail. This can have a selective advantage in terms of energy expenditure, but more cannot be speculated without a large-scale analysis. Such a large scale analysis is conceivable given that losing swim bladder is not as uncommon as one might think (McCune & Carlson, 2004).

There is at least one analytical model, which suggests that in negatively buoyant animals, a continuous swimming may not be, in fact, energetically the most efficient mechanism to swim (Weihs, 1973). The authors demonstrated that a hop-and-sink swimming mechanism (similar to burst-and-glide) could be energetically more efficient in negatively buoyant organisms. So, it does not necessarily mean that a fish without a swim bladder would prefer to continuously hover to maintain its height in a water column. It is to be noted that the above model was proposed based on zooplankton and a difference in density of animals can influence their energetics of swimming; although the larval fish in this study do not measure very different in terms of length from the zooplankton reported in the above study.

In conclusion, while swim bladder inflation delays as noted in Chapter 3 can plausibly influence the swimming pattern and make it more continuous, it alone cannot explain the differences observed in swimming pattern. This is also what we observe in Figure 6.3 where 2-weeks old DT are still seen to execute long continuous swim events despite inflation of the swim bladder. The duration of swim events appears to be shorter than the 1-week old DT but they are still more continuous and longer compared to the tiny bouts of ZF. As the change in swimming is not dramatic, the change between 1-week and 2-weeks old fish may not be directly attributed to swim bladder inflation as other morphological/physiological changes might have also taken

place simultaneously during this period. All in all, from an organismal perspective, this points to a multi-factorial reason, likely combining both low-DO availability and delayed swim bladder inflation, for the observed differences in swimming pattern. Most of the suggestions discussed here at the organismal level are based on empirical observations and no direct causality has been validated. Nonetheless, they are falsifiable hypotheses which can be tested using an experimental evolution or evolutionary ecology approach.

5.4 Anatomy

Anatomical atlas:

To investigate physiological differences that might explain the observed differences in exploratory swimming, I asked the question in two broad themes: firstly, to evaluate the degree of conservation in anatomy between the two fish by virtue of their evolutionary closeness. Secondly, to capture the differences in neuronal activity which might explain the observed differences.

Cell types and their distribution are often very conserved among animals, more so among closely related animals. For instance, *engrailed-1* positive neurons were first described in zebrafish (Higashijima, Masino, et al., 2004). Later on, *engrailed-1* positive neurons were identified in *Xenopus* and mammals. More recently, medial stripe of this glycinergic *engrailed-1b* positive neurons in ZF were shown to be implicated in swimming (Severi et al., 2018).

In the anatomy experiments, I first tested for the distribution of excitatory (glutamatergic) and inhibitory (glycinergic and GABAergic) cell types in DT. I found the distribution to be very conserved to what has been described in ZF before (shown in Chapter 6 for reference). I used the same markers for labelling these neurons as were first used in ZF. To visualize the pattern of glutamatergic neurons or the distribution of vesicular glutamate transporter (VGLUT) genes, I used a combination of *vglut2a* and *vglut2b* probes. For glycinergic neurons, to understand the pattern of distribution of neuronal glycine transporter (GLYT), only *glyt2* marker was used as *glyt1*is predominately expressed in the spinal cord (Adams et al., 1995). To visualize the GABAergic cells, I used anti-GAD65/67 antibody due to lack of information on the *gad65/67*

gene sequences in DT. It is to be noted that this work was being carried out at a time when the completely annotated genome assembly of DT was not available. The aforementioned staining was also carried out on a *Tg(HuC:H2B-GCaMP6s)* DT along with an immunohistochemistry against GFP to visualize the cells labelled by the *Tg(HuC:H2B-GCaMP6s)* line along with the distribution of glutamatergic, glycinergic and GABAergic cell. This can be useful to identify the neurotransmitter phenotype of any particular cell population labeled by *Tg(HuC:H2B-GCaMP6s)*. This is shown in Figure 6.6. The dual staining would still need to be improved. In the meantime, given the similarity in brain regions and distribution of cell types, an alternative method would be to register the DT brain on ZF brain to gain a better understanding of the identified nuclei while also transferring the newly acquired knowledge into ZF community.

In ZF, the arrangement of glutamatergic and glycinergic neurons in the ZF hindbrain was first described by Higashijima et al. (2004). They showed non-overlapping rostro-caudal running stripes for all three neuronal cell types. Interestingly, Koyama et al. (2011) observed a functional and morphological significance to this patterning. Majorly using the alx transcription factor to target a stripe of glutamatergic neurons in the hindbrain, they showed a trend in the distribution of the neurons along the dorso-ventral axis with respect to their relative time-of-birth, axon length, input resistance and swimming frequency. Moreover, Koyama et al. (2011) showed that excitatory and inhibitory interneurons which form the underlying network for escape behavior are recruited based on their age and function from these cell-type based stripes. Pujala & Koyama (2019) went on to look at projections of hindbrain V2a neurons into the spinal cord and discovered that new projections are layered lateral to the existing ones and can lead to distinct parallel functional pathways. So, this conserved overall arrangement might provide a ground plan which is suitable for easy integration of newly formed circuits to the existing network to add new behaviors to the behavioral repertoire of the animal.

After showing conservation in distribution of the excitatory and inhibitory neurons, I looked at the reticulospinal (RS) neurons in DT and compared their distribution in ZF. Due to a moderate fish-to-fish variance in labelling, the backfilling experiments were performed in both the fish simultaneously and the results were directly compared. Based on the description of RS neurons in ZF by Kimmel et al. (1982) and Orger et al. (2008), a high degree of conservation was observed between DT and ZF. I could identify cells of the mesencephalic nucleus of the medial longitudinal fascicle (nuc MLF/ nMLF), the rhombocephalic reticular formation (nuc RE) and the rhombocephalic vestibular nucleus (nuc VE) in DT that has been described in ZF before.

Specifically, the various cells from the rostral (RoL, RoM, RoV), middle (Mauthner neuron, MiR, MiM, MiV, MiD) and caudal (CaD, CaV) RE nucleus were identified. In the nuc MLF, MeM and MeL cells were identified. Dendrites crossing the midline from MeM cells were identified in DT as has been described in ZF earlier (Kimmel et al., 1982). Although a detailed description of the connectivity is not possible using this method, nevertheless, I could also reproducibly find long laterally running projections from the RoL1 as described in ZF (Kimmel et al., 1982). Anatomically, similar RS neurons (MeM and RoL1 equivalent) have also been described in lamprey (Rovainen, 1967 and Rovainen et al., 1973), indicating that these neurons might be phylogenetically very old. Such anatomically homologous neurons and their conserved distribution points to a common ancestry between DT, ZF and even the evolutionarily more distant animal, lamprey. However, it does not necessarily point to a conserved functional role of these neurons. For instance, homologous neurons are found to have differing functions in divergent feeding behaviors of nematodes (Bumbarger et al., 2013). A more striking example is that of whirligig beetle, an aquatic insect which lacks olfactory antennae, where the role of its mushroom body is shifted from olfaction to vision (Lin & Strausfeld, 2012).

5.5 Physiology

Next, I asked whether the conserved form follows a conserved function. Although high degree of anatomical conservation is noted among animals, one need to be more careful while extrapolating it to functional conservation. For instance, glutamatergic Chx-10 expressing V2a neurons in zebrafish are found to provide excitatory drive to the spinal central pattern generator (CPG) (Kimura et al., 2013). On the other hand, a restricted population of glutamatergic V2a neurons have recently been shown to be involved in termination of locomotion in mice – this is in complete contrast to what has been observed in zebrafish. It is possible that both animals have a functionally heterogenous population of V2a neurons and some of the functional groups remain undiscovered yet. Another particular case from ZF which exemplifies the importance of making careful assumptions about functional properties from transcriptionally defined neuronal classes comes from the spinal V2a neurons. There are at least three functional subtypes of spinal V2a neurons responsible for slow, intermediate and fast locomotion (Song et al., 2018).

Where does the change in neuronal code underlying the difference in swim events originate?

To understand the physiological implementation of the long continuous swims, the first question that needed to be answered was: where to look for – would the change in neuronal code originate in spinal cord or supraspinal centers? Evolutionarily, a more parsimonious mechanism to implement a long continuous swimming might be to introduce changes in the more peripheral networks of the spinal cord without altering the more central supraspinal code. Indeed, there are ways in which this can be solely implemented at the spinal level.

Central pattern generators (CPGs) in the spinal cord generate rhythmic contractions responsible for locomotion. A spontaneous stimulus-independent stop to the locomotion can arise from the intrinsic properties of the CPGs itself. Hence, the duration of locomotion can, in principle, be controlled at the level of CPGs to some extent. There are at least two such "run-down" mechanisms at the CPG-level that can implement this.

One of these run-down mechanisms was described in *Xenopus* by Dale & Gilday (1996): during swimming, ATP is released in the spinal cord and keeps the excitability high by inhibiting the voltage-gated K^+ channels via activation of P2Y receptors. Eventually, ATP breaks down to adenosine, which can inhibit the voltage-gated Ca^{2+} channels via activation of P1 receptors. This will lead to a run-down of the CPG activity.

Another mechanism at the level of CPGs that can bring an end to a locomotor event involves the Na^+/K^+-ATPase pump and it was also demonstrated in *Xenopus* tadpole (Zhang & Sillar, 2012). This is based on an activity and sodium spike dependent enhancement of Na^+/K^+ pump function that can lead to an ultraslow, minute-long afterhyperpolarization (usAHP) in network neurons following the locomotor events. In this study, the activity of the Na^+/K^+-ATPase pump was suppressed using ouabain, a pump blocker. This blocked the usAHP and also caused an increase in the swimming duration. Thus, there can be an independent activity-dependent shut-down of the CPGs without any supraspinal command.

As this is dependent on activity and sodium spike, it opens up interesting possibilities. As we know, zebrafish executes a fast and rigorous swim bout when compared to DT; it is possible

that this is often accompanied by large Na^+ influx in the CPG neurons of ZF and triggers the aforementioned mechanism. On the contrary, this may not be achieved in DT with its slow swims where the spiking activity might be lower in the CPG neurons. We have to be cautious here and remember that we are discussing activity of neurons between two different species and this would not be directly comparable as many factors such as cell size and distribution of ion channels can change the conductance properties of the cell very easily. This can in turn lead to a very different dynamics of Na^+ /K^+ ions. In fact, the 'threshold' for triggering the usAHP could be different in the CPG neurons of the two animals, thereby the two animals can still follow the same mechanism, but at two different timescales.

However, given the very long durations of swims in DT, I hypothesized that there would be a supraspinal component of control over the locomotion. It doesn't seem efficient to drive a system without any control over the steering for a duration of hundreds of seconds, especially for a system which needs to constantly update its motor program based on environmental cues. While there could still be some concurrent adaptations in the CPG and/or musculature of DT, the main control unit would likely be supraspinal in nature. In fact, it is plausible that in DT, the infrequent stop signal mostly relies on a supraspinal command whereas in ZF it is majorly regulated by the run-down mechanisms intrinsic to the CPG network due to its faster swimming. Indeed, in ZF, there is evidence that spinalized preparations can still generate episodic swimming without any supraspinal input and it is dependent on the rostral segments of the spinal cord (Wiggin et al., 2012).

To probe the neuronal activity of the suraspinal centers in the brain, I created a transgenic fish model of DT with a near pan-neuronal nuclear-localized expression of the genetically encoded calcium indicator (GECI), GCaMP6s. The indicator was driven under the promoter *HuC* (also known as *elav3*); it is expressed in a large fraction of the neurons in the brain. Despite the slower kinetics of GCaMP6slow over a GCaMP6fast indicator, I used GCaMP6s indicator as its sensitivity is higher and hence is likely to detect a more proportion of active cells (Chen et al., 2013). The whole brain imaging of this fish was performed under a light-sheet microscope during spontaneous swimming to investigate the neuronal activity corresponding to the swimming events. Broadly, there were two motivations to perform this: 1) to understand the nature of change in the neuronal code which can explain the long swimming events in DT. 2) to take advantage of the long swim events in DT to temporally resolve the neuronal activity with respect to various phases of the swimming.

Based on the regression analysis performed on the whole brain activity with swimming behavior, activity in specific brain regions were identified to be correlated with swimming activity. Similar brain nuclei were already seen to be correlated with swimming in ZF by Dunn, Mu et al. (2016). In their study, hindbrain nuclei were identified to be highly direction selective whereas a non-direction selective mid-brain nucleus was also identified which likely also constitutes the nMLF cells. In ZF, activity in nMLF neurons have been earlier shown to be implicated in swimming (Thiele et al., 2014 and Wang & McLean, 2014), and more specifically to be correlated with duration of swim bouts (Severi et al., 2014). So, this nucleus is a good candidate for modulating the length of swim events. It is to be noted that it cannot be said with certainty as to which of the swimming correlated neurons are actually driving locomotion in DT or which ones are merely involved in the modulation of the ongoing swimming. I did note a significant modulation of spontaneous swimming, but as I have not looked at the ongoing modulation of tail-beats during the whole-brain imaging, this will be a question reserved for future studies. Some of the neurons might, in fact, simply receive an internal copy of the ongoing swimming state and not have an actuator role. Loss-of-function or gain-of-function experiments would be inevitable to validate any causation. However, the fact that I see a scaling in the activity of the neuronal population in the midbrain and hindbrain nuclei indicates that there is a constant drive for steering and maintenance of locomotion that is supraspinal in nature and is unlikely implemented at CPG-level alone.

The finding of supraspinal swimming correlated neurons also agrees with what has been reported from various studies across many other animal species. Juvin et al. (2016) identified three sets of reticulospinal (RS) neurons in the middle rhombencephalic reticular nucleus that showed activation during the start, maintenance and end of locomotion. In addition to the RS neurons which directly project to the spinal cord, another important set of neurons implicated in locomotion are located in the brainstem region, called the mesencephalic locomotor region (MLR). MLR and its equivalent structures have been identified in many organisms including lamprey, mice and humans (Ryczko & Dubuc, 2013). So far there is no clear evidence of an equivalent region in ZF. Based on the location of the nucleus (mid-brain/hind-brain junction) that I have identified in DT, it is possible that this nucleus consists of nMLF and as well as MLR-equivalent cells of DT/ZF (Dunn, Mu, et al., 2016). A thorough anatomical and physiological study of this region will be essential to validate this. DT can serve as a good model here as one of the features of the MLR is the graded control that it exerts over locomotor

output and this can be easily studied with the continuous modulation of locomotion that is noted in DT.

So, the change in neuronal behavior is supraspinal in nature; but mechanistically how can the long-lasting neuronal activity be produced?

In the previous section it is shown that supraspinal neurons are active for long periods of activity which correlates with the long swim events in DT. This leads to a pertinent question: how do the neurons change their activity pattern? As described earlier, I used a GECI to carry out the physiological recordings. While this non-invasive optical recording method has the advantage of surveying large number of cells simultaneously, its temporal resolution is poor and cannot resolve spiking activity of the neurons. An electrophysiological approach is more suited to pursue this question once a population of interest in identified.

However, based on the vast literature on locomotion in other animal species, I can propose a few models for the implementation of long neuronal activity based on the circuit and membrane properties of a neuronal network. Non-linear intrinsic response properties of neurons such as plateau potentials can cause a bistable behavior in neurons. With respect to supraspinal motor control, Antri, Fenelon et al. (2009) investigated the sensory stimulus initiated long depolarizations in the reticulospinal (RS) neurons of lamprey. The results suggested a role of calcium-activated non-selective cationic current (I_{CAN}) in the long-lasting depolarization. It also demonstrated the role of glutamatergic synaptic inputs from spinal cord and elsewhere, in the temporal amplification of the sustained depolarizations. As the I_{CAN} activity diminishes, the glutamatergic inputs could provide more excitation for the required activation. The I_{CAN} does not show a voltage dependency and can lead to long-lasting influx of calcium. Their activity can still be preceded by the activity of voltage-dependent L-type calcium channels (Morisset & Nagy, 1999, Voisin & Nagy, 2001 and Baufreton et al., 2003).

In contrast, in frog tadpoles, Li et al. (2006) demonstrated that the prolonged swimming cannot be explained by intrinsic membrane properties of the neurons. They showed that a small region of caudal hindbrain and rostral spinal cord was sufficient to generate prolonged swimming. Instead of bistability of the neurons, they found a reverberation hypothesis to be the underlying mechanism. According to this, the authors found neurons forming reciprocal excitatory

synapses and providing direct mutual excitation to keep the network active for long periods. In addition to descending feed-forward excitation from these neurons, the authors also identified feed-back ascending excitation.

So, while these mechanisms can explain the long-lasting activity of supraspinal neurons in DT, to test this directly, we would require to use electrophysiological methods.

Apart from the membrane or network properties of the supraspinal command neurons, neuromodulation of these neurons can also be another source of change which can keep the circuit tonically active. Dopaminergic (DA) system plays an important role in the modulation of the activity of the supraspinal control centers. A long-known pathway is the ascending DA pathway from meso-diencephalic DA neurons that projects from A9 to the striatum in mice [see Grillner & Robertson (2016) for a review]. Within the basal ganglion, D1-expressing neurons of the direct pathway and D2-expressing neurons of the indirect-pathway form the targets of these projections. More recently, descending DA projections directly innervating MLR in the brainstem have been discovered. Ryczko et al. (2013) had first shown direct descending DA projections in lampreys from the posterior tuberculum (homologue of the mammalian substantia nigra pars compacta and/or ventral tegmental area) to the MLR region. Later on, such projections were also shown to be conserved in salamander and mice (Ryczko et al., 2016). The DA cell group A13 is shown to exclusively form descending projections (Sharma et al., 2018). With the dopamine sensor transgenic lines that are now available in ZF, the role of these nuclei can be directly investigated during swimming in fish (Sun et al., 2018).

Can more be said on the role of neurons in the identified nuclei in the regulation of swimming behavior?

Brain nuclei are often described on the basis of anatomical localization, expression of a particular transcription factor, effects of electrical stimulation or calcium imaging/ optogenetic stimulation carried out under the expression of a particular sensor/actuator driven by a specific promoter. In all of the above cases, it cannot be ruled out that the described nucleus consists of a functionally heterogeneous population of neurons or networks of neurons.

For instance, a recent study found that optogenetic stimulation of entire lateral paragigantocellular nucleus (LPGi) in the caudal brainstem in mice failed to induce or modulate locomotion but a selective targeting of the glutamatergic and glycinergic LPGi produced locomotor initiation and arrest respectively (Capelli et al., 2017). Roseberry et al. (2016) identified that glutamatergic MLR neurons in mice were necessary for locomotion whereas GABAergic MLR cells could decelerate ongoing locomotion using local projections to these glutamatergic cells. Moreover, a cholinergic MLR population was able to modulate ongoing locomotion. Again, glutamatergic neurons in two subregions of the MLR in mice, namely the cuneiform nucleus (CnF) and the pedunculopontine nucleus (PPN) are also shown to be required for distinct component of locomotion: high- and low-speed respectively (Josset et al., 2018). In lamprey as well, MLR neurons were identified for both initiation of locomotion and termination (Grätsch et al., 2019).

Due to the kinetics of the calcium indicators used widely in ZF optical physiology and used in this study, it is difficult to assign neuronal activity to various phases of the swimming in ZF. As a result, the functional diversity of neurons as described above in other animals is often missed by the studies that employ GECIs in ZF. Recently, using *in-vivo* voltage imaging in ZF, Abdelfattah, Kawashima, et al. (2018) classified swimming related neurons into various functional sub-types. The authors used a *vglut2a:gal4* line and focused on a mid-brain nucleus. They identified neurons which correlated with onset, swimming phase and off phase of the swimming. Although impressive, current optical methods wouldn't allow a scaling of this voltage imaging to a brain-wide scale. Here, in the current study, taking advantage of the long swim events in DT, I tried to cluster neurons into onset, maintenance and offset neurons on a brain-wide scale. One of the disadvantages of the method was the few numbers of onset and offset events, if any, in the swimming during the brain acquisitions due to the innately long swim events in DT. However, based on the few swim events (n=36) I obtained from DT (N=4), all the swimming correlated nuclei appear to consist of a functionally heterogenous population of neurons.

A rather approximate regressor (-3 to +1 seconds) was used to identify the onset and offset neurons. This decision was based on factors such as acquisition frequency and information from fluorescence change in the brain acquisitions averaged around the onset and offset events. The onset/offset regressors may not strictly simulate the onset/offset behavior in fish leading to a lower regression coefficient. Based on the analysis, two functional subtypes, onset and offset

neurons were detected and as described above, they formed a heterogeneous population with the maintenance neurons described above. The two symmetrically laterally located nuclei which appear similar to the GABAergic nuclei described by Severi et al., (2018) seemed to consist of a large proportion of onset and offset neurons which has not been suggested before in ZF. Majorly, the offset neurons were found to located in the dorsal hindbrain, whereas onset neurons were found to be more widely distributed, heterogenously with the swim maintenance neurons. Such a functionally heterogeneous neuronal population might be a more optimal layout for forming local functional circuits with reduced wiring lengths (Chklovskii et al., 2002) as opposed to having functionally defined clusters of nuclei across the brain.

The end of locomotion is of particular interest to us as ZF executes very frequent stops to the locomotion whereas in DT, it is very infrequent. The mechanism for the underlying stop command could have independently diverged to adapt to the differing frequency of the stop commands utilized. A consistent firing during the termination of swim events is observed except for few events in DT3 where the activity appears to be a little uncorrelated with termination. The exact reasons for this are yet unknown. It could be that although I group all swim events in a single category, this category could actually constitute different types of swim events and this variability might be able to explain the anomalous behavior observed in few events of DT3. It is also possible that termination of some swim events (likely high intensity movements) can indeed depend on earlier discussed run-down mechanisms at the CPG-level.

Anatomically, these offset neurons seem to be very heterogeneously distributed, especially in the dorsal hindbrain nuclei. These could be inhibitory interneurons or RS neurons, part of the reticular formation. Such offset neurons have not been described in ZF before – this could be simply because most studies employing calcium imaging methods were not sufficient to identify such neurons at a brain-wide scale. However, similar neurons have been described in a variety of other animal species - Juvin et al. (2016) have described stop cells involved in the end phase of the swimming in lamprey. Activation of stop cells was observed during MLR (mesencephalic locomotor region) stimulation, sensory-evoke locomotion and spontaneous locomotion. The authors carried out pharmacological activation and inactivation of the cells using D-glutamate and a glutamate receptor antagonist respectively to successfully manipulate the termination of a swimming event. Similarly, Bouvier et al., 2015 identified glutamatergic V2a neurons in mice brainstem responsible for halting ongoing locomotion. Takakusaki et al., 2003 showed a locomotor arrest in cats when stimulated in the medullary reticulospinal tract.

In tadpole, Perrins et al., 2002 identified a contralaterally projecting mid-hindbrain reticulospinal neuron (MHR) which reliable stopped locomotion. The current study points to existence of functionally similar offset cells in fish.

On the contrary, neurons similar in activity to the onset neurons that I describe here have been reported earlier in ZF. Firstly, Arrenberg et al. (2009) had carried out an "optogenetic scanning" to identify a region in the hindbrain which could reliably induce swimming in larval ZF. Then, Kimura et al. (2013) had showed a glutamatergic Chx-10 expressing V2a neurons in ZF which provide an excitatory drive to the spinal central pattern generator (CPG). Among the onset neurons identified in this study, many cannot be strictly classified as 'swim onset' in nature. These cells form a continuum between onset and maintenance of swimming and show a strong correlation to both onset and maintenance of swimming. A tiny burst of activity is seen in the onset neurons during the two long swim events in DT4 (in Figure 4.9), it is to be noted that an activity of offset neurons in DT4 (in Figure 4.11) is also observed around the same time point. This possibly indicates that the period of pause was very short to be translated into an observable behavioral change.

Based on the swimming correlation and the anatomical evidence, I would hypothesize that the identified ventral mid-brain nucleus consist of nMLF (as shown in Dunn et al., 2016) projecting to spinal cord and other MLR-like neurons which might activate downstream RS neurons in the hindbrain to continuously feed the spinal CPGs and keep them active. I did not look at the graded control of this nucleus over swimming speed (or half beat frequency in head-embedded preparation) which would be a feature of the MLR nucleus. This can be tested in the future to comment on whether this nucleus in DT (and possibly in ZF) is an equivalent of the MLR. The role of this nucleus in maintaining the length of swim events and acting as maintenance neurons can be validated by spatially targeting this cell population using optogenetic methods to tonically stimulate the neurons in ZF to simulate the long swimming activity as observed in DT. A more thorough characterization of the nucleus would involve explicitly demonstrating anatomical projections from this nucleus to the RS neurons.

5.6 Conclusions and future directions

Using two closely related fish species, *Danionella translucida* (DT) and *Danio rerio* / Zebrafish (ZF), I show that two anatomically conserved neuronal circuits are able to produce two different behavioral outputs based on their functional differences.

Firstly, I demonstrate that the two fish species utilize different strategies to execute spontaneous swimming. DT performs slower swimming with a lower half beat frequency and lower maximum tail angle when compared to ZF. With escape response, I show difference at the millisecond scale with respect to delay in achieving the maximum velocity. This opens up interesting questions on influence of locomotion on sensory integration and sensory-motor transformation which can be tested in the future.

At the level of neuronal circuits, I show a high degree of conservation in the distribution of excitatory and inhibitory neurons and reticulospinal neurons in the hindbrain. I show that the activity of supraspinal centers in the midbrain and hindbrain is scaled to the long swim events in DT suggesting that these supraspinal centers play a role in the long swim events of DT. Using the close conservation of the brain structures in DT and ZF and the available genetic tools in ZF, a causal relationship can be tested by performing a tonic excitation of the identified (most upstream) midbrain nuclei in ZF to simulate the long swim events of DT. I also propose mechanisms at neuronal membrane and circuit levels to explain the origin of the long-lasting activity in the network. These hypotheses can be tested using electrophysiological methods to specifically record from the identified neuronal populations to characterize their cellular and network properties.

Moreover, taking advantage of the long swim events in DT, I characterized neurons implicated in various phases of swimming, namely onset, maintenance and offset. Using the currently available genetically encoded calcium indicators (GECIs), it is not achievable directly in ZF. However, in principle, by virtue of the anatomical conservation in the two fish species, these findings from DT can be translated to ZF by performing a brain registration of DT acquisitions on ZF brain. This can approximately identify the same brain nuclei in ZF and also help in identifying their cellular properties more precisely based on the large repertoire of genetic lines and literature available for ZF.

While I have made suggestions on how a particular behavior or neuronal network might have been evolutionarily selected in nature, I have refrained from making any direct claim at an evolutionary level from the present study as it was not the aim here: only two samples in the course of evolution were investigated. One would have to incorporate many more species to comment on the evolution of behavior (or neuronal networks) that I have noted in this study. To put it according to Tinbergen's classical paper on ethology, biologically, behavior can be investigated at four distinct levels (Tinbergen, 1963): (1) how is it caused physiologically? (2) what is its survival value? (3) how has it evolved? (4) how does it develop in the individual? In the current work, I have focused on the first two levels. Nevertheless, this lays a foundation for future work to directly compare neuronal circuits and behaviors in vertebrate species. This is particularly interesting to do in danionins as many related species are known and can be easily adapted to the same fish facility that is developed for ZF/DT. With the ability to dissect behaviors to their genetic and neuronal circuit components, this would be the modern approach to comparative neuroethology which can directly inform us about evolution of behaviors and neuronal circuits.

Chapter 6

Appendix

"Measure what can be measured, and make measurable what cannot be measured."

— Galileo Galilei

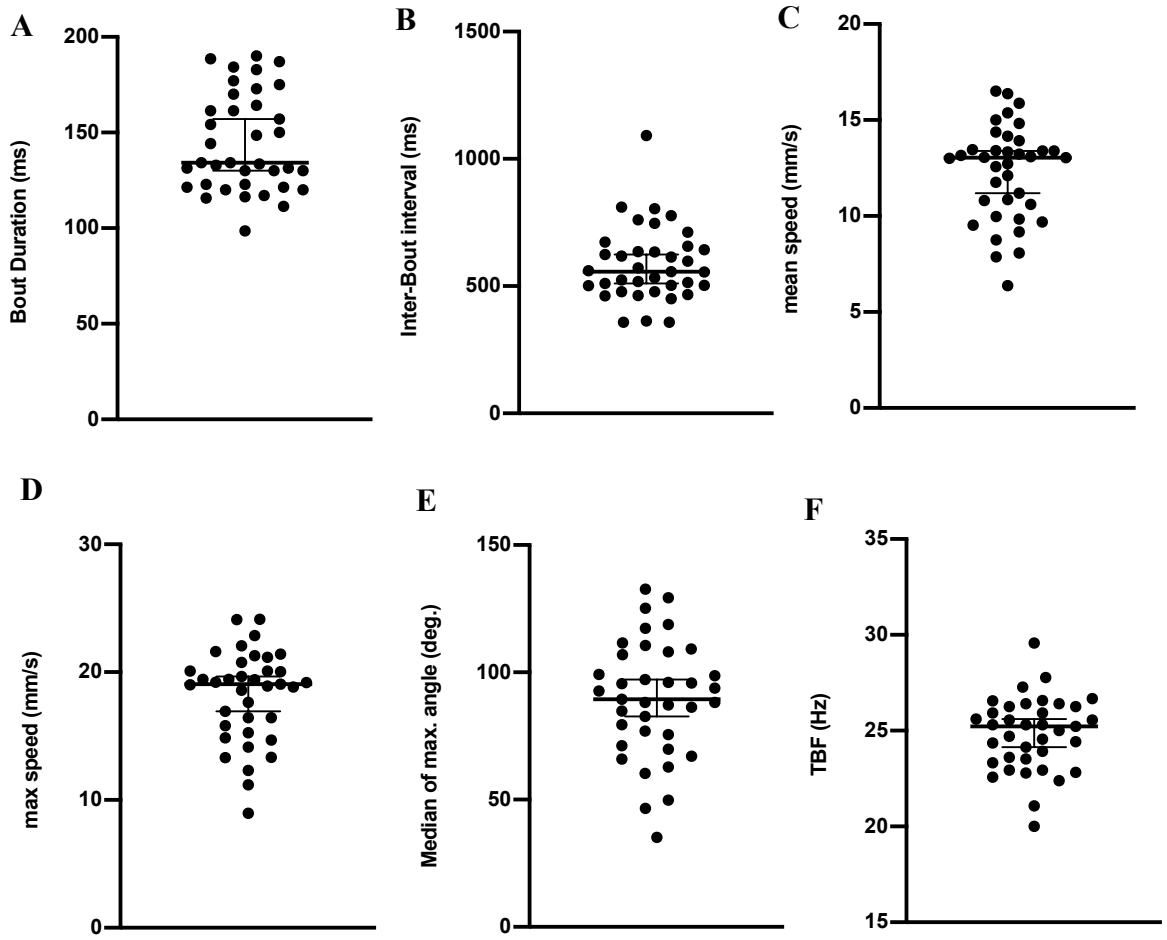

Figure 6.1: Bout-wise kinematics of ZF. (A) and (B) show the bout and inter-bout duration in ZF. (C) Mean speed, (D) maximum speed, (E) maximum angle and (F) tail-beat frequency (TBF) of ZF bouts. (N=37 ZF each)

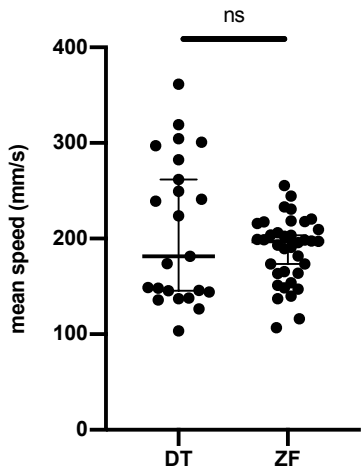

Figure 6.2: Mean speed in DT and ZF was comparable over long time scale. Average speed of DT was obtained after adjusting for the fraction of time spent swimming according to the head-embedded data. For ZF, this was obtained after adjusting for the fraction of time spent swimming based on the bout and inter-bout durations from the free-swimming data. (N=23 DT and 37 ZF).

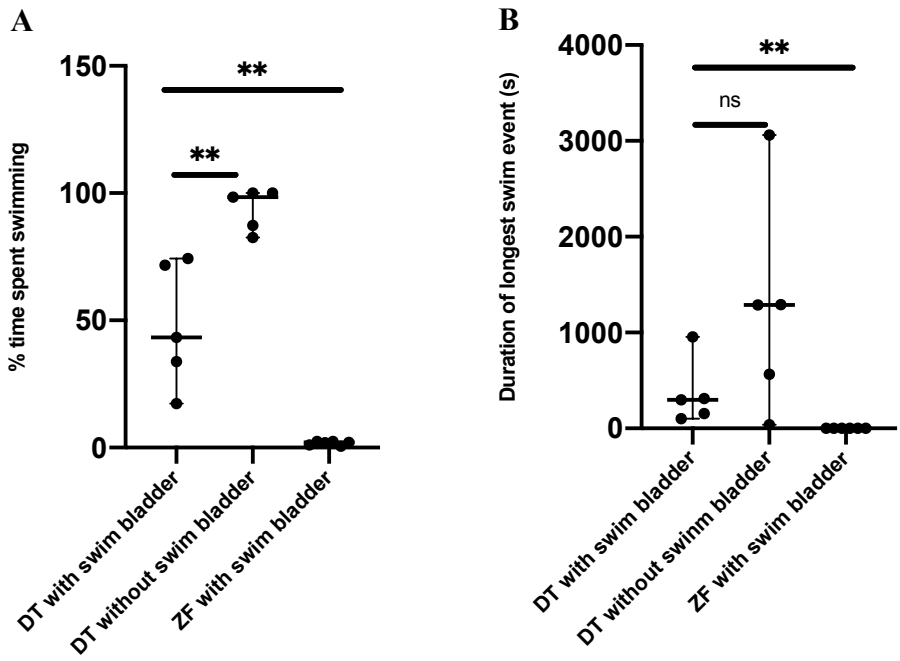

Figure 6.3: Swimming in 1-week and 2-week old DT larvae. (A) percentage of time spent swimming in 2-week old DT with swim bladder (n=5), 1-week old DT without swim bladder (n=5) and 1-week old ZF with swim bladder (n=6) (** $p<0.01$, Mann-Whitney test). (B) Duration of the longest swim event in 2-week old DT with swim bladder (n=5), 1-week old DT without swim bladder (n=5) and 1-week old ZF with swim bladder (n=6) (** $p<0.01$, Mann-Whitney test).

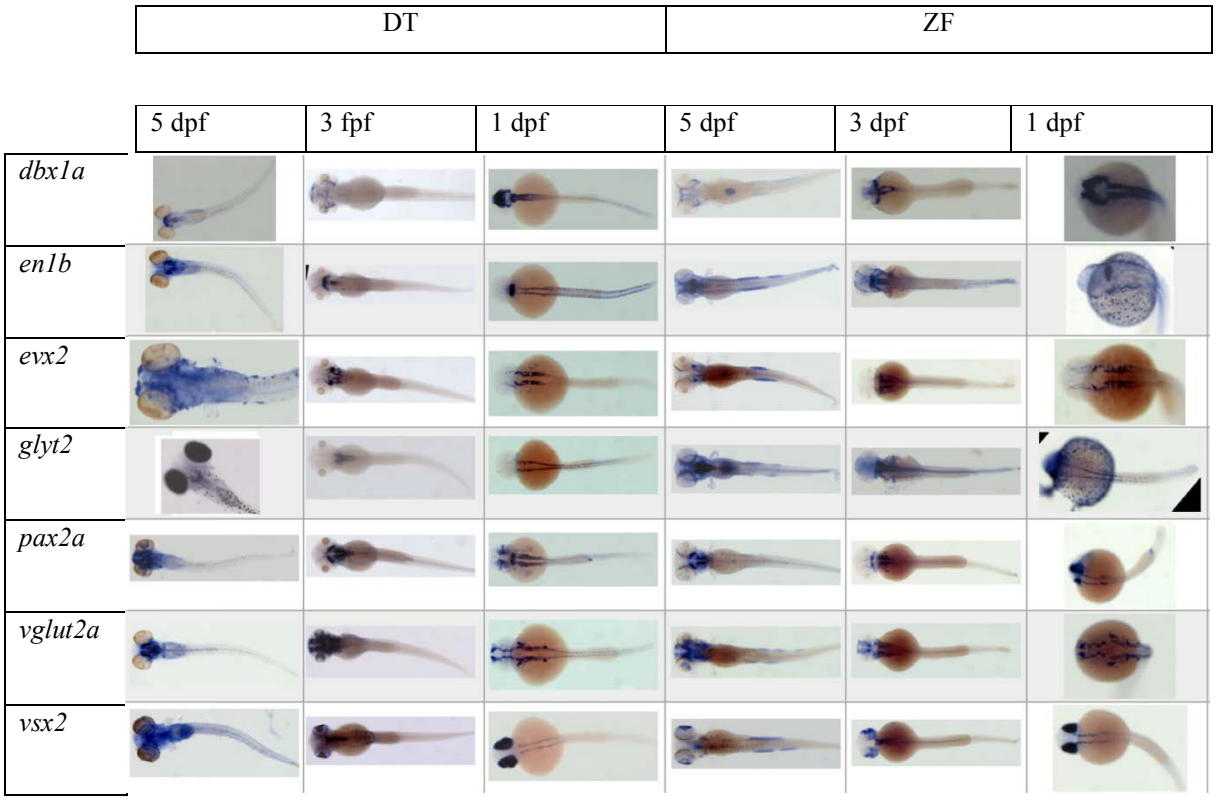

Figure 6.4: *in-situ* hybridization performed on ZF and DT. *in-situ* hybridization was performed at various stages in ZF and DT against various genes.

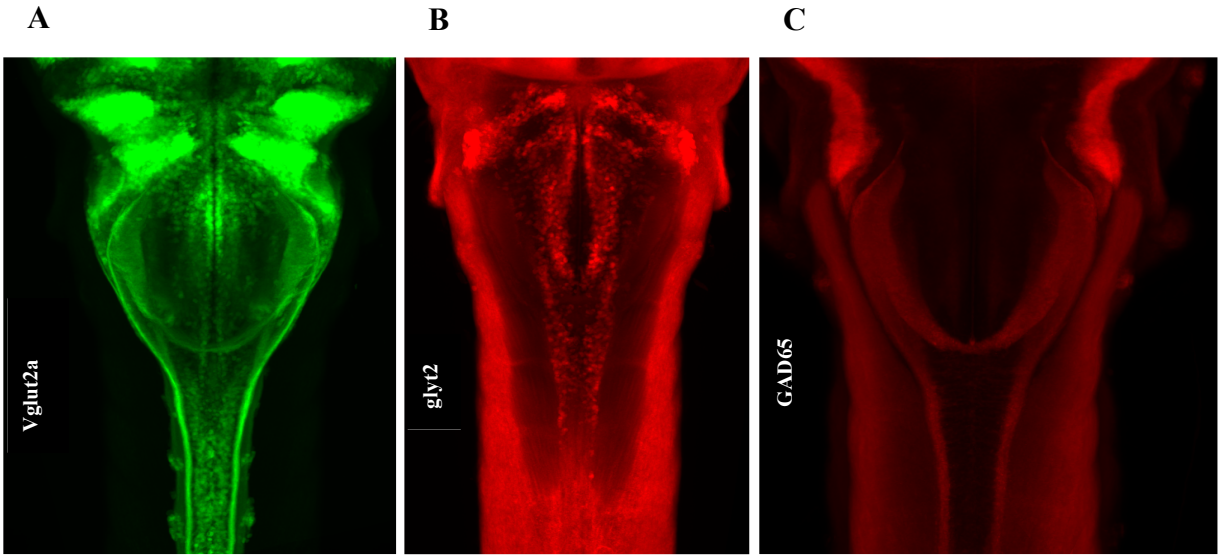

Figure 6.5: Distribution of glutamatergic, glycinergic and GABAergic neurons in the hindbrain of ZF obtained from Z-brain atlas (Randlett et al., 2015). Maximum projection of (A) *vglut2a*-GFP (Bae et al., 2009), (B) *glyt2*-GFP (Mclean et al., 2007) and (C) anti-GAD67 (Randlett et al., 2015) ZF lines showing the distribution of glutamatergic, glycinergic and GABAergic cells respectively in the hindbrain of ZF.

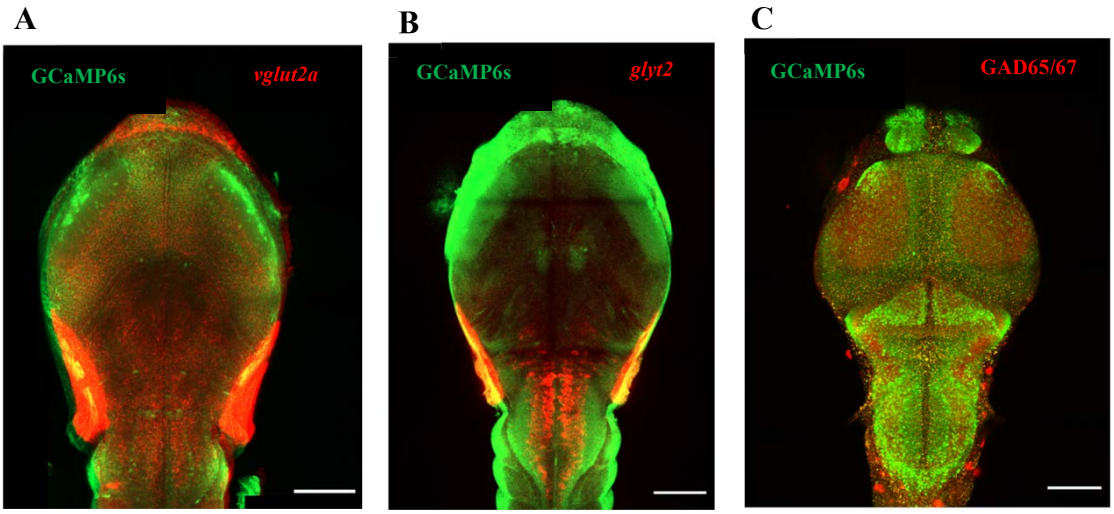

Figure 6.6: Distribution of (A) glutamatergic (B) glycinergic and (C) GABAergic neurons in the DT brain is shown in red along with distribution of HuC:H2B-GCaMP6s expressing neurons in green. Anti-*glyt2* ISH and anti-*vglut2a* ISH in (A) and (B) respectively. Anti-GAD65/67 IHC in (C). Anti-GFP IHC to label the GCaMP6s expressing neurons. Scale bar is 100 µm.

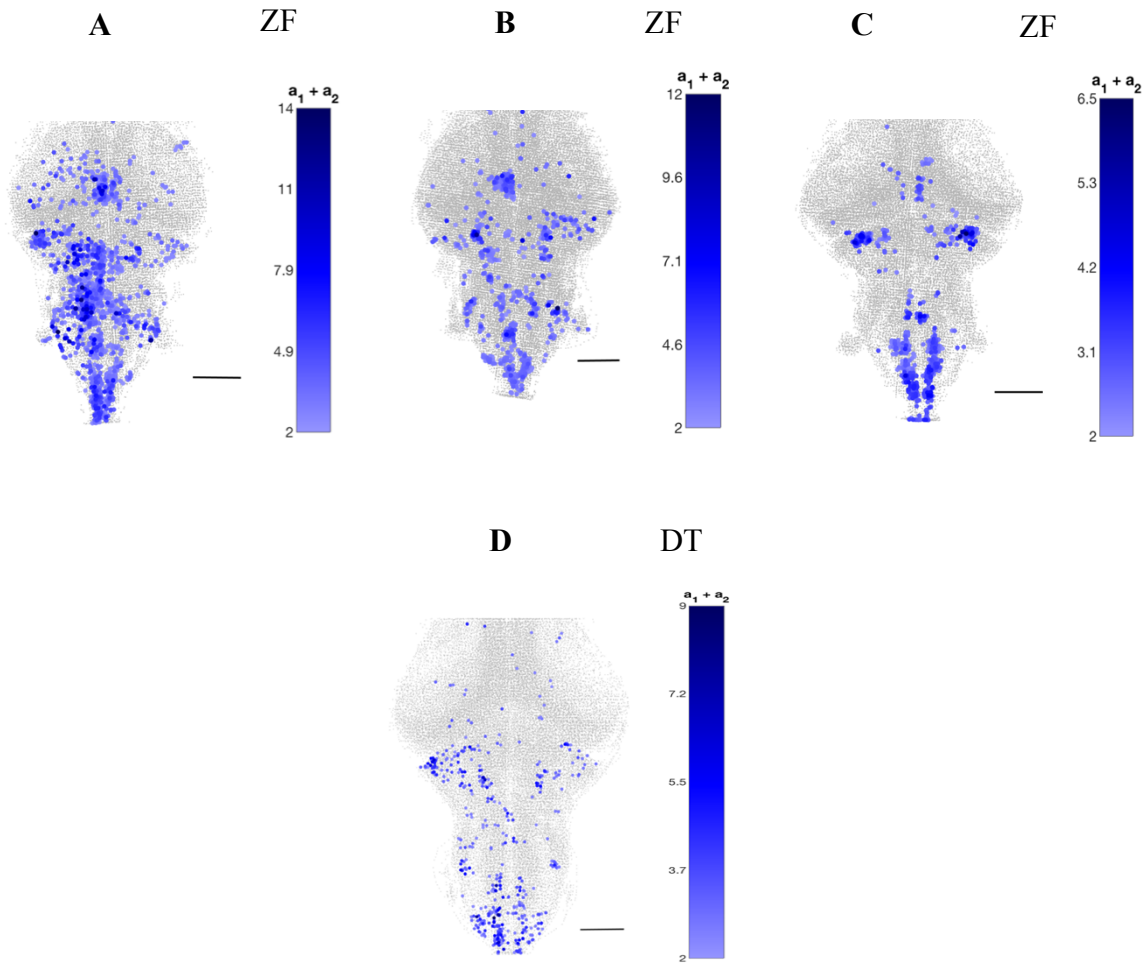

Figure 6.7: Neuronal correlates of swimming in ZF and DT. (A), (B) and (C) show neuronal correlates of swimming in ZF. Highly correlated neurons of ZF are color-coded in blue. The identification is based on the regression coefficient and t-score. (D) shows neuronal correlates of swimming in a DT with 2 long swim events. Highly correlated neurons of DT are color-coded according to their identification confidence based on the regression coefficient (a1) and t-score (a2). See Figure 6.8 (A) for an example of the method. The nuclei located in the medial mid-brain, lateral midbrain and hindbrain are conserved in DT and ZF. Scale bar is 100 µm.

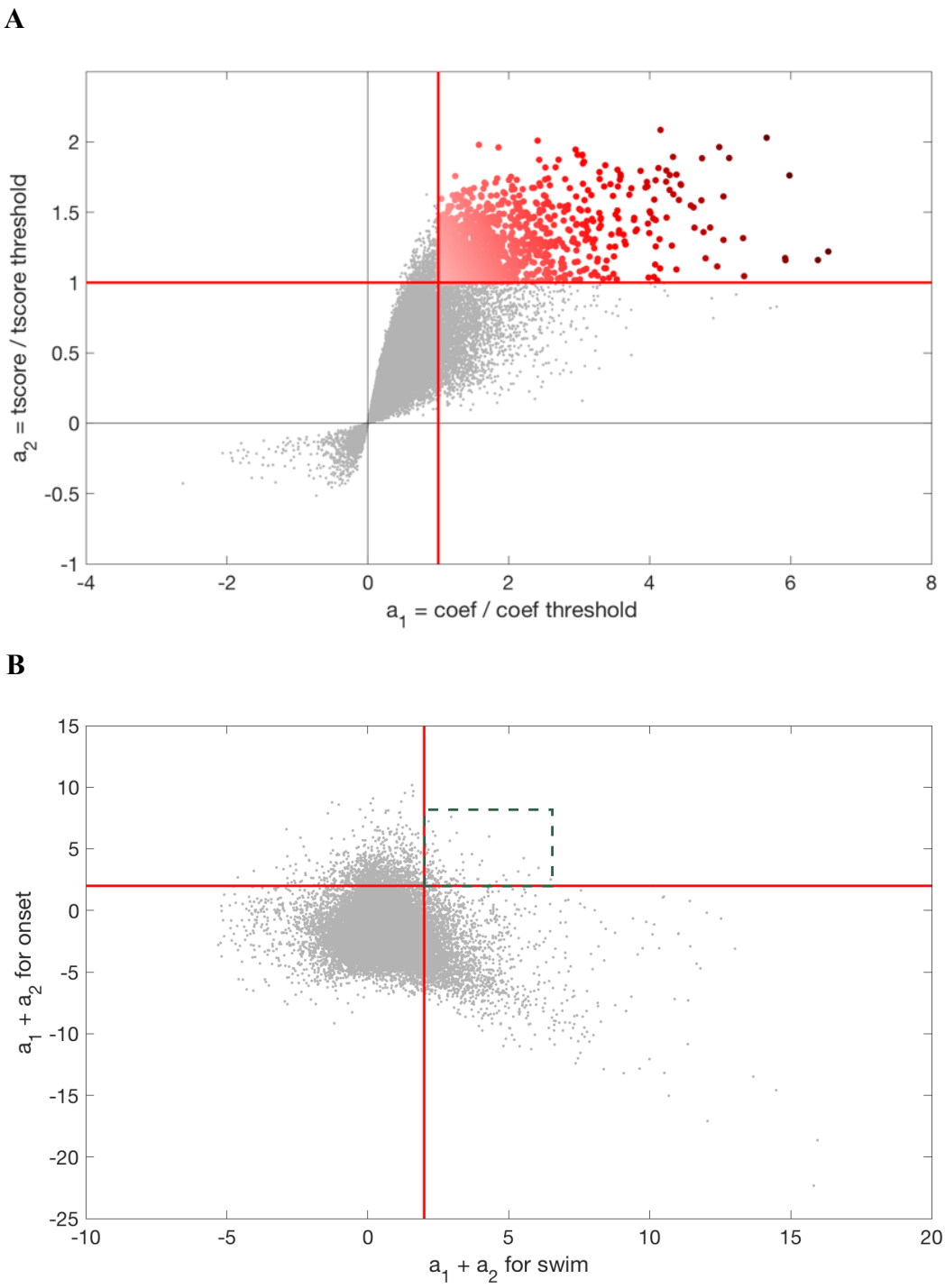

Figure 6.8: Identification of swim maintenance neurons and diversity of onset neuron in DT. (A) shows an example of selection of swim "maintenance" cells in DT based on the regression coefficient (a_1) and t-score (a_2). (B) shows the identification of onset neurons which have a swim maintenance component. The green rectangle captures all the neurons with both, onset ($onset_{(a1+a2)}$) and swim maintenance coefficients ($swim_{(a1+a2)}$) greater than the threshold.

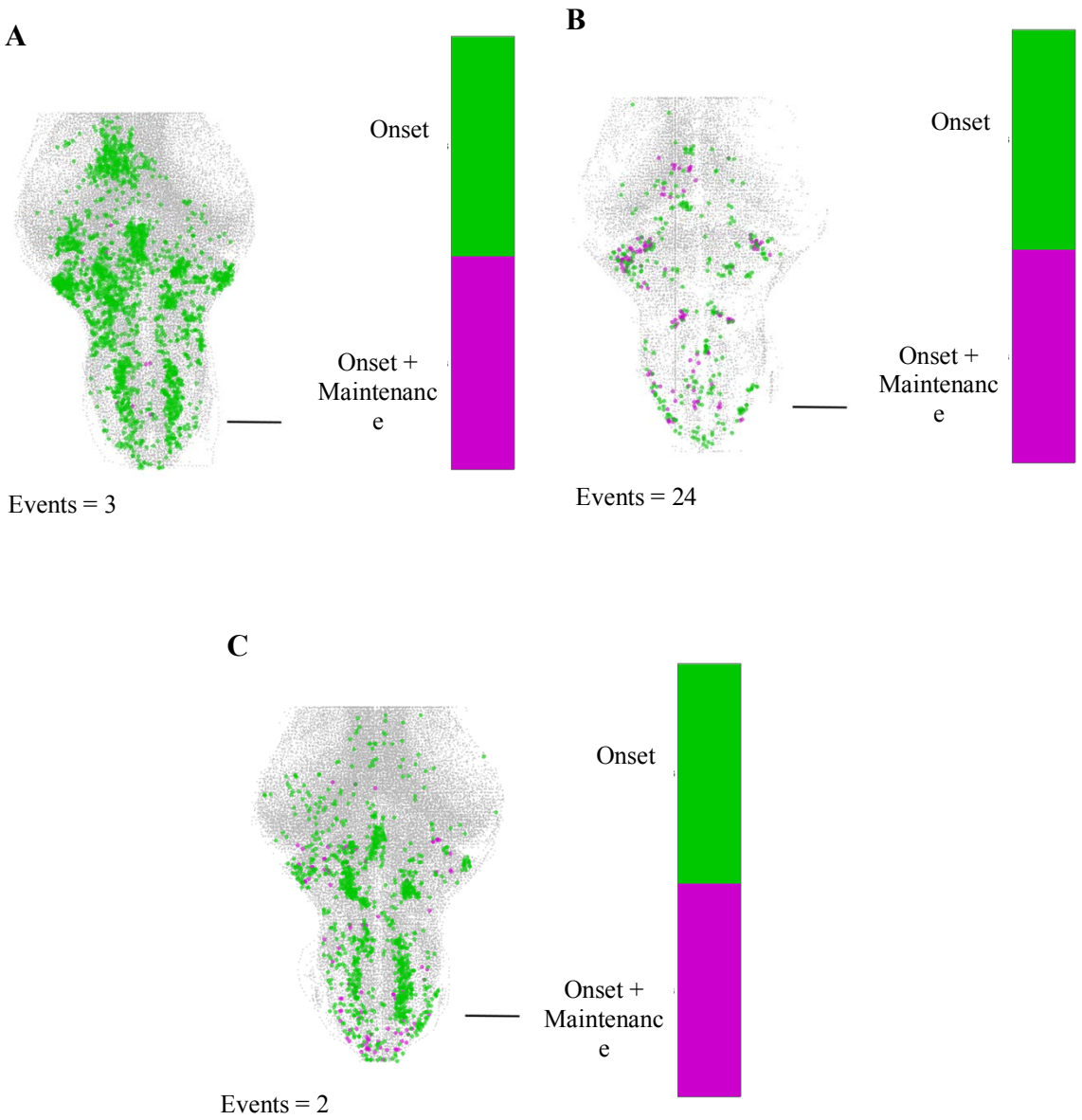

Figure 6.9: DT brains showing a continuum between onset and swimming components in the onset neurons. The activity in onset neurons in all the nuclei appear in a continuum from onset to swimming. Fish in (A), (B) and (C) had 3, 24 and 2 swim onset events respectively. The distribution of identification confidence (a_1+a_2) for onset and swim maintenance was used to identify the onset and swim maintenance contribution of the onset neurons. The neurons are accordingly color-coded for their contribution to onset (green) and onset + swim maintenance (magenta) in DT. Scale bar is 100 µm.

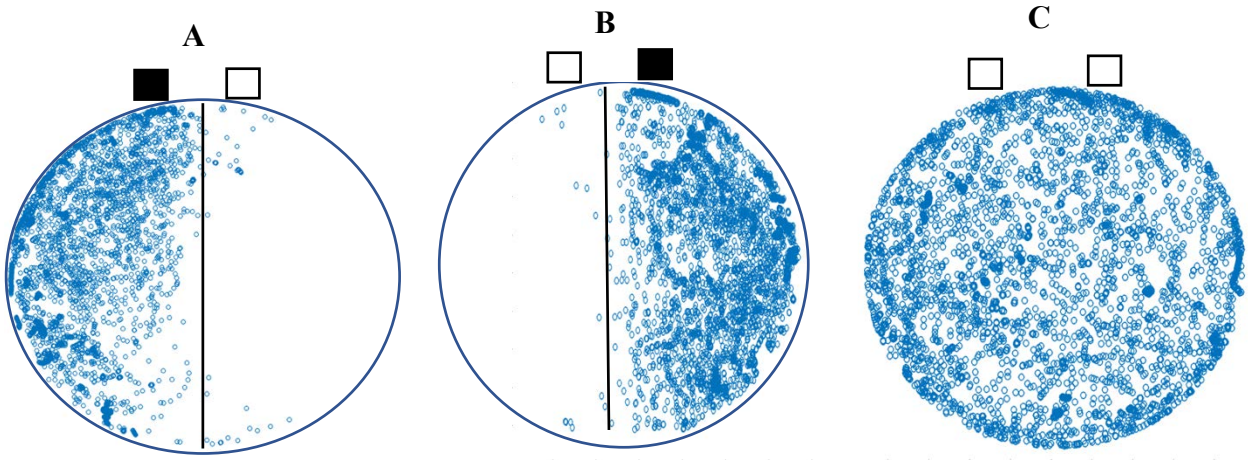

Figure 6.10: DT shows negative phototaxis. (A) and (B) show preference of 21 dpf DT larvae to the dark partition in a phototaxis assay. 5 fish per Petri dish were used in the assay. Their positions in a 20 minutes interval is represented here. The colored box on the top indicates whether the partition was dark or lit. The vertical bar represents the partition between the dark and lit halves of the arena. (C) is a control group of 5 fish, recorded for 20 minutes with no dark partition.

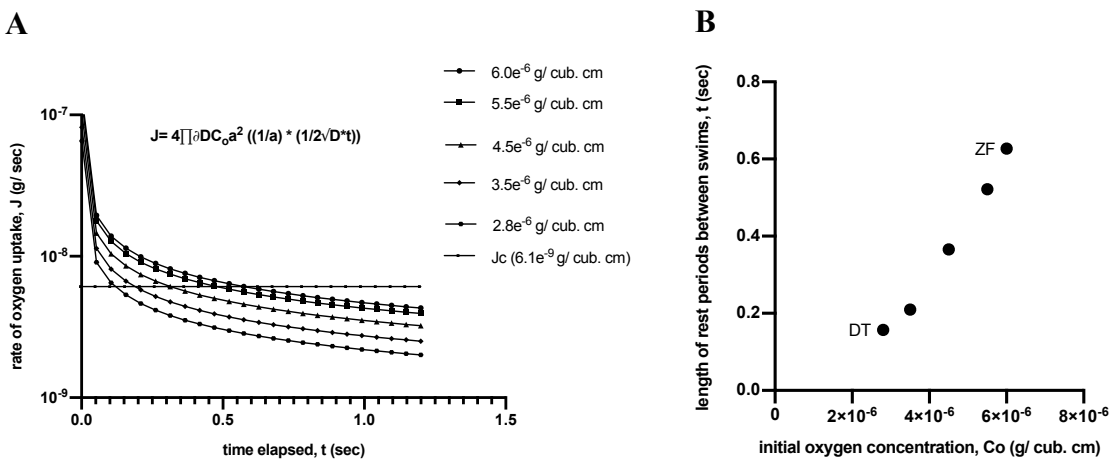

Figure 6.11: Analytical model showing lower availability of dissolved oxygen (DO) in the surrounding can lead to a shorter inactivity time (based on Weihs, 1980). (A) shows the dependence of the rate of oxygen uptake over time (t=0, when the object stops moving) on initial concentration of dissolved oxygen (DO) in the surrounding water. Horizontal line (J_c) indicates the approximation of the critical oxygen uptake rate when the larvae would have to start to swim again to replenish oxygen in its surrounding (calculated based on the inter-bout duration information available on ZF. Initial DO concentration is assumed to be the highest for ZF in this calculation). Based on the analytical model from Weihs (1980); see Chapter 5 for more info. (B) shows the length of stationary

periods attainable at various initial oxygen concentrations based on the model in (A) described by Weihs (1980).It indicates how this length would decrease with decreasing initial DO concentration, selecting a more continuous swimming pattern. Data points at the highest and lowest concentrations are labelled as ZF and DT respectively. It is for the representation of the effect of lowering DO in the surrounding on the inactivity duration. The actual DO concentration in the wild for DT and ZF are not known. A range of DO reported for ZF was chosen here for the model for simplicity (Shukla & Bhat, 2017).

Bibliography

Abdelfattah, A., Kawashima, T., Singh, A., Novak, O., Liu, H., Shuai, Y., Huang, Y.-C., Grimm, J., Patel, R., Friedrich, J., Mensh, B., Paninski, L., Macklin, J., Podgorski, K., Lin, B.-J., Chen, T.-W., Turner, G., Liu, Z., Koyama, M., … Schreiter, E. (2018). Bright and photostable chemigenetic indicators for extended in vivo voltage imaging. *BioRxiv*. https://doi.org/10.1101/436840

Adams, R. H., Sato, K., Shimada, S., Tohyama, M., Puschel, A. W., & Betz, H. (1995). Gene structure and glial expression of the glycine transporter GlyT1 in embryonic and adult rodents. *Journal of Neuroscience*, *15*(3), 2524–2532. https://doi.org/10.1523/jneurosci.15-03-02524.1995

Ahrens, M. B., Orger, M. B., Robson, D. N., Li, J. M., & Keller, P. J. (2013). Whole-brain functional imaging at cellular resolution using light-sheet microscopy. *Nature Methods*, *10*(5), 413. https://doi.org/10.1038/NMETH.2434

Andersson, L. S., Larhammar, M., Memic, F., Wootz, H., Schwochow, D., Rubin, C. J., Patra, K., Arnason, T., Wellbring, L., Hjälm, G., Imsland, F., Petersen, J. L., McCue, M. E., Mickelson, J. R., Cothran, G., Ahituv, N., Roepstorff, L., Mikko, S., Vallstedt, A., … Kullander, K. (2012). Mutations in DMRT3 affect locomotion in horses and spinal circuit function in mice. *Nature*, *488*(7413), 642–646. https://doi.org/10.1038/nature11399

Antri, M., Fénelon, K., & Dubuc, R. (2009). The contribution of synaptic inputs to sustained depolarizations in reticulospinal neurons. *Journal of Neuroscience*, *29*(4), 1140–1151. https://doi.org/10.1523/JNEUROSCI.3073-08.2009

Arrenberg, A. B., Bene, D., & Baier, H. (2009). Optical control of zebrafish behavior with halorhodopsin. *Proceedings of the National Academy of Sciences of the United States of America*, *106* (42), 17968-17973. doi.org/10.1073/pnas.0906252106

Bae, Y. K., Kani, S., Shimizu, T., Tanabe, K., Nojima, H., Kimura, Y., Higashijima, S. ichi, &

Hibi, M. (2009). Anatomy of zebrafish cerebellum and screen for mutations affecting its development. *Developmental Biology*, *330*(2), 406–426. https://doi.org/10.1016/j.ydbio.2009.04.013

Bagatto, B., Pelster, B., & Burggren, W. W. (2001). Growth and metabolism of larval zebrafish: effects of swim training. *Journal of Experimental Biology, 204* (24), 4335-4343.

Baufreton, J., Garret, M., Rivera, A., De la Calle, A., Gonon, F., Dufy, B., Bioulac, B., & Taupignon, A. I. (2003). D5 (not D1) dopamine receptors potentiate burst-firing in neurons of the subthalamic nucleus by modulating an L-type calcium conductance. *Journal of Neuroscience*, *23*(3), 816–825. https://doi.org/10.1523/jneurosci.23-03-00816.2003

Berg, H. C., & Brown, D. A. (1972). Chemotaxis in Escherichia coli analysed by three-dimensional tracking. *Nature*, *239*(5374), 500–504. https://doi.org/10.1038/239500a0

Bhattacharyya, K., McLean, D. L., & MacIver, M. A. (2017). Visual Threat Assessment and Reticulospinal Encoding of Calibrated Responses in Larval Zebrafish. *Current Biology, 27*(18), 2751-2762. https://doi.org/10.1016/j.cub.2017.08.012

Boehrer, B., & Schultze, M. (2008). Stratification of lakes. *Reviews of Geophysics*, *46*(2), 1–27. https://doi.org/10.1029/2006RG000210

Borla, M. A., Palecek, B., Budick, S., & O'Malley, D. M. (2002). Prey capture by larval zebrafish: Evidence for fine axial motor control. *Brain, Behavior and Evolution*, *60*(4), 207–229. https://doi.org/10.1159/000066699

Bouvier, J., Caggiano, V., Leiras, R., Balueva, K., Fuchs, A., & Correspondence, O. K. (2015). Descending Command Neurons in the Brainstem that Halt Locomotion. *Cell*, *163*, 1191–1203. https://doi.org/10.1016/j.cell.2015.10.074

Brett, J. R. (1964). The Respiratory Metabolism and Swimming Performance of Young Sockeye Salmon. *Journal of the Fisheries Research Board of Canada*, *21*(5), 1183–1226. https://doi.org/10.1139/f64-103

Britz, R., & Conway, K. W. (2009). Osteology of paedocypris, a miniature and highly developmentally truncated fish (Teleostei: Ostariophysi: Cyprinidae). *Journal of Morphology*, *270*(4), 389–412. https://doi.org/10.1002/jmor.10698

Buchanan, J., & Grillner, S. (1987). Newly identified "glutamate interneurons" and their role in locomotion in the lamprey spinal cord. *Science*, *236*(4799), 312–314. https://doi.org/10.1126/science.3563512

Budick, S. A., & O'Malley, D. M. (2000). Locomotion of larval zebrafish. *The Journal of Experimental Biology*, *203*, 2565–2579. http://jeb.biologists.org/content/jexbio/203/17/2565.full.pdf

Bumbarger, D. J., Riebesell, M., Rödelsperger, C., & Sommer, R. J. (2013). System-wide rewiring underlies behavioral differences in predatory and bacterial-feeding nematodes. *Cell*, *152*(1–2), 109–119. https://doi.org/10.1016/j.cell.2012.12.013

Burgess, H. A., & Granato, M. (2007). Sensorimotor Gating in Larval Zebrafish. *Journal of Neuroscience, 27*(18), 4984-4994. https://doi.org/10.1523/JNEUROSCI.0615-07.2007

Capelli, P., Pivetta, C., Esposito, M. S., & Arber, S. (2017). Locomotor speed control circuits in the caudal brainstem. *Nature*, *551*(7680), 373–377. https://doi.org/10.1038/nature24064

Cartner, S. C., Eisen, J. S., Farmer, S. C., Guillemin, K. J., Kent, M. J., & Sanders, G. E. (2020). The Zebrafish in Biomedical Research: Biology, Husbandry, Diseases, and Research Applications. *Academic Press* (first edition: August 2019).

Chen, T.-W., Wardill, T. J., Sun, Y., Pulver, S. R., Renninger, S. L., Baohan, A., Schreiter, E. R., Kerr, R. A., Orger, M. B., Jayaraman, V., Looger, L. L., Svoboda, K., & Kim, D. S. (2013). Ultra-sensitive fluorescent proteins for imaging neuronal activity. *Nature, 499*(7458), 295-300.

Childress, J. J., & Seibel, A. B. (1997). Life at Stable low oxygen levels: Adaptations of animals to oceanic oxygen minimum layers. *Journal of Experimental Biology*, *201*, 1223–1232.

Chklovskii, D. B., Schikorski, T., & Stevens, C. F. (2002). Wiring optimization in cortical circuits. *Neuron*, *34*(3), 341–347. https://doi.org/10.1016/S0896-6273(02)00679-7

Dadarlat, M. C., & Stryker, M. P. (2017). Locomotion enhances neural encoding of visual stimuli in mouse V1. *Journal of Neuroscience*, *37*(14), 3764–3775. https://doi.org/10.1523/JNEUROSCI.2728-16.2017

Dale, N., & Gilday, D. (1996). Regulation of rhythmic movements by purinergic neurotransmitters in frog embryos. *Nature*, *383*(6597), 259–263. https://doi.org/10.1038/383259a0

Darnton, N. C., Turner, L., Rojevsky, S., & Berg, H. C. (2007). On torque and tumbling in swimming Escherichia coli. *Journal of Bacteriology*, *189*(5), 1756–1764. https://doi.org/10.1128/JB.01501-06

Davis, J. C. (1975). Minimal Dissolved Oxygen Requirements of Aquatic Life with Emphasis on Canadian Species: a Review. *Journal of the Fisheries Research Board of Canada*, *32*(12), 2295–2332. https://doi.org/10.1139/f75-268

Denton, E. J., & Marshall, N. B. (1958). The buoyancy of bathypelagic fishes without a gas-filled swimbladder. *Journal of the Marine Biological Association of the United Kingdom*, *37*(3), 753–767. https://doi.org/10.1017/S0025315400005750

Domenici, P., Steffensen, J. F., & Batty, R. S. (2000). The effect of progressive hypoxia on swimming activity and schooling in Atlantic herring. *Journal of Fish Biology*, *57*(6), 1526–1538. https://doi.org/10.1006/jfbi.2000.1413

Dreosti, E., Lopes, G., Kampff, A. R., & Wilson, S. W. (2015). Development of social behavior in young zebrafish. *Frontiers in Neural Circuits*, *9*, 39. https://doi.org/10.3389/fncir.2015.00039

Dunn, T. W., Gebhardt, C., Naumann, E. A., Riegler, C., Ahrens, M. B., Engert, F., & Del Bene, F. (2016). Neural Circuits Underlying Visually Evoked Escapes in Larval Zebrafish.

Neuron, *89*(3), 613–628. https://doi.org/10.1016/j.neuron.2015.12.021

Dunn, T. W., Mu, Y., Narayan, S., Randlett, O., Naumann, E. A., Yang, C. T., Schier, A. F., Freeman, J., Engert, F., & Ahrens, M. B. (2016). Brain-wide mapping of neural activity controlling zebrafish exploratory locomotion. *ELife*, *5*, 1–29. https://doi.org/10.7554/eLife.12741

Edwards, D. H., Heitler, W. J., & Krasne, F. B. (1999). Fifty years of a command neuron: The neurobiology of escape behavior in the crayfish. *Trends in Neurosciences,* 22(4), 153–161. Elsevier Ltd. https://doi.org/10.1016/S0166-2236(98)01340-X

Fero, Kandice Yokogawa, T., & Burgess, H. A. (2011). Zebrafish Models in Neurobehavioral Research. *NeuroMethods* 52(3). https://doi.org/10.1007/978-1-60761-922-2

Grätsch, S., Auclair, F., Demers, O., Auguste, E., Hanna, A., Büschges, A., & Dubuc, R. (2019). A brainstem neural substrate for stopping locomotion. *Journal of Neuroscience*, *39*(6), 1044–1057. https://doi.org/10.1523/JNEUROSCI.1992-18.2018

Green, M. H., Ho, R. K., & Hale, M. E. (2011). Movement and function of the pectoral fins of the larval zebrafish (*Danio rerio*) during slow swimming. *Journal of Experimental Biology*, *214*(18), 3111–3123. https://doi.org/10.1242/jeb.057497

Green, Matthew H, Curet, O. M., Patankar, N. A., & Hale, M. E. (2013). Fluid dynamics of the larval zebrafish pectoral fin and the role of fin bending in fluid transport. *Bioinspiration & Biomimetics, 8*, 16002–16013. https://doi.org/10.1088/1748-3182/8/1/016002

Grillner, S., & Robertson, B. (2016). The Basal Ganglia Over 500 Million Years. In *Current Biology.* 26(20), 1088–R1100). Cell Press. https://doi.org/10.1016/j.cub.2016.06.041

Higashijima, S. I., Mandel, G., & Fetcho, J. R. (2004). Distribution of prospective glutamatergic, glycinergic, and gabaergic neurons in embryonic and larval zebrafish. *Journal of Comparative Neurology*, *480*(1), 1–8. https://doi.org/10.1002/cne.20278

Hikosaka, O., & Wurtz, R. H. (1985). Modification of saccadic eye movements by GABA-

related substances. II. Effects of muscimol in monkey substantia nigra pars reticulata. *Journal of Neurophysiology*, *53*(1), 292–308. https://doi.org/10.1152/jn.1985.53.1.292

Freeman, J., Vladimirov, N., Kawashima, T., Mu, Y., Sofroniew, N. J., Bennett, D. V., Rosen, J., Yang, C. T., Looger, L. L., & Ahrens, M. B. (2014). Mapping brain activity at scale with cluster computing. *Nature Methods*, *11*(9), 941–950. https://doi.org/10.1038/nmeth.3041

Josset, N., Roussel, M., Lemieux, M., Lafrance-Zoubga, D., Rastqar, A., & Bretzner, F. (2018). Distinct Contributions of Mesencephalic Locomotor Region Nuclei to Locomotor Control in the Freely Behaving Mouse. *Current Biology*, *28*(6), 884-901.e3. https://doi.org/10.1016/j.cub.2018.02.007

Juvin, L., Grätsch, S., Trillaud-Doppia, E., Gariépy, J. F., Büschges, A., & Dubuc, R. (2016). A Specific Population of Reticulospinal Neurons Controls the Termination of Locomotion. *Cell Reports*, *15*(11), 2377–2386. https://doi.org/10.1016/j.celrep.2016.05.029

Kadobianskyi, M., Schulze, L., Schuelke, M., & Judkewitz, B. (2019) Hybrid genome assembly and annotation of Danionella translucida, a transparent fish with the smallest known vertebrate brain. *BioRxiv*. https://doi.org/10.1101/539692

Kaneko, M., Fu, Y., & Stryker, M. P. (2017). Locomotion induces stimulus-specific response enhancement in adult visual cortex. *Journal of Neuroscience*, *37*(13), 3532–3543. https://doi.org/10.1523/JNEUROSCI.3760-16.2017

Katz, P. S., & Hale, M. E. (2017). Evolution of Motor Systems. Neurobiology of Motor Control: Fundamental Concepts and New Directions. *John Wiley and Sons, Inc.* (first edition: 2017). https://doi.org/10.1002/9781118873397.ch6

Kimmel, C. B., Powell, S. L., & Metcalfe, W. K. (1982). Brain neurons which project to the spinal cord in young larvae of the zebrafish. *Journal of Comparative Neurology*, *205*(2), 112–127. https://doi.org/10.1002/cne.902050203

Kimura, Y., Satou, C., Fujioka, S., Shoji, W., Umeda, K., Ishizuka, T., Yawo, H., & Higashijima, S. (2013). Hindbrain V2a Neurons in the Excitation of Spinal Locomotor Circuits during Zebrafish Swimming. *Current Biology*, *23*(10), 843–849. https://doi.org/10.1016/J.CUB.2013.03.066

Koyama, M., Kinkhabwala, A., Satou, C., Higashijima, S. I., & Fetcho, J. (2011). Mapping a sensory-motor network onto a structural and functional ground plan in the hindbrain. *Proceedings of the National Academy of Sciences of the United States of America*, *108*(3), 1170–1175. https://doi.org/10.1073/pnas.1012189108

Kullander, K., Butt, S. J. B., Lebret, J. M., Lundfald, L., Restrepo, C. E., Rydström, A., Klein, R., & Kiehn, O. (2003). Role of EphA4 and EphrinB3 in local neuronal circuits that control walking. *Science*, *299*(5614), 1889–1892. https://doi.org/10.1126/science.1079641

Li, W. C., Soffe, S. R., Wolf, E., & Roberts, A. (2006). Persistent responses to brief stimuli: Feedback excitation among brainstem neurons. *Journal of Neuroscience*, *26*(15), 4026–4035. https://doi.org/10.1523/JNEUROSCI.4727-05.2006

Lin, C., & Strausfeld, N. J. (2012). Visual inputs to the mushroom body calyces of the whirligig beetle Dineutus sublineatus: Modality switching in an insect. *The Journal of Comparative Neurology*, *520*(12), Spc1–Spc1. https://doi.org/10.1002/cne.23158

Marques, J. C., Lackner, S., Félix, R., & Orger, M. B. (2018). Structure of the Zebrafish Locomotor Repertoire Revealed with Unsupervised Behavioral Clustering. *Current Biology*, *28*(2), 181-195.e5. https://doi.org/10.1016/j.cub.2017.12.002

Martins, E. P., & Bhat, A. (2014). Population-level personalities in zebrafish: aggression-boldness across but not within populations. *Behavioral Ecology*, *25*(2), 368–373. https://doi.org/10.1093/beheco/aru007

McCune, A. R., & Carlson, R. L. (2004). Twenty ways to lose your bladder: Common natural mutants in zebrafish and widespread convergence of swim bladder loss among teleost fishes. *Evolution and Development*, *6*(4), 246–259. https://doi.org/10.1111/j.1525-142X.2004.04030.x

McElligott, M. B., & O'Malley, D. M. (2005). Prey tracking by larval zebrafish: Axial kinematics and visual control. *Brain, Behavior and Evolution*, *66*(3), 177–196. https://doi.org/10.1159/000087158

Mclean, D. L., Fan, J., Higashijima, S.-I., Hale, M. E., & Fetcho, J. R. (2007). *LETTERS A topographic map of recruitment in spinal cord*. *446*. https://doi.org/10.1038/nature05588

Ménard, A., & Grillner, S. (2008). Diencephalic Locomotor Region in the Lamprey—Afferents and Efferent Control. *Journal of Neurophysiology*, *100*(3), 1343–1353. https://doi.org/10.1152/jn.01128.2007

Migault, G., Van Der Plas, T. L., Trentesaux, H., Panier, T., Candelier, R. L., Emi Proville, R., Englitz, B., Debr, G., & Bormuth, V. (2018). Whole-Brain Calcium Imaging during Physiological Vestibular Stimulation in Larval Zebrafish Article Whole-Brain Calcium Imaging during Physiological Vestibular Stimulation in Larval Zebrafish. *Current Biology*, *28*, 3723–3735. https://doi.org/10.1016/j.cub.2018.10.017

Morisset, V., & Nagy, F. (1999). Ionic basis for plateau potentials in deep dorsal horn neurons of the rat spinal cord. *Journal of Neuroscience*, *19*(17), 7309–7316. https://doi.org/10.1523/JNEUROSCI.19-17-07309.1999

Mueller, K. P., & Neuhauss, S. C. F. (2014). Sunscreen for Fish: Co-Option of UV Light Protection for Camouflage. *PLoS ONE*, *9*(1), e87372. https://doi.org/10.1371/journal.pone.0087372

Müller, U. K., & Van Leeuwen, J. L. (2004). Swimming of larval zebrafish: Ontogeny of body waves and implications for locomotory development. *Journal of Experimental Biology*, *207*(5), 853–868. https://doi.org/10.1242/jeb.00821

Nair, A., Nguyen, C., & McHenry, M. J. (2017). A faster escape does not enhance survival in zebrafish larvae. *Proceedings of the Royal Society B: Biological Sciences*, *284*(1852). https://doi.org/10.1098/rspb.2017.0359

Newcomb, J. M., Sakurai, A., Lillvis, J. L., Gunaratne, C. A., & Katz, P. S. (2012). Homology and homoplasy of swimming behaviors and neural circuits in the Nudipleura (Mollusca, Gastropoda, Opisthobranchia). *Proceedings of the National Academy of Sciences of the United States of America,* 109(1), 10669–10676). National Academy of Sciences. https://doi.org/10.1073/pnas.1201877109

Niell, C. M., & Stryker, M. P. (2010). Modulation of Visual Responses by Behavioral State in Mouse Visual Cortex. *Neuron*, *65*(4), 472–479. https://doi.org/10.1016/j.neuron.2010.01.033

Orger, M. B., & De Polavieja, G. G. (2017). NE40CH06-Orger Zebrafish Behavior: Opportunities and Challenges. *Annu. Rev. Neurosci*, *40*, 125–147. https://doi.org/10.1146/annurev-neuro-071714

Orger, M. B., Kampff, A. R., Severi, K. E., Bollmann, J. H., & Engert, F. (2008). *Control of visually guided behavior by distinct populations of spinal projection neurons*. *11*(3), 327–333. https://doi.org/10.1038/nn2048

Oswald, M. E., Singer, M., & Robison, B. D. (2013). The Quantitative Genetic Architecture of the Bold-Shy Continuum in Zebrafish, *Danio rerio*. *PLoS ONE*, *8*(7), e68828. https://doi.org/10.1371/journal.pone.0068828

Parichy, D. M. (2015). Advancing biology through a deeper understanding of zebrafish ecology and evolution. *ELife*, *4*. https://doi.org/10.7554/eLife.05635

Parsons, G. R., & Carlson, J. K. (1998). Physiological and behavioral responses to hypoxia in the bonnethead shark, Sphyrna tiburo: routine swimming and respiratory regulation. *Fish Physiology and Biochemistry*, *19*.

Paul, D. H. (1991). Pedigrees of neurobehavioral circuits: Tracing the evolution of novel behaviors by comparing motor patterns, muscles, and neurons in members of related taxa. *Brain, Behavior and Evolution*, *38*(4–5), 226–239. https://doi.org/10.1159/000114390

Penalva, A., Bedke, J., Cook, E. S. B., Barrios, J. P., Bertram, E. P. L., & Douglass, A. D.

(2018). Establishment of the miniature fish species *Danionella translucida* as a genetically and optically tractable neuroscience model. *BioRxiv*. https://doi.org/10.1101/444026

Perrins, R., Walford, A., & Roberts, A. (2002). Sensory Activation and Role of Inhibitory Reticulospinal Neurons that Stop Swimming in Hatchling Frog Tadpoles. *Journal of Neuroscience*, *22*(10), 4229–4240. https://doi.org/10.1523/jneurosci.22-10-04229.2002

Pujala, A., & Koyama, M. (2019). Chronology-based architecture of descending circuits that underlie the development of locomotor repertoire after birth. *ELife*, *8*. https://doi.org/10.7554/eLife.42135

Raff, R. A. (2000). Evo-devo: The evolution of a new discipline. *Nature Reviews Genetics*, *1*(1), 74–79. https://doi.org/10.1038/35049594

Randlett, O., Wee, C. L., Naumann, E. A., Nnaemeka, O., Schoppik, D., Fitzgerald, J. E., Portugues, R., Lacoste, A. M. B., Riegler, C., Engert, F., & Schier, A. F. (2015). Whole-brain activity mapping onto a zebrafish brain atlas. *Nature Methods*, *12*(11), 1039–1046. https://doi.org/10.1038/nmeth.3581

Roberts, T. R. (1986). *Danionella translucida*, a new genus and species of cyprinid fish from Burma, one of the smallest living vertebrates. *Environmental Biology of Fishes*, *16*(4), 231–241. https://doi.org/10.1007/BF00842977

Robison, B. D., & Rowland, W. (2005). A potential model system for studying the genetics of domestication: behavioral variation among wild and domesticated strains of zebra danio (*Danio rerio*). *Canadian Journal of Fisheries and Aquatic Sciences*, *62*(9), 2046–2054. https://doi.org/10.1139/f05-118

Roseberry, T. K., Lee, A. M., Lalive, A. L., Wilbrecht, L., Bonci, A., & Kreitzer, A. C. (2016). Cell-Type-Specific Control of Brainstem Locomotor Circuits by Basal Ganglia. *Cell*, *164*(3), 526–537. https://doi.org/10.1016/j.cell.2015.12.037

Rovainen, C. M. (1967). Physiological and anatomical studies on large neurons of central nervous system of the sea lamprey (Petromyzon marinus). I. Müller and Mauthner cells.

Journal of Neurophysiology, *30*(5), 1000–1023. https://doi.org/10.1152/jn.1967.30.5.1000

Rüber, L., Kottelat, M., Tan, H. H., Ng, P. K. L., & Britz, R. (2007). Evolution of miniaturization and the phylogenetic position of Paedocypris, comprising the world's smallest vertebrate. *BMC Evolutionary Biology*, *7*(1), 38. https://doi.org/10.1186/1471-2148-7-38

Ryczko, D., & Dubuc, R. (2013). The Multifunctional Mesencephalic Locomotor Region. *Current Pharmaceutical Design*, *19*(24), 4448–4470. https://doi.org/10.2174/1381612811319240011

Ryczko, D., Cone, J. J., Alpert, M. H., Goetz, L., Auclair, F., Dubé, C., Parent, M., Roitman, M. F., Alford, S., & Dubuc, R. (2016). A descending dopamine pathway conserved from basal vertebrates to mammals. *Proceedings of the National Academy of Sciences of the United States of America*, *113*(17), E2440–E2449. https://doi.org/10.1073/pnas.1600684113

Ryczko, D., Grätsch, S., Auclair, F., Dubé, C., Bergeron, S., Alpert, M. H., Cone, J. J., Roitman, M. F., Alford, S., & Dubuc, R. (2013). Forebrain dopamine neurons project down to a brainstem region controlling locomotion. *Proceedings of the National Academy of Sciences of the United States of America*, *110*(34), E3235–E3242. https://doi.org/10.1073/pnas.1301125110

Sakurai, A., & Katz, P. S. (2017). Artificial Synaptic Rewiring Demonstrates that Distinct Neural Circuit Configurations Underlie Homologous Behaviors. *Current Biology*, *27*(12), 1721-1734.e3. https://doi.org/10.1016/J.CUB.2017.05.016

Schulze, L., Henninger, J., Kadobianskyi, M., Chaigne, T., Faustino, A. I., Hakiy, N., Albadri, S., Schuelke, M., Maler, L., Del Bene, F., & Judkewitz, B. (2018). Transparent Danionella translucida as a genetically tractable vertebrate brain model. *Nature Methods*, *15*(11), 977–983. https://doi.org/10.1038/s41592-018-0144-6

Severi, K. E., Böhm, U. L., & Wyart, C. (2018). Investigation of hindbrain activity during

active locomotion reveals inhibitory neurons involved in sensorimotor processing. *Scientific Reports*, *8*(1), 13615. https://doi.org/10.1038/s41598-018-31968-4

Severi, K. E., Portugues, R., Marques, J. C., O'Malley, D. M., Orger, M. B., & Engert, F. (2014). Neural Control and Modulation of Swimming Speed in the Larval Zebrafish. *Neuron*, *83*(3), 692–707. https://doi.org/10.1016/j.neuron.2014.06.032

Sharma, S., Kim, L. H., Mayr, K. A., Elliott, D. A., & Whelan, P. J. (2018). Parallel descending dopaminergic connectivity of A13 cells to the brainstem locomotor centers. *Scientific Reports*, *8*(1), 1–15. https://doi.org/10.1038/s41598-018-25908-5

Shukla, R., & Bhat, A. (2017). Morphological divergences and ecological correlates among wild populations of zebrafish (*Danio rerio*). *Environmental Biology of Fishes*, *100*(3), 251–264. https://doi.org/10.1007/s10641-017-0576-3

Smit, H., Amelink-Koutstaal, J. M., Vijverberg, J., & Von Vaupel-Klein, J. C. (1971). Oxygen consumption and efficiency of swimming goldfish. *Comparative Biochemistry and Physiology -- Part A: Physiology*, *39*(1), 1–28. https://doi.org/10.1016/0300-9629(71)90343-4

Song, J., Dahlberg, E., & El Manira, A. (2018). V2a interneuron diversity tailors spinal circuit organization to control the vigor of locomotor movements. *Nature Communications*, *9*(1), 1–14. https://doi.org/10.1038/s41467-018-05827-9

Spence, R., Gerlach, G., Lawrence, C., & Smith, C. (2008). The behaviour and ecology of the zebrafish, *Danio rerio*. *Biological Reviews*, *83*(1), 13–34. https://doi.org/10.1111/j.1469-185X.2007.00030.x

Sun, F., Zeng, J., Jing, M., Zhou, J., Feng, J., Owen, S. F., Luo, Y., Li, F., Wang, H., Yamaguchi, T., Yong, Z., Gao, Y., Peng, W., Wang, L., Zhang, S., Du, J., Lin, D., Xu, M., Kreitzer, A. C., … Li, Y. (2018). A Genetically Encoded Fluorescent Sensor Enables Rapid and Specific Detection of Dopamine in Flies, Fish, and Mice. *Cell*, *174*(2), 481-496. https://doi.org/10.1016/j.cell.2018.06.042

Takakusaki, K., Kohyama, J., & Matsuyama, K. (2003). Medullary reticulospinal tract mediating a generalized motor inhibition in cats: III. Functional organization of spinal interneurons in the lower lumbar segments. *Neuroscience*, *121*(3), 731–746. https://doi.org/10.1016/S0306-4522(03)00542-6

Thiele, T. R., Donovan, J. C., & Baier, H. (2014). Descending Control of Swim Posture by a Midbrain Nucleus in Zebrafish. *Neuron*, *83*(3), 679–691. https://doi.org/10.1016/j.neuron.2014.04.018

Thisse, C., & Thisse, B. (2008). High-resolution in situ hybridization to whole-mount zebrafish embryos. *Nature Protocols*, *3*(1), 59–69. https://doi.org/10.1038/nprot.2007.514

Tinbergen, N. (1963). Tinbergen1963.pdf. *Zeitschrift fur Tierpsychologie*, *20*, 410–433.

Torres, J. J., & Childress, J. J. (1983). Relationship of oxygen consumption to swimming speed in Euphausia pacifica 1. Effects of temperature and pressure. *Marine Biology*, *74*. http://www.polarpelagic.com/wp-content/uploads/2016/05/Torres-and-Childress-1983.pdf

Valente, A., Huang, K. H., Portugues, R., & Engert, F. (2012). Ontogeny of classical and operant learning behaviors in zebrafish. *Learning and Memory*, *19*(4), 170–177. https://doi.org/10.1101/lm.025668.112

Van Leeuwen, J. L., Voesenek, C. J., & Müller, U. K. (2015). How body torque and Strouhal number change with swimming speed and developmental stage in larval zebrafish. *Journal of the Royal Society Interface*, *12*. https://doi.org/10.1098/rsif.2015.0479

Voisin, D. L., & Nagy, F. (2001). Sustained L-type calcium currents in dissociated deep dorsal horn neurons of the rat: Characteristics and modulation. *Neuroscience*, *102*(2), 461–472. https://doi.org/10.1016/S0306-4522(00)00468-1

Wang, W. C., & McLean, D. L. (2014). Selective Responses to Tonic Descending Commands by Temporal Summation in a Spinal Motor Pool. *Neuron*, *83*(3), 708–721. https://doi.org/10.1016/j.neuron.2014.06.021

Watari, N., & Larson, R. G. (2010). The hydrodynamics of a run-and-tumble bacterium propelled by polymorphic helical flagella. *Biophysical Journal*, *98*(1), 12–17. https://doi.org/10.1016/j.bpj.2009.09.044

Webb, P. W. (1971). The swimming energetics of trout. *Journal of Experimental Biology*, *55*, 521–540.

Webb, P. W., & Weihs, D. (1986). Functional Locomotor Morphology of Early Life History Stages of Fishes. *Transactions of the American Fisheries Society*, *115*(1), 115–127. https://doi.org/10.1577/1548-8659(1986)115<115:flmoel>2.0.co;2

Weihs, D. (1973). Mechanically efficient swimming techniques for fish with negative buoyancy. *Journal of Marine Research*, *31*, 194–209.

Weihs, D. (1980). Respiration and depth control as possible reasons for swimming of northern anchovy, Engraulis mordax, yolk-sac larvae. *Fishery Bulletin*, *78*(10), 109-117. https://www.st.nmfs.noaa.gov/spo/FishBull/78-1/weihs.pdf

Weihs, D. (1980). Energetic significance of changes in swimming modes during growth of larval anchovy Engraulis mordax. *Fishery Bulletin*, *77*(3), 597–604.

Wiggin, T. D., Anderson, T. M., Eian, J., Peck, J. H., & Masino, M. A. (2012). Episodic swimming in the larval zebrafish is generated by a spatially distributed spinal network with modular functional organization. *Journal of Neurophysiology*, *108*(3), 925–934. https://doi.org/10.1152/jn.00233.2012

Zhang, H. Y., & Sillar, K. T. (2012). Short-term memory of motor network performance via activity-dependent potentiation of Na +/K + pump function. *Current Biology*, *22*(6), 526–531. https://doi.org/10.1016/j.cub.2012.01.058

Annex #1

In the following annex, you will find a book chapter prepared for publication in: The laboratory fish: Biology, Husbandry, and Research Applications of the most used species in research (book chapter, *Elsevier*, 2020).

The chapter covers the research applications of *Danionella translucida* in neuroscience, developmental biology and the evolution of genome architecture. Moreover, it provides a documentation on breeding and husbandry of the fish species, along with notes on its natural history.

† Book chapter being submitted to: *The laboratory fish: Biology, Husbandry, and Research Applications of the most used species in research* (2020), Elsevier publication.

Danionella translucida, a tankful of new opportunities

Gokul Rajan, Karine Duroure and Filippo Del Bene

Abstract (100-150 words)

Danionella translucida (DT) are cyprinid fish with the smallest known vertebrate brain, a small transparent body and a partially open cranium. They are also very closely related to the more popular genetic model zebrafish. This makes the adaptability of established genetic tools for transgenesis and mutagenesis easier. These features, along with a diverse behavioral repertoire make them an interesting model organism in neuroscience to investigate complex behaviors. In addition to neuroscience, they can also be valuable model in developmental and evolutionary biology. Here, we describe the biology and ecology of this fish with an emphasis on the research questions that are made more accessible with this new fish model. We also report the husbandry and breeding practices used in our laboratory which can make it easier for other laboratories to house this fish species.

Keywords (5-10 words): *Danionella translucida*, miniaturization, neuroscience, behaviors, development, evolution, husbandry, breeding

Biology and ecology of *Danionella translucida*

Danionella translucia (DT) are cyprinid fish belonging to the Danioninae subfamily, the same group of fish to which the popular model organism zebrafish (ZF) belongs. The adults of this species measure only 10-12 mm in length as seen in figure 1.1. DT was first reported by Roberts (1986) from the roots of floating aquatic plants in Myanmar. They were found in shallow (maximum 1 m deep), slow flowing streams in the Pegu Division of Myanmar. Some other fishes collected from this site included other cyprinids – *Danio* and *Microrasbora*, and other fishes like *Hara* and *Oryzias*.

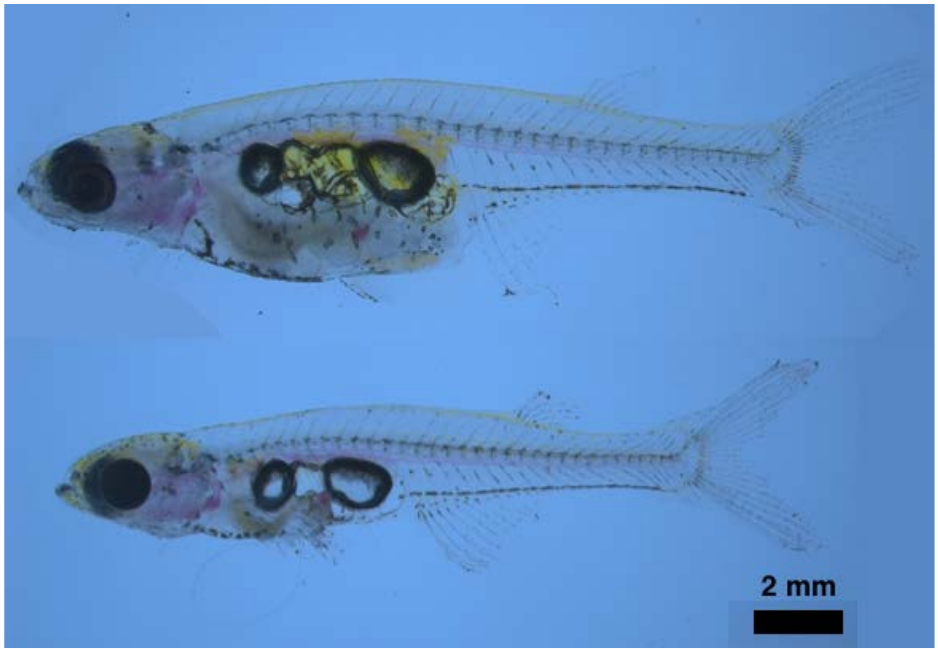

Figure 1.1: 11-month-old adult female and male *Danionella translucida*.

Both DT and ZF are found in the freshwaters of the tropical regions in the South-East Asia. A comparison of recent reported sightings of ZF and DT based on Parichy (2015) and Roberts (1986) respectively is shown in figure 1.2. DT share the unique features of danionins which include a large indentation in the medial margin of mandibles (Howes 1979, as cited in Roberts 1986), longer anal fin and a higher number of caudal vertebrae when compared to abdominal vertebrae. Their reduced adult size makes them an interesting candidate model organism. This reduction in size is a result of miniaturization, a developmental phenomenon observed in at

least 36 species of Cyprinidae (Kottelat et al, 2006). It is suggested that this phenomenon might have evolved independently several times in the cyprinid family (Ruber *et al.*, 2007). Some of these miniature fish show developmental truncation and DT is one of them. Among these, *D. translucida* along with *Danionella mirifa* and *Paedocypris* are some of the most truncated fish (Britz & Conway 2009). They have a two chambered swim bladder with the anterior and posterior chambers widely separated. Wild-type DT has very little pigmentation except in the eyes. More melanophores are present on the ventral side compared to the dorsal side where the few melanophores are mostly limited to the head.

Figure 1.2: Distribution of *Danio rerio* and *Danionella translucida* in south and South-East Asia.

Neuroscience:

Larval ZF has become a very popular model organism in systems neuroscience. The popularity can be ascribed to their small size, transparency and development of tools over the years to perform genetic manipulations. One of the major advantages is the ability to image whole brain activity at single cell resolution using genetically encoded calcium indicators (GECI) (Ahrens *et al.*, 2013). By virtue of the close evolutionary relationship between ZF and DT, a lot of these genetic tools are easily transferable from the former to latter. To create a mutant lacking any pigmentation, including in the eye -- based on the fact that *tyr* gene encoding tyrosinase is involved in melanin synthesis pathway in ZF -- Schulze, Henninger *et al.* (2018) successfully used CRISPR-Cas9 genome editing technique to target *tyr* gene in DT. They have been also successful in generating a stable Tg(NeuroD:GCaMP6f) transgenic line using Tol2 mediated transgenesis technique. Moreover, Kadobianskyi *et al.* (2019) have recently published an assembled and annotated genome sequence of DT. This will aid all the future work on targeted genetic manipulations in DT.

In ZF, most studies have focused on simple behavioral questions pertaining to perception, locomotion or sensorimotor transformations of reflexive nature. It is mainly due to the fact that most complex behaviors appear in the later stages of larval development. ZF larvae start to show reliable learning at 3 weeks (Valente *et al.*, 2012). Similarly, social preference starts to appear in 3 weeks old larvae (Dreosti *et al.*, 2015). This is where the advantages of DT become more obvious. While the adults of DT are small in size and transparent, they also show a rich repertoire of behaviors. They perform visually mediated shoaling and schooling. The males also exhibit vocalization which is likely related to male-male aggression (Schulze, Henninger *et al.* 2018). Penalva *et al.* (2018) also showed socially reinforced learning in adult DT. As shown in figure 1.3, imaging of adult fish can be carried out non-invasively in moderately sedated fish embedded in agar where the gills are still free to move. This rich behavioral repertoire in adult DT combined with its small size, lack of pigmentation and the ease of transfer of genetic tools from ZF to DT makes adult DT a very favorable system to understand neuronal underpinnings of complex behaviors.

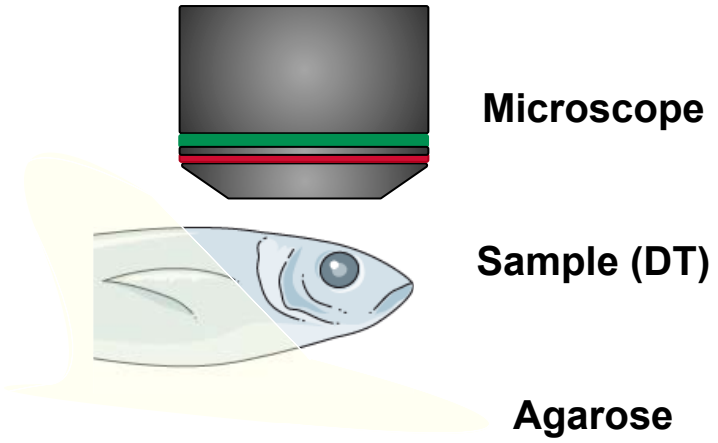

Figure 1.3: Mounting of adult *Danionella translucida* for non-invasive *in-vivo* brain imaging.

In addition to the aforementioned neurobehavioral applications in adult DT, there can be at least two other interesting applications of DT in neuroscience: 1) To study ontogeny of behaviors. In a vertebrate organism, it can be often challenging to closely follow the development of a behavior and its underlying neuronal circuit over various developmental stages in life. DT fares well here due to its small size and transparency throughout the life cycle. We can track the changes in neuronal networks as they mature. 2) To identify general principles and evolution of neuronal circuits. Given the high degree of evolutionary closeness between DT and ZF, they can be used to understand functional divergence of neuronal circuit if divergent behaviors can be identified between the two species which may or may not be a result of miniaturization in DT. As studies on ossification in *Danionella dracula* and *Paedocypris* show that most bones affected by truncation are those which appear late in the development of zebrafish, it suggests that the developmental truncation occurs later in the ontogeny of these fish species. Hence, developmentally the two species are very much comparable in early stages. This should come as an advantage to comparative studies of DT and ZF which look at the larval and juvenile stages of the two fish species. Comparatives studies following this methodology can be seen in invertebrates like Nudipleura (Newcomb *et al.*, 2012), but such studies at the level of neuronal circuits are not common in vertebrates due to the inherent difficulty of working with organisms of higher biological complexity.

Development and evolution:

The advantages of a small, non-pigmented, adult fish are not limited to neuroscience. The transparency of the fish throughout its life does offer a great opportunity to the developmental biologists to track the growth of various organs during its maturation. It also offers the advantage of studying developmental defects and other pathologies in a matured system.

On the other hand, miniaturization, which is more common among fishes, amphibians and reptiles, can lead to size reduction and structural simplification in body plan (Hanken and Wake, 1993). Previous work has suggested that miniaturization can introduce morphological novelties that can increase variability (Hanken and Wake, 1993). For instance, a number of sexually dimorphic and non-dimorphic morphological novelties have been described in DT (Britz & Conway 2009). From an organismal and evolutionary perspective, this is interesting and calls for more attention. At the genomic level, Kadobianskyi *et al.* (2019) have reported that the genome size of DT is around half of that reported for zebrafish genome and this reduction can be a result of extensive intron truncation that is observed in DT. The origin and role of introns in eukaryotes have long been a source of much speculation (Rogozin *et al.*, 2012) and DT genome can be a possible tool to investigate this.

Animal husbandry – early larval stages

It is critical to pay attention to the early stage larval fish as this is usually the period with the most mortality. We particularly pay more attention to the fish from 0 to 16 days post-fertilization (dpf). From 0 dpf to 4 dpf, we keep the larvae in incubator at 28° C. The fish is kept in E3 medium (without methylene blue). The density is maintained at a maximum of 4 clutches (~48 eggs) per 90 cm Petri plate and the E3 medium in the plates is changed every day. The incubator follows a light/dark cycle of approximately 14/10 hours.

During 4 to 16 dpf, we use a co-culture of rotifers and algae to grow the larvae. The rotifers are prepared in a 2L instant ocean (Aquastore – catalog # 342142) solution of 15 ppt concentration with 1.5 ml algae added twice a day. The rotifer system is continuously aerated using a pump. Algal stock used is RGcomplete (Planktovie – catalog # B001). To create the co-culture, we prepare an 800 ml solution (in 1L beaker) of 3.75 ppt instant ocean solution (1/4th of the salt

concentration used in the rotifer culture) along with 200 µl algae. Rotifers collected from the culture are sequentially filtered using filters of 250, 150 and 50 µm pore-size respectively (VWR, catalog # 510-0507, 510-0520, 510-0525). The filtered rotifers collected on the 50 µm filter are mixed in a 3.75 ppt solution and added to the above co-culture beaker to make a final rotifer density of ~60 rotifers/ml in a volume of 800 ml. The larvae (at most 30) at 4 dpf are added to the above beaker of rotifer-algae co-culture and maintained in this until 16 dpf. The resulting culture is maintained at room temperature (~24° C) until day 16. Figure 1.4 shows DT larvae at 10 dpf. The co-culture is checked daily, and rotifers and algae are replenished when needed based on their density. Rotifer density is maintained at ~60 rotifers/ ml. Dead algae is periodically removed and the beaker is changed occasionally when necessary.

Figure 1.4: Larval *Danionella translucida* at 10 days post-fertilization.

Animal husbandry – early stages to adulthood

At around 16 dpf, the larvae are transferred to the system water in the main fish facility. The fish are transferred to nursery tanks with filter. Maximum density at this stage is kept at 60 larvae/tank. Until 28 dpf, they remain in this tank and the water inflow is only kept very minimal (slow dripping). At 28 dpf, they are moved to adult tanks with a filter size of 800 µm and a constant stream of water inflow. In the adult tanks, the density can be at most 90. We use adult tanks of 8L volume, so the normalized density is at most 11.25 fish/L. Although it is still less than 12 fish/L as recommended for zebrafish (Castranova *et al.*, 2011), considering that the size of adult DT is less than 1/3 of ZF adult, it should be possible to accommodate more fish. We

will now discuss more about the physico-chemical parameters and the food regime in use after moving the fish into the system water of the animal house.

As most of the danionin species are found in the freshwaters of tropical and subtropical regions, they show considerable degree of similarity in terms of tolerance to physico-chemical parameters and food source. Zebrafish, for instance, can tolerate a wide range of temperatures (below 10 to 40° C), pH (6 to 10) and conductivities (10 to 271 µS/cm) in nature (Aleström *et al.*, 2019) but a narrower range of these parameters are used in the animal housing's system water. Similarly, we use a narrow range of these parameters for DT which are not very off from the values used for zebrafish husbandry. Hence, the housing systems can be shared by the two species if needed. For DT, as shown in table 1.1, the room temperature of the facility is maintained from 21 to 23° C. The temperature of the water is in the range of 25 to 28° C. The pH is balanced at 7.3±1. The conductivity of the system water can vary from 250 to 450 µS/cm. 20 g of instant ocean (aquarium systems) and 10 g $CaCl_2$ is added per 1L of system water to attain desired conductivity and pH is maintained with $NaHCO_3$. The water renewal is fixed at 10% in 24 hours. The light/dark cycle is maintained at 14/10 hours in our facility for both zebrafish and *D. translucida*.

Parameter	Range
Room temperature	20° C to 24° C
Water temperature	25° C to 28° C
pH	6.3 to 8.3
Conductivity	250 µS to 450 µS

Table 1.1: Physico-chemical parameters used for *Danionella translucida* in the animal housing.

Regarding the food, McClure *et al.*, (2006) had analyzed the gut content of 327 individual fish representing 17 populations of eight danionin species in the wild to conclude that insects were the primary source of food in these species. For DT in the laboratory setting, larval fish starting from 16 dpf are fed with regular diet of Gemma Micro 75 (Skretting, USA) (twice a day) with

occasional rotifers (three times a week). The water inlet at this point is maintained very slow with constant dripping. Once the fish are at 28 dpf, they are transferred to a feeding regime with regular Gemma Micro 150 (Skretting, USA) (twice a day) and live *Artemia* (once a day). The water inlet at this point is increased to a constant flow. Spawning, schooling and vocalization – signs of social behavior - can be seen as a proxy for a good health status of the fish.

Our system and therefore the components thereof including the tanks come from Tecniplast, France.

Breeding

DT spawn in clutches of eggs. They are also known to spawn in crevices. Hence, we add 2 to 4 silicone tubes (~ 5 cm long) in the adult tanks to aid spawning. Figure 1.5 shows an adult tank with such tubes. Supplementary video S1.1 shows a video of the same. We also observe that spawning is often initiated immediately after the first feeding cycle of *Artemia* in the morning indicating that food also may directly aid mating.

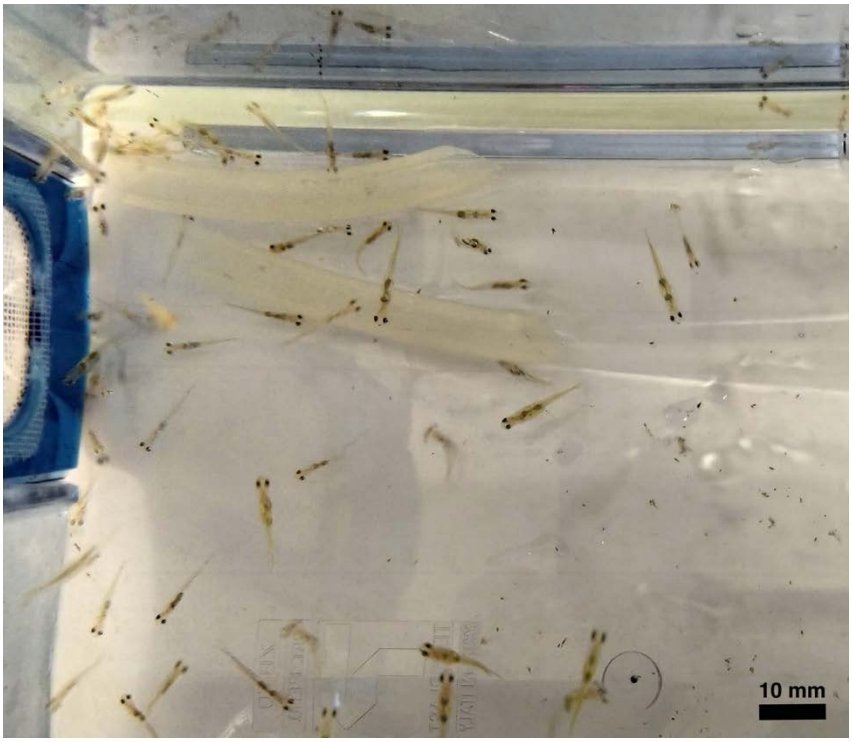

Figure 1.5: Adult *Danionella translucida* in their home tanks with two silicone tubes to aid spawning in the fish.

DT do not require special breeding tanks as they do not feed on their eggs like zebrafish. They lay eggs around the silicone tubes in their home tanks. So, the eggs can be collected at a later time of the day. We perform breeding of the fish in community in their home tanks. Mating in smaller groups have not been tried enough as with the limited number of mutants and transgenics at the moment, it was not necessary. However, we have had anecdotal success in breeding with 3 fish (both 2 males/ 1 female and 1male/ 2 females).

We have now carried out at most 3 generations of inbreeding of DT in our animal house and we have not observed any signs of inbreeding depression such as reduced fecundity or emergence of sick progenies. In fact, the 2 to 3 years old fish stocks in our facility still appear mostly healthy. Although, the egg production can decrease with age as we note below.

Although not specifically in DT, it has been observed in general that a reduction in body size is linked with a reduction in fecundity and an increase in size of the egg (Hanken & Wake, 1993; Duarte & Alcaraz, 1989). We carried out a small observational study to quantify the egg production in DT. All the housing parameters in the study are maintained at the aforementioned range and breeding details are also kept the same (number of silicone tubes = 4 per tank). We observed that 1-year-old adult DT produce on an average: 8.26 clutches/ 50 females/ day or 99.12 eggs/ 50 females/ day (at an average of 12 eggs/ clutch). Figure 1.6 shows two clutches of DT eggs. We also observed that 1-year-old DT females produced more clutches than the 2-years-old fish at 1.57 clutches/ 50 females/ day. A 1 female: 2 males sex ratio was maintained in both, 1-year and 2-years old groups. With regards to sex ratio, we had tanks with two different sex ratios in the 2-years-old group. The tanks with 1 female: 2 males ratio produced 2.62 times more clutches per day than the tank with 1 female: 1 male ratio.

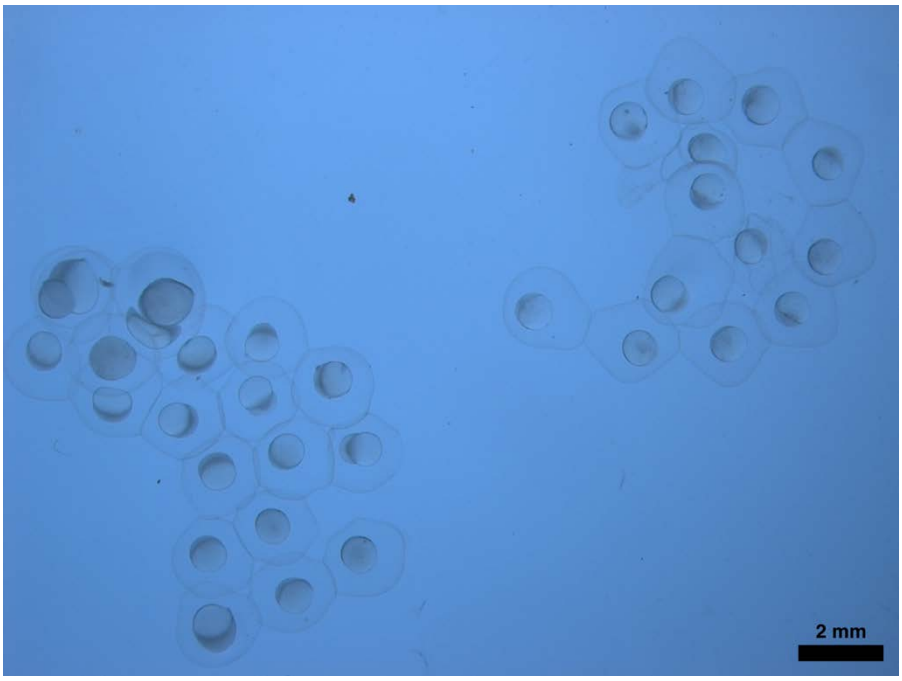

Figure 1.6: Clutches of eggs of *Danionella translucida*.

The number of eggs produced per female in DT is very low if one compares it to ZF, but this had been mostly sufficient for our purposes. The best breeding outcome of 8.26 clutches/ 50 females/ day was obtained in 1-year-old DT fish at 1 female: 2 males ratio. However, while breeding 3 fish (1 female/2 males) in a tank, we have had an almost constant production of 1 clutch/ female/ day. This might indicate that a community breeding comes at a cost of high intra-community competition to mate. So, we believe that the egg production can be eventually increased further with improvement in breeding techniques. Breeding in many smaller communities compared to one large community might be just one of the many changes that one can try.

Acknowledgements:

We thank the fish facility at Instiut Curie for their support in animal husbandry. We also extend our thanks to Judkewitz lab in Berlin for the initial stock of *Danionella translucida*.

Artwork list:

Figure 1.1: 11-month-old adult female and male *Danionella translucida*. Original image.

Figure 1.2: Distribution of *Danio rerio* and *Danionella translucida* in south and south-east Asia. Original image.

Figure 1.3: Mounting of adult *Danionella translucida* for non-invasive *in-vivo* brain imaging. Original image.

Figure 1.4: Larval *Danionella translucida* at 10 days post-fertilization. Original image.

Figure 1.5: Adult *Danionella translucida* in their home tanks with two silicone tubes to aid spawning in the fish. Original image.

Figure 1.6: Clutches of eggs of *Danionella translucida*. Original image.

Table 1.1: Physico-chemical parameters used for *Danionella translucida* in the animal housing. Original material.

Supplementary video S1.1: adult *Danionella translucida* in their home tank. (https://drive.google.com/file/d/1lqm20TLdpLe22LdsyzqzyjvG5lGL0rRg/view?usp=sharing) Original video.

References:

Ahrens, M. B., Orger, M. B., Robson, D. N., Li, J. M., & Keller, P. J. (2013). Whole-brain functional imaging at cellular resolution using light-sheet microscopy. *Nature Methods*, *10*(5), 413–420. https://doi.org/10.1038/nmeth.2434

Aleström, P., D'Angelo, L., Midtlyng, P. J., Schorderet, D. F., Schulte-Merker, S., Sohm, F., & Warner, S. (2019). Zebrafish: Housing and husbandry recommendations. *Laboratory Animals*, https://doi.org/10.1177/0023677219869037

Britz, R., & Conway, K. W. (2009). Osteology of *Paedocypris*, a miniature and highly developmentally truncated fish (Teleostei: Ostariophysi: Cyprinidae). *Journal of Morphology*, *270*(4), 389–412. https://doi.org/10.1002/jmor.10698

Castranova, D., Lawton, A., Lawrence, C., Baumann, D. P., Best, J., Coscolla, J., … Weinstein, B. M. (2011). The Effect of Stocking Densities on Reproductive Performance in Laboratory Zebrafish (*Danio rerio*). *Zebrafish, 8*(3), 141-146. https://doi.org/10.1089/zeb.2011.0688

Dreosti, E., Lopes, G., Kampff, A. R., & Wilson, S. W. (2015). Development of social behavior in young zebrafish. *Frontiers in Neural Circuits*, *9*. https://doi.org/10.3389/fncir.2015.00039

Duarte, C. M., & Alcaraz, M. (1989). To Produce Many Small or Few Large Eggs: A Size-Independent Reproductive Tactic of Fish. *Oecologia*, *80*(3), 401–404.

Hanken, J., & Wake, D. B. (1993). Miniaturization of body size: Organismal consequences and evolutionary significance. In *Annual Review of Ecology and Systematics 24*, 501–519. https://doi.org/10.1146/annurev.es.24.110193.002441

Kadobianskyi, M., Schulze, L., Schuelke, M., & Judkewitz, B. (2019). Hybrid genome assembly and annotation of Danionella translucida , a transparent fish with the smallest known vertebrate brain. *BioRxiv*. https://doi.org/10.1101/539692

Kottelat, M., Britz, R., Tan, H. H. & Witte, K. E. (2006). *Paedocypris*, a new genus of southeast Asian cyprinid fish with a remarkable sexual dimorphism, comprises the world's smallest vertebrate. Royal Society B-Biological Sciences, *273*, 895–899. doi:10.1098/rspb.2005.3419

McClure, M. M., McIntyre, P. B., & McCune, A. R. (2006). Notes on the natural diet and habitat of eight danionin fishes, including the zebrafish *Danio rerio*. *Journal of Fish Biology*, *69*(2), 553–570. https://doi.org/10.1111/j.1095-8649.2006.01125.x

Newcomb, J. M., Sakurai, A., Lillvis, J. L., Gunaratne, C. A., & Katz, P. S. (2012). Homology and homoplasy of swimming behaviors and neural circuits in the Nudipleura (Mollusca, Gastropoda, Opisthobranchia). *Proceedings of the National Academy of Sciences of the United States of America 109* (1), 10669–10676. https://doi.org/10.1073/pnas.1201877109

Parichy, D. M. (2015). The natural history of model organisms: Advancing biology through a deeper understanding of zebrafish ecology and evolution. *ELife*, *2015*(4), 1–11. https://doi.org/10.7554/eLife.05635.001

Penalva, A., Bedke, J., Cook, E. S. B., Barrios, J. P., Bertram, E. P. L., & Douglass, A. D. (2018). Establishment of the miniature fish species *Danionella translucida* as a genetically and optically tractable neuroscience model. *BioRxiv*. https://doi.org/10.1101/444026

Roberts, T. R. (1986). *Danionella translucida*, a new genus and species of cyprinid fish from Burma, one of the smallest living vertebrates. *Environmental Biology of Fishes, 16*(4), 231–241. https://doi.org/10.1007/BF00842977

Rogozin, I. B., Carmel, L., Csuros, M., & Koonin, E. V. (2012). Origin and evolution of spliceosomal introns. *Biology Direct 7*, 11. BioMed Central. https://doi.org/10.1186/1745-6150-7-11

Rüber, L., Kottelat, M., Tan, H. H., Ng, P. K. L., & Britz, R. (2007). Evolution of miniaturization and the phylogenetic position of Paedocypris, comprising the world's smallest vertebrate. *BMC Evolutionary Biology*, *7*, 38. https://doi.org/10.1186/1471-2148-7-38

Schulze, L., Henninger, J., Kadobianskyi, M., Chaigne, T., Faustino, A. I., Hakiy, N., … Judkewitz, B. (2018). Transparent *Danionella translucida* as a genetically tractable vertebrate brain model. *Nature Methods*, *15*(11), 977–983. https://doi.org/10.1038/s41592-018-0144-6

Valente, A., Huang, K. H., Portugues, R., & Engert, F. (2012). Ontogeny of classical and operant learning behaviors in zebrafish. *Learning and Memory*, *19*(4), 170–177. https://doi.org/10.1101/lm.025668.112

Annex #2

During my PhD, I also contributed to the following research work which looked at the role of a population of intertectal neurons (ITN) in binocular integration of visual cues and its importance in prey capture.

Specifically, during my PhD, I built a high-speed behavioral imaging system. On this system, I had developed behavioral assays such as tap-induced escape, loom-induced escape, opto-motor response, phototaxis and prey capture assay. Of these, prey capture assay was used in this study. The set-up comprised of a low angle LED ring light to create a dark field illumination so as to image both the ZF larvae and the prey (rotifers) simultaneously.

I performed the prey capture experiments on ITN:Gal4 zebrafish larvae expressing UAS:BoTxBLC-GFP (BoTx), a zebrafish-optimized botulinum toxin. This would silence vesicular release in the neurons expressing Gal4. As expected, the larvae showed a decrease in prey consumption when compared to the control siblings. However, when I compared the swimming kinematics between the test fish and control siblings, I observed that the test fish spent significantly less time exploring its environment. It is likely due to a weak expression of Gal4 in the spinal cord. Using these experiments, it was concluded that a loss-of-function experiment using a genetic line would be difficult to interpret because of the expression of Gal4 outside the ITN cells, specifically in the spinal cord. Hence, a more spatially targeted approach using laser-ablation was utilized in the study.

nature COMMUNICATIONS

ARTICLE

https://doi.org/10.1038/s41467-019-13484-9 OPEN

An interhemispheric neural circuit allowing binocular integration in the optic tectum

Christoph Gebhardt [1], Thomas O. Auer [1], Pedro M. Henriques[2], Gokul Rajan [1,3], Karine Duroure[1,3], Isaac H. Bianco [2,4*] & Filippo Del Bene [1,3,4*]

Binocular stereopsis requires the convergence of visual information from corresponding points in visual space seen by two different lines of sight. This may be achieved by superposition of retinal input from each eye onto the same downstream neurons via ipsi- and contralaterally projecting optic nerve fibers. Zebrafish larvae can perceive binocular cues during prey hunting but have exclusively contralateral retinotectal projections. Here we report brain activity in the tectal neuropil ipsilateral to the visually stimulated eye, despite the absence of ipsilateral retinotectal projections. This activity colocalizes with arbors of commissural neurons, termed intertectal neurons (ITNs), that connect the tectal hemispheres. ITNs are GABAergic, establish tectal synapses bilaterally and respond to small moving stimuli. ITN-ablation impairs capture swim initiation when prey is positioned in the binocular strike zone. We propose an intertectal circuit that controls execution of the prey-capture motor program following binocular localization of prey, without requiring ipsilateral retinotectal projections.

[1] Institut Curie, PSL Research University, INSERM U934, CNRS UMR3215, Paris, France. [2] Department of Neuroscience, Physiology & Pharmacology, University College London, London WC1E 6BT, UK. [3] Present address: Sorbonne Université, INSERM, CNRS, Institut de la Vision, Paris, France. [4] These authors jointly supervised: Isaac H. Bianco, Filippo Del Bene. *email: i.bianco@ucl.ac.uk; filippo.del-bene@inserm.fr

In order to feed on moving prey, predatory animals must recognize, pursue, and finally capture their target. Hunting sequences of zebrafish larvae consist of a pursuit phase that sometimes culminates in a capture maneuver[1,2]. The pursuit phase is characterized by discrete approach swims (AS) and asymmetric bouts (J-turns and high-angle turns) that enable the larva to orient toward and approach its prey[1,3–6]. Capture maneuvers consist of specific high-acceleration capture swims (also called rams) or suction feedings[1,7].

Having two forward facing eyes with a binocular field of view may enable predating animals to evaluate target distance (binocular stereopsis) and thereby increase the likelihood of successfully capturing prey. Zebrafish larvae have laterally positioned eyes resulting in a negligible binocular field of view under most behavioral conditions. However, during hunting sequences, larvae consistently converge their eyes, resulting in a substantial increase in their binocular visual field[3]. Vergence angle varies with target distance[8] and capture swims are initiated once the target is located in a stereotypic strike zone within the binocular visual field, around 500 µm directly in front of a larva[1,3,8]. Furthermore, prey capture is strongly impaired when retinal input is unilaterally removed[9]. This evidence suggests that zebrafish larvae use binocular depth cues to locate and capture prey.

A binocular stereopsis mechanism for localizing an object in a three-dimensional environment depends on visual information about corresponding object features, as viewed by each eye, converging on binocular downstream neurons. For example, in mammals, it has been suggested that this convergence is achieved by direct superposition of corresponding retinal input via ipsi- and contralaterally projecting optic nerve fibers from the two eyes[10]. However, in zebrafish larvae, retinotectal fibers project exclusively contralaterally[11]. It is thus unclear how a convergence of binocular visual information for localizing prey in the strike zone is accomplished.

The optic tectum (OT) is the main retinorecipient area in the midbrain of teleosts and is homologous to the superior colliculus (SC) in mammals. It is an important sensorimotor integrator that is essential for visually guided behaviors including predator avoidance[12] and prey capture[9,13]. The OT consists of two main areas: a synaptic neuropil and a cellular *stratum periventriculare* (SPV). The OT neuropil receives input from contralateral retinal ganglion cells (RGCs)[11] which innervate four retinorecipient layers, from superficial to deep: the *stratum opticum* (SO), the *stratum fibrosum et griseum superficiale* (SFGS), the *stratum griseum centrale* (SGC), and the *stratum album centrale* (SAC)[14,15].

In this study, we report the surprising discovery of activity in the deep layers of the tectal neuropil in response to visual stimulation of the ipsilateral eye of zebrafish larvae. We identify a population of intertectal interneurons, ITNs, that responds to visual motion and innervates both left and right OT. ITNs are GABAergic and establish synapses in the deep layers of the neuropil. Furthermore, these neurons respond to small moving spots that resemble prey of zebrafish larvae such as *Paramecia*. ITN-ablation uncovers a specific requirement of these neurons for the initiation of capture swims when prey is positioned in the binocular strike zone directly in front of the larva. We propose that ITNs are a central component of a bilateral neural circuit that integrates binocular visual information to enable localization and capture of prey, in the absence of ipsilateral retinotectal projections (IRPs).

Results

Visually evoked activity in the ipsilateral tectum. First, we wanted to know if visual information from one eye is represented in the ipsilateral tectal hemisphere, despite the lack of ipsilaterally projecting retinotectal axons. To this end, we used 2-photon microscopy to image the OT of 5 days-post-fertilization (dpf) larvae that expressed the calcium indicator GCaMP5G under control of a pan-neuronal promoter. One eye was visually stimulated with moving bars (width: 9°, speed: 20° s^{-1}, 12 angular directions spaced 30° apart) and the second eye was surgically removed prior to functional imaging to ensure monocular visual input (Fig. 1a). The absence of regenerative re-routing of retinal fibers from the remaining eye to the non-innervated tectal hemisphere after monocular enucleation was confirmed by anterograde DiO tracing (Supplementary Fig. 1). After correcting for motion artefacts, image timeseries from each larva were registered to the corresponding *z*-plane of a 5 dpf *Tg(elavl3: GCaMP5G)* reference larva. We computed average stimulus-triggered fluorescence responses for 6 anatomical subregions of the OT (SPV, deep and superficial neuropil in the ipsi- or contralateral tectal hemisphere, Fig. 1a). Consistent with fully crossed retinotectal projections in zebrafish, we observed strong calcium transients in all 3 regions of the tectum contralateral to the stimulated eye (Fig. 1b, upper three traces). Surprisingly, we also detected visually evoked responses in the tectal neuropil ipsilateral to the stimulated eye, i.e., contralateral to the enucleated eye (Fig. 1b, lowest two traces). This activity appeared confined to the neuropil as almost no response to moving bars was detected in ipsilateral periventricular neurons (PVNs) (Fig. 1b, ipsilateral SPV trace). To generate anatomical maps of stimulus-correlated activity, we used a regression-based approach[16] and, consistent with our previous observations, found highly-correlated voxels in the tectal neuropil and SPV contralateral to the stimulated eye but also within the deep laminae of the ipsilateral tectal neuropil (comprising SGC and SAC) (Fig. 1c, d).

ITNs connect the two hemispheres of the optic tectum. To explain these observations, we hypothesized that a population of commissural neurons might exist that preferentially targets the deep laminae of the tectal neuropil. Moreover, this population would likely be visual motion responsive and directly or indirectly activated by retinal afferents.

Our lab isolated a *Gal4*-expressing transgenic zebrafish line, *Gal4ic3034Tg* (referred to as *ITNGal4* hereafter), which labels a population of neurons interconnecting the two tectal hemispheres (Fig. 2a, b). Based on this anatomical feature we named the neuronal population intertectal neurons (ITNs). In addition to labeling ITNs, the *Gal4ic3034Tg* transgene is also expressed in the pineal gland, spinal cord, superficial interneurons in the OT (SINs), and sparsely in PVNs (Fig. 2a). The number of ITNs labeled in *ITNGal4, UAS:GFP* larvae varied across animals with a minimum of 22 labeled cells (12 on the right, 10 on the left) and a maximum of 48 (27 right, 21 left) (average from 18 randomly chosen larvae: 32 ITNs in total, 16 per side). This variability is likely due to variegation in transgene expression[17].

The cell bodies of ITNs are situated in two bilaterally symmetric nuclei below the OT in the mesencephalic tegmentum (Fig. 2a, lower left panel), and send their neurites dorsally, crossing the tectal commissures in ladder-like trajectories (Fig. 2a, upper left panel). ITN neurites develop concomitantly with retinal innervation of the OT: They cross the midline and arborize in the OT starting from 3.5 dpf as revealed by single ITN neurite tracing (Fig. 2c). By 4 dpf, individual ITNs form increasingly complex arborization patterns in both the ipsi- and contralateral OT neuropil (Fig. 2d). Arbors of individual ITNs localize to the deep neuropil layers, between the SGC and the SAC (Supplementary Fig. 2a, b).

2-photon imaging of ITN somata revealed that cells contralateral to the stimulated eye showed visually evoked activity in response to moving bars (Supplementary Fig. 2c, d) indicating

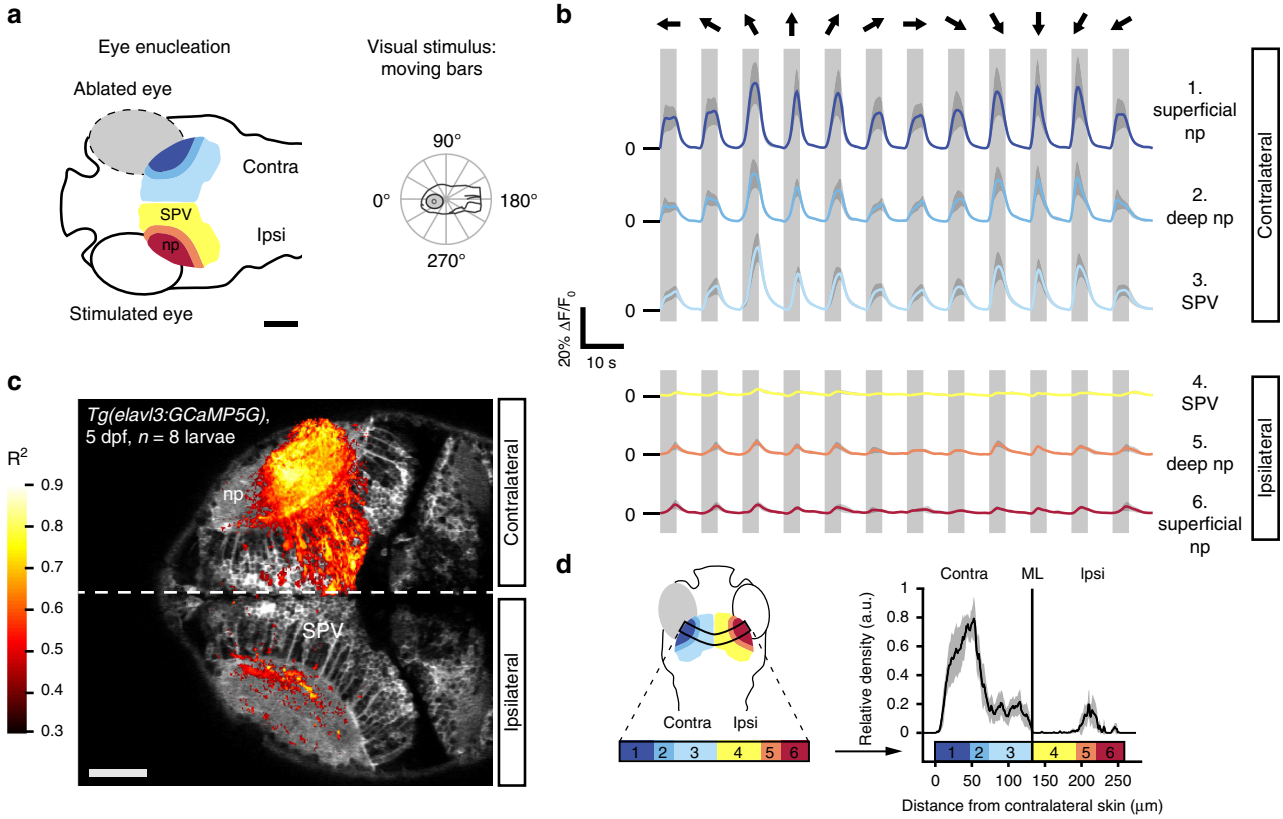

Fig. 1 Visually evoked activity in the deep neuropil of the tectal hemisphere ipsilateral to the visually stimulated eye. **a** Optic tecta of 5 days-post-fertilization (dpf) larvae expressing GCaMP5G were imaged after monocular enucleation at 3–4 dpf. The remaining eye was visually stimulated with moving bars running across the larva's field of view (bar width: 9°, speed: 20° s^{-1}, direction: randomly chosen from 12 angular directions 30° apart for each individual stimulus presentation interval, see polar plot inset). Scale bar = 100 µm (np: tectal neuropil, SPV: *stratum periventriculare*). **b** Average fluorescence modulations of all voxels in six anatomically identified zones during visual stimulation with moving bars ($n = 8$ larvae, color code: 1. dark blue = superficial contralateral neuropil, 2. blue = deep contralateral neuropil, 3. light blue = contralateral SPV, 4. yellow = ipsilateral SPV, 5. orange = deep ipsilateral neuropil, 6. red = superficial ipsilateral neuropil, dark gray shading indicates the 95% confidence intervals, light gray vertical bars indicate the stimulus interval). In addition to the expected stimulus-synchronized activity in the tectal hemisphere contralateral to the stimulated eye, visually evoked activity was also observed in the neuropil of the ipsilateral tectum. Moving bar directions for each stimulus presentation interval are indicated by black arrows above the traces with respect to a larva's orientation as shown in the polar plot inset in **a**. Source data are provided as Source Data File. **c** Highly stimulus-correlated voxels ($R^2 > 0.4$) were found in the tectal hemisphere contralateral to the stimulated eye, consistent with direct contralateral retinal input. However, stimulus-correlated voxels were also observed in the ipsilateral tectal hemisphere, which in this experiment does not receive any direct retinal input due to eye enucleation. Scale bar = 50 µm. Source data are provided as Source Data File. **d** The average density projection of voxels (calculated as the mean over the short axis of the curved rectangle in the left panel) that are highly correlated with a moving bar stimulus ($R^2 > 0.4$, as in **c** shows an enrichment in the tectal hemisphere contralateral to the stimulated eye and in the deep ipsilateral neuropil. Anatomical regions were color-coded as in **a** and **b** ($n = 8$ larvae, gray shading indicates the 95% confidence interval, np: tectal neuropil, SPV: *stratum periventriculare*, ML: midline).

that they must receive direct or indirect visual input. ITNs thus match the anatomical and functional profile of the commissural neuronal population whose existence was predicted from ipsilateral activity in the deep neuropil of the OT.

ITNs are GABAergic interneurons and form synapses in the OT. Next, we analyzed the neurotransmitter phenotype and synaptic connections of ITNs. We performed fluorescent whole-mount in situ hybridization in combination with anti-GFP immunostaining in 4 dpf *ITNGal4, UAS:GFP* zebrafish larvae. Expression of *vglut2a/2b* did not show any overlap with anti-GFP immunostaining suggesting that ITNs are not glutamatergic (Supplementary Fig. 3a). We furthermore found that ITN nuclei were located in the mesencephalic tegmentum, anterior to the midbrain–hindbrain boundary, and showed no overlap with *chata*-positive cells of the nucleus isthmus, in rhombomere 1 (Supplementary Fig. 3b)[2]. However, expression of *gad65/67* colocalized with anti-GFP labeling in the ITN nuclei, indicating that ITNs are GABAergic inhibitory interneurons (Fig. 3a).

To find out where ITNs form synapses, we genetically targeted the presynaptic marker synaptophysin, conjugated to GFP (Syp-GFP)[18], to ITNs. We discovered that ITNs establish putative presynaptic contacts on their arbors in both tectal hemispheres. Presynaptic puncta were localized to the deep neuropil layers (Fig. 3b, upper right panel and Supplementary Fig. 2a, b), extending along the rostral-caudal axis of the OT (Fig. 3b, lower right panels). Furthermore, we transiently expressed the post-synaptic marker psd95-GFP[19] in ITNs and found putative postsynaptic specializations in the deep layers of the neuropil, ipsilateral to ITN cell bodies (Fig. 3c).

In summary, ITNs are a class of inhibitory interneurons that interconnect the two tectal hemispheres.

ITNs respond to prey-like moving target stimuli. In order to explore if ITNs are involved in visual processing during hunting

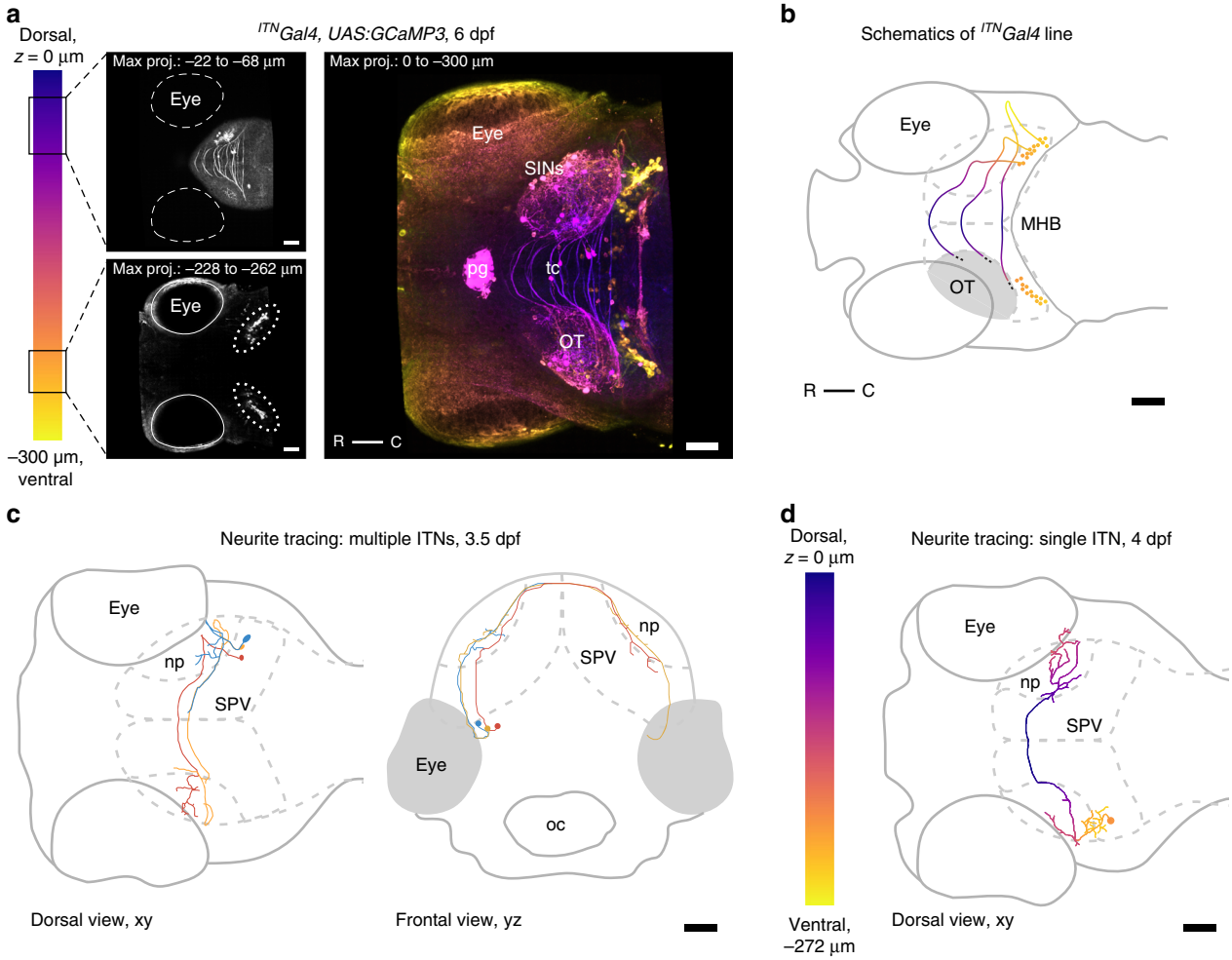

Fig. 2 Intertectal neurons connect the two hemispheres of the optic tectum. **a** Maximum intensity projections of an *ITNGal4* transgenic larva viewed dorsally at 6 dpf in which neurons that connect the two hemispheres of the optic tectum (intertectal neurons, ITNs) are labeled (most dorsal plane through the larva is indicated by $z = 0$ µm). The cell bodies of ITNs are situated in two bilateral symmetric nuclei below the respective tectal lobes (ITN nuclei highlighted by dotted ellipses in lower left panel) and send their axons dorsally through the tectum crossing the tectal commissure in ladder-like trajectories (upper left panel). In addition to labeling ITNs in the mesencephalic tegmentum, *Gal4* is also expressed in the pineal gland, SINs, scattered periventricular neurons (PVNs), and the spinal cord in this transgenic line. All scale bars = 50 µm. (pg: pineal gland, tc: tectal commissure, OT: optic tectum, R: rostral, C: caudal, SINs: superficial interneurons). **b** Schematic of the transgenic ITNGal4 line depicted in **a**. ITN cell bodies and axon tracts are color-coded according to the position in the dorsoventral *z*-plane. To increase readability only the right ITN's connectivity with respect to the larva is shown. Scale bar = 50 µm. (MHB: midbrain-hindbrain boundary, OT: optic tectum, R: rostral, C: caudal). **c** Neurite tracing of multiple ITNs in a larva at 3.5 dpf. At 3.5 dpf ITN neurites start to cross the midline (e.g., the blue ITN). In addition, ITNs begin to form arbors at the boundaries between the deep layers of the neuropil and the PVN layer. Scale bar = 50 µm. (oc: mouth/oral cavity, np: tectal neuropil, SPV: *stratum periventriculare*). Color-coded to simplify distinction between single ITNs. **d** Neurite tracing of a representative ITN at 4 dpf, color-coded according to the position in the dorsoventral *z*-plane (most dorsal plane of the larva is indicated by $z = 0$ µm). ITN axons cross the midline superficially and form arborization patterns of increasing complexity in the ipsi- and contralateral neuropil structures of the optic tectum. Scale bar = 50 µm. (np: tectal neuropil, SPV: *stratum periventriculare*).

behavior, we first tested if ITNs respond to prey-like stimuli in a virtual hunting assay for tethered zebrafish larvae combined with 2-photon calcium imaging[13]. We presented 5–6 dpf *ITNGal4, UAS:GCaMP3* larvae with small moving spots (speed: 30° s^{-1}, size: 5°) running horizontally across the frontal visual field (Fig. 4a) while simultaneously imaging ITN activity bilaterally. ITNs were strongly responsive to prey-like stimuli (Fig. 4b). Plotting the angular position of the moving spot at the onset of the calcium transient revealed that ITNs responded when the stimulus was in the contralateral visual hemifield. This is consistent with ITNs receiving visual input deriving from the contralateral eye via RGC terminals in the ipsilateral OT, or ipsilateral tectal interneurons (Fig. 4c). Simple light flashes did not evoke ITN responses and we did not observe activity modulations associated with convergent saccades (i.e., initiation of hunting). This suggests that ITNs do not display premotor activity but rather visual sensory responses to prey-like moving target stimuli.

ITNs are required for the binocular localization of prey. Based on their anatomy and physiology, we hypothesized that ITNs might be required for the binocular localization of prey during hunting behavior. We examined this hypothesis using two loss of function approaches:

We generated *ITNGal4, UAS: BoTxBLC-GFP* larvae to genetically silence vesicle release in *Gal4*-expressing neurons using zebrafish-optimized Botulinum toxin light chain[20], and assessed prey capture performance[9]. *ITNGal4, UAS: BoTxBLC-GFP* larvae showed a large reduction in prey consumption compared with

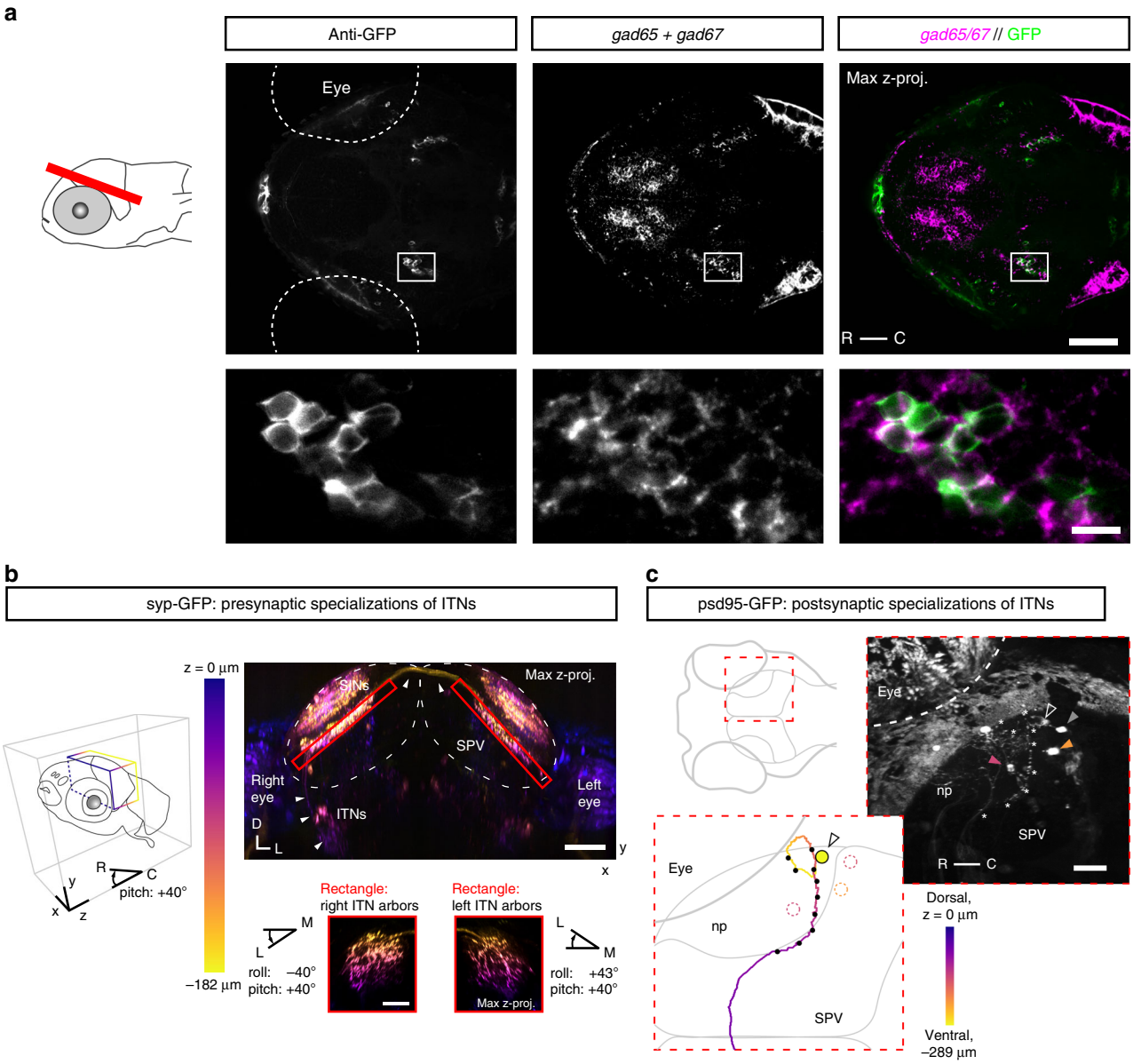

Fig. 3 Intertectal neurons are GABAergic interneurons and form pre- and post-synaptic specializations in the OT. **a** Expression of *gad65/gad67* and anti-GFP immunoreactivity in the brain of a 4 dpf *ITNGal4, UAS:GCaMP3* larvae (red bar in larva to the left indicates microscopic plane, scale bar = 50 µm). Two bilateral symmetric ITN nuclei are labeled by anti-GFP (left nucleus enlarged and shown in the lower images, scale bar = 10 µm). **b** Maximum intensity projection through the OT of a 5 dpf *ITNGal4, UAS:GCaMP3, UAS:Syp-GFP)* larva (view from the front and below of the larva). Syp-GFP signal is color-coded according to depth along *z*. Pre-synaptic specializations of ITNs (Syp-GFP puncta, red rectangles) are in the deep neuropil ipsi- and contralaterally to the ITN cell bodies. Small panels: maximum intensity projections of the pre-synaptic specializations of ITNs viewed dorso-laterally (larva first rotated along the roll axis by −40° for right ITN arbors or along the roll axis by 43° for left ITN arbors, then rotated along the larval pitch axis by +40°, color code according to depth in *z*). White arrows indicate the ITN axon tract. Syp-GFP-labeled puncta in upper layers of the tectal neuropils belong to superficial interneurons (SINs) in the SO and SFGS[54]. All scale bars = 50 µm. **c** Postsynaptic specializations labeled in a 3 dpf *ITNGal4 UAS:GCaMP3* larva, transiently expressing *UAS:psd-95-GFP*. Right panel shows a maximum intensity projection viewed dorsally through the right OT (skin autofluorescence partially removed). A single ITN was labeled in this larva (cell body indicated by open white arrow) and locations of puncta with strong psd-95-GFP expression are indicated by white asterisks along the ITN neurite. The ITN was traced and its trajectory color-coded according to the position in the dorsoventral *z*-plane (lower-left inset). Black dots along the neurite indicate the positions of psd-95-GFP puncta. Post-synaptic specializations of ITNs were found predominantly in the deep layers of the tectal neuropil ipsilateral to the ITN cell body. Periventricular neuron cell bodies (PVNs) were sometimes labeled in *ITNGal4* larvae (dotted circles or filled arrows color-coded according to their *z*-position in right panel). Scale bar = 30 µm. (np: tectal neuropil, R: rostral, C: caudal, D: dorsal, L: left, SO: *stratum opticum*, SFGS: *stratum fibrosum et griseum superficiale*, SPV: *stratum periventriculare*).

sibling controls (Supplementary Fig. 4a). However, further analysis revealed that *BoTxBLC-GFP*-expressing larvae did not inflate their swim bladder and thus spent significantly less time swimming and covered less distance during prey capture trials (Supplementary Fig. 4b). Therefore, reduced prey consumption is likely secondary to locomotor deficits, perhaps due to *BoTxBLC-GFP* expression in the spinal cord.

Next we performed 2-photon laser ablation of ITN cell bodies to specifically examine the behavioral requirement of these neurons. We unilaterally ablated ITNs in 4 dpf *ITNGal4, UAS:*

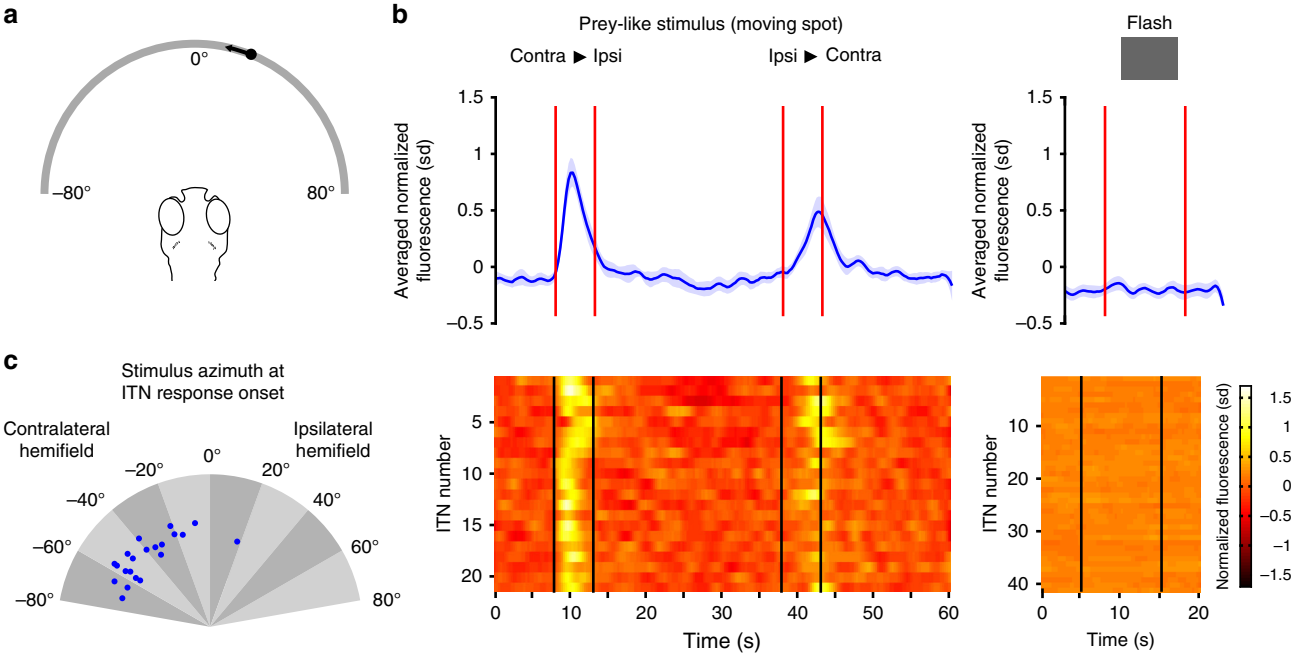

Fig. 4 ITNs display visual sensory responses to prey-like moving target stimuli. **a** Schema of the virtual hunting assay. 5–6 dpf *ITNGal4, UAS:GCaMP3* larvae were tethered in agarose with their eyes free to move. Small moving spots (size: 5°, speed: 30° s^{-1}) moving horizontally from right to left or vice versa were projected on a curved screen covering ~160° of visual space. At the same time, a 2-photon microscope was used to record fluorescent calcium signals in ITNs in response to the visual stimuli as well as eye kinematics using an infrared imaging camera. **b** ITN cell bodies showed strong Ca-transient modulations in response to moving spots (stimulus intervals indicated by the red/black vertical lines, $n = 21$ ITNs from five larvae) whereas ITNs did not respond to flashes ($n = 41$ ITNs from three larvae). Traces show mean normalized fluorescence intensities with 95% confidence intervals. Source data are provided as Source Data File. **c** Azimuth of moving spots at the onset of the response of each ITN to visual prey-like stimuli. ITNs collectively respond to moving spots spanning almost the whole contralateral visual hemifield ($n = 21$ ITNs from five larvae). Source data are provided as Source Data File.

GCaMP3 larvae (12–26 ablated ITNs, Fig. 5a) and, after a recovery period, assessed hunting performance of individual animals. Control larvae, of identical genetic background, underwent the same mounting and imaging procedure but were not ablated. As a further control, sham-ablations were performed by randomly ablating PVNs directly above the ITN nucleus. ITN-ablated larvae were imaged the next day, which confirmed that ITNs were successfully removed (Fig. 5a). At 6 dpf, control, sham-ablated and ITN-ablated larvae were tested in a prey capture performance assay that quantified consumption of paramecia over the course of 4 h.

ITN-ablated larvae consumed fewer paramecia than unablated controls (Fig. 5b) and the strength of this hunting deficit correlated with the number of ablated ITNs (Supplementary Fig. 4c). Sham-ablated larvae did not show a significant difference in paramecia consumption compared with control larvae and were thus pooled with the control group.

ITN-ablated larvae did not show differences in time spent swimming (Fig. 5c), swim bout duration, maximum bout speed, interbout interval or swim bout turn angles (Supplementary Fig. 4d–g), indicating that general motor defects do not account for the impairment of predatory performance. Moreover, prey recognition and hunting-specific motor outputs remained unchanged following ITN ablation: total hunting duration (as estimated from periods of ocular convergence) was unaffected (Fig. 5c) as was average hunting sequence duration and eye vergence angles during hunting (Supplementary Fig. 4h, i). Thus, despite capturing fewer prey than control larvae, ITN-ablated larvae do not display motor defects and can recognize prey and initiate hunting.

We further hypothesized that ITN ablation might result in reduced prey consumption if ITNs are required for larvae to estimate prey location and accordingly initiate capture swims. To uncover at which point during the hunting sequence ITN-ablated larvae deviated from normal hunting behavior, we analyzed a total of 2149 individual hunting sequences from 29 control and 12 ITN-ablated larvae. We subdivided individual hunting routines into a sequence of events enabling us to quantify probabilities of specific outcomes at each stage, including target switching, target fixation, successful capture swims etc. (Fig. 5d). Through this analysis, we detected a specific deficit at the penultimate fixation stage of a hunting sequence, immediately prior to striking at prey (Supplementary Movies 1 and 2). Specifically, when the prey was localized in the binocular strike zone (prey at 0.5 mm distance, ±10° azimuth), ITN-ablated larvae showed a significantly reduced probability of initiating a capture maneuver (Fig. 5g). By contrast, other aspects of hunting behavior of ITN-ablated larvae, including the probability and distance of target fixation, did not appear to differ versus controls (Fig. 5e, f and Supplementary Fig. 5a–f).

In summary, ablating commissural ITNs led to a specific behavioral deficit during binocular localization of prey[3], namely a failure to initiate capture strikes. This is consistent with reduced hunting performance in ITN-ablated larvae and supports the idea that ITNs mediate an interhemispheric neural computation that initiates capture swims at the final moment of hunting when prey is located in the binocular strike zone in front of the predator.

Discussion

Ipsilateral retinal projections (IRPs) exist in members of almost all vertebrate classes. Their presence in basal cyclostomes suggests that IRPs are an ancestral trait[21] and seem to have been lost at multiple times during evolution such that they are absent or

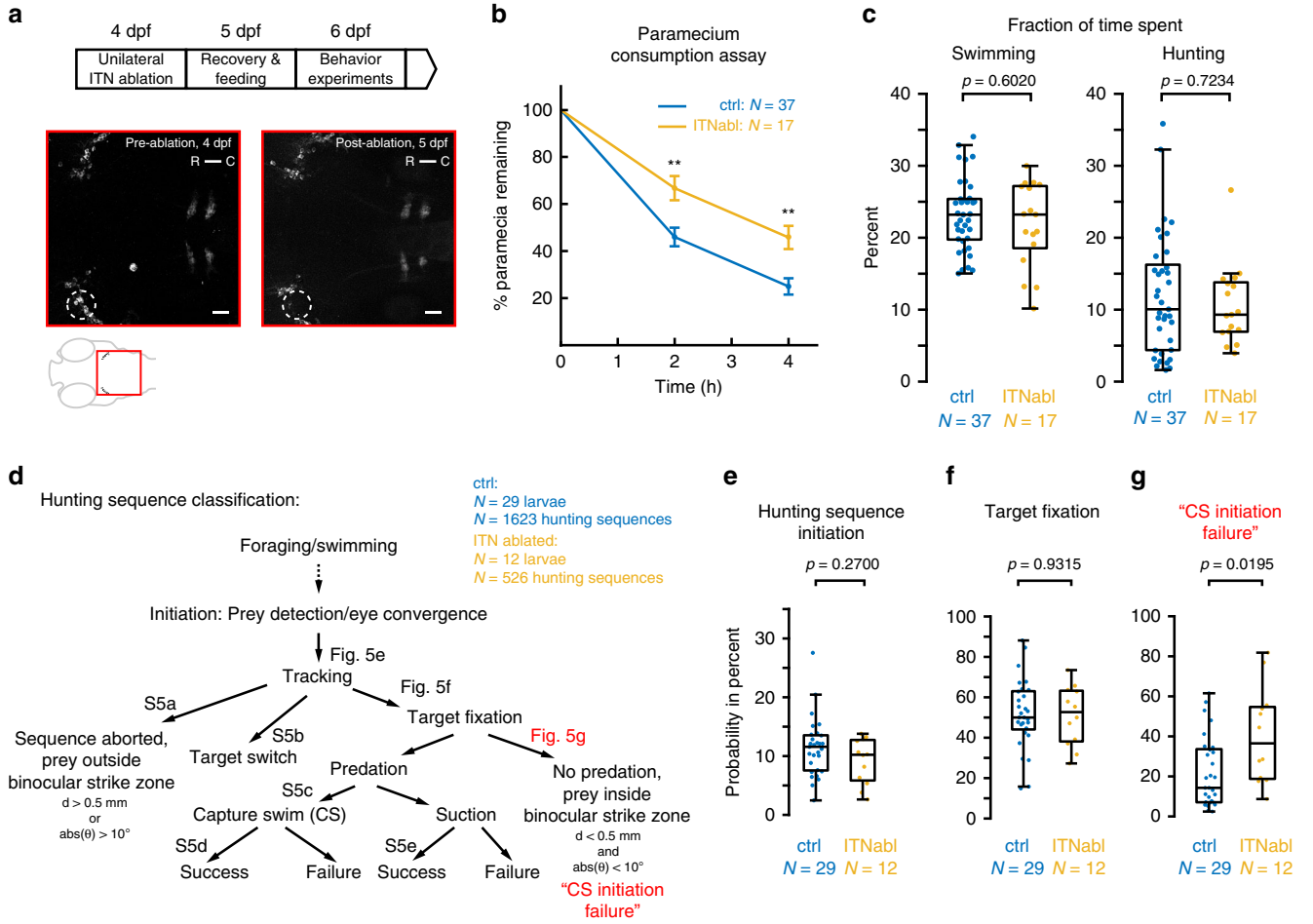

Fig. 5 ITNs are required for the initiation of capture swims when prey is positioned in the binocular strike zone. **a** Experimental design for ablations and subsequent behavioral tracking. 12–26 ITNs were unilaterally laser-ablated in 4 dpf *ITNGal4, UAS:GCaMP3* larvae, left to recover and fed with paramecia on 5 dpf. Behavior experiments were performed at 6 dpf. ITN-ablated *ITNGal4, UAS:GCaMP3* larvae were imaged at 4 dpf (lower panels, pre-ablation) and again at 5 dpf (post-ablation). Dotted ellipse indicates ablated cells. Scale bars = 25 µm. **b** Paramecium consumption for control ($n = 34$ non-ablated larvae and $n = 3$ sham-ablated larvae) and ITN-ablated larvae ($n = 17$ larvae, 12–26 ITNs ablated). ITN-ablated larvae consume paramecia at a reduced rate compared with control larvae (percentage of remaining paramecia relative to the number of paramecia at $t = 0$ h, whiskers denote 95% confidence intervals, Mann–Whitney *U*-test, $t = 2$ h: $p = 0.0036$, $t = 4$ h: $p = 0.0013$). **c** Fraction of time spent swimming and time spent hunting for control ($n = 37$) and ITN-ablated ($n = 17$) larvae (Mann–Whitney *U*-test, swimming: median (ctrl) = 23.2%, median (ITNabl) = 23.2%, $p = 0.6020$//hunting: median (ctrl) = 10%, median (ITNabl) = 9.3%, $p = 0.7234$). **d** Schematic illustrating classification of individual hunting sequences. Figure references refer to the respective panels in Fig. 5 and Supplementary Fig. 5. In total, 1623 hunting sequences from 29 control larvae and 526 hunting sequences from 12 ITN-ablated larvae were analyzed. **e** ITN-ablated larvae initiate hunting with comparable probability to control larvae (control: median hunting sequence initiation probability = 11.6 %, ITN-ablated: median hunting sequence initiation probability = 10.2%, Mann–Whitney *U*-test, $p = 0.2700$). **f** ITN-ablated larvae fixate targets with a comparable probability to control larvae (control: median target fixation probability = 50.0%, ITN-ablated: median target fixation probability = 52.7%, Mann–Whitney *U*-test, $p = 0.9315$). **g** ITN-ablated larvae initiate capture swims at lower probability when prey is positioned in the binocular strike zone (prey at <0.5 mm distance, ±10° azimuth) compared with controls (Mann–Whitney *U*-test, $p = 0.0195$, control: median failure rate = 14.3 %, ITN-ablated: median failure rate = 36.5 %). Central marks of boxplots indicate the respective median. Bottom and top edges correspond to 25th and 75th percentiles. Source data for Fig. 5b–g are provided as Source Data File.

reduced in certain species (for a comprehensive review see ref.[22]). The existence of IRPs is sometimes attributed to a high degree of overlap of the field of views from both eyes and/or a predatory life style relying on binocular stereoscopic vision. However, this cannot be considered a general rule since there are species that have extensive IRPs but no overlapping field of views (e.g., the hagfish *Eptatretus*)[21] as well as predators such as the chameleon, which lack IRPs entirely[23].

Zebrafish larvae are predatory, also lack IRPs to the OT[11] but show behavioral responses consistent with processing of binocular cues during prey hunting[3,8,9]. In this study, we have presented evidence for an intertectal neural circuit that could enable a vertebrate without IRPs to process binocular visual cues.

To our surprise, 2-photon calcium-imaging in zebrafish larvae revealed visual motion-evoked neuronal activity in the deep layers of the tectal neuropil ipsilateral to the stimulated eye, despite the lack of ipsilateral retinotectal projections. We identified a *Gal4*-expressing transgenic line which labels a previously unknown class of commissural neurons (ITNs) that connect both tectal hemispheres. ITNs respond to visual motion stimuli in the contralateral visual field and extend arbors in the deep neuropil laminae of the OT where ipsilateral visual activity is observed. It is therefore likely that ITNs transfer visual information across the midline, which in turn would enable tectal integration of visual information from the two eyes. Unilateral ablation of ITNs impaired prey hunting performance and produced a specific deficit in the initiation of capture

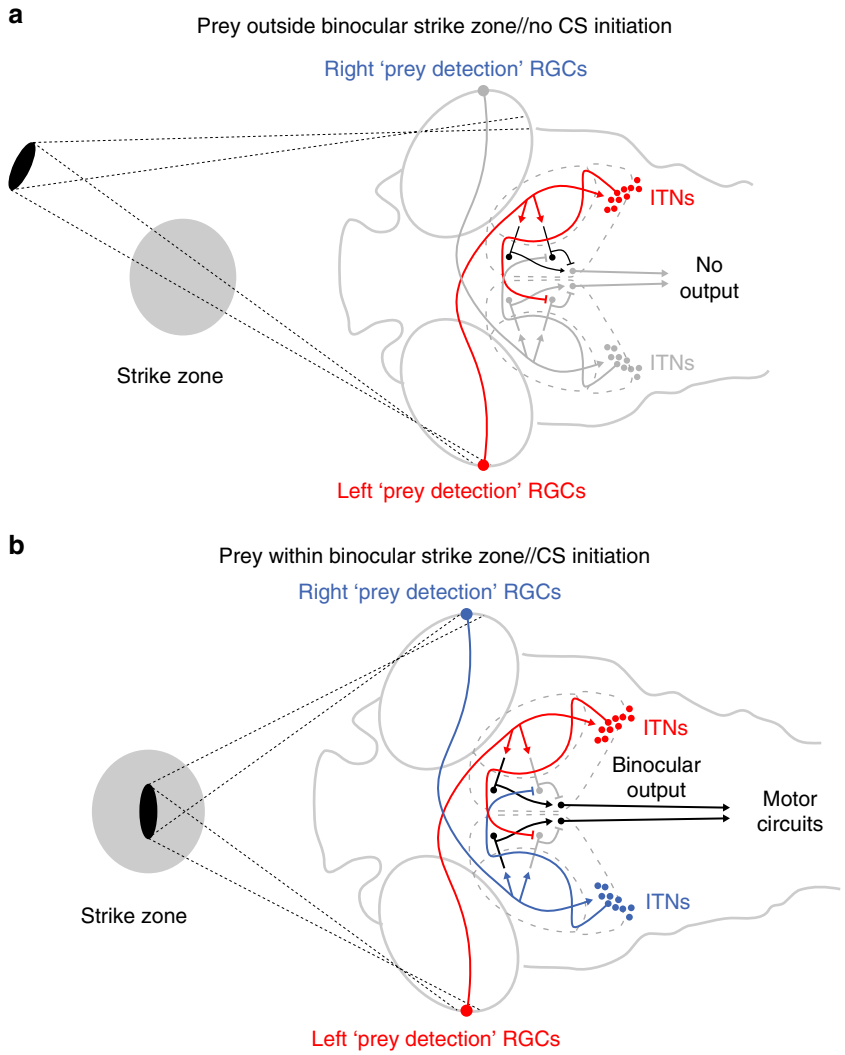

Fig. 6 Model circuit for the integration of binocular visual input to localize prey and initiate capture swims. **a** Prey located outside the strike zone will at most activate the trigger zone of just one eye. RGCs transmit visual information to the contralateral OT and contralateral ITNs. ITNs in turn cross the midline to convey visual information to the opposite OT. In this case, local inhibitory interneurons in the oppposite OT prevent a capture swim from being triggered. **b** When prey is positioned inside the binocular strike zone, both trigger zones are activated. Thus, each tectum receives direct contralateral retinal input, as well as indirect, ITN-mediated input carrying information from the ipsilateral eye. The coincidence of excitatory drive and disinhibition, respectively, allows a premotor command to be generated to initiate a capture swim.

swims. Although ITN-ablated larvae continued to fixate prey at equivalent distances compared to controls, they failed to initiate capture maneuvers when prey was localized to the binocular strike zone. The presence of intertectal connections in zebrafish larvae was previously suggested based on anatomical data from immunohistochemistry[24,25] or single cell labeling approaches[26,27]. However, our study represents the first anatomical, physiological, and behavioral assessment of a genetically accessible class of commissural intertectal neurons.

At the penultimate fixation stage of hunting epochs, eye vergence angles are almost invariant[3]. Thus, lines of sight to the binocular strike zone will be represented at consistent locations in temporal retinae of the two eyes in accordance with anatomical evidence showing increased photoreceptor density in the temporal retina of larval zebrafish[28,29]. Coincident activation of these retinal trigger zones could be the neural signal indicating the correct localization of prey that in turn is used to initiate a capture swim[3]. This simple triangulation mechanism is reminiscent of that proposed for the striking behavior of preying mantids[30,31].

In particluar, we suggest that ITNs participate in a circuit that detects the presence of prey in the binocular strike zone by signaling coincident, bilateral activation of specialized trigger zones in the left and right temporal retinae (Fig. 6). In our model, retinal activity is relayed to contralateral tectal neurons as well as contralateral ITNs, consistent with ITN activation by prey-like stimuli in the contralateral visual field (Fig. 4). ITNs in turn project across the midline (Fig. 2) to transfer visual information to the opposite hemisphere (Fig. 1). As ITNs are inhibitory (Fig. 3), we propose a disinhibition mechanism whereby they silence inhibitory interneurons in the contralateral tectum. This enables a circuit motif in which the tectum can detect simultaneous activation of both trigger zones: activation of the contralateral retina is communicated by direct retinal input, and activation of the ipsilateral temporal retina is signaled by ITN-mediated disinhibition of intrinsic interneurons. The combination of excitatory drive and removal of inhibitory block together allow the generation of a pre-motor command that triggers execution of a capture swim.

Binocular neural responses have been previously reported in zebrafish larvae in the context of behaviors driven by whole field motion: the optokinetic reflex (OKR) and the optomotor response (OMR)[32–34]. Here convergence of monocular visual information is thought to be mediated via the posterior commissure[33] and because these behaviors do not depend on retinotectal connections[15] it is likely that binocular integration of whole field motion cues is independent of ITNs.

Intertectal connections have been studied in multiple species[35,36]. In anurans, neurons of the *nucleus isthmi* indirectly connect the tectal hemispheres and mediate binocular visual responses in the anterior part of the OT[37,38]. However, bilateral ablation of these nuclei does not impair binocular depth perception during hunting[37,39]. Direct commissural connections between the superior colliculi, the mammalian homolog of the OT, were also reported in mammals but their function remains rather obscure: Severing the collicular commissure restored visual fixation capabilities of hemianopic cats to the blind hemifield that was originally caused by unilateral ablations of the visual neocortex (Sprague effect)[40]. While the interpretation of this experiment is not straight forward, it suggests a mostly underappreciated role of intercollicular neurons in visually guided behavior, even in mammals.

Finally, it has been convincingly shown that binocular stereopsis is present in very different evolutionary lineages[41–43]. However, common and distinct principles of binocular stereopsis have not been addressed yet on the neural circuit level. Our study contributes to defining these principles by providing evidence for a neural circuit that establishes a simple form of binocular stereopsis in the absence of direct superposition of retinal input from both eyes.

Methods

Contact for reagent and resource sharing. Further information and requests for resources and reagents should be directed to and will be fulfilled by Filippo Del Bene (filippo.del-bene@inserm.fr).

Zebrafish embryo maintenance. Zebrafish (*Danio rerio*) were maintained at 28 °C on a 14 h light/10 h dark cycle. Fish were housed in the animal facility of our laboratories at UCL or Institut Curie, which were built according to the respective local animal welfare standards. All animal procedures were performed in accordance with French, British, and European Union animal welfare guidelines. Animal handling and experimental procedures were approved by the Committee on ethics of animal experimentation—Institut Curie and the UK Home Office under the Animal (Scientific Procedures) Act 1986. No statistical methods were used to predetermine sample size. Where indicated the experiments were randomized and the investigators blinded to allocation during experiments and outcome assessment.

ITN neurite and synapse labeling. Transient single cell labeling to analyze ITN neurite morphology was achieved by injecting 1 nl of a *UAS:tagRFP, UAS:GFP* plasmid DNA (25 ng µl^{-1}) at 1 cell stage into ^{ITN}*Gal4, UAS:GCaMP3* embryos. To transiently label post-synaptic densities of ITNs, 1 nl of a *UAS:psd95-GFP* plasmid DNA (25 ng µl^{-1}) were injected at 1 cell stage into ^{ITN}*Gal4, UAS:GCaMP3* embryos. Presynaptic sites were labeled by crossing ^{ITN}*Gal4, UAS:GCaMP3* with *Tg (Brn3c:Gal4, UAS:Syp-GFP)* larvae and the offspring screened against *Brn3c* and for *Gal4ic3034Tg*—and *Syp-GFP* expression. Larvae were imaged at 3–5 dpf using a Zeiss LSM 780 confocal microscope (Zeiss, Oberkochen, Germany), equipped with a water immersion objective (Zeiss, Plan-Apochromat 40 ×/1.00). Image stacks were analyzed using MATLAB (The MathWorks Inc., Natick, MA, USA) and FIJI[44]. Skin autofluorescence was removed manually in FIJI to enable an unobstructed view onto ITN synaptic structures and neurites.

Neurite tracing. ITN neurites were traced using the simple neurite tracer plugin[45] provided in FIJI. Individual ITNs labeled in ^{ITN}*Gal4, UAS:GCaMP3* larvae injected with *UAS:tagRFP, UAS:GFP* were followed through the confocal stack based on their color and/or marker intensity. The vector files containing the traced neurites were then exported to MATLAB for further processing using the MatlabIO toolbox included in visualization and analysis software Vaa3D[46].

Whole-mount in situ hybridization and immunohistochemistry. *Vglut2a/vglut2b, gad67/gad65* probe mixtures were generated from cDNA using the following primers:

vglut2a_fwd: GATTCTCCTCACGTCCACACTGAA
vglut2a_rev: AACACATACTGCCACTCTTCTCGG
vglut2b_fwd: CGTCGACATGGTCAATAACAGCAC
vglut2b_rev: ATAGCACCTACAATCAGAGGGCAG
gad67_fwd: CATCATCCTCACCAGCTGCTGGAG
gad67_rev: AACATTGTAAAGGCACACCCATCATC
gad65_fwd: TCACCTATGAGGTGGCTCCAGTCTTC
gad65_rev: GTCATAATGCTTGTCCTGCTGGAAC

The mRNA anti-sense riboprobes for *chata* were kindly provided by Marnie Halpern[47]. For in situ hybridization, larvae were stored in 100% methanol and rehydrated stepwise into 0.1% Tween in PBS. Tissue permeabilization was achieved by proteinase K treatment adapted to larval age at room temperature, followed by post-fixation in 4% PFA in PBS. After prehybridization, hybridization with digoxigenin-UTP-labeled and fluorescein-UTP-labeled riboprobes (Roche Applied Science) was performed overnight at 65/68 °C and larvae were kept in the dark for all subsequent steps. Larvae were washed with TNT (0.1 M Tris, pH 7.5, 0.15 M NaCl, 0.1% Tween 20), incubated in 1% H_2O_2 in TNT for 20 min, washed several times and blocked in TNB [2% DIG Block (Roche) in TNT] for 1 h. Incubation with anti-digoxigenin-POD (peroxidase) Fab fragments (Roche, 1:50 in TNB) was performed for 24 h at 4 °C. Signals were detected using the Cy3-TSA kit (PerkinElmer) for 60 min (*vglut2a/2b* mixture) or 30 min (*gad65/67* mixture), respectively. Larvae were incubated in DAPI in TNT overnight at 4 °C and washed with TNT prior to imaging. For subsequent immuno-staining, chicken anti-GFP (1:500, Genetex, GTX13970) and mouse anti-ERK (1:500, p44/42 MAPK (Erk1/2), 4696) were used as primary antibodies followed by goat anti-chicken Alexa Fluor 488-conjugated (1:400, Invitrogen, A11039) and anti-mouse Alexa Fluor 594-conjugated (1:500, Invitrogen, A11005) secondary antibodies.

3D Brain registration. Registration of image volumes of 18 ^{ITN}*Gal4, UAS:GCaMP3* at 6 dpf, co-immunolabeled with anti-tErk and anti-GFP, to a tErk reference brain[48] was performed using the CMTK toolbox version 3.2.2[49].

Eye ablations. 3 to 4 dpf *Tg(elavl3:GCaMP5G)* larvae were mounted in 2% low-melting-point agarose and one eye was removed using fine forceps. The larvae were then left to recover in Ringer solution supplemented with Calcium for 1 h. Subsequently, the larvae were transferred into fish medium until 2-photon Calcium imaging was performed on 5 or 6 dpf.

Lipophilic dye tracing. For tracing of retinotectal projections, eye-ablated larvae where fixed in 4% PFA/PBS for 2 h following injection of the lipophilic dye DiO into the remaining eye.

Calcium imaging and visual stimulation. Larvae were mounted in 2.5% low melting-point agarose such that one eye was facing an OLED screen (800 pixel × 600 pixel, eMagin, Bellevue, WA, USA) subtending around 70° × 55° of a larva's visual field. The screen was covered with a red long-pass filter (Kodak Wratten No. 25) to enable simultaneous imaging and visual stimulation. Larvae were then imaged in vivo using a two-photon microscope (LaVision Biotec, Bielefeld, Germany), equipped with a mode-locked Chameleon Ultra II Ti–Sapphire laser tuned to 920 nm (Coherent Inc., Santa Clara, CA, USA) and a Zeiss Plan-APOCHROMAT 20× water immersion objective (NA 1, Zeiss, Oberkochen, Germany). Emitted fluorescence was detected using a bandpass filter (ET525/50 M, Chroma Technology GmbH, Olching Germany) in front of a GaAsP photomultiplier tube (H7422-40, Hamamatsu Photonics K.K., Hamamatsu City, Japan). The average laser power at the sample during scanning was 10–20 mW and frames were scanned at 4 Hz resulting in 1.33 µs dwell time per pixel (pixel size: 0.85 µm^2). Scanning and image acquisition were controlled with LaVision Biotec's proprietary ImSpector software.

Visual stimulation was handled by a computer separate from the image acquisition setup using Psychophysics Toolbox[50]. Stimuli were either moving bars running across the eye's field of view (bar width: 9°, speed: 20° s^{-1}, direction: pseudo-randomly chosen for each stimulus epoch from 12 angular directions 30° apart, stimulus repetitions: three times per direction, stimulus presentation interval: 10 s) or light flashes instantaneously covering the entire field of view (stimulus repetitions: five times, stimulus presentation interval: 10 s). The image acquisition was synchronized with the visual stimulation by recording the imaging frame number in parallel to stimulus presentation timing via a U3 LabJack DAQ (LabJack, Lakewood, CO, U.S.A.).

Virtual prey-hunting assay. 5 to 6 dpf ^{ITN}Gal4, UAS:GCaMP3 larvae were individually mounted in 2% low-melting-point agarose in a 35 mm petri dish and the eyes and tail subsequently freed from the agarose with a scalpel. Visual stimuli consisted of small moving spots (subtending 5° visual angle) back-projected onto a curved screen in front of the animal, appeared at 76° to the left or right of the midline and then moving 152° right or left across the frontal region of visual field (at an average angular velocity with respect to the fish of 30°/s). At each imaging

plane, 12–18 repetitions of each of the visual stimuli (L > R, R > L) were presented in pseudo-random order.

2-photon calcium imaging was simultaneously performed using a custom-built microscope equipped with a 20 × /1.00 NA Olympus objective and a Ti:Sapphire ultra-fast laser (Chameleon Ultra II, Coherent Inc) tuned to 920 nm. Average laser power at the sample was 5–10 mW. Images were acquired by frame scanning at 3.6 Hz with 1 µs dwell time per pixel. For each larva, 1–3 focal planes through the ITN nuclei of the larva were imaged. Image acquisition and visual stimulus presentation were controlled using software written in LabView and MATLAB.

Image analysis for calcium imaging experiments. A voxel-based analysis strategy was chosen for the Calcium-imaging experiments following eye ablations. Acquired timeseries were motion-corrected by calculating the shift between an average image and each timeseries image based on the inverse Fourier-transformed normalized cross-power spectra. Each image timeseries was further registered to the corresponding *z*-plane of a 5 dpf *Tg(elavl3:GCaMP5G)* reference larva using MATLAB's *align_nonrigid* function. Individual image timeseries were re-shuffled due to the randomized stimulus order during visual stimulation and averaged across repetitions. To identify voxels that were correlated with stimulus presentation we used a regression-based approach[16]. In short, a binary matrix was generated indicating when a stimulus was present independent of its directionality. For every voxel, the average temporal response profile was estimated using least-squares regression. Voxels with a p value > 0.0001 were discarded from analysis and the maximum value of the regression coefficient from eight larvae was kept for each voxel. Voxels that had a regression coefficient > 0.4 were considered strongly correlated with stimulus presentation and thus active. The intensity values for all voxels in one of six anatomically defined ROIs in the ipsilateral and contralateral tectal hemisphere were averaged over time for each larva. The deltaF/F_0 average profiles were calculated by estimating the baseline using MATLAB's *imerode* function with a 10 s kernel (i.e., the stimulus presentation interval). DeltaF/F_0 was obtained by calculating $F_{<\mathrm{ROI}>}/F_{<\mathrm{ROI\ baseline}>} - 1$. Delta$F/F0$ average profiles were then averaged across larvae.

The response of ITNs to moving bars and light flashes covering the contralateral field of view was analyzed using a ROI based approach. First, acquired timeseries were registered by calculating the shift between an average image and each timeseries image based on the inverse Fourier-transformed normalized cross-power spectra. ROIs were manually selected from a standard deviation projection of the image timeseries and based on anatomical landmarks. ROI timeseries were re-shuffled to account for the randomized stimulus order during visual stimulation and averaged across repetitions. The deltaF/F_0 average profiles were calculated by estimating the baseline using MATLAB's *imerode* function with a 10 s kernel and calculating $F_{<\mathrm{ROI}>}/F_{<\mathrm{ROI\ baseline}>} - 1$. Finally, the delta$F/F0$ averages were normalized to the maximal value.

Analysis of data collected during virtual hunting assays was performed by correcting motion artefacts of timeseries using cross-correlation[13]. ROIs were selected manually based on an anatomical stack of the brain volume. ROI trials were discarded from analysis if the *z*-scored motion-error exceeded two standard deviations. The ROI intensity profiles were *z*-scored and then averaged over trials. Lateral ITN position (i.e., left or right) was recorded from an anatomical stack of the larva and stimulus direction (right to left and vice versa) was remapped to contralateral to ipsilateral and vice versa with respect to the ITN position in the larva. For calculating the onset of the ITN activity with respect to the stimulus position in the visual field, the maximum of the ROI timeseries within the stimulus interval (contra > ipsi and ipsi > contra) was identified. Subsequently, the response onset was defined as timepoint when the response curve was smaller than the maximum and falling below 0.5 standard deviations. Timepoints for contra > ipsi and ipsi > contra were averaged and the corresponding azimuth was calculated based upon the trajectory of the visual cue.

Synaptic silencing. *^{ITN}Gal4, UAS:RFP larvae* were crossed to *UAS:BoTxBLC-GFP* larvae[20], screened at 3 dpf and separated into GFP-positive (*^{ITN}Gal4, UAS:BoTxBLC-GFP*) and GFP-negative (control) siblings. On 5 dpf, all larvae were fed with rotifers to gain feeding experience.

ITN laser ablations. At 4 dpf, *^{ITN}Gal4, UAS:GCaMP3* larvae, in which more than 12 ITNs were labeled in one nucleus, were randomly assigned to either the control, sham-ablated or ITN-ablated group. Larvae from the two ablation groups were then randomly selected for unilateral cell ablation (i.e., only cells on either the left or right side with respect to the larval rostral–caudal axis to be ablated per larva). Then all larvae independent of the assigned group were anesthetized using 0.02% tricaine (MS-222, Sigma) diluted in fish medium, mounted in 3% low-melting-point agarose and imaged using a custom-made 2-photon microscope[13]. Single target cells (either ITNs or PVNs) were identified by first taking a full frame scan. Then a mode-locked laser beam (800 nm) was scanned in a spiral pattern around a defined target cell position for ~100 ms. A cell was regarded as successfully ablated when after ablation a small point of saturated intensity was detected at the target position instead of the cell. Then the procedure was repeated and finally the number of successfully ablated cells recorded for each larva. After the procedure, each larva's brain was inspected under the microscope and only larvae with clearly visible heartbeat and blood flow in both brain hemispheres were kept for further experiments. Control, sham-ablated and ITN-ablated larvae were then removed from the agarose and kept individually. On 5 dpf ITN-ablated larvae were re-imaged to ensure that neurons were successfully removed and were otherwise left to recover. All larvae were subsequently separated into 12-well plates and assigned a code for anonymization. Each larva was fed with *Paramecia* on 5 dpf to gain feeding experience.

Prey consumption assays. At 6 dpf, all larvae were tested in a prey consumption assay[9] and, since the larvae received food more than 12 h earlier, they were at this point considered starved[51,52]. At the beginning of the assay ($t = 0$ h) paramecia or rotifers were added to petri dishes containing either a single larva (for ITN-ablations) or 4 larvae (for the *BoTxBL-GFP*-expression experiments). Short movies of the dishes were then recorded at $t = 0$ h, $t = 1$ h, t = 2 h and $t = 4$ h after the start of the experiment using high-speed infrared sensitive cameras (MC1362 or MC4082, Mikrotron GmbH, Germany) positioned above the dish. Dishes were dark field-illuminated using a custom-made LED-ring (850 nm) placed around the dishes. To obtain temporal prey consumption curves, the number of living prey per dish was counted at each time point during the assay using FIJI's Cell Counter plugin. These numbers were then normalized to the initial prey number at $t = 0$ h.

Larva tracking and data analysis. For the behavioral analysis of *UAS:BoTxBLC-GFP*-expressing larvae, individual larvae were imaged with a Mikrotron MC1362 high-speed camera at 700 Hz. Each recording lasted between 5 to 10 min. The larva's position in each frame was extracted online using a custom-made tracking software[1].

For the analysis of ITN-ablated larvae, individual animals were filmed for around 15 min at 100 frames s^{-1} and illuminated by a custom-made LED-based diffusive backlight (850 nm) placed below the dish. For each frame, the x/y -position and orientation of the larva's body centroid and the angles of the larva's eyes were extracted in real-time based upon image moments computed by OpenCV routines within the open-source visual programming language Bonsai[53].

Data Analysis was performed off-line in MATLAB. Hunting sequences were detected by calculating the vergence angles from the difference between the left and right eye angles filtered by a 50 ms boxcar filter. Vergence distributions are mostly bimodal (i.e., representing eyes parallel and convergences) thus thresholds for start (on) and end (off) of hunting sequences were determined by fitting the vergence distributions for each larva with a Two-Term Gaussian Model (using MATLABs *fit* function). The on-threshold for hunting sequences for each larva was then determined by subtracting 1 standard deviation from the mean of the gaussian distribution with the higher mean (representing convergences). The off-threshold for hunting sequences was the intersection point of two gaussians minus 5°. The start of a hunting sequence was then defined by the point when the vergence angle exceeded the on-threshold and the end was indicated by the vergence angle falling below the off-threshold. From these hunting sequence start and end timepoints, the fraction of time spent hunting could be calculated by taking the number of video frames during hunting sequences normalized by the total number of frames during the experiment. Furthermore, hunting sequence duration and average vergence angle during hunting sequences were determined.

Swim bouts were detected by calculating a larva's instant velocity in mm s^{-1} from the x- and y-centroid position difference filtered with a 30 ms (for determining the start of a swim bout) or a 100 ms (for determining the swim bout end) boxcar filter. Putative swim bouts were then detected using MATLABS *findpeaks* function. Then start and end timepoints of swim bouts were determined based on the on-threshold of 2 mm s^{-1} in the 30 ms-boxcar-filtered velocity curve and an off-threshold of 1.25 mm s^{-1} in the 100 ms-boxcar-filtered velocity curve. From the swim bout start and end timepoints, the fraction of time spent swimming could be calculated by taking the number of video frames during swim bouts normalized by the total number of frames during the experiment. Furthermore, swim bout duration, maximum bout speed and interbout intervals were calculated for bouts and interbout intervals occurring during hunting sequences for each larva. To obtain turning angles for each bout during hunting sequences the difference between average orientation changes 30 ms before and 30 ms after a swim bout was calculated. For ITN-ablated larvae turning angles were re-mapped according to the side of the ablation to control for potential unpsecific ablation defects induced through unilateral ablation.

For all analyzed hunting sequence and swim bout parameters, the relative frequency distribution and the cumulative relative frequency distribution per larva were calculated and then averaged for all larvae within the control and ITN-ablated group. To test for equality of the average distributions a Two-Sample Kolmogoroff–Smirnov test was performed.

Single hunting sequence evaluation of ITN-ablated larvae and data analysis. To evaluate the outcome of single hunting sequences, 15 min videos of hunting larvae were taken at 100 frames s^{-1}. Dishes were dark field-illuminated using a custom-made LED-ring (850 nm) placed around the dish to simplify the detection of paramecia. Hunting sequences were identified based on visible eye vergences and assigned to either of the categories shown in Fig. 5d based on their outcome: 1. sequence aborted when prey outside of binocular strike zone (prey at distance

smaller than 0.5 mm and smaller than ±10° azimuth between prey and larva), 2. targets were switched or 3. target was fixated i.e., the larva was positioning the target in a stereotypic binocular strike zone around 0.5 mm in front of the larva. If the target was fixated during the hunting sequence it was furthermore evaluated if a capture swim, a suction or sequence abortion when the target was inside the binocular strike zone occurred. Finally, if a capture swim or a suction was performed the success or failure was recorded. Only sequences with an unequivocally identifiable fixated target were included for analysis. In rare cases in which multiple paramecia were fixated by a larva during a single hunting sequence (43/2149 hunting sequences from 29 control and 12 ITN-ablated larvae), the entire hunting sequence was assigned to the target switch category. Data analysis was performed off-line in MATLAB. Category probabilities for a given larva were calculated by counting the total number of events (e.g., successful capture swims) normalized to the number of events of the superordinate node (e.g., capture swims).

Quantification and statistical analysis. All statistical analyses were performed in either MATLAB or FIJI. Statistical tests, p values and sample size are reported in the text or figure legends. All tests were two-tailed. No statistical methods were used to predetermine sample size. Where indicated the experiments were randomized and the investigators blinded to allocation during experiments and outcome assessment.

Reporting summary. Further information on research design is available in the Nature Research Reporting Summary linked to this article.

Data availability

The datasets generated and analyzed during the current study are available from the corresponding authors on request. The source data underlying Figs. 1b, c, 4b, c, 5b–g and Supplementary Figs. 2d, 4a–i and 5a–f are provided as a Source Data file.

Received: 2 January 2019; Accepted: 30 October 2019;
Published online: 29 November 2019

References

1. Marques, J. C., Lackner, S., Félix, R. & Orger, M. B. Structure of the zebrafish locomotor repertoire revealed with unsupervised behavioral clustering. *Curr. Biol.* **28**, 181–195.e5 (2018).
2. Henriques, P. M., Rahman, N., Jackson, S. E. & Bianco, I. H. Nucleus isthmi is required to sustain target pursuit during visually guided prey-catching. *Curr. Biol.* **29**, 1771–1786.e5 (2019).
3. Bianco, I. H., Kampff, A. R. & Engert, F. Prey capture behavior evoked by simple visual stimuli in larval zebrafish. *Front. Syst. Neurosci.* **5**, 101 (2011).
4. Borla, M. A., Palecek, B., Budick, S. & O'Malley, D. M. Prey capture by larval zebrafish: evidence for fine axial motor control. *Brain. Behav. Evol.* **60**, 207–229 (2002).
5. McElligott, M. B. & O'Malley, D. M. Prey tracking by larval zebrafish: axial kinematics and visual control. *Brain. Behav. Evol.* **66**, 177–196 (2005).
6. Trivedi, C. A. & Bollmann, J. H. Visually driven chaining of elementary swim patterns into a goal-directed motor sequence: a virtual reality study of zebrafish prey capture. *Front. Neural Circuits* **7**, 86 (2013).
7. Budick, S. A. & O'Malley, D. M. Locomotor repertoire of the larval zebrafish: swimming, turning and prey capture. *J. Exp. Biol.* **203**, 2565–2579 (2000).
8. Patterson, B. W., Abraham, A. O., MacIver, M. A. & McLean, D. L. Visually guided gradation of prey capture movements in larval zebrafish. *J. Exp. Biol.* **216**, 3071–3083 (2013).
9. Gahtan, E., Tanger, P. & Baier, H. Visual prey capture in larval zebrafish is controlled by identified reticulospinal neurons downstream of the tectum. *J. Neurosci.* **25**, 9294–9303 (2005).
10. Petros, T. J., Rebsam, A. & Mason, C. A. Retinal axon growth at the optic chiasm: to cross or not to cross. *Annu. Rev. Neurosci.* **31**, 295–315 (2008).
11. Burrill, J. D. & Easter, S. S. Development of the retinofugal projections in the embryonic and larval zebrafish (Brachydanio rerio). *J. Comp. Neurol.* **346**, 583–600 (1994).
12. Dunn, T. W. et al. Neural circuits underlying visually evoked escapes in larval zebrafish. *Neuron* **89**, 613–628 (2016).
13. Bianco, I. H. & Engert, F. Visuomotor transformations underlying hunting behavior in zebrafish. *Curr. Biol.* **25**, 831–846 (2015).
14. Meek, J. Functional anatomy of the tectum mesencephali of the goldfish. An explorative analysis of the functional implications of the laminar structural organization of the tectum. *Brain Res.* **287**, 247–297 (1983).
15. Roeser, T. & Baier, H. Visuomotor behaviors in larval zebrafish after GFP-guided laser ablation of the optic tectum. *J. Neurosci.* **23**, 3726–3734 (2003).
16. Freeman, J. et al. Mapping brain activity at scale with cluster computing. *Nat. Methods* **11**, 941–950 (2014).
17. Roberts, J. A. et al. Targeted transgene integration overcomes variability of position effects in zebrafish. *Development* **141**, 715–724 (2014).
18. Meyer, M. P. & Smith, S. J. Evidence from in vivo imaging that synaptogenesis guides the growth and branching of axonal arbors by two distinct mechanisms. *J. Neurosci.* **26**, 3604–3614 (2006).
19. Niell, C. M., Meyer, M. P. & Smith, S. J. In vivo imaging of synapse formation on a growing dendritic arbor. *Nat. Neurosci.* **7**, 254–260 (2004).
20. Sternberg, J. R. et al. Optimization of a neurotoxin to investigate the contribution of excitatory interneurons to speed modulation in vivo. *Curr. Biol.* **26**, 2319–2328 (2016).
21. Wicht, H. & Northcutt, R. G. Retinofugal and retinopetal projections in the pacific hagfish, *Eptatretus stouti* (Myxinoidea) (Part 1 of 2). *Brain. Behav. Evol.* **36**, 315–321 (1990).
22. Ward, R., Repérant, J., Hergueta, S., Miceli, D. & Lemire, M. Ipsilateral visual projections in non-eutherian species: random variation in the central nervous system? *Brain Res. Rev.* **20**, 155–170 (1995).
23. Bennis, M., Repérant, J., Rio, J.-P. & Ward, R. An experimental re-evaluation of the primary visual system of the European chameleon, Chamaeleo chameleon. *Brain. Behav. Evol.* **43**, 173–188 (1994).
24. Ronneberger, O. et al. ViBE-Z: a framework for 3D virtual colocalization analysis in zebrafish larval brains. *Nat. Methods* **9**, 735–742 (2012).
25. Wilson, S. W., Ross, L. S., Parrett, T. & Easter, S. S. The development of a simple scaffold of axon tracts in the brain of the embryonic zebrafish, Brachydanio rerio. *Development* **108**, 121–145 (1990).
26. Helmbrecht, T. O., dal Maschio, M., Donovan, J. C., Koutsouli, S. & Baier, H. Topography of a visuomotor transformation. *Neuron* **100**, 1429–1445.e4 (2018).
27. Sato, T., Hamaoka, T., Aizawa, H., Hosoya, T. & Okamoto, H. Genetic single-cell mosaic analysis implicates ephrinB2 reverse signaling in projections from the posterior tectum to the hindbrain in zebrafish. *J. Neurosci.* **27**, 5271–5279 (2007).
28. Schmitt, E. A. & Dowling, J. E. Early retinal development in the zebrafish, Danio rerio: light and electron microscopic analyses. *J. Comp. Neurol.* **404**, 515–536 (1999).
29. Zimmermann, M. J. Y. et al. Zebrafish differentially process color across visual space to match natural scenes. *Curr. Biol.* **28**, 2018–2032.e5 (2018).
30. Nityananda, V. & Read, J. C. A. Stereopsis in animals: evolution, function and mechanisms. *J. Exp. Biol.* **220**, 2502–2512 (2017).
31. Prete, F. R., Wells, H., Wells, P. H. & Hurd, L. E. *The Praying Mantids*. (JHU Press, 1999).
32. Kubo, F. et al. Functional architecture of an optic flow-responsive area that drives horizontal eye movements in zebrafish. *Neuron* **81**, 1344–1359 (2014).
33. Naumann, E. A. et al. From whole-brain data to functional circuit models: the zebrafish optomotor response. *Cell* **167**, 947–960.e20 (2016).
34. Portugues, R., Feierstein, C. E., Engert, F. & Orger, M. B. Whole-brain activity maps reveal stereotyped, distributed networks for visuomotor behavior. *Neuron* **81**, 1328–1343 (2014).
35. Auen, E. L. Axonal transport of HRP in descending tectal fibers of the pit viper. *Neurosci. Lett.* **9**, 137–140 (1978).
36. Voneida, T. J. & Mello, N. K. Interhemispheric projections of the optic tectum in pigeon. *Brain. Behav. Evol.* **11**, 91–108 (1975).
37. Glasser, S. & Ingle, D. The nucleus isthmus as a relay station in the ipsilateral visual projection to the frog's optic tectum. *Brain Res.* **159**, 214–218 (1978).
38. Gruberg, E. et al. Influencing and interpreting visual input: the role of a visual feedback system. *J. Neurosci.* **26**, 10368–10371 (2006).
39. Collett, T. S., Udin, S. B. & Finch, D. J. A possible mechanism for binocular depth judgements in anurans. *Exp. Brain Res.* **66**, 35–40 (1987).
40. Sprague, J. M. Interaction of cortex and superior colliculus in mediation of visually guided behavior in the cat. *Science* **153**, 1544–1547 (1966).
41. Collett, T. Stereopsis in toads. *Nature* **267**, 349–351 (1977).
42. Ptito, M., Lepore, F. & Guillemot, J.-P. Stereopsis in the cat: behavioral demonstration and underlying mechanisms. *Neuropsychologia* **29**, 443–464 (1991).
43. Rossel, S. Binocular stereopsis in an insect. *Nature* **302**, 821–822 (1983).
44. Schindelin, J. et al. Fiji: an open-source platform for biological-image analysis. *Nat. Methods* **9**, 676–682 (2012).
45. Longair, M. H., Baker, D. A. & Armstrong, J. D. Simple Neurite Tracer: open source software for reconstruction, visualization and analysis of neuronal processes. *Bioinformatics* **27**, 2453–2454 (2011).
46. Peng, H., Ruan, Z., Long, F., Simpson, J. H. & Myers, E. W. V3D enables real-time 3D visualization and quantitative analysis of large-scale biological image data sets. *Nat. Biotechnol.* **28**, 348–353 (2010).
47. Hong, E. et al. Cholinergic left-right asymmetry in the habenulo-interpeduncular pathway. *Proc. Natl Acad. Sci. USA* **110**, 21171–21176 (2013).
48. Randlett, O. et al. Whole-brain activity mapping onto a zebrafish brain atlas. *Nat. Methods* **12**, 1039–1046 (2015).

49. Rohlfing, T. & Maurer, C. R. Jr. Nonrigid image registration in shared-memory multiprocessor environments with application to brains, breasts, and bees. *IEEE Trans. Inform. Technol. Biomed.* **7**, 16–25 (2003).
50. Brainard, D. H. The psychophysics toolbox. *Spat. Vis.* **10**, 433–436 (1997).
51. Filosa, A., Barker, A. J., Dal Maschio, M. & Baier, H. Feeding state modulates behavioral choice and processing of prey stimuli in the zebrafish tectum. *Neuron* **90**, 596–608 (2016).
52. Jordi, J. et al. A high-throughput assay for quantifying appetite and digestive dynamics. *Am. J. Physiol. -Regul. Integr. Comp. Physiol.* **309**, R345–R357 (2015).
53. Lopes, G. et al. Bonsai: an event-based framework for processing and controlling data streams. *Front. Neuroinform.* **9**, 7 (2015).
54. Preuss, S. J., Trivedi, C. A., vom Berg-Maurer, C. M., Ryu, S. & Bollmann, J. H. Classification of object size in retinotectal microcircuits. *Curr. Biol.* **24**, 2376–2385 (2014).

Acknowledgements

We would like to thank Kristen Severi and Roshan Jain for comments on the manuscript and all members of the Del Bene and Bianco labs for discussions. The Tg(*UAS:BoTxBLC-GFP)* zebrafish line was a gift from Claire Wyart. We thank the Developmental Biology Curie imaging facility (PICT-IBiSA@BDD, Paris, France, UMR3215/U934), member of the France-BioImaging national research infrastructure, for their help and advice with everything microscopy related. The Del Bene laboratory Neural Circuits Development is part of the Laboratoire d'Excellence (LABEX) entitled DEEP (ANR -11-LABX-0044), and of the École des Neurosciences de Paris Ile-de-France network. This work has been in part funded by an ATIP/AVENIR program starting grant (F.D.B.), ERC-StG #311159-Zebratectum (F.D.B.), CNRS, INSERM and Institut Curie (F.D.B) core funding. I.H.B. received a UCL Excellence Fellowship and a Sir Henry Dale Fellowship (101195/Z/13/Z) from the Wellcome Trust and Royal Society. C.G. was supported by an EMBO Short-term Fellowship, an Institut Curie Postdoctoral Fellowship and an FRM Postdoctoral Fellowship. T.O.A. was supported by a Boehringer Ingelheim Fonds PhD Fellowship. P.H. was supported by a UCL IMPACT studentship. G.R. received funding from the European Union's Horizon 2020 Research and Innovation program under the Marie Skłodowska-Curie grant agreement no. 666003.

Author contributions

C.G., I.H.B., and F.D.B. conceived and designed experiments. C.G. performed all experimental procedures unless otherwise indicated. T.O.A. and C.G. identified the ^{ITN}*Gal4* line. P.H. performed the virtual hunting assay experiments. T.O.A. performed in situ hybridizations, morphological ITN characterization, and the synaptic labeling experiments. K.D. helped with immunostaining experiments and zebrafish line maintenance. G.R. performed the behavioral analysis of ^{ITN}*Gal4* fish expressing *BoTxBLC-GFP*. C.G. analyzed the data. C.G., I.H.B. and F.D.B. wrote the manuscript with input from all coauthors.

Competing interests

The authors declare no competing interests.

Additional information

Supplementary information is available for this paper at https://doi.org/10.1038/s41467-019-13484-9.

Correspondence and requests for materials should be addressed to I.H.B. or F.D.B.

Peer review information *Nature Communications* thanks Robert Hindges and the other, anonymous, reviewer(s) for their contribution to the peer review of this work.

Reprints and permission information is available at http://www.nature.com/reprints

Publisher's note Springer Nature remains neutral with regard to jurisdictional claims in published maps and institutional affiliations.

Open Access This article is licensed under a Creative Commons Attribution 4.0 International License, which permits use, sharing, adaptation, distribution and reproduction in any medium or format, as long as you give appropriate credit to the original author(s) and the source, provide a link to the Creative Commons license, and indicate if changes were made. The images or other third party material in this article are included in the article's Creative Commons license, unless indicated otherwise in a credit line to the material. If material is not included in the article's Creative Commons license and your intended use is not permitted by statutory regulation or exceeds the permitted use, you will need to obtain permission directly from the copyright holder. To view a copy of this license, visit http://creativecommons.org/licenses/by/4.0/.

© The Author(s) 2019

Supplementary Information

An interhemispheric neural circuit allowing binocular integration in the optic tectum

(Gebhardt et al.)

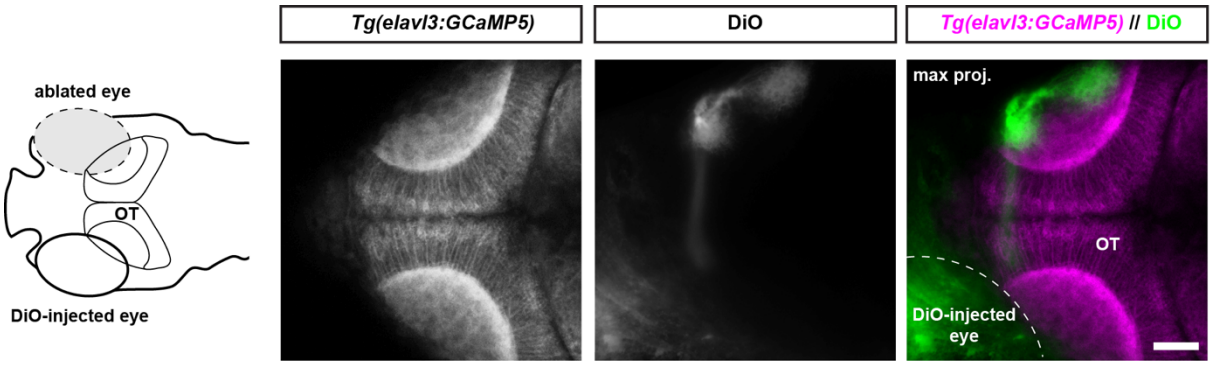

Supplementary Fig. 1

Supplementary Fig. 1. Eye enucleation.

Monocular ablation at 3 dpf does not induce re-routing of retinal fibres of the remaining eye to the ipsilateral tectal hemisphere by 5 dpf as shown by anterograde labelling of retinal ganglion cell axons with DiO (pseudo-coloured in green). The optic tectum is labelled by the pan-neuronal transgene *Tg(elavl3:GCaMP5G)* (pseudo-coloured in magenta). Scale bar = 50 µm.

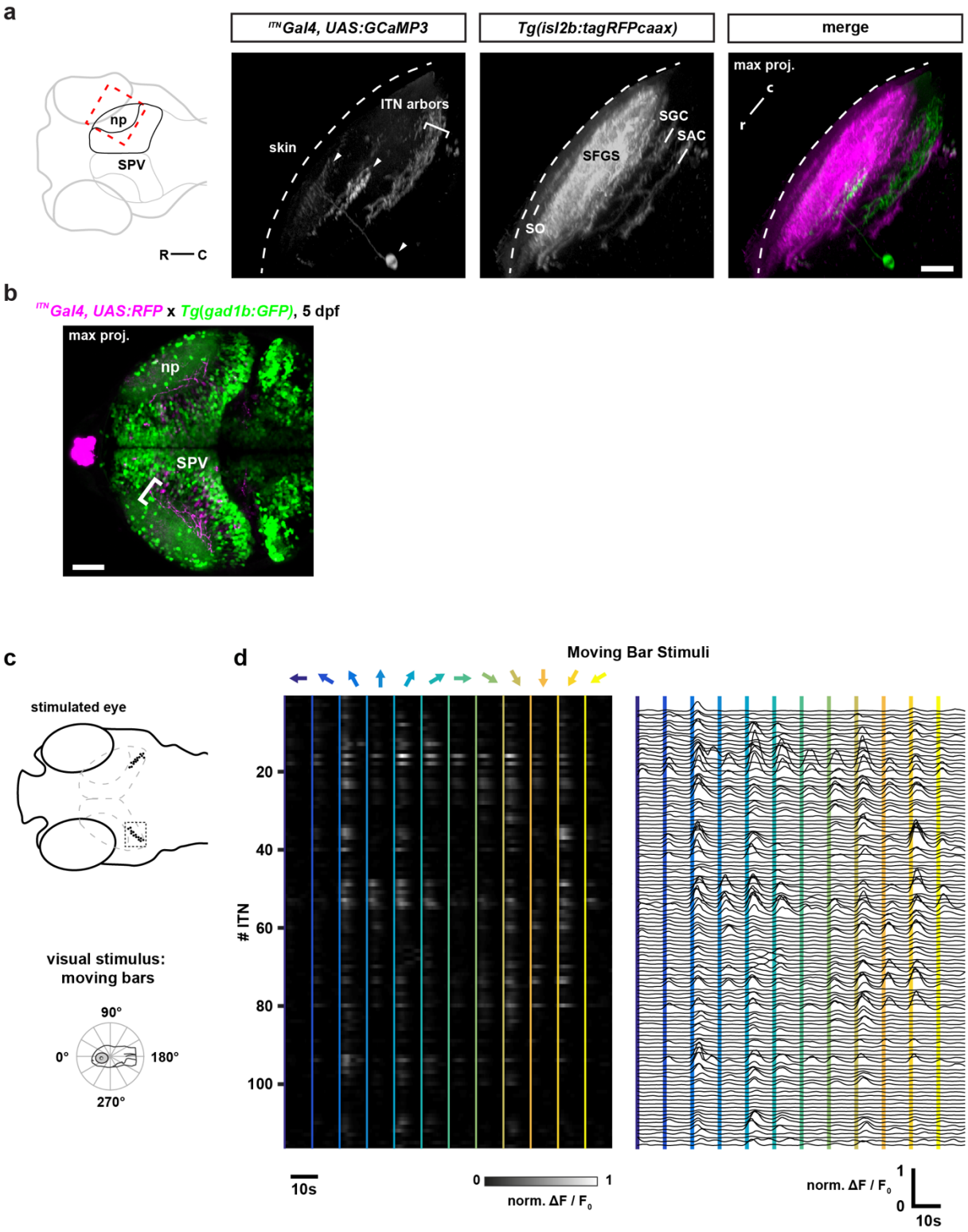

Supplementary Fig. 2

Supplementary Fig. 2. ITNs arborize in the deep layers of the tectal neuropil and respond to visual stimuli.

(a) Maximum intensity projection of the right tectal neuropil viewed dorsally of a representative 3 dpf *^{ITN}Gal4, UAS:GCaMP3*, *Tg(isl2b:tagRFPcaax* larva*)*. ITN arbours are exclusively observed in the deep layers of the tectal neuropil in between the SGC and SAC layer. Occasionally, single PVNs are labelled by the *^{ITN}Gal4* transgene but PVN neurites are rarely overlapping with ITN arbours and can be easily distinguished based on their morphology. A single bi-stratified periventricular neuron in the SPV is labelled in this particular ^{ITN}Gal4 larva (white arrows pointing at the PVN's cell body and its arbours) and was used as anatomical reference. Retinal arbours labelled by the *isl2b* promotor are pseudo-coloured in magenta. Scale bar = 20 µm. (R: rostral, C: caudal, np: tectal neuropil, SO: *stratum opticum*, SFGS: *stratum fibrosum et griseum superficiale*, SGC: *stratum griseum centrale*, SAC: *stratum album centrale*, SPV: *stratum periventricuare*).

(b) ITN arbours are predominantly found in the deep layers of the tectal neuropil (most likely between the SAC and SGC in the tectal neuropil, indicated by the white bracket). This is consistent with the location of visually-evoked activity observed in the ipsilateral deep neuropil after monocular enucleation (see Fig. 1d). Single PVNs were also labelled by the *^{ITN}Gal4* transgene but PVN neurites were mostly non-overlapping with ITN arbours and could thus be easily distinguished based on their morphology. Scale bar = 50 µm. (np: tectal neuropil, SPV: *stratum periventricuare*).

(**c**) 5 dpf larvae expressing GCaMP3 in ITNs were imaged with a 2-photon microscope while visually stimulating the contralateral eye with moving bars (bar width: 9 °, speed: 20 °/s, direction: randomly chosen for each stimulus epoch from 12 angular directions 30 ° apart) running across the field of view.

(**d**) ITNs responded strongly to visual motion stimuli (n = 116 ITNs from 14 larvae). Vertical lines indicate the begin of a stimulus interval color-coded according to the stimulus direction. Source data are provided as a Source Data file.

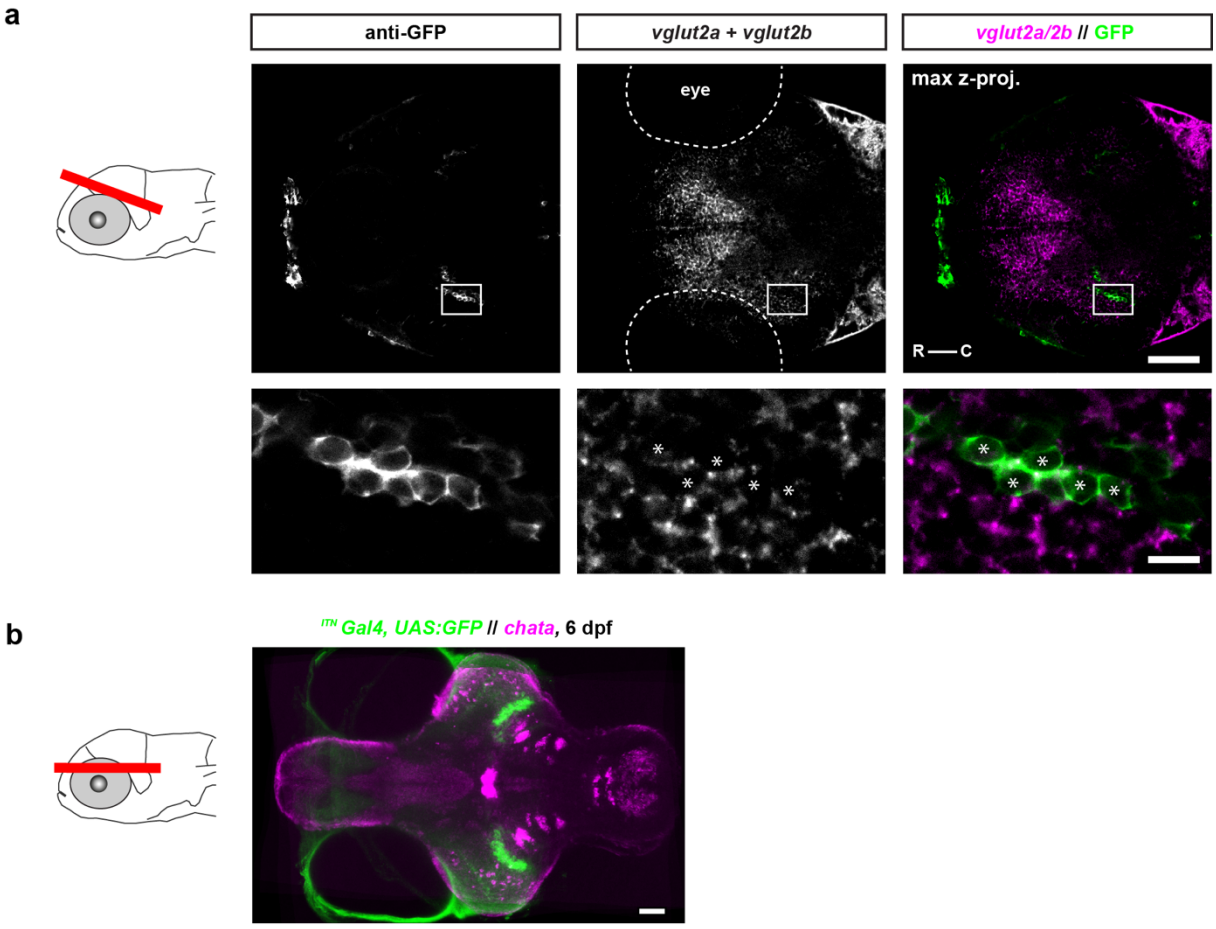

Supplementary Fig. 3

Supplementary Fig. 3. ITNs are neither glutamatergic nor cholinergic.

(a) Expression of *vglut2a*/*vglut2b* as markers for glutamatergic neurons and anti-GFP immunoreactivity in the brain of a 4 dpf ^{ITN}*Gal4, UAS:GCaMP3* larvae (shown cryo-section indicated by the red bar in the schematic larva to the left, scale bar = 50 µm). The ITN cell bodies are visible in the GFP channel (left nucleus highlighted by white rectangle which was then magnified and shown in the lower images for each channel, scale bar = 10 µm). GFP and *vglut2a/vglut2b* expression are mainly non-overlapping (ITNs indicated by asterisks in the lower images).

(b) Overlay of average intensity images derived from datasets of whole-brain GFP-immunoreactivity (green) and *chata* expression (magenta) each registered to the z-brain atlas. GABAergic ITN nuclei are located in the mesencephalic tegmentum, anterior to the midbrain-hindbrain boundary and are not overlapping with cholinergic isthmic nuclei in rhombomere 1. Scale bar = 50 µm.

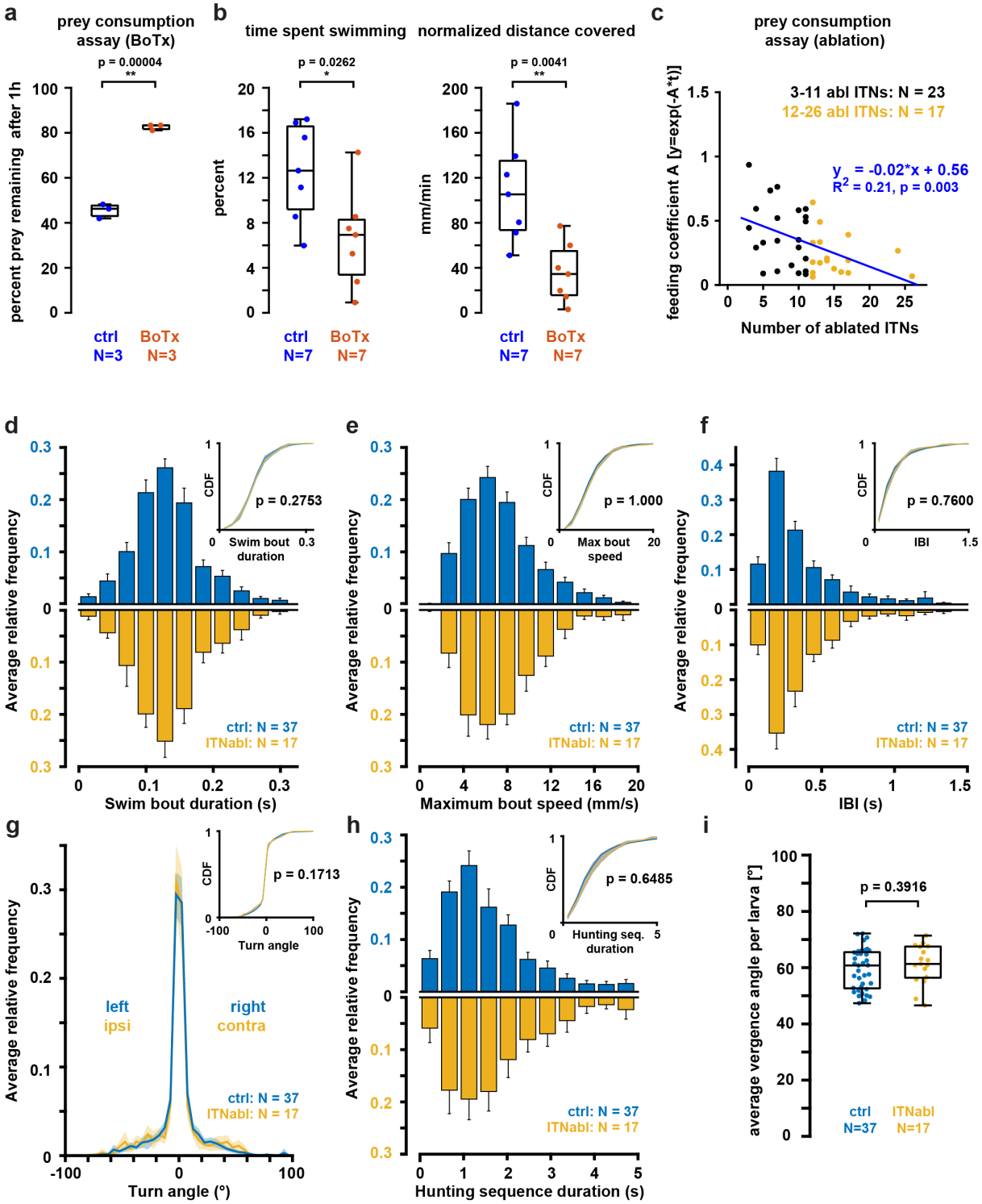

Supplementary Fig. 4

Supplementary Fig. 4. ITN-ablated larvae are indistinguishable from control larvae regarding locomotion and prey recognition.

(a) Silencing of vesicular release in 5 dpf ^{ITN}Gal4 larvae by zebrafish-optimized Botulinum toxin BoTxBLC-GFP (BoTx) caused a severe reduction in prey consumption compared to control siblings in a prey consumption assay (control: median percent prey left after 1h = 46.25 %, BoTx: median percent prey left after 1h = 83.3 %, Mann-Whitney U-test, p = 0.00004, both groups: N = 3 trials, 4 larvae each).

(b) Individual BoTx-expressing larvae spent significantly less time swimming (Mann-Whitney U-test, p = 0.0262) and covered less distance (Mann-Whitney U-test, p = 0.0041) during experimental trials than control siblings (both groups: N = 7 larvae).

(c) The number of ablated ITNs plotted against the feeding coefficient A, derived from temporal feeding curves in the prey consumption assays [y = exp(-A*t)].

(d) Average relative frequencies of swim bout duration during hunting sequences for control (blue) and ITN-ablated larvae (yellow). No significant difference of swim bout duration distributions was found between control and ITN-ablated larvae (control: n = 6749 swim bouts from 37 larvae, median duration = 0.138 s, ITN-ablated: n = 2519 swim bouts from n = 17 larvae, median duration = 0.135 s, Kolmogorov-Smirnov-test, p = 0.2753). Error bars of all following relative frequency plots indicate the +95 % confidence interval. The insets show the cumulative distribution function for control and ITN-ablated histograms with the grey shaded boundaries indicating the 95 % confidence intervals.

(e) Average relative frequencies of maximum swim bout speed during hunting sequences for control (blue) and ITN-ablated larvae (yellow). No significant difference of maximum swim bout speed distributions was found between control and ITN-ablated larvae (control: n = 6749 swim bouts from 37 larvae, median maximum speed = 7.123 mm/s, ITN-ablated: n = 2519 swim bouts from n = 17 larvae, median maximum speed = 7.734 mm/s, Kolmogorov-Smirnov-test, p = 1.000).

(f) Average relative frequencies of interbout interval (IBI) duration during hunting sequences for control (blue) and ITN-ablated larvae (yellow). No significant difference of IBI duration distributions was found between control and ITN-ablated larvae (control: n = 4655 interbout intervals from 37 larvae, median duration = 0.338 s, ITN-ablated: n = 1649 interbout intervals from n = 17 larvae, median duration = 0.339 s, Kolmogorov-Smirnov-test, p = 0.7600).

(g) Average relative frequencies of changes in orientation per swim bout (= turn angle) during hunting sequences with the shaded boundaries indicating the respective 95 % confidence intervals. No difference of swim bout angle distributions was observed between control and ITN-ablated larvae (control: n = 6749 swim bouts / turns from 37 larvae, ITN-ablated: n = 2519 swim bouts / turns from n = 17 larvae, Kolmogorov-Smirnov-test, p = 0.1713).

(h) Average relative frequencies of hunting sequence duration for control (blue) and ITN-ablated larvae (yellow). No significant difference of hunting sequence duration distributions was found between control and ITN-ablated larvae (control: n = 2263 hunting sequences from 37 larvae, median duration = 1.689 s, ITN-ablated: n = 948 hunting sequences from n = 17 larvae, median duration = 1.722 s, Kolmogorov-Smirnov-test, p = 0.6485).

(i) ITN-ablated larvae do not show significantly different average vergence angles during hunting compared to control larvae (control: n = 2263 hunting sequences from 37 larvae, median vergence angle = 60.8 °, ITN-ablated: n = 948 hunting sequences from n = 17 larvae, median vergence angle = 61.3 °, Mann-Whitney U-test, p = 0.3916). Source data for all panels in this figure are provided as a Source Data file.

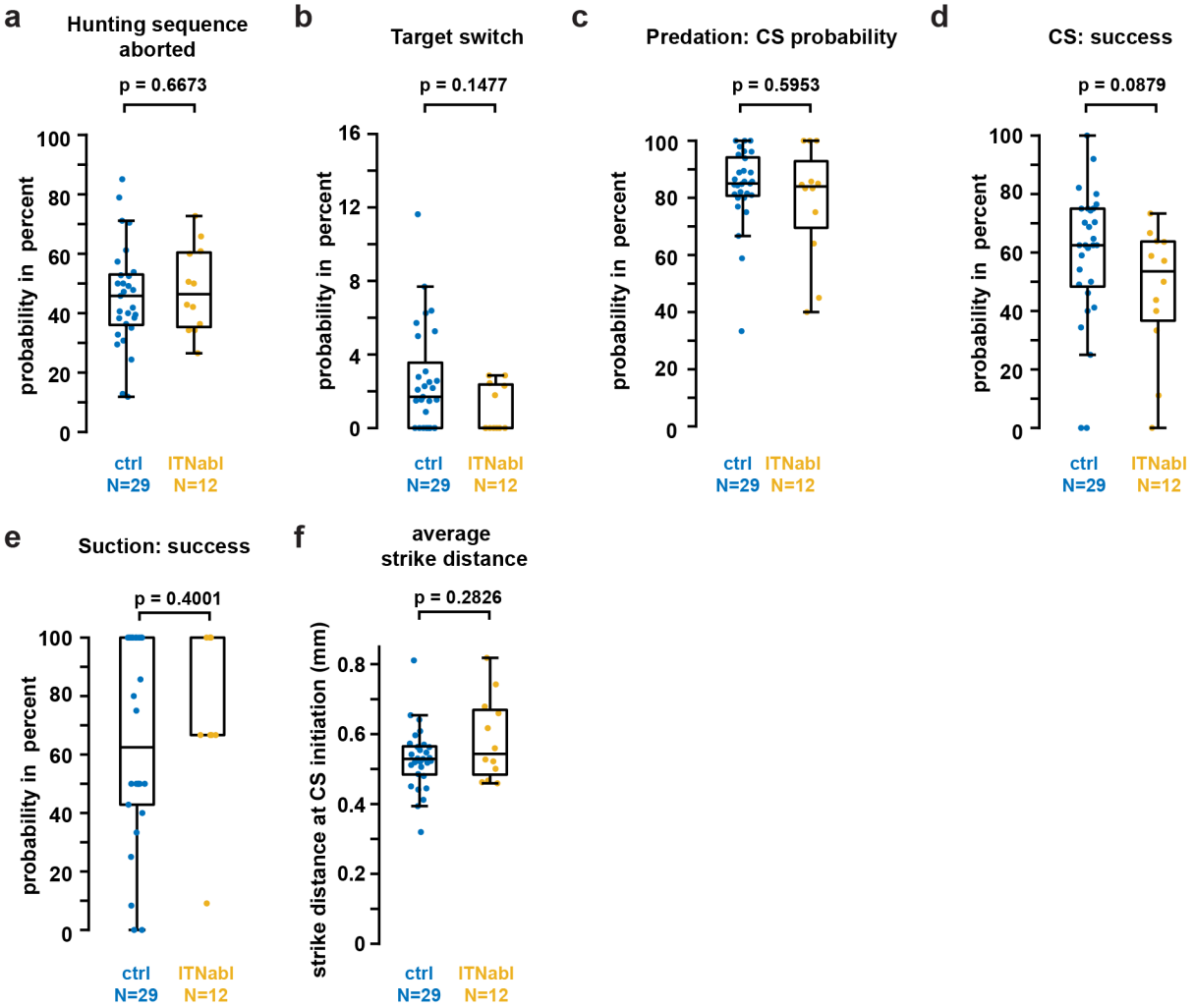

Supplementary Fig. 5

Supplementary Fig. 5. Hunting sequence classification.

(a) ITN-ablated larvae did not abort hunting sequences while the target was outside the binocular strike zone (d > 0.5 mm and/or abs(azimuth) > 10 °) with a different probability compared to control larvae (control: median probability = 45.8 %, ITN-ablated: median probability = 46.4 %, Mann-Whitney U-test, p = 0.6673).

(b) ITN-ablated larvae also did not show a significantly different probability to switch, once one prey target was being pursued, to another target compared to control larvae (control: median target switch probability = 1.7 %, ITN-ablated: median target switch probability = 0 %, Mann-Whitney U-test, p = 0.1477).

(c) If they engaged in predation once targeted prey was in the binocular striking zone, ITN-ablated larvae did not perform capture swims (CS) with a different probability compared to control larvae. This suggests that ITN-ablated larvae did not change their hunting strategy, e.g. by performing more suctions (control: median CS initiation probability = 85.0 %, ITN-ablated: median CS initiation = 84.0 %, Mann-Whitney U-test, p = 0.5953).

(d) ITN-ablated larvae did show a slightly decreased, although not significantly different, probability of successful capture swims (CS) compared to control larvae (control: median probability = 62.5 %, ITN-ablated: median probability = 53.6 %, Mann-Whitney U-test, p = 0.0879).

(e) ITN-ablated larvae did not show a significant different probability of successful suctions compared to control larvae (control: median probability = 62.5 %, ITN-ablated: median probability = 66.6 %, Mann-Whitney U-test, p = 0.4001).

(f) ITN-ablated larvae did not show significantly different average striking distances per larva during capture swims (CS) compared to control larvae (control: median distance = 0.529 mm, ITN-ablated: median distance = 0.543 mm, Mann-Whitney U-test, p = 0.2826). Source data for all panels in this figure are provided as a Source Data file.

Annex #3

This annex contains a manuscript based on the results in Chapters 3 and 4 and is prepared for a peer-reviewed publication. This will be the primary publication from this thesis work and includes content from all the Chapters, 1 to 6. The manuscript is provided with a primary document covering the main results and a supplemental document providing additional supporting data.

Divergence of exploratory locomotion in two closely related vertebrate species

Gokul Rajan[1,2], Julie Lafaye[3], Martin Carbo Tano[4], Karine Duroure[1,2], Dimitrii Tanese[5], Giulia Faini[5], Thomas Panier[3], Jörg Henninger[6], Benjamin Judkewitz[6], Ralf Britz[7], Christoph Gebhardt[1,8], Raphaël Candelier[3], Valentina Emiliani[5], Georges Debregeas[3], Claire Wyart[4], *Filippo Del Bene[1,2]

[1]Institut Curie, PSL Research University, INSERM U934, CNRS UMR3215, Paris, France

[2]present address: Sorbonne Université, INSERM, CNRS, Institut de la Vision, Paris, France

[3]Sorbonne Université, CNRS, Institut de Biologie Paris-Seine (IBPS), Laboratoire Jean Perrin (LJP), 75005, Paris, France

[4]Institut du Cerveau et de la Moelle épinière (ICM), Sorbonne Universités, UPMC Univ Paris 06, Inserm, CNRS, Hôpital Pitié-Salpêtrière, France

[5]Institut de la Vision, Sorbonne Université, INSERM S968, CNRS UMR7210, Paris, France

[6]Einstein Center for Neurosciences, NeuroCure Cluster of Excellence, Charité–Universitätsmedizin Berlin, Berlin, Germany

[7]Department of Life Sciences, Natural History Museum, Cromwell Road, London, SW7 SBD, UK

[8]present address: Zuckerman Mind Brain Behavior Institute and Department of Ecology, Evolution, and Environmental Biology, Columbia University, New York, NY 10027, USA

Key words: *Danionella translucida*; *Danio rerio*; divergence; locomotion; neuronal circuits

*Corresponding author: filippo.del-bene@inserm.fr

Abstract

Diverse forms of locomotion exist in nature and is adapted to the environmental constraints of an animal. We established an approach to understand how neuronal circuits underlying locomotion diverge in nature by comparing larvae of two closely related species, *Danionella translucida* (DT) and *Danio rerio* or zebrafish (ZF), that occupy similar environments and yet exhibit different swimming behaviors. Using transgenesis, *in-situ* staining, light sheet imaging, optogenetic stimulation and field study, we investigated the proximate (cellular and physiological) and ultimate (organismal) causes behind this divergence in swimming behavior despite the phylogenetic and environmental proximity that the two species share. DT is shown to utilize lower half tail-beat frequencies and maximum tail angles to generate a lower thrust producing a continuous swimming at lower speed compared to ZF. The reorientation kinematics of the two fish are also found to be very different where DT tend have a long ballistic swim phase. We show a high degree of conservation in brain anatomy and identified a mid-brain nucleus in DT and ZF to be responsible to maintain the long-lasting swim events in the larvae. Moreover, we propose two organismal characteristics which add ethological relevance to the observed differences in swimming.

Introduction

Danionella translucida (DT) undergo a developmental truncation which leads to a small body size in adults with a partially developed cranium. This is indeed what makes them interesting for functional neuroscience studies (Schulze et al., 2018). However, studies on ossification in *Danionella dracula* demonstrate that most bones affected by truncation are formed later in the development of zebrafish (Britz et al., 2009). Hence, developmentally the two species should be very much comparable in the early stages of development. Most studies on neuronal circuits try to characterize a functional circuit in a single organism at a given timepoint. Within an animal, the functional circuits change over the ontogenic time course. Changes can also be observed across different animal species due to differences that emerged over the evolutionary time course. Studies looking at such comparisons would increase the scope of the discipline of evolutionary-development to include neuroscience in its purview (Raff, 2000).

Two important concepts while considering such changes at an evolutionary time course are homoplasy and homology. Homoplasy can arise from convergent or parallel evolution. Convergence is an important phenomenon in evolution which points to specific conserved ways of laying out an optimal system. In contrast, homologous systems can show divergence over time and acquire new functions. The concept can, of course, be extended to genes, proteins, cells, networks and behaviors. In the current study, we demonstrate the differences in the explorative swimming of DT and zebrafish (ZF) despite their evolutionary closeness, and investigate the factors underlying these differences. For a new behavior to emerge, it can broadly happen in at least three ways from a neuronal circuit viewpoint (Katz & Hale, 2017): (1) Changes in peripheral systems without major changes to the central neuronal networks. (2) Rewiring of functional neuronal circuits involved in the behavior. (3) Changes in neuronal network activity without any changes in the hardwiring. This can be due to the cellular and network properties of the neurons involved, or due to neuromodulation.

We used high-speed imaging we show that DT performs long-lasting swim events with a continuous tail-beat activity as opposed to the short burst-and-glide swimming in ZF. A high degree of anatomical conservation is demonstrated using *in-situ* and immunohistochemistry methods. Using a novel DT *Tg(HuC:H2B-GCaMP6s)* and light sheet imaging, we identified a mid-brain nuclei correlated with maintenance of the long swim events in DT. The role of this nuclei in sustaining the long swim events was validated using optogenetic stimulation in ZF to induce increased swimming. Moreover, based on laboratory and field evidence, we suggest two organismal characteristics which form a strong argument for the ethological relevance of the difference in swimming pattern in the two fish species. To our knowledge, such a comprehensive comparison encompassing behavior, anatomy, physiology and ecology has not been carried out in vertebrates before. To put it according to Tinbergen's classical paper on ethology, biologically, behavior can be investigated at four distinct levels (Tinbergen, 1963): (1) how

is it caused physiologically? (2) what is its survival value? (3) how has it evolved? (4) how does it develop in the individual? It is the first two aspects, physiology and survival advantage, that we tackle in this work.

Results

Larval *Danionella translucida* (DT) and zebrafish (ZF) are comparable in size. However, DT executes a continuous pattern of swimming unlike ZF.

DT and ZF are found in similar freshwater environments in Asia and are evolutionarily very closely related as documented in Figure S1. This is an advantage to comparative studies of larval DT and ZF which look at divergent phenomena. During undulatory swimming, propulsive forces result from the fluid-body interaction. The resulting thrust and hydrodynamic resistance strongly depend on the animal's body size (Muller, 2004 and Van Leeuwen et al., 2015). Here, in Figure 1A-B, an overview of the size of the two larvae at 5 dpf is shown. Although there is a subtle difference in their length, they fall in a similar range. In our dataset, the length of DT ranges from 4.4 to 4.9 mm and the length of ZF ranges from 4.1 to 4.7 mm. With this comparable range in size, they would be expected to develop similar propulsive forces and hydrodynamic resistance during swimming.

ZF are known to swim in a beat-and-glide pattern wherein a burst of tail activity lasting ~140 ms is followed by a small glide phase (Budick & O'Malley, 2000). In contrast to this, in DT, we observe sequences of continuous tail activity lasting for hundreds or thousands of seconds. A high speed (700 Hz) imaging system was used to record spontaneous swimming in fish. Figure 1C and 1D show the behavioral acquisition system and the resultant swimming tracks of a fish respectively. Movies #1 and #2 represent a spontaneous swimming video of DT and ZF respectively. The swimming speed of the fish was determined based on the x/y coordinates of the fish and the tail angle can be considered as the angle of the farthest tail segment from the body with respect to the body axis. Figure 1E shows the behavioral difference in a time window of 10 seconds for a representative fish from both the fish species. One can note the continuous swimming at a lower speed throughout the 10 s window in DT. In contrast, the swimming in ZF is clearly intermittent with longer pauses as compared to their period of activity.

Danionella translucida (DT) use lower tail angle and half tail beat frequency to achieve slower swimming when compared to zebrafish (ZF)

The finer kinematics of swimming behavior in the two fish species is explored in this section. To achieve this, half tail beats were defined using the tail angle information (Figure S2-A). Approximately thousands of half beats per fish were used in the analysis to calculate the kinematic parameters such as

half tail beat frequency (Hz), maximum tail angle (degree) and mean instantaneous speed (mm/s). This is shown below in Figure 1F. In DT, the median half beat frequency is 41.18 Hz and in ZF, it is 63.64 Hz. In terms of tail angle, the maximum tail angle lies at 19.23 degree and 42.73 degree for DT and ZF respectively. This lower half beat frequency combined with lower tail angle in DT would lead to generation of a lower thrust when compared to ZF. Such lower thrust leads to a slower mean swimming speed in DT (3.07 mm/s) when compared to ZF (16.93 mm/s). This shows how DT can sustain long swimming periods by executing slower swims at lower thrust.

The above results are based on the half beat analysis, specifically ~460,000 half beats from 23 DT and 190,000 half beats from 37 ZF. It was important to formulate the analysis based on half-beats to be able to work with two comparable units of locomotion. It is important to note that although the half beat based analysis would lead to slightly different kinematic results in ZF when compared to the classical bout-based analysis, this would not change the conclusions in terms of the large differences that we note in the kinematics of DT and ZF. The bout-wise analysis was also performed on the same dataset and is presented in Figure S2(B-G) for comparison.

Danionella translucida (DT) maintain longer and continuous swimming in head-embedded preparation when compared to zebrafish (ZF)

A drawback of the spontaneous free-swimming assay is that the long continuous stretches of swim events in DT are often split into smaller fragments of swim tracks when the fish approaches the edges of the arena as the background illumination at the edges causes a problem with reliable tracking of the fish. This can lead to an underestimation of the duration of the swim events in DT. To overcome the aforementioned caveat in estimation of duration of swim events and to make our behavioral recordings as close as the later brain imaging experiments, we used a head-embedded preparation of DT and ZF as shown in Figure 1G. This gives the ability to confine the animal with its tail-free to continuously monitor the tail activity and comment on the maximum duration of the swim events. The animals were acclimatized to the recording conditions for >90 minutes. The recordings lasted for 10-20 minutes.

In Figure 1G, the difference in the duration of swimming is shown as a raster plot. The black regions indicate swimming, while the white regions indicate the periods of rest. The 4 DT fish swim for most part of the recording. On the contrary, the 4 ZF swim in small bursts of activity, interspersed with long pauses. The median percentage of the total time spent swimming is shown in Figure 1H. DT swims for 98.5 % of the total recording whereas ZF swims only 2%. Additionally, the absolute duration of the swims was found to be very variable for DT, ranging from a minimum of 106 sec to a maximum of 1289 sec (which is the same as the maximum duration of the acquisition). For ZF, this range was between 460 ms and 938 ms. This is higher than what we see in a free-swimming ZF and such a difference in

bout durations between free-swimming and head-embedded preparations is already reported (Severi et al., 2014).

Escape response is conserved between *Danionella translucida* (DT) and *Danio rerio* but DT shows a lower latency to attain peak speed

The auditory escape response is very conserved among various fish species and is known to follow a very stereotypical pattern in ZF. We examined if this response differed in the two fish species by virtue of their differing pattern of spontaneous swimming. We built a tap-induced escape assay to study this. Briefly, a tap was delivered to the behavioral arena platform when the fish swims in the center region of the arena (Movie #3). The stimulation events are spaced in time by at least 50 secs to avoid any habituation. Figure 1I shows the striking similarity in the escape strategy between DT and Z. Both fish species initiate a fast escape response with a C-turn followed by a counter bend. This highly conserved escape response was expected to be similar between the two fish.

However, there are minor differences in the kinematics. The analysis of the kinematics was carried out in a window of 140 ms around the escape maneuver as shown in Figure S3. This window was empirically selected based on exploratory analysis of escape events in both the fish species. As can be seen in Figure IJ, DT swims with a lower mean speed and covers a smaller distance during this period compared to ZF. Despite that, the mean escape speed of DT at 30.5 mm/s is as much as a 10-fold increase from its free-swimming speed. In ZF, this increase is only ~3 folds at 42.9 mm/s. This has to be interpreted cautiously though as the free-swimming velocity and escape velocity are estimated using very different time windows. DT seems to undergo a larger change in speed during the escape. The distance covered by DT (4.3 mm) is less when compared to ZF (6.0 mm). This alone does not quantify the efficiency of the escape very well though. Another important parameter would have been the variability in the directionality of the escapes but this parameter is not suitable to the tap-induced escape assay being tested here. On the other hand, the delay to achieve maximum speed during escape is different in the two fish species. The delay is found to be surprisingly smaller in DT at 28.6 ms when compared to 33.6 ms in ZF. This appears to be an interesting tradeoff between response time and escape speed.

Swimming in *Danionella translucida* (DT) consists of a long ballistic phase

Mean squared displacement (MSD) can be thought of as a measure of the space explored by a motile agent over a given time. This quantity can help us to get an idea of the extent of spatial spread of an animal's trajectory over time. The MSD obviously depends on the instantaneous speed as examined earlier, but it also depends on the dynamics of reorientation. To quantify the latter, the decorrelation in heading angle (R) was calculated, from which we extracted the time-scale over which the motion of the

fish can be considered to be ballistic. Figure 2A and 2B represent a few swimming tracks isolated from a single DT and ZF respectively. Such tracks were used to quantify the R and MSD. There is a faster randomization of orientation in ZF compared to DT, as evidenced by the comparison of the heading decorrelation dynamics in Figure 2C. For ZF, the decorrelation function R(t) decays in about 1 second down to 0.3, then reaches zero in 6-7 seconds. By comparison, for DT, R(t) shows a small initial drop (down to 0.8) then reaches 0 exponentially over ~8 seconds. For DT, this randomization can be understood by describing the fish navigation as a series of straight ballistic periods interspersed by discrete reorientation events, akin to the classical run-and-tumble mechanisms of motile bacteria (Berg & Brown, 1972, Watari & Larson, 2010 and Darnton et al., 2007). The small initial decay can be interpreted as a short time-scale fluctuation in heading direction during run periods. The subsequent slow exponential decay has a decay time of ~6 seconds that corresponds to the mean duration of the straight segments. This slower decay in heading decorrelation of DT is expected to yield a longer ballistic regime compared to ZF.

To illustrate this fact, we estimated the ballistic component of the MSD as:

$$MSD_{bal}(t) = \langle \left[\int_{t_0}^{t_0+t} v * R(t' - t_0).dt' \right]^2 \rangle_{t_0}$$

As shown in Figure 2C, for DT, this quantity correctly captures the MSD of the ballistic regime up to ~6 seconds. In contrast, for ZF, the MSD departs from the ballistic component from 1 second (or approximately 2 bouts) onwards, indicating that beyond this threshold the diffusive component becomes dominant. Although ZF's instantaneous velocity is larger than DT as shown before, the MSD of both species are comparable over our experimental range as shown in Figure 2D. This is due to the slower reorientation kinematics of DT as discussed above. In conclusion, although ZF is significantly faster at short-time scales, the longer ballistic regime of DT would lead to a comparable exploratory kinematics at long time-scale (beyond 10 seconds). Figure S4 illustrates that during these long swimming periods, DT is also capable of executing a modulation of swimming speed.

Lower availability of dissolved oxygen and delayed inflation of swim bladder could have contributed to the differing swimming pattern

A pertinent question is what selective forces, physiological or environmental if any, would have led to the differing pattern of swimming at the smaller time-scale. Fish were tested in a long column (36 cm) of water for their preference of depth. For analysis, the column was divided into three zones - upper, middle and lower. As can be seen in Figure 2E, larval DT show a strong preference for the bottom of the water column and larval ZF prefer the top zone of the water column. Upper layers of a water column

are richer in dissolved oxygen (DO) when compared to the bottom layers (Boehrer & Schultze, 2008 and Davis, 1975). Hence, the preference of DT to deeper water would accompany a lower availability of DO. A lower availability of DO (from depth preference shown in Figure 2E) would prevent the animal from executing high speed swims which would demand a higher consumption of oxygen as shown in Figure S5-A. A slower swimming would be selected in this case as seen in DT. In addition to slow swimming, a continuous movement would also be beneficial as it will allow the animal to replenish the DO in its surrounding by either continuously displacing itself to a new location or by locally mixing the DO in its immediate surrounding with motion. The latter has been shown analytically shown by Weihs (1980) and is illustrated in Figure S5-B.

The laboratory finding of larval DT's preference to the bottom of the water column was also found to be conserved in adult DT in our field study. The field study was carried out in Myanmar (Figure S5-C). The DO concentration that we recorded at this depth of the stream in Myanmar was 2.83 mg/L. Compared to this, adult zebrafish are reported in waters with a median DO concentration of 5.55 mg/L (Shukla & Bhat, 2017).

Another observation of plausible consequence is the delayed inflation of swim bladder in DT. A complete inflation of swim bladder in DT has been observed at ~15 dpf as shown in Figure 2F. In ZF, the inflation of swim bladder already occurs at ~4dpf, which is around the same time (~5dpf) when the animal has to start actively feeding as the yolk is used up. The yolk disappears at ~4 dpf in DT as well but the swim bladder inflation is delayed. It would imply that DT has to actively swim without a swim bladder and explore its environment to be able to feed and survive. A fish without swim bladder would have to continuously swim and exert a downward force.

However, it is important to note that the delayed inflation of swim bladder alone would not explain the difference in swimming pattern. Swimming was evaluated in a population of 15 dpf DT larvae with inflated swim bladder. This is shown in Figure S6. Although, a decrease is seen in the proportion of time spent swimming in 15 dpf DT when compared to 6 dpf DT, it is still very high when compared to the burst-and-glide swims of ZF. This would suggest that the swimming pattern of DT might be a result of a combination of factors which include lower availability of DO and delayed inflation of swim bladder.

Distribution of reticulospinal neurons and excitatory and inhibitory neurons in the hindbrain is conserved

Determining the anatomy was the first step to understand the cellular underpinnings of the change in swimming. Since the RS neurons project directly from the brainstem to the spinal cord, as command neurons, they are good candidates for controlling the pattern of locomotion. To visualize these neurons,

we carried out backfill experiments using Texas Red in DT and ZF. Figure 3A shows the labelling of reticulospinal (RS) neurons in DT. In both DT and ZF, a similar experimental protocol was used to label the RS neurons to be able to directly compare them.

In Figure 1B, we tried to carry out a cell-to-cell comparison of the reticulospinal neurons between the two species. We could identify cells of the mesencephalic nucleus of the medial longitudinal fascicle (nucMLF/nMLF), the rhombocephalic reticular formation (nucRE) and the rhombocephalic vestibular nucleus (nucVE) that are described in ZF. Specifically, the various cells from the rostral (RoL, RoM, RoV), middle (Mauthner neuron, MiR, MiM, MiV, MiD) and caudal (CaD, CaV) RE nucleus were also identified in DT. In the nMLF, MeM and MeL cells were recognized. Dendrites crossing the midline from MeM cells were identified in DT as described in ZF earlier (Figure 1C). The annotations are based on the cell descriptions in ZF (Kimmel et al., 1982 and Orger et al., 2008).

Next, we investigated the distribution of excitatory (glutamatergic) and inhibitory (glycinergic and GABAergic) neurons in the hindbrain as this has been already well characterized in the ZF brain. For labelling glutamatergic and glycinergic cells, we used *in-situ* hybridization and for GABAergic cells, immunohistochemistry was used. As can be seen from Figure 3D-F, the distribution of the excitatory and inhibitory neurons forms roustro-caudally running stripes in the hindbrain. This has been reported widely in ZF and is represented in Figure S7. The cross-sectional views of these markers are illustrated in Figure S8. The developmental and functional consequences arising from this spectacularly conserved patterning might also be conserved between the two species.

Similar supraspinal nuclei are correlated with swimming in both fishes; however, with long-lasting neuronal activity in DT

To identify functionally relevant nuclei in the brain corresponding to swimming activity, we created a transgenic line, *Tg(HuC:H2B-GCaMP6s)* expressing a near pan-neuronal nuclear-localized GCaMP6s indicator. A comparison with an equivalent transgenic in ZF is shown in Figure S9. For the whole-brain imaging experiments, we used 5dpf DT and ZF and acquired a brain volume of ~200 µm at ~1 Hz while the tail of the fish was freed to record the swimming movements simultaneously (Figure S10).

The foremost goal of the analysis was to identify the supraspinal centers of locomotion in the brain and to compare their activity between the two species. The whole brain acquisitions were segmented into thousands of regions of interest (ROIs) representing individual neurons. The behavior of the fish was extracted from the tail acquisitions and converted into a binary on/off signal. A regression analysis was performed between the neuronal fluorescence signal and the regressor representing the swim events. An illustration of the methodology used for selecting the best swim cells using regression coefficient (a_1) and t-score (a_2) as a confidence value (a_1+a_2) is shown in Figure 4A. A set of nuclei were obtained in

DT and ZF brains that were highly correlated with the swimming behavior – these neurons will be referred to as swim neurons or swim "maintenance" neurons. The distribution of the nuclei in the medial mid-brain, lateral mid-brain and hindbrain is very conserved between the two fish species (Figure 4B-C). More representative brains for ZF and DT are shown in Figure S11. In Figure 4D, the mean neuronal activity of the identified neurons is plotted with swim events (in grey). As can be seen from the Figure 4D, the activity in these identified nuclei in DT scale with the long swim events of DT. This points to a role of these nuclei in the maintenance of the long swim events in DT.

Optogenetic activation of the mid-brain swim nucleus in ZF leads to increased swimming

To verify the role of the identified mid-brain nucleus in sustaining the long swim events in DT, we carried out optogenetic stimulation in ZF. We performed this experiment in ZF as transgenic lines, such as *Tg(HuC:CoChR-eGFP)*, are available in ZF to carry out optogenetic manipulation. The idea was to stimulate the identified swim maintenance neurons in ZF and to verify whether such a stimulation would lead to a prolonged swimming in ZF. We selected the medial mid-brain neuron for the stimulation. The region is highlighted in the Figure 4E (top). The embedded fish which were able to swim at the recording chamber underwent the stimulation protocol. As can be seen in Figure 4E (bottom), the stimulation caused an increased swimming in ZF. The increase in swimming was caused by both, a recruitment of more bouts and an increase in the duration of bouts. This evidence establishes the role of this novel mid-brain nuclei in the maintenance of long swim events.

Discussion

The similar morphology and evolutionary closeness of the two larval species provided a unique opportunity to understand how differences in behaviors can arise from relatively conserved neuronal circuits. We demonstrated the striking differences in the swimming of DT and ZF at the milliseconds- and seconds- timescale, identified a mid-brain neuronal population whose differential activity might underlie the differences in the swimming behavior of the two fish and proposed ethologically relevant reasons which might explain the survival advantage of the swimming types.

While undertaking such a study, it can be difficult to decipher which stage of the two fish species is directly comparable. No single marker or a combination of markers can be assumed to have an effective readout of the relative age of the two fish species. To overcome this, we used fish of the same age based on their absolute developmental stage. This approach is more effective as it does not assume anything about the developmental stage of the fish based on a few physiological/ morphological markers and the behaviors under investigation do not change by a matter of few days in either of the fish species. The primary focus of the study has been on the long-lasting continuous swimming in DT and its

consequences at the behavioral (mechanistic and ethological) and neuronal circuit levels. We found that DT utilizes low half tail beat frequency and maximum tail angle to generate a low propulsive force leading to a swimming at lower speeds as opposed to the fast swimming observed in ZF (Van Leeuwen et al., 2015). An important difference in the analysis of spontaneous swimming that we introduce is, instead of analyzing the swimming based on bouts as is classically done in ZF (Severi et al., 2014), we use half tail beats which are defined as a peak-to-peak tail beat cycles. This was important to be able to evaluate swimming in the two species at a level that is comparable to each other and half tail beats were the most basic common unit of locomotion. Such slow swimming is sustained for long periods of time in DT. These long continuous swim events were also well captured in the head-embedded swimming experiment.

Given the differences in spontaneous swimming pattern in ZF and DT, we asked if this would cause a difference in the escape swim executed by the two fish species. While qualitatively the escape strategy appeared to be very conserved, subtle differences were noted in the kinematics. The mean escape speed and the response time to achieve peak escape speed were lower in DT compared to ZF. So, DT makes a slower escape but can respond faster than ZF; an interesting trade-off. However, the efficacy of an escape depends on other factors as well which are not considered here. Directionality of escape is one such parameter (Bhattacharyya et al., 2017). Also, there is evidence that sensory modality, the ability to locate a predatory stimulus from a distance, serves as best predictor of a successful escape response (Nair et al., 2017). The low-latency escape response in DT could be mediated at the motor level by a faster motor transformation or/and at the sensory level by a quicker sensory integration (Niell & Stryker, 2010, Dadarlat & Stryker, 2017, Kaneko, Fu, & Stryker, 2017).

The influence of this swimming mechanism on explorative swimming in DT and ZF. We compared the mean squared displacement (MSD) which depends on both, instantaneous speed and the reorientation in heading angle. Although ZF's instantaneous velocity is higher than DT, the MSD is comparable in the two fish. This can be explained by studying the heading decorrelation curve. ZF is seen to show a rapid drop in heading decorrelation, reaching R=0.3 in 1 sec. In DT, on the contrary, although an initial small decline of R=0.8 is seen – it later drops to R=0 slowly over a period of over 8 seconds. This delay in decay of heading decorrelation indicates a longer ballistic regime in DT compared ZF. It is to be noted that the length of ballistic swims in DT can still be an underestimation as swimming in the confined space of the arena in the experimental set-up can influence its reorientation frequency.

We briefly looked at organismal characteristics which might be able to explain the interesting differences in the swimming that we have noted above. The long generation time of DT and ZF prevent the use of experimental evolution approach to demonstrate link between differences at organismal level and its role in the development of the swimming pattern. Nevertheless, we describe two plausible factors that can contribute to this observed difference in swimming pattern. The first of these is: DT's preference

to the bottom layers of the water column and the accompanied exposure to lower dissolved oxygen (DO) concentrations. The preference to the bottom water column was also confirmed in our field study with adult DT. Although we were unable to cite larval DT in the wild, the presence of adult DT at the bottom of the water column and their spawning behavior at the crevices would strongly point towards the occurrence of the larval habitat in the bottom layers of the water column as well. In contrary, ZF adults spawn in the shallower ephemeral pools created in the monsoons (Parichy, 2015). To study efficiency of swimming, many authors have used oxygen consumption as a readout for energy input. For instance, it has been shown in trout, goldfish, *Euphausia pacifica* and others that oxygen consumption increases with increase in swim speed (Webb, 1971, Smit et al., 1971, Torres & Childress, 1983, Brett, 1964). Figure S5 shows such a dependency in larval ZF-like fish (Bagatto et al., 2001). Lower oxygen availability in DT would limit the maximum oxygen consumption and thus lead to a lower swim speed. Of course, many animals thrive in deep sea environments with extremely low oxygen levels but this might be dependent on a large number of adaptations which might have promoted lower oxygen consumption (Childress & Seibel, 1997). In closely related freshwater species, more subtle adaptation such as a difference in swimming can be expected. In addition to a decreased swimming speed, a decreased DO concentration has also been shown to promote a more continuous swimming (Green et al., 2011 and Weihs 1979).

The second characteristic that we observed which seemed to offer an explanation to the difference in swimming pattern was the delayed inflation of the swim bladder. At first, the preference to the bottom might seem to be associated with the delayed inflation of the swim bladder but this might not be necessarily be true as the preference seems to be also conserved in adult DT with inflated swim bladder. A swim bladder provides the ability to swim at various levels of the water columns without expending significant amount of energy to stay afloat. Without a swim bladder, a fish would have to continuously exert a downward force equivalent to 5% of its weight in air to maintain a level in the water (Denton & Marshall, 1958). For instance, mackerels (*Scomber scombrus*) do not possess a swim bladder and are observed to swim vigorously, likely to maintain their height in water column. Since we provide evidence that the swimming in 2-weeks old DT larvae with inflated swim bladder still remains very high compared to ZF at 1 or 2 week(s), it is apparent that delayed inflation of swim bladder alone cannot explain the long, continuous swimming in larval DT and that it is likely a result of a combination of factors.

In the anatomy experiments, we tested for the distribution of excitatory (glutamatergic) and inhibitory (glycinergic and GABAergic) cell types in DT. We found the distribution to be very conserved to what has been described in ZF before. The same markers were used for labelling these neurons as were first used in ZF (Higashijima et al. 2004). To visualize the pattern of glutamatergic neurons or the distribution of vesicular glutamate transporter (VGLUT) genes, we used a combination of *vglut2a* and *vglut2b* probes. For glycinergic neurons, to understand the pattern of distribution of neuronal glycine transporter

(GLYT), only *glyt2* marker was used as *glyt1*is predominately expressed in the spinal cord (Adams et al., 1995). To visualize the GABAergic cells, we used anti-GAD65/67 antibody. Moreover, based on the description of RS neurons in ZF by Kimmel et al. (1982) and Orger et al. (2008), a high degree of conservation in their distribution was observed between DT and ZF. We could identify cells of the mesencephalic nucleus of the medial longitudinal fascicle (nuc MLF/ nMLF), the rhombocephalic reticular formation (nuc RE) and the rhombocephalic vestibular nucleus (nuc VE) in DT that has been described in ZF before. Specifically, the various cells from the rostral (RoL, RoM, RoV), middle (Mauthner neuron, MiR, MiM, MiV, MiD) and caudal (CaD, CaV) RE nucleus were identified. In the nuc MLF, MeM and MeL cells were identified. Dendrites crossing the midline from MeM cells were identified in DT as has been described in ZF earlier (Kimmel et al., 1982). Such anatomically homologous neurons and their conserved distribution points to a common ancestry between DT, ZF and even the evolutionarily more distant animal, lamprey. However, it does not necessarily point to a conserved functional role of these neurons. For instance, homologous neurons are found to have differing functions in divergent feeding behaviors of nematodes (Bumbarger et al., 2013). A more profound example is that of whirligig beetle, an aquatic insect which lacks olfactory antennae and where the role of its mushroom body is shifted from olfaction to vision (Lin & Strausfeld, 2012).

Based on the regression analysis performed on the whole brain activity with swimming behavior, activity in specific brain regions were identified to be correlated with swimming activity. Similar brain nuclei were already seen to be correlated with swimming in ZF by Dunn, Mu et al. (2016). In ZF, activity in nMLF neurons have been earlier shown to be implicated in swimming (Thiele et al., 2014 and Wang & McLean, 2014), and more specifically to be correlated with duration of swim bouts (Severi et al., 2014). So, this nucleus is a good candidate for modulating the length of swim events. The finding of supraspinal swimming correlated neurons also agrees with the findings from various studies across many other animal species including lamprey (Juvin et al. 2016). In addition to the RS neurons which directly project to the spinal cord, another important set of neurons implicated in locomotion are located in the brainstem region, called the mesencephalic locomotor region (MLR). As suggested by Dunn, Mu, et al. (2016) earlier, the highly correlated medial mid-brain nucleus could consist of nMLF as well as other unidentified mesencephalic neurons which may include the fish-equivalent of MLR. A thorough anatomical and physiological study of this region will be essential to validate this. Moreover, optogenetic stimulation of the medial mid-brain nucleus in ZF has validated the causal link between the swim “maintenance” neurons and their ability to maintain long-lasting swimming activity. It is to be noted that the despite the increased swimming on optogenetic stimulation, the bout-wise swimming pattern is still conserved in ZF. This could be arising due to inherent constraints of ZF spinal circuitry. Indeed, in ZF, there is evidence that spinalized preparations can still generate episodic swimming without any supraspinal input and it is dependent on the rostral segments of the spinal cord (Wiggin et al., 2012). An autonomous stop to the locomotion can arise from the intrinsic properties of the Central

pattern generators (CPGs) itself. Hence, the duration of locomotion can, in principle, be controlled at the level of CPGs to some extent. Two such mechanisms are known to exist in *Xenopus*: ATP-mediated high excitability by inhibiting the voltage-gated K^+ channels via activation of P2Y receptors (Dale & Gilday, 1996) and sodium spike dependent enhancement of Na^+/K^+ pump function that can lead to an ultraslow, minute-long afterhyperpolarization (usAHP) in network neurons following the locomotor events (Zhang & Sillar, 2012).

An open question that remains is, mechanistically how can the long-lasting neuronal activity be produced in DT? Non-linear intrinsic response properties of neurons such as plateau potentials can cause a bistable behavior in neurons. With respect to supraspinal motor control, Antri, Fenelon et al. (2009) investigated the sensory stimulus initiated long depolarizations in the reticulospinal (RS) neurons of lamprey. The results suggested a role of calcium-activated non-selective cationic current (I_{CAN}) in the long-lasting depolarization. The I_{CAN} does not show a voltage dependency and can lead to long-lasting influx of calcium. Their activity can still be preceded by the activity of voltage-dependent L-type calcium channels (Morisset & Nagy, 1999, Voisin & Nagy, 2001 and Baufreton et al., 2003). In contrast, in frog tadpoles, Li et al. (2006) demonstrated that the prolonged swimming cannot be explained by intrinsic membrane properties of the neurons. Instead of bistability of the neurons, they found a reverberation hypothesis to be the underlying mechanism. According to this, the authors found neurons forming reciprocal excitatory synapses and providing direct mutual excitation to keep the network active for long periods. In addition to descending feed-forward excitation from these neurons, the authors also identified feed-back ascending excitation. In addition to these possibilities, the influence of neuromodulators, especially dopamine (DA) on the swimming associated neurons is worth exploring. This can be investigated with the DA sensor transgenic lines that are now available in ZF (Sun et al., 2018). Moreover, DT and ZF does create a unique opportunity to increase our understanding of a common danionin brain using two different pieces of evidence. For instance, we were able to take advantage of the long swim events in DT to temporally resolve the neuronal activity with respect to various phases of the swimming. This is otherwise not possible with ZF with the currently used GECIs. Using this method, we identified a population of offset neurons in the hindbrain of at 3 DTs which fired reliably during the termination of a swim events (Figure S12).

In conclusion, using two closely related fish species, DT and ZF, we show that two anatomically conserved neuronal populations are able to produce two different behavioral outputs based on their functional differences. This lays a foundation for future work to directly compare neuronal circuits and behaviors in vertebrate species. This is particularly interesting to do in danionins as many related species are known and can be easily adapted to the same fish facility that is developed for ZF/DT. With the ability to dissect behaviors to their genetic and neuronal circuit components in danionins, this would be the modern approach to comparative neuroethology which can directly inform us about evolution of behaviors and neuronal circuits.

Methods

Fish breeding and husbandry

6 days post-fertilization (dpf) zebrafish (ZF) and *Danionella translucida* (DT) larvae were used for behavioral experiments. For imaging experiments, 5 dpf ZF and DT were used. DT adults were grown at a water temperature of 25 to 28° C, pH of 6.3 to 8.3 and a conductivity of 250 to 450 uS. Adult DT are fed with Gemma Micro 150 (Skretting, USA) (twice a day) and live *Artemia* (once a day). DT are known to spawn in crevices. Hence, 2 to 4 silicone tubes (~ 5 cm long) were added in the adult tanks to aid spawning.

The larvae were grown at a density of <50 larvae per 90 cm Petri plate in E3 egg medium (without methylene blue). For behavioral experiments, at 5 dpf, both larval ZF and DT were transferred to a 250 ml beaker with 100 ml E3 egg medium (without methylene blue) and fed with rotifers. They were maintained at 28°C in an incubator until the experiment.

All animal procedures (zebrafish and *D. translucida*) were performed in accordance with the animal welfare guidelines of France and the European Union. Animal experimentations were approved by the committee on ethics of animal experimentation at Institut Curie and Institut de la Vision, Paris.

Free-swimming behavioral acquisition, fish tracking and tail segmentation

A high-speed camera (MC1362, Mikrotron-GmbH, Germany) and a Schneider apo-Xenoplan 2.0/35 objective (Jos. Schneider Optische Werke GmbH, Germany) were used to carry out the free-swimming acquisitions. The resolution of the images were 800 x 800 pixels with 17 pixels /mm and the acquisition was carried out at 700 Hz. The fish were illuminated with an infrared LED array placed below the swimming arena. An 850 nm infrared bandpass filter (BP850-35.5, Midwest Optical Systems, Inc.) was used on the objective to block all the visible light.

The behavioral arena was illuminated with visible light at 220 lux which was similar to the light intensity in the home incubator. Both DT and ZF were fed at 5 dpf with filtered rotifers and 6 dpf fish were used for the experiment. The fish were transferred to 35 mm Petri plates and acclimatized for > 2 hours before the behavioral acquisitions. 23 DT and 37 ZF were tested with the acquisition lasting for ~ 20 - 30 mins.

Image acquisition, fish tracking and tail segmentation were performed using a custom-written C# (Microsoft, USA) program. The online tracking of the fish and tail segmentation was carried out as described in Marques et al., (2018). Briefly, the following method was performed. A background was calculated by taking the mode of a set of frames which are separated in time so that the fish occupies a different position in each frame. This background image was subtracted from each acquired frame. The

subtracted image was smoothened using a boxcar filter. A manually selected threshold was used to separate the fish from the background. The fish blob was selected by performing a flood fill starting at the maximum intensity point. The center of mass of this shape was considered the position of the larva. The middle point on a line joining the center of mass of each eye was defined as the larva's head position. The direction of the tail was identified by finding the maximum pixel value on a 0.7 mm diameter circle around the head position. Then, a center of mass was calculated on an arc centered along this direction. The angles of ~10 tail segments measuring 0.3 mm were calculated. To do this, successive tail segments were identified by analyzing the pixel values along a 120-degree arc from the previous segment. This same algorithm was used for both DT and ZF. The empirically selected threshold to separate the fish from background was different in the two fish.

Analysis pipeline for free-swim data

Poor tracking was identified using pixel intensities of the tail segments. The lost frames, if any, were identified based on a 32-bit time stamp encoded in the first 4 pixels of all the images. These lost frames are then interpolated and filled with NaN values for the recorded parameters.

Discontinuities in turning when the fish turns from 0 to 360 degree or vice versa were corrected. The raw X and Y coordinates were smoothened using the savitzky golay digital filter: in MATLAB (MathWorks, USA), *sgolayfilt* function is used to implement this. A 2nd order polynomial fit was employed on a window size of 21 units (30 ms). Displacement was calculated using these X and Y coordinates of the centroid of the fish.

The measure of tail curvature was used to identify the bouts as described in (Marques et al., 2018). The first 8 tail segments were incorporated in the analysis based on the reliability of the tracking as assessed by the raw pixel intensities. The change in the curvature of the tail was emphasized over local fluctuations by taking a cumulative sum of the values along the tail. The differences in tail angles were calculated as we wanted to detect movements. The tail movements were then smoothened using a boxcar filter of size equivalent to ~14.30 ms. The absolute of the segment angles were then convolved into a single curvature measure. A maxima/minima filter of 28.6 ms/ 572 ms was specifically applied to this tail curvature dataset of zebrafish based on the knowledge of bout and inter-bout durations available to us. An empirically validated cut-off was used on the convolved and smoothened tail curvature measure to identify the starts and ends of swim bouts. It is important to note that in the analysis, only the 'burst' phase of 'burst-and-glide' swims were identified in ZF.

The 7th tail segment was used for calculating tail beat frequency and maximum tail angle. The trace of the tail segment was smoothened and small gaps (less than 7 ms) in the swim events due to tracking were interpolated. Swim events with larger gaps were eliminated from the analysis. Any identified events shorter than 71.5 ms in length, if present, were discarded as well to avoid artefacts. On the bout-

based kinematics, the bout distance, inter-bout duration, mean and maximum speed, maximum tail angle and tail beat frequency were calculated.

Half beat based kinematics in Zebrafish and *Danionella translucida*

A peak-to-peak half cycle was defined as a half tail beat cycle and this was used for the kinematic calculations to be able to compare a similar unit of locomotion between the two fish.

In zebrafish: to identify the half-beats, on every swim bout, the absolute of the tail angles was calculated from the 8th segment of the tail and the peaks of tail angle were identified using the *findpeaks* function in MATLAB. Figure S2(A) shows this for a swim bout in zebrafish.

In *Danionella translucida*: the trace of the tail segment is smoothened using a savitzky golay digital filter function of 3rd order with a window size of 50 ms. Small gaps (less than 7 ms) in the tracking were interpolated. Using *bwlabel* function in MATLAB on the binary matrix of good/ bad tracking, all continuous stretches of good tracking were labelled. From this, only the stretches longer than 35 frames (or 50ms) were selected for further analysis to avoid small tracking artefacts if any. On these identified stretches, half beats were identified as mentioned above for zebrafish.

On every half beat in both the fishes, the following kinematic parameters were calculated: duration, distance, mean and maximum speed, maximum tail angle and half beat frequency. The 8th tail segment was used for calculating tail beat frequency and max tail angle.

Head-embedded swimming

A high-speed camera (MC4082, Mikrotron-GmbH, Germany) with a Navitar Zoom 7000 macro lens was used to carry out the head-embedded acquisitions. The resolution of the images were 400 x 400 pixels with 75 pixels /mm and the temporal resolution of the acquisition was 100 or 250 Hz. The fish were illuminated with an infrared LED array placed below the swimming arena. An 850 nm infrared bandpass filter (BP850-35.5, Midwest Optical Systems, Inc.) was used on the objective to block all the visible light.

6 dpf DT and ZF were embedded in 0.5 ml of 1.5% agarose. For ZF, nacre incross fish were used. The agarose covered the head up to the pectoral fins. Each fish was acclimatized for at least 90 minutes before acquisition. Recordings lasted for 10-20 mins per fish. 4 DT and 5 ZF were used in this experiment. The head-embedded videos were primarily used to determine the amount of time spent in swimming. 6 dpf ZF (n=6) and DT (n=5) were used for the experiment. The duration of swimming was normalized to the total length of the acquisition and reported as a percentage of the total duration of acquisition.

Tail tracking

The tail tracking was either performed manually or using a custom-written program in MATLAB. The methodology was kept the same within an experiment to be consistent. Briefly, the following approach was employed for the automated tracking. An ROI was drawn around the tail. A threshold was selected empirically for every video to binarize the image to be able to segment the tail. The image was divided into 12 vertical bocks perpendicular the tail segment. A mask was used to run through the image block-by-block to determine the center of mass of the largest blob (tail segment) per block. This center of mass information was used to calculate the angle between two consecutive tail spots. Of the 11 tail segment angles, the first nine were used to determine a curvature of the tail throughout the video. A cut-off value on the curvature was used to determine regions of active swimming.

Tap-induced escape behavior

An Arduino controlled solenoid was added to the free-swimming behavioral set-up. The Arduino was triggered from the image acquisition program written in C# (Microsoft, USA). When triggered, the solenoid would hit the surface of the arena from the bottom and cause the fish to escape in response to this stimulus. The trigger was only initiated if the fish was not at the edges of the Petri dish and if there was an inter-stimulus interval of at least 50 seconds between two consecutive trials. The delay between the trigger onset and the delivery of the solenoid on the arena was estimated and incorporated in the analysis to calculate an accurate reaction time. 19 DT (n=141 trials) and 15 ZF (n=159 trials) were tested in the assay.

To analyze the escape kinematics, the peak escape velocities were identified in a window of approx. 450 ms after the stimulus delivery. A peak speed was considered as at least 2 times the peak speed during free-swimming (9.25mm/s and 42.5 mm/s for DT and ZF respectively). In case of multiple peak escape velocities in the window, only the first one was considered. Now a 140 ms region of interest was selected around the peak speed to include 40 ms before the peak and 100 ms after the peak as shown in Figure S3 for a zebrafish. The region of interest was empirically decided after exploring many trials across both the fish species. Mean and maximum speeds, total distance covered and the delay to reach the peak speed after the stimulus delivery – these parameters were computed for all the trials in each fish.

The major differences in the processing pipeline from the free-swimming analysis pipeline were as follows. The X/Y displacement vectors were further filtered using zero-phase digital filtering (*filtfilt* function in MATLAB) with a filter size of 11 ms to identify the peak escape velocities. Kinematics were neither calculated on half beats nor bouts, but on the custom defined 140 ms window for a better comparison of the escape events in the two species of fish.

Mean squared displacement (MSD) and reorientation analysis

Information on X/Y- coordinates was used to compute the Mean squared displacement (MSD) and decorrelation in heading orientation (R) over time. A Savitsky-Golay filter was applied on the X and Y traces to fit a 2nd order polynomial on a 200 ms window. The filtered trajectories were then downsampled to 70 Hz. For each fish, discrete continuous trajectories were identified in a circular region of interest of radius of 300 pixels (18mm) to mitigate border-induced bias. These trajectories were used for the computation.

The time-evolution of MSD and R were calculated at every 100 ms time-step and averaged over all trajectories for each animal. To compute R, we extracted at each time t a unit vector **u**(t) aligned along the fish displacement [dx,dy] calculated over a 1s time window. Notice that this vector was only calculated if the fish had moved by at least 0.5 mm in this time period. The heading decorrelation over a period Δt was then computed as $R(\Delta t)=\langle \mathbf{u}(t).\mathbf{u}(t+\Delta t)\rangle_t$. This function R quantifies the heading persistence over a given period: R=1 corresponds to a perfect maintenance of the heading orientation, whereas R=0 corresponds to a complete randomization of the orientations. The MSD and R values were plotted over time for DT (n=23 fish) and ZF (n=37 fish).

Quantification of depth preference

Three vertical glass cylinders with 36 cm water height were used in this experiment. 6 dpf zebrafish larvae (n=30 per cylinder) were added to three cylinders. 6 dpf *Danionella translucida* (DT) larvae (n=30 per cylinder) were added to another three cylinders.

The cylinders were considered as consisting of three sections and marked accordingly: the bottom 12 cm, middle 12 cm and the top 12 cm sections. The number of fish in each section of the column was manually counted once every hour for 10 hours. This was used to calculate the average normalized fish density in every section of the water column.

Quantification of body length and swim bladder inflation

Body length was measured in 5 dpf larvae of the two species (n = 10 for DT and n = 9 for ZF). Pictures of the larvae were captured using AxioCam MR3 camera. The magnification of the optics was noted and the physical dimension of camera pixel was used to calculate the pixel size in µm as follows: pixel size = (260/magnification) x binning factor.

To quantify swim bladder inflation, from a population of growing larvae (3 dpf to 15 dpf), five or more larvae were sampled for each age and the proportion of larvae with inflated swim bladder was quantified. A moving averaging was performed using a window size of two units to smoothen the curve and the swim bladder inflation results were reported from 3.5 to 14.5 days.

Fluorescence In-situ hybridization (FISH) and Immuno-histochemistry (IHC)

To generate anti-sense probes, DNA fragments were obtained by PCR using Phusion™ High-Fidelity DNA Polymerase (Thermo Scientific™) and the following primers (5'->3'): vglut2a (forward primer: *AGTCGTCTAGCCACAACCTC*; reverse primer: *CACACCATCCCTGACAGAGT)*, vglut2b (forward primer: *GCAATCATCGTAGCCAACTTC*; reverse primer: *ACTCCTCTGTTTTCTCCCATC)* and glyt2 (forward primer: *TGGAAGGATGCTGCTACACA*; reverse primer: *TGACCATAAGCCAGCCAAGA).* Total cDNA for ZF and DT were used as a template. PCR fragments were cloned into the pCRII-TOPO vector (Invitrogen) according to manufacturer's instructions. All plasmids used were sequenced for confirmation.

Digoxigenin RNA-labeled or Fluorescein RNA-labeled probes were transcribed *in vitro* using the RNA Labeling Kit (Roche Diagnostics Corporation) according to manufacturer's instructions. Dechorionated embryos at the appropriate developmental stages were fixed in fresh 4% paraformaldehyde (PFA) in 1X phosphate buffered saline (pH 7.4) and 0.1% Tween 20 (PBST) for at least 4 hours at room temperature or overnight at 4° C. Following this, the samples were preserved in methanol at -20° C until the *in-situ* experiments described below.

Whole-mount digoxigenin (DIG) *in-situ* hybridization was performed according to standard protocols (Thisse & Thisse, 2008). Briefly, the fixed samples were then rehydrated in a decreasing series of methanol/PBST solution. A protease-K (10 µg/mL) treatment was performed depending on the age and species of the sample (90 mins and 120 mins for 5 dpf DT and ZF respectively). The fish were again incubated in 4% PFA and added to HY4 buffer for 1 hour at 68° C. The samples were then incubated overnight at 68°C in a solution of DIG-labeled probe at a dilution of 1:50 in HY4 buffer. Excess probes were removed by several washes. The samples were blocked using 2% blocking solution (Roche) for at least 1 hour before adding the Fab fragments of the alkaline phosphatase-conjugated anti-DIG-AP antibody (Roche) to detect DIG. This reaction mixture was kept overnight at 4° C. A chromogenic NBT-BCIP substrate (Roche) was used to detect the hybridization.

After staining, the whole-mount DIG labeled embryos were washed twice in PBST. The embryos/larvae were again fixed overnight in 4% PFA/PBST. Glycerol was added to the samples before imaging on a stereoscope with AxioCam MR3 camera.

Whole-mount Fluorescence *in-situ* hybridizations (FISH)

The samples stored in methanol at -20^oC from above were rehydrated by two baths of 50% methanol/PBST followed by two baths of PBST. This was incubated for 10 min in a 3% H_2O_2, 0.5% KOH solution, then rinsed in 50% methanol/ 50% water and again dehydrated for 2 hours in 100%

methanol at -20°C. Samples were rehydrated again by a series of methanol baths from 100% to 25% in PBST, and washed two times in PBST. This was followed by an age and species dependent treatment of proteinase-K (10 µg/mL) at room temperature. At 5 dpf, DT and ZF underwent treatment of proteinase-K for 90 and 120 mins respectively.

Following this, the samples were again fixed in 4% PFA/PBST. After 2 hours of pre-hybridization in HY4 buffer at 68° C, hybridization with fluorescein-labelled probes (40ng probes in 200 µl HY4 buffer) was performed overnight at 68°C with gentle shaking. Embryos were rinsed and blocked in TNB solution (2% blocking solution (Roche) in TNT) for 2 hours at room temperature. This was then incubated overnight with Fab fragments of anti-Fluo-POD (Roche) diluted 1:50 in TNB. For signal revelation, embryos were washed with 100 µl Tyramide Signal Amplification (TSA, PerkinElmer) solution and incubated in the dark with Fluorescein (FITC) Fluorophore Tyramide diluted 1:50 in TSA. The signal was then followed for 30 minutes for *glyt* and 1 hour for *vgult2b* until a strong signal was observed. After which, the reactions were stopped by 5 washes with TNT, and incubated for 20 minutes with 1% H_2O_2 in TNT. All the steps after Fluorescein (FITC) incubation were processed in the dark.

Antibody staining

Following fluorescent *in situ* hybridisation staining, whole mount embryos were washed twice in TNT solution. Subsequently, they were blocked for 1 hour at room temperature in 10% Normal Goat Serum (Invitrogen) and 1% DMSO in TNT solution. Rabbit GAD65/67 primary antibody (AbCam) diluted 1/5000 in 0.1% blocking solution was incubated overnight at 4°C. The Alexa Fluor 635 secondary antibody goat anti-rabbit IgG (1/500) (Life Technologies) was added in 0.1% blocking solution and incubated overnight at 4°C. After 5 washes in PBST buffer, microscopic analysis was performed.

Confocal imaging of the whole brain FISH/IHC samples

To image the whole brain *in-situ* hybridization and immunohistochemistry samples, we used Zeiss LSM 780, LSM 800 and LSM 880 confocal microscopes with a 10x or 40x objective using appropriate lasers and detection schemes suitable to the labelled sample. Whole brain images were acquired in tiles and stitched together using the stitching algorithm available in Zeiss ZEN blue and ZEN black (on LSM 800). The images are shown as maximum intensity projections created on imageJ. In GAD65/67, non-specific blobs of signal likely originating from residual dye left on the skin after the washing step was removed using image processing in the representative image.

Retrograde labelling of reticulospinal (RS) neurons

A solution containing 10% w/v Texas Red dextran (TRD, 3,000 MW, Invitrogen) in water was pressure injected in the spinal cord (between body segment 7 to 14) of 4dpf ZF and DT. In DT, this method resulted less efficient in labeling the whole RS neurons. The best results were obtained by cutting the tail beyond segment 14th with fine scissors and pressure injecting the TRD in the exposed spinal cord. After the labeling, the fish were allowed to recover in E3 egg medium for 24 hours at 28° C.

At 5dpf, the surviving injected larvae were anaesthetized with 0.02% Tricaine (MS-222, Sigma), mounted in 1.5% low melting point agarose and imaged under a VIVO 2-photon microscope (3I, Intelligent Imaging Innovations Ltd). Labelling was often sparse and varied among the injected fish which survived to 5dpf (n=4 fish per species). Maximum intensity projection images of the reticulospinal neurons in ZF and DT is shown from the animals where almost all the RS neurons were labelled. RS neurons in DT brain were annotated based on their anatomical similarity to the ones in zebrafish (Kimmel et al., 1982a).

Generation of pan-neuronal calcium sensor Tg(HuC-H2B:GCaMP6s) line

To create Tg(HuC:H2B-GCaMP6s) DT fish, 6 ng/µl of the plasmid and 25 ng/µl of Tol2 was used. Injections were performed in embryos which were less than or equal to 4-cell stage. The injection was performed free-hand and the egg was targeted directly. Tol2-elavl3-H2B-GCaMP6s plasmid was a gift from Misha Ahrens (Addgene plasmid # 59530; http://n2t.net/addgene:59530; RRID: Addgene_59530). It was published in (Freeman et al., 2014).

Light-sheet imaging

Transgenic DT and ZF expressing H2B-GCaMP6s under the HuC promoter was utilized. The GCaMP is nuclear tagged, so its expression is limited to the nucleus which makes it easier for segmentation of the neurons. The fishes were embedded in a capillary with 2.5% agar. The tail was freed and recorded simultaneously to extract a readout of the spontaneous swimming behavior. Before each recording, the embedded fish were acclimatized to the recording chamber with the blue laser switched on for at least 10 minutes. The scanning objective was lateral and the beam entered from the left side of the fish and the detection objective was placed upright on the top. Both the objectives were moved with a piezo so that the light sheets were always in the focal plane of the detection objective. Average laser power was at 0.05 mW. Approximately 280 µm of the brain volume was imaged in each fish. Brain imaging was carried out at approximately 1 Hz (1 whole brain volume / sec) and the tail movement was acquired at ~ 40-80 Hz. Each acquisition lasted for ~ 20 minutes.

Image processing and analysis pipeline for whole-brain light-sheet data

For ZF and DT, image processing was performed offline using MATLAB. Based on visual inspection, if needed, image drift was corrected by calculating the cross-correlation on a manually selected region of interest (ROI). The dx and dy values employed to correct the drift in this ROI were extrapolated to the whole stack. Brain contour was manually outlined on mean graystack images for each layer. Background value for each layer was estimated from the average intensity of pixels outside the brain contour. The segmentation procedure consisted of a regression with a gaussian regressor convolved with the same gaussian regressor. The result was regressed a second time with the same regressor. Baseline and fluorescence were calculated for each neuron identified by the segmentation. The fluorescence *F(t)* signal was extracted by evaluating the mean intensity across the pixels within each neuron. For ZF, the baseline was calculated by the running average of the 10th percentile of the raw data in sliding windows of 50 sec. For DT, the baseline for identifying "swim" neurons was calculated as the 10th percentile of the raw data within each inactive period defined as the time period between 5 sec after the end of a swim event and 3 sec before the beginning of the next swim event (from tail acquisition data). The baseline values for the active periods were interpolated using the values in the inactive periods. For both ZF and DT, the relative variation of fluorescence intensity *dF/F* was calculated as *dF/F* = (*F(t)* – baseline) / (baseline-background).

Brain registration

We used the Computational Morphometry ToolKit CMTK ((http://www.nitrc.org/projects/cmtk/) to compute and average the morphing transformation from high resolution brain stacks (184 layers, 1um deep) to create a common brain for the *Tg(HUC:H2B:GCaMP6s)* DT line. All the calcium imaging results were mapped to this reference brain. To compare neuronal populations across different brain samples, we calculated the spatial densities of the considered clusters by using the Kernel Density Estimation (KDE) with a Gaussian kernel with a bandwidth of 12.8 µm. Discrete cluster densities were determined for all points of an inclusive common 3D rectangular grid with an isotropic resolution of 5 µm.

Statistical methods

Behavior data: All the averaged values per fish were prepared in MATLAB 2017b (Mathworks) and statistical tests between the populations were carried out in Prism 8 (GraphPad). Kruskal-Wallis test by ranks was performed in all cases where the dataset did not follow a normal distribution.

Light-Sheet imaging data: For both ZF and DT, neurons from the more rostral part of the brain were removed (y coordinates between y_{max} – 10 um and y_{max}) because of dF/F artefact due to image border.

A multi-linear regression was performed using the classical normal equations. In DT, this was performed on dF/F for the whole duration of the experiment and in ZF, on dF/F for a manually selected time period with many well isolated swim bouts. The analysis determines the best-fit coefficient β to explain the neuronal data (y) by the linear combination $y = \sum \beta_j * x_j + \beta_o$, where x_j is the regressor. For ZF, a constant regressor and a swim maintenance regressor (based on the tail acquisition data) were used. For DT, four regressors were used: constant, swim maintenance, swim onset and swim offset. The onset and offset regressors were obtained from the initiation and termination of swim events (based on the tail acquisition data) with a time window of -3 sec to +1 sec around the event. Swim maintenance, onset and offset regressors were convolved with a single exponential of 3.5 sec decay time which approximates the H2B-GCaMP6s response kernel in ZF (Migault et al., 2018). T-scores were computed for every neuron/regressor combination.

To characterize highly responsive neurons for a specific regressor, the regression coefficient and t-score distributions were first fitted with a gaussian model (μ_{dist}, σ_{dist}) to estimate a sub-distribution responsible for noise (neurons that are not correlated well with the regressor). These sub-distributions, defined as the maximum distribution ± σ_{dist}, were then fitted again with a gaussian model (μ_{nosie}, σ_{noise}). The highly responsive neurons were defined as neurons with both, a regression coefficient higher than regression threshold $_{coefficient} = \mu_{noise\ coefficient} + 3\ \ \sigma_{noise\ coefficient}$ (or threshold $_{coefficient} = \mu_{noise\ coefficient} + 4\ \ \sigma_{noise\ coefficient}$) and a t-score higher than t-score threshold $_{t\text{-}score} = \mu_{noise\ t\text{-}score} + 3\ \ \sigma_{noise\ t\text{-}score}$ (or threshold $_{coefficient} = \mu_{noise\ t\text{-}score} + 4\ \ \sigma_{noise\ t\text{-}score}$).

To quantify the responsiveness of highly correlated neurons, a score was created for each neuron based on the sum of the regression coefficient normalized by the regression threshold$_{coefficient}$ (a_1) and the t-score normalized by the t-score threshold$_{t\text{-}score}$ (a_2). The higher the score, the more responsive is the neuron. For characterization of the swim onset and maintenance components of the onset neurons, the distribution of all the onset neurons was first visualized on a $[a_1+a_2]_{swim\ regressor}$ versus $[a_1+a_2]_{onset\ regressor}$ plot. The angle of a vector from the point of intersection of the normalized thresholds of $[a_1+a_2]_{swim\ regressor}$ and $[a_1+a_2]_{onset\ regressor}$ (at [2,2]) to an individual neuron's position was calculated for every onset neuron. An onset neuron with an angle between pi and pi/2 was considered to possess only a swim onset component (green) whereas an onset neuron with an angle between pi/2 and zero was considered to possess both, strong onset and maintenance components.

Figures

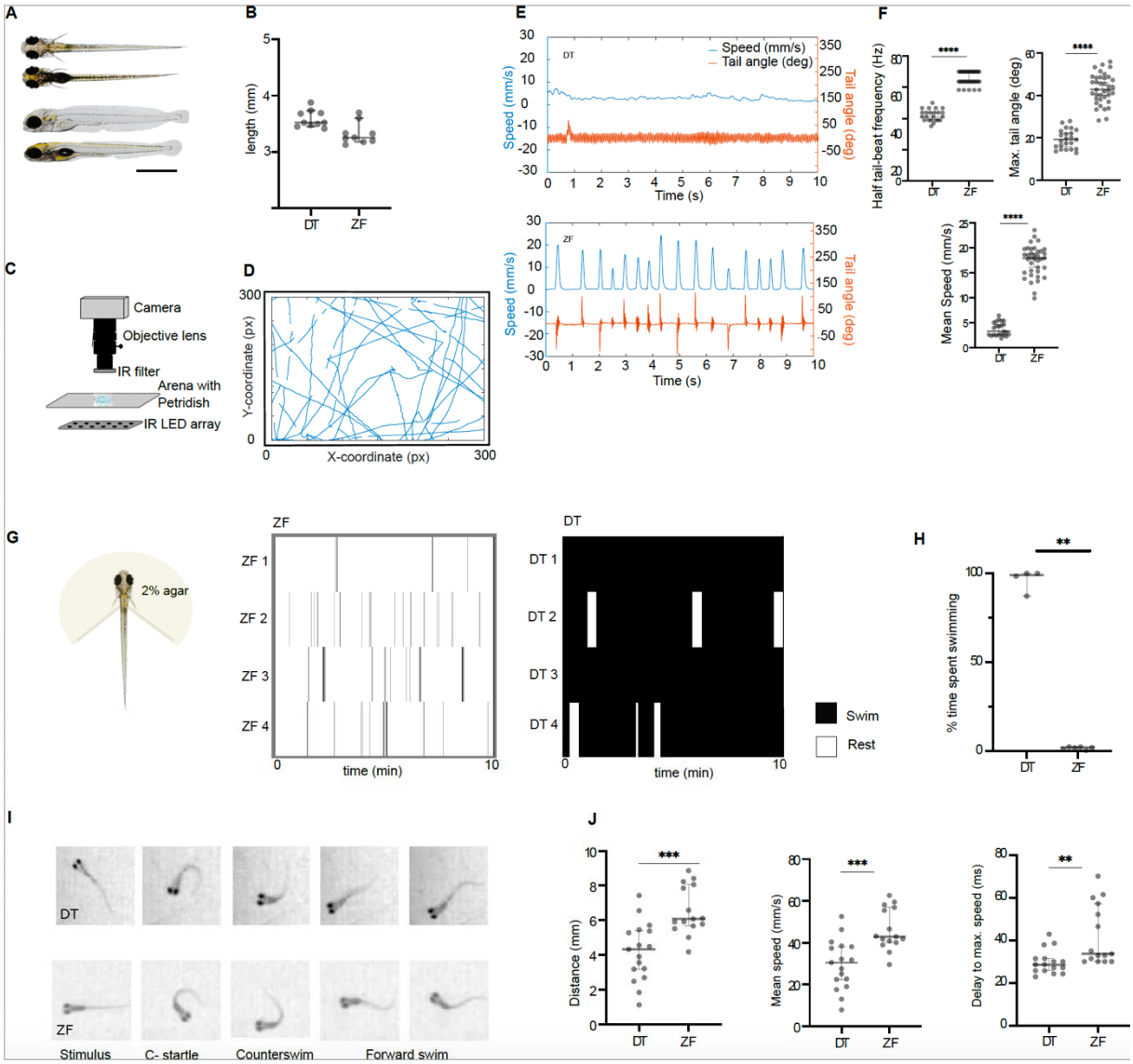

Figure 1: Fine kinematics of spontaneous swimming, head-embedded swimming and escape response. DT and ZF measure similar in size at 5 dpf. (A) A dorsal and lateral view of DT and ZF at 5 dpf is shown. (B) Measurement of body length in 5 dpf DT and ZF (N= 10 DT; N= 9 ZF). (C) An illustration of the free-swimming behavioral analysis set-up comprising of a high-speed camera. The arena is illuminated with an IR-LED array. (D) Representative swim trajectories of a single DT obtained from the animal tracking. Such swim trajectories are used in further analysis. (E) A comparison of representative swimming pattern of DT and ZF. It demonstrates swimming in DT and ZF for 10 seconds, illustrating the continuous swimming in DT with lower translational speed (blue) and tail angle (orange) over time when compared to ZF. (F) Swimming kinematics of DT and ZF in a spontaneous swimming assay. DT utilizes lower half tail beat frequency (Hz) and lower maximum tail angles (degree) to achieve swimming at lower speeds (mm/s) when compared to ZF (N= 23 DT, n = 494628 half tail beats and N=

37 ZF, n = 202176 half tail beats). (G) Tail movements were recorded in head-embedded fish preparations. The raster plots illustrate the long swim durations in DT (right) when compared to the intermittent swimming in ZF (left). (H) The normalized time spent actively swimming (% of total acquisition time) is higher in DT compared to ZF (N=5 DT and N= 6 ZF). (I) Qualitatively, the escape strategy in DT and ZF is highly conserved. The sequence of escape response in DT and ZF immediately after the tap stimulus delivery is illustrated. (J) Although DT covers a shorter distance at a lower mean speed, the time delay (ms) to achieve the maximum escape speed is lower in DT (DT: N=19 fish, n=141 events; ZF: N=15 fish, n=159 events). The swim kinematics are calculated on a 140 ms window around the escape swim after stimulus delivery. ** p<0.01, *** p=0.001, **** p<0.0001, Mann-Whitney test. All error bars show 95 % confidence interval.

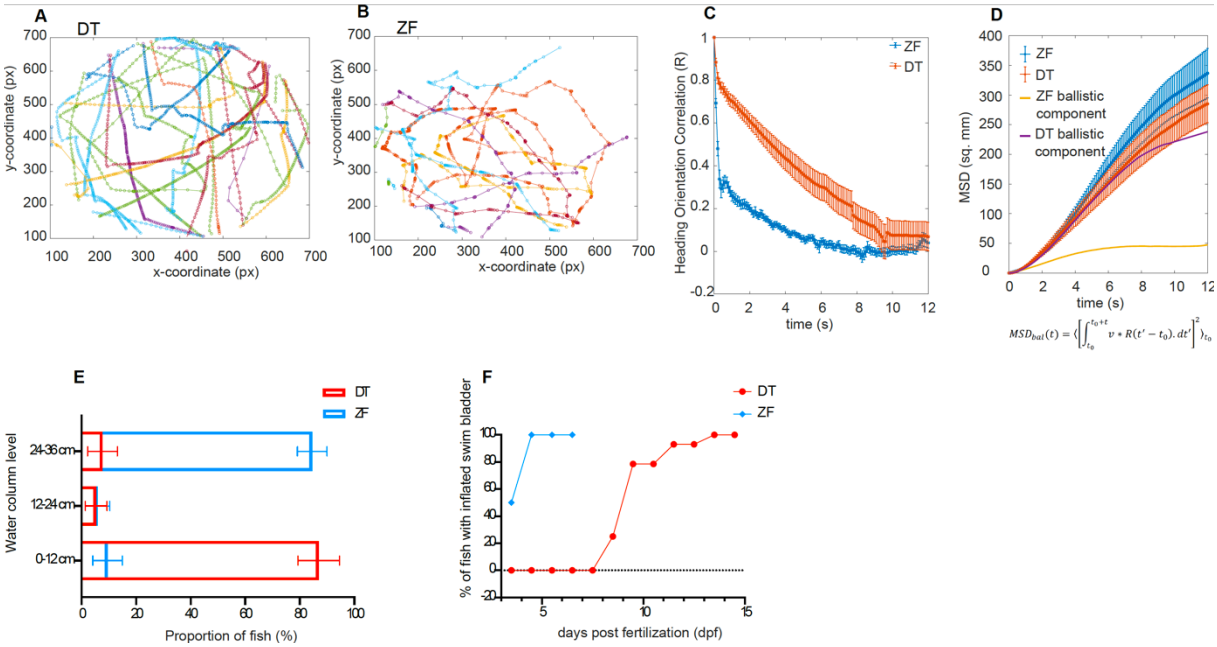

Figure 2: Differences in the longer timescale swimming pattern during exploration and other organismal level traits

(A) and (B) represent a few tens of trajectories (each trajectory with a different color) picked from a single DT and ZF. Such trajectories from many fish were utilized for the calculation of Mean squared displacement (MSD) and heading orientation correlation (R). (C) Change in heading persistence over time. At R=1, the animal is moving in a straight trajectory and at R=0, it is completely random. In ZF, R drops rapidly whereas this drop happens over longer period of time in DT. Hence, exploratory swimming in DT has a longer ballistic phase. The error bars show SEM. (D) Mean squared displacement (MSD) in DT and ZF over time. The MSD over time for the ballistic component of DT and ZF is also overlapped on the plot. The ballistic component of the MSD was estimated as: $\boldsymbol{MSD_{bal}(t)} = \langle\left[\int_{t_0}^{t_0+t} \boldsymbol{v * R(t' - t_0).dt'}\right]^2\rangle_{t_0}$. The error bars show SEM. (E) DT larvae prefer the bottom of the water

column whereas ZF larvae prefer the top. (N= ~30 fish and n = 10 readings in 3 replicates for each fish species). The error bars show 95% confidence interval. (F) Swim bladder inflation in ZF occurs earlier than in DT. A complete inflation of swim bladder in ZF occurs at ~ 4dpf whereas the DT population undergoes a complete inflation of its swim bladder at around 15 dpf. N = 10 DT and 9 ZF.

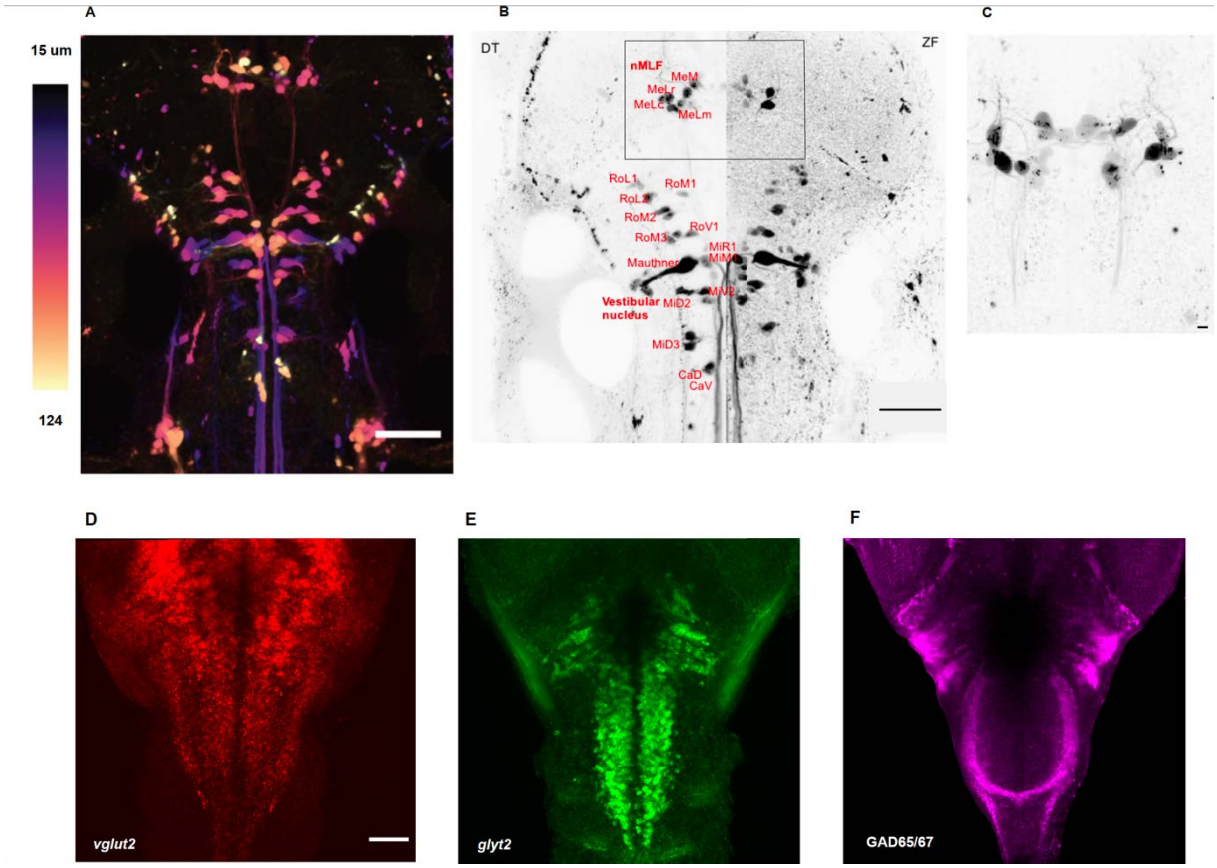

Figure 3: Conserved distribution of reticulospinal neurons and excitatory and inhibitor neurons in the hindbrain of DT and ZF

(A) Distribution of reticulospinal (RS) neurons in the brainstem of DT. Maximum intensity is color coded for depth. Scale bar is 100 µm. (B) Comparison of RS neurons in DT and ZF. A cell-to-cell comparison of RS neurons in a maximum intensity projection of RS neurons in DT and ZF. The RS neurons in DT are annotated based on the description of RS neurons in ZF as described in Kimmel et al., 1982 and Orger et al., 2008. A high degree of conservation is observed. Scale bar is 100 µm. (C) A closer look at the rectangular ROI from (B). Maximum intensity projection of the nucleus of the medial longitudinal fasciculus (nMLF) in another DT fish is shown. Contralateral dendritic projections are observed in DT as noted in ZF (Kimmel et al., 1982). Scale bar is 10 µm. Distribution of (D) glutamatergic (E) glycinergic and (F) GABAergic neurons in the hindbrain of DT using *in-situ* hybridization (ISH) and immunohistochemistry (IHC). Rostrocaudally running striped pattern of these neuronal types is observed in DT as noted in ZF (Higashijima et al., 2004). Anti-*vglut2a* + anti-*vglut2b*

ISH and anti-*glyt2* ISH in (D) and (E) respectively. Anti-GAD65/67 IHC in (F). All images are a maximum intensity projection. Scale bar is 50 µm.

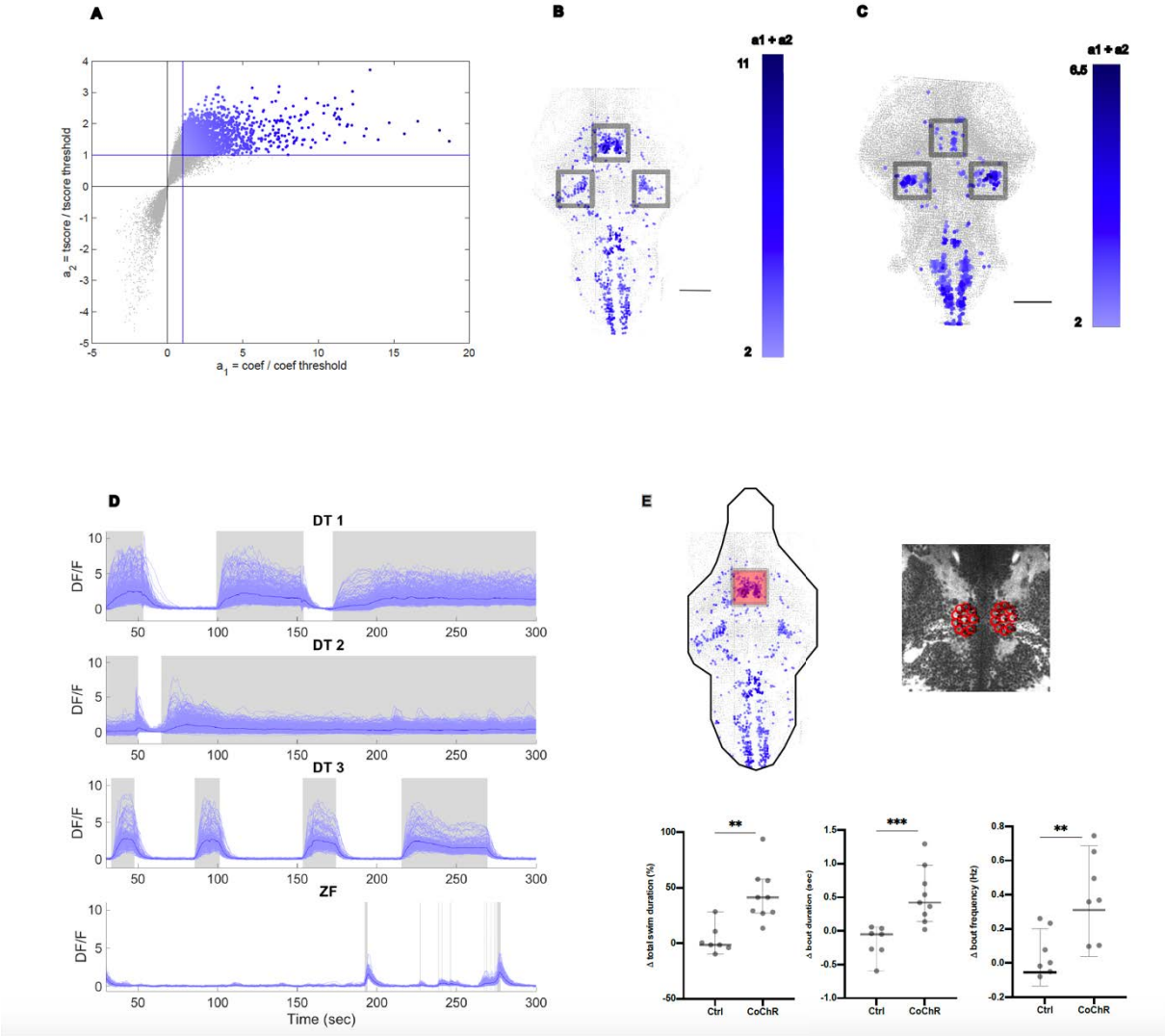

Figure 4: Supraspinal nuclei associated with swim maintenance

(A) An illustration of the selection of swim maintenance cells based on their regression coefficient (a_1) and t-score (a_2). The neurons are encoded in a color gradient based on their (a_{1+} a_2) score. The color gradient increases as the score increases. (B) and (C) show a representative figure of neuronal correlates of swimming identified in DT and ZF brain respectively. The nuclei correlated with swimming are located in the medial mid-brain, lateral midbrain and the hindbrain, and appear to be conserved between DT and ZF. Scale bar is 100 µm. (E) Neuronal activity of swim maintenance neurons in three DT compared to their activity in a ZF for a duration of 300 secs. The activity of the conserved nuclei in DT is sustained for long durations unlike ZF, scaling with their long swim events. The grey shaded regions represent active swimming. N= 3 DT and 1 ZF. (F) The region of interest (ROI) for optogenetic stimulation is shown (top): the deep mid-brain nuclei. The time spent swimming is prolonged by the

activation; this increase is caused by both, an increase in the frequency of recruitment of bouts and an increase in the duration of the bouts as shown in the Figure (bottom). N = 7 Ctrl ZF and 9 CoChR ZF. ** $p<0.01$, *** $p=0.001$, Mann-Whitney test. All error bars show 95 % confidence interval.

Acknowledgement

We would like to thank Mykola Kadobianskyi (Judkewitz lab, Charité Universitätsmedizin Berlin) for providing us with an early access to the *Danionella translucida* genome. Thanks to Dr. Adrien Jouary and Dr. Michael Orger (Champalimaud, Lisbon) for sharing their expertise in animal tracking. Discussions with Dr. Roshan Jain (Haverford College, USA) and members of the Del Bene lab and Laboratoire Jean Perrin at Sorbonne were useful and much appreciated.

References

Adams, R. H., Sato, K., Shimada, S., Tohyama, M., Puschel, A. W., & Betz, H. (1995). Gene structure and glial expression of the glycine transporter GlyT1 in embryonic and adult rodents. *Journal of Neuroscience*, *15*(3 II), 2524–2532. https://doi.org/10.1523/jneurosci.15-03-02524.1995

Antri, M., Fénelon, K., & Dubuc, R. (2009). The contribution of synaptic inputs to sustained depolarizations in reticulospinal neurons. *Journal of Neuroscience*, *29*(4), 1140–1151. https://doi.org/10.1523/JNEUROSCI.3073-08.2009

Bagatto, B., Pelster, B., & Burggren, W. W. (2001). Growth and metabolism of larval zebrafish: Effects of swim training. *Journal of Experimental Biology*, *204*(24), 4335–4343.

Baufreton, J., Garret, M., Rivera, A., De la Calle, A., Gonon, F., Dufy, B., Bioulac, B., & Taupignon, A. I. (2003). D5 (not D1) dopamine receptors potentiate burst-firing in neurons of the subthalamic nucleus by modulating an L-type calcium conductance. *Journal of Neuroscience*, *23*(3), 816–825. https://doi.org/10.1523/jneurosci.23-03-00816.2003

Berg, H. C., & Brown, D. A. (1972). Chemotaxis in Escherichia coli analysed by three-dimensional tracking. *Nature*, *239*(5374), 500–504. https://doi.org/10.1038/239500a0

Bhattacharyya, K., McLean, D. L., & MacIver, M. A. (2017). *Visual Threat Assessment and Reticulospinal Encoding of Calibrated Responses in Larval Zebrafish*. https://doi.org/10.1016/j.cub.2017.08.012

Boehrer, B., & Schultze, M. (2008). Stratification of lakes. *Reviews of Geophysics*, *46*(2), 1–27. https://doi.org/10.1029/2006RG000210

Brett, J. R. (1964). The Respiratory Metabolism and Swimming Performance of Young Sockeye Salmon. *Journal of the Fisheries Research Board of Canada*, *21*(5), 1183–1226. https://doi.org/10.1139/f64-103

Britz, R., Conway, K. W., & Rüber, L. (2009). Spectacular morphological novelty in a miniature cyprinid fish, Danionella dracula n. sp. *Proceedings of the Royal Society B: Biological Sciences*, *276*(1665), 2179–2186. https://doi.org/10.1098/rspb.2009.0141

Budick, S. A., & O'Malley, D. M. (2000). Locomotion of larval zebrafish. *The Journal of Experimental Biology*, *203*, 2565–2579. http://jeb.biologists.org/content/jexbio/203/17/2565.full.pdf

Bumbarger, D. J., Riebesell, M., Rödelsperger, C., & Sommer, R. J. (2013). System-wide rewiring underlies behavioral differences in predatory and bacterial-feeding nematodes. *Cell*, *152*(1–2), 109–119. https://doi.org/10.1016/j.cell.2012.12.013

Childress, J. J., & Seibel, A. B. (1997). Life at Stable low oxygen levels: Adaptations of animals to oceanic oxygen minimum layers. *Journal of Experimental Biology*, *201*, 1223–1232.

Dadarlat, M. C., & Stryker, M. P. (2017). Locomotion enhances neural encoding of visual stimuli in mouse V1. *Journal of Neuroscience*, *37*(14), 3764–3775. https://doi.org/10.1523/JNEUROSCI.2728-16.2017

Dale, N., & Gilday, D. (1996). Regulation of rhythmic movements by purinergic neurotransmitters in frog embryos. *Nature*, *383*(6597), 259–263. https://doi.org/10.1038/383259a0

Darnton, N. C., Turner, L., Rojevsky, S., & Berg, H. C. (2007). On torque and tumbling in swimming Escherichia coli. *Journal of Bacteriology*, *189*(5), 1756–1764. https://doi.org/10.1128/JB.01501-06

Davis, J. C. (1975). Minimal Dissolved Oxygen Requirements of Aquatic Life with Emphasis on Canadian Species: a Review. *Journal of the Fisheries Research Board of Canada*, *32*(12), 2295–2332. https://doi.org/10.1139/f75-268

Denton, E. J., & Marshall, N. B. (1958). The buoyancy of bathypelagic fishes without a gas-filled swimbladder. *Journal of the Marine Biological Association of the United Kingdom*, *37*(3), 753–767. https://doi.org/10.1017/S0025315400005750

Dunn, T. W., Mu, Y., Narayan, S., Randlett, O., Naumann, E. A., Yang, C. T., Schier, A. F., Freeman, J., Engert, F., & Ahrens, M. B. (2016). Brain-wide mapping of neural activity controlling zebrafish exploratory locomotion. *ELife*, *5*(MARCH2016), 1–29. https://doi.org/10.7554/eLife.12741

Freeman, J., Vladimirov, N., Kawashima, T., Mu, Y., Sofroniew, N. J., Bennett, D. V., Rosen, J., Yang, C. T., Looger, L. L., & Ahrens, M. B. (2014). Mapping brain activity at scale with cluster computing. *Nature Methods*, *11*(9), 941–950. https://doi.org/10.1038/nmeth.3041

Green, M. H., Ho, R. K., & Hale, M. E. (2011). Movement and function of the pectoral fins of the larval zebrafish (Danio rerio) during slow swimming. *Journal of Experimental Biology*, *214*(18), 3111–3123. https://doi.org/10.1242/jeb.057497

Higashijima, S. I., Mandel, G., & Fetcho, J. R. (2004). Distribution of prospective glutamatergic, glycinergic, and gabaergic neurons in embryonic and larval zebrafish. *Journal of Comparative Neurology*, *480*(1), 1–8. https://doi.org/10.1002/cne.20278

Juvin, L., Grätsch, S., Trillaud-Doppia, E., Gariépy, J. F., Büschges, A., & Dubuc, R. (2016). A Specific Population of Reticulospinal Neurons Controls the Termination of Locomotion. *Cell Reports*, *15*(11), 2377–2386. https://doi.org/10.1016/j.celrep.2016.05.029

Kaneko, M., Fu, Y., & Stryker, M. P. (2017). Locomotion induces stimulus-specific response enhancement in adult visual cortex. *Journal of Neuroscience*, *37*(13), 3532–3543. https://doi.org/10.1523/JNEUROSCI.3760-16.2017

Katz, P. S., & Hale, M. E. (2017). Evolution of Motor Systems. In *Neurobiology of Motor Control: Fundamental Concepts and New Directions* (Issue February). https://doi.org/10.1002/9781118873397.ch6

Kimmel, C. B., Powell, S. L., & Metcalfe, W. K. (1982a). *Brain Neurons Which Project to the Spinal Cord in Young Larvae of the Zebrafish*. *127*.

Kimmel, C. B., Powell, S. L., & Metcalfe, W. K. (1982b). Brain neurons which project to the spinal cord in young larvae of the zebrafish. *Journal of Comparative Neurology*, *205*(2), 112–127. https://doi.org/10.1002/cne.902050203

Li, W. C., Soffe, S. R., Wolf, E., & Roberts, A. (2006). Persistent responses to brief stimuli: Feedback excitation among brainstem neurons. *Journal of Neuroscience*, *26*(15), 4026–4035. https://doi.org/10.1523/JNEUROSCI.4727-05.2006

Lin, C., & Strausfeld, N. J. (2012). Visual inputs to the mushroom body calyces of the whirligig beetle Dineutus sublineatus: Modality switching in an insect. *The Journal of Comparative Neurology*, *520*(12), Spc1–Spc1. https://doi.org/10.1002/cne.23158

Marques, J. C., Lackner, S., Félix, R., & Orger, M. B. (2018). Structure of the Zebrafish Locomotor Repertoire Revealed with Unsupervised Behavioral Clustering. *Current Biology*, *28*(2), 181-195.e5. https://doi.org/10.1016/j.cub.2017.12.002

Migault, G., Van Der Plas, T. L., Trentesaux, H., Panier, T., Candelier, R. L., Emi Proville, R., Englitz, B., Debr, G., & Bormuth, V. (2018). Whole-Brain Calcium Imaging during Physiological Vestibular Stimulation in Larval Zebrafish Article Whole-Brain Calcium Imaging during Physiological Vestibular Stimulation in Larval Zebrafish. *Current Biology*, *28*, 3723–3735. https://doi.org/10.1016/j.cub.2018.10.017

Morisset, V., & Nagy, F. (1999). Ionic basis for plateau potentials in deep dorsal horn neurons of the rat spinal cord. *Journal of Neuroscience*, *19*(17), 7309–7316. https://doi.org/10.1523/JNEUROSCI.19-17-07309.1999

Müller, U. K., & Van Leeuwen, J. L. (2004). Swimming of larval zebrafish: Ontogeny of body waves and implications for locomotory development. *Journal of Experimental Biology*, *207*(5), 853–868. https://doi.org/10.1242/jeb.00821

Nair, A., Nguyen, C., & McHenry, M. J. (2017). A faster escape does not enhance survival in zebrafish larvae. *Proceedings of the Royal Society B: Biological Sciences*, *284*(1852). https://doi.org/10.1098/rspb.2017.0359

Niell, C. M., & Stryker, M. P. (2010). Modulation of Visual Responses by Behavioral State in Mouse Visual Cortex. *Neuron*, *65*(4), 472–479. https://doi.org/10.1016/j.neuron.2010.01.033

Orger, M. B., Kampff, A. R., Severi, K. E., Bollmann, J. H., & Engert, F. (2008). *Control of visually guided behavior by distinct populations of spinal projection neurons*. *11*(3), 327–333. https://doi.org/10.1038/nn2048

Parichy, D. M. (2015). Advancing biology through a deeper understanding of zebrafish ecology and evolution. *ELife*, *4*. https://doi.org/10.7554/eLife.05635

Raff, R. A. (2000). Evo-devo: The evolution of a new discipline. *Nature Reviews Genetics*, *1*(1), 74–79. https://doi.org/10.1038/35049594

Schulze, L., Henninger, J., Kadobianskyi, M., Chaigne, T., Faustino, A. I., Hakiy, N., Albadri, S., Schuelke, M., Maler, L., Del Bene, F., & Judkewitz, B. (2018). Transparent Danionella translucida as a genetically tractable vertebrate brain model. *Nature Methods*, *15*(11), 977–983. https://doi.org/10.1038/s41592-018-0144-6

Severi, K. E., Portugues, R., Marques, J. C., O'Malley, D. M., Orger, M. B., & Engert, F. (2014). Neural Control and Modulation of Swimming Speed in the Larval Zebrafish. *Neuron*, *83*(3), 692–707. https://doi.org/10.1016/j.neuron.2014.06.032

Shukla, R., & Bhat, A. (2017). Morphological divergences and ecological correlates among wild populations of zebrafish (Danio rerio). *Environmental Biology of Fishes*, *100*(3), 251–264. https://doi.org/10.1007/s10641-017-0576-3

Smit, H., Amelink-Koutstaal, J. M., Vijverberg, J., & Von Vaupel-Klein, J. C. (1971). Oxygen consumption and efficiency of swimming goldfish. *Comparative Biochemistry and Physiology -- Part A: Physiology*, *39*(1), 1–28. https://doi.org/10.1016/0300-9629(71)90343-4

Sun, F., Zeng, J., Jing, M., Zhou, J., Feng, J., Owen, S. F., Luo, Y., Li, F., Wang, H., Yamaguchi, T., Yong, Z., Gao, Y., Peng, W., Wang, L., Zhang, S., Du, J., Lin, D., Xu, M., Kreitzer, A. C., … Li, Y. (2018). A Genetically Encoded Fluorescent Sensor Enables Rapid and Specific Detection of Dopamine in Flies, Fish, and Mice. *Cell*, *174*(2), 481-496.e19. https://doi.org/10.1016/j.cell.2018.06.042

Thiele, T. R., Donovan, J. C., & Baier, H. (2014). Descending Control of Swim Posture by a Midbrain Nucleus in Zebrafish. *Neuron*, *83*(3), 679–691. https://doi.org/10.1016/j.neuron.2014.04.018

Thisse, C., & Thisse, B. (2008). High-resolution in situ hybridization to whole-mount zebrafish embryos. *Nature Protocols*, *3*(1), 59–69. https://doi.org/10.1038/nprot.2007.514

Tinbergen, N. (1963). Tinbergen1963.pdf. In *Zeitschrift fur Tierpsychologie* (Vol. 20, pp. 410–433).

Torres, J. J., & Childress, J. J. (1983). Relationship of oxygen consumption to swimming speed in Euphausia pacifica 1. Effects of temperature and pressure. In *Marine Biology* (Vol. 74). http://www.polarpelagic.com/wp-content/uploads/2016/05/Torres-and-Childress-1983.pdf

Van Leeuwen, J. L., Voesenek, C. J., & Müller, U. K. (2015). How body torque and Strouhal number change with swimming speed and developmental stage in larval zebrafish. *J. R. Soc. Interface*, *12*. https://doi.org/10.1098/rsif.2015.0479

Voisin, D. L., & Nagy, F. (2001). Sustained L-type calcium currents in dissociated deep dorsal horn neurons of the rat: Characteristics and modulation. *Neuroscience*, *102*(2), 461–472. https://doi.org/10.1016/S0306-4522(00)00468-1

Wang, W. C., & McLean, D. L. (2014). Selective Responses to Tonic Descending Commands by Temporal Summation in a Spinal Motor Pool. *Neuron*, *83*(3), 708–721. https://doi.org/10.1016/j.neuron.2014.06.021

Watari, N., & Larson, R. G. (2010). The hydrodynamics of a run-and-tumble bacterium propelled by polymorphic helical flagella. *Biophysical Journal*, *98*(1), 12–17. https://doi.org/10.1016/j.bpj.2009.09.044

Webb, P. W. (1971). The swimming energetics of trout. *Journal of Experimental Biology*, *55*, 521–540.

Weihs, D. (1980). Respiration and depth control as possible reasons for swimming of northern anchovy, Engraulis mordax, yolk-sac larvae. *Fishery Bulletin*, *78*(10).

https://www.st.nmfs.noaa.gov/spo/FishBull/78-1/weihs.pdf

Wiggin, T. D., Anderson, T. M., Eian, J., Peck, J. H., & Masino, M. A. (2012). Episodic swimming in the larval zebrafish is generated by a spatially distributed spinal network with modular functional organization. *Journal of Neurophysiology*, *108*(3), 925–934. https://doi.org/10.1152/jn.00233.2012

Zhang, H. Y., & Sillar, K. T. (2012). Short-term memory of motor network performance via activity-dependent potentiation of Na +/K + pump function. *Current Biology*, *22*(6), 526–531. https://doi.org/10.1016/j.cub.2012.01.058

Supplemental Information

Divergence of exploratory locomotion in two closely related vertebrate species

Gokul Rajan, Julie Lafaye, Martin Carbo Tano, Karine Duroure, Dimitrii Tanese, Giulia Faini, Thomas Panier, Jörg Henninger, Benjamin Judkewitz, Ralf Britz, Christoph Gebhardt, Raphaël Candelier, Valentina Emiliani, Georges Debregeas, Claire Wyart, Filippo Del Bene

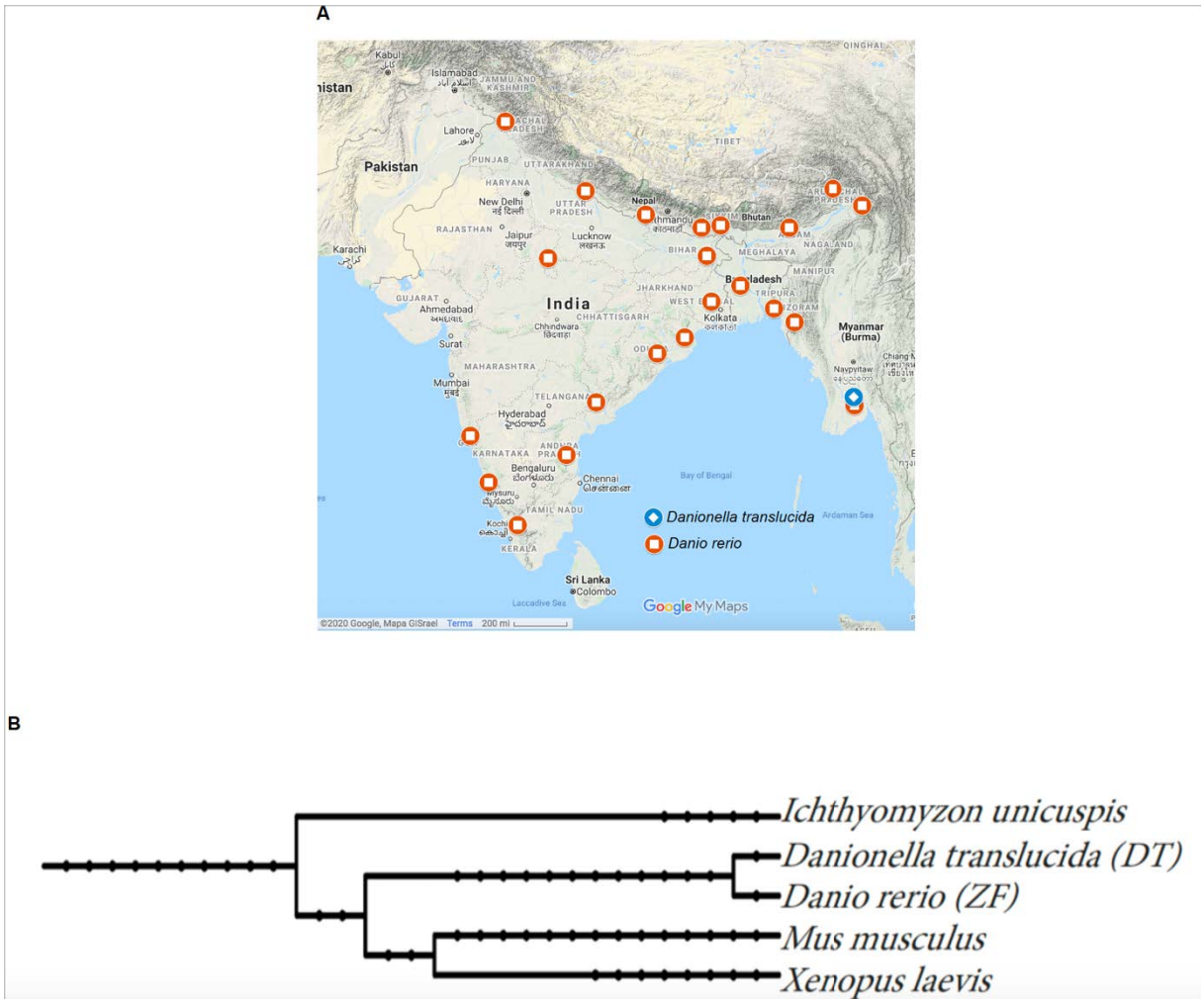

Figure S1: Natural habitat and evolutionary relationship

(A) Recent ZF reports (from Parichy, 2015) with the report of DT from Roberts, 1986. Both the fish species are found in similar freshwater environments in south east Asia. (B) Evolutionary relationship among some common model organisms along with DT. Both DT and ZF share a common sub-family, Danioninae. The tree is based on NCBI taxonomy. Each internal node represents a taxonomic category as obtained from NCBI taxonomy.

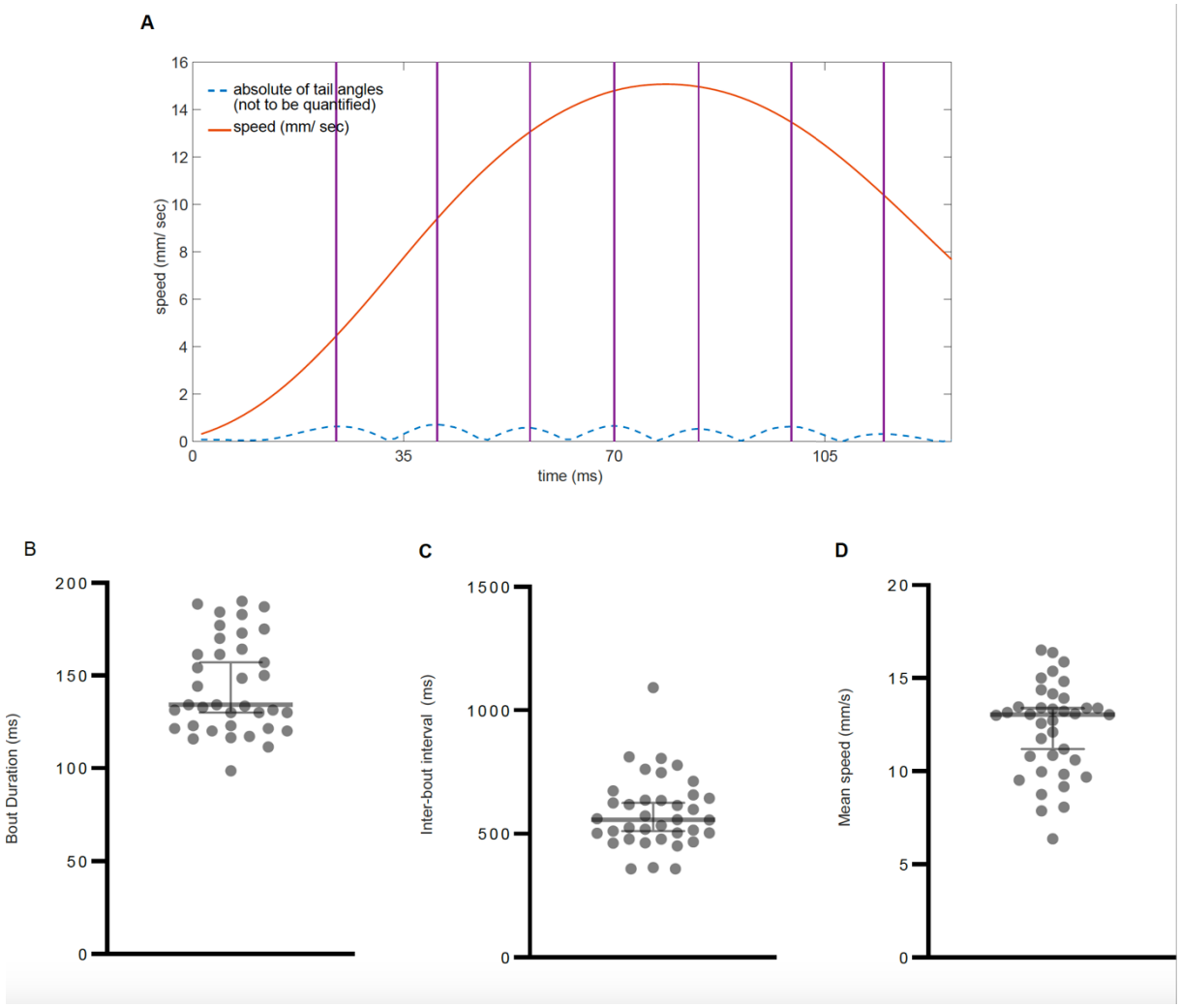

Figure S2: Half tail-beat detection and bout-wise kinematic analysis

(A) Illustration of half tail-beat identification in a swim bout of zebrafish. The vertical lines show the peak of tail bend which is considered as the start and/or end of a half beat. (B) The median bout duration and (C) inter-bout duration, (D) median of mean speed and (E) maximum speed, (F) median of maximum tail angle and (G) tail-beat frequency (TBF) of ZF after analyzing the same dataset utilizing a bout-wise analysis method (N=37 ZF each). The values obtained by performing such a bout-wise analysis were found to be close to what has been reported for zebrafish earlier (Budick & O'Malley, 2000).

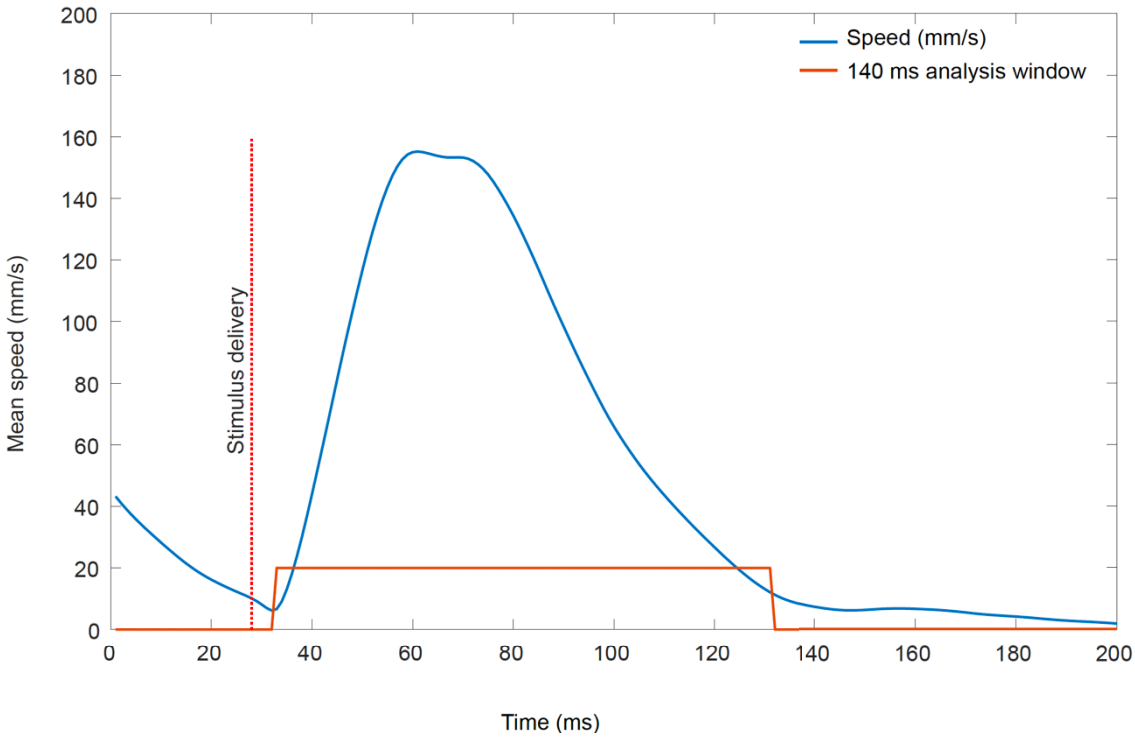

Figure S3: Analysis of escape kinematics

Figure 2.1: Illustration of the 140 ms window selected for the analysis of tap-induced escape kinematics in ZF. The vertical red line shows the time of stimulus delivery. The vertical red line illustrates the 140 ms window used for analysis of the escape kinematics in DT and ZF.

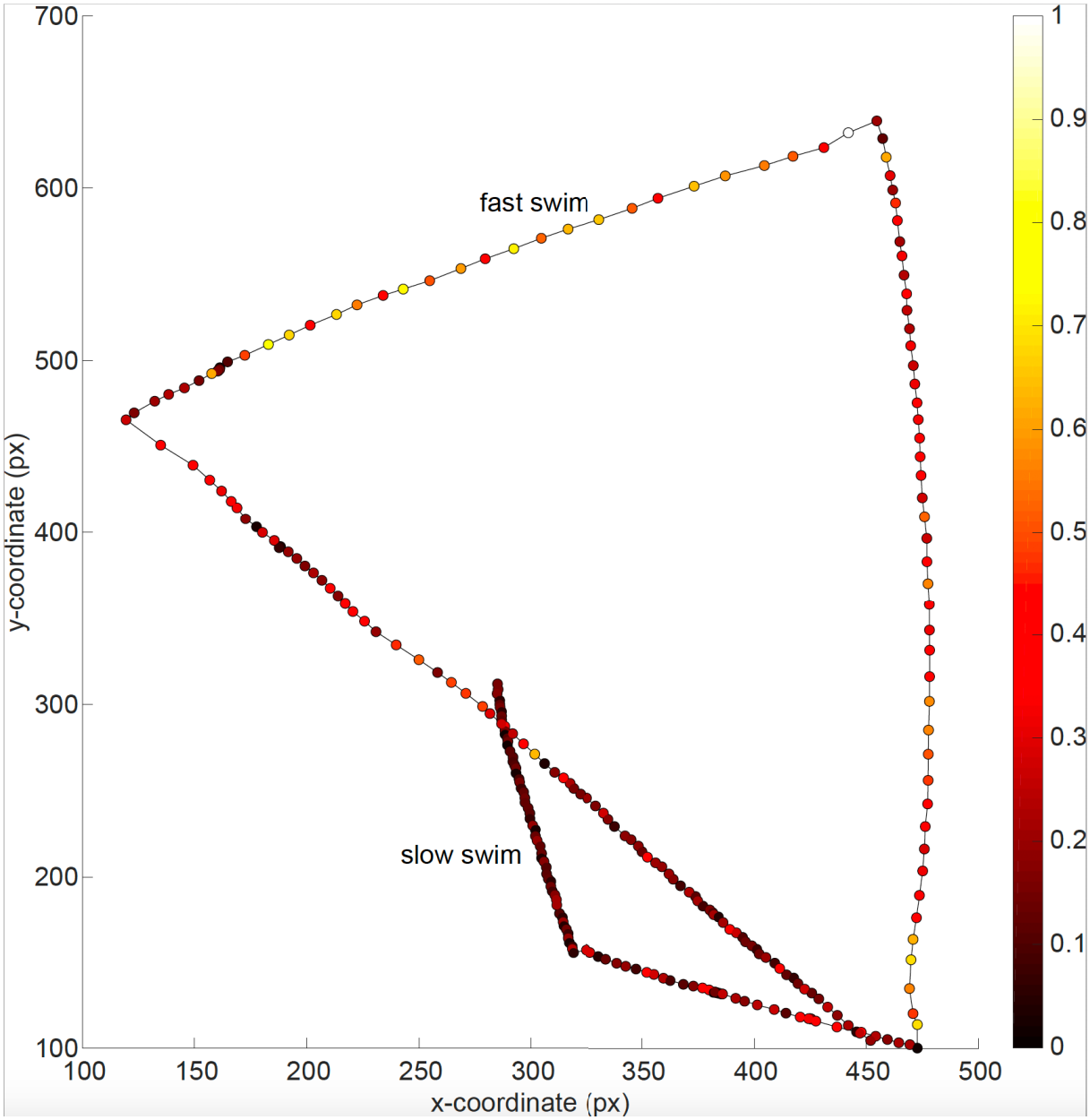

Figure S4: Modulation swimming speed in DT

Figure 3.2: Slow and fast swims in DT. A ~25s long trajectory of a DT representing a slow and fast track of swimming. Each step is 100 ms apart.

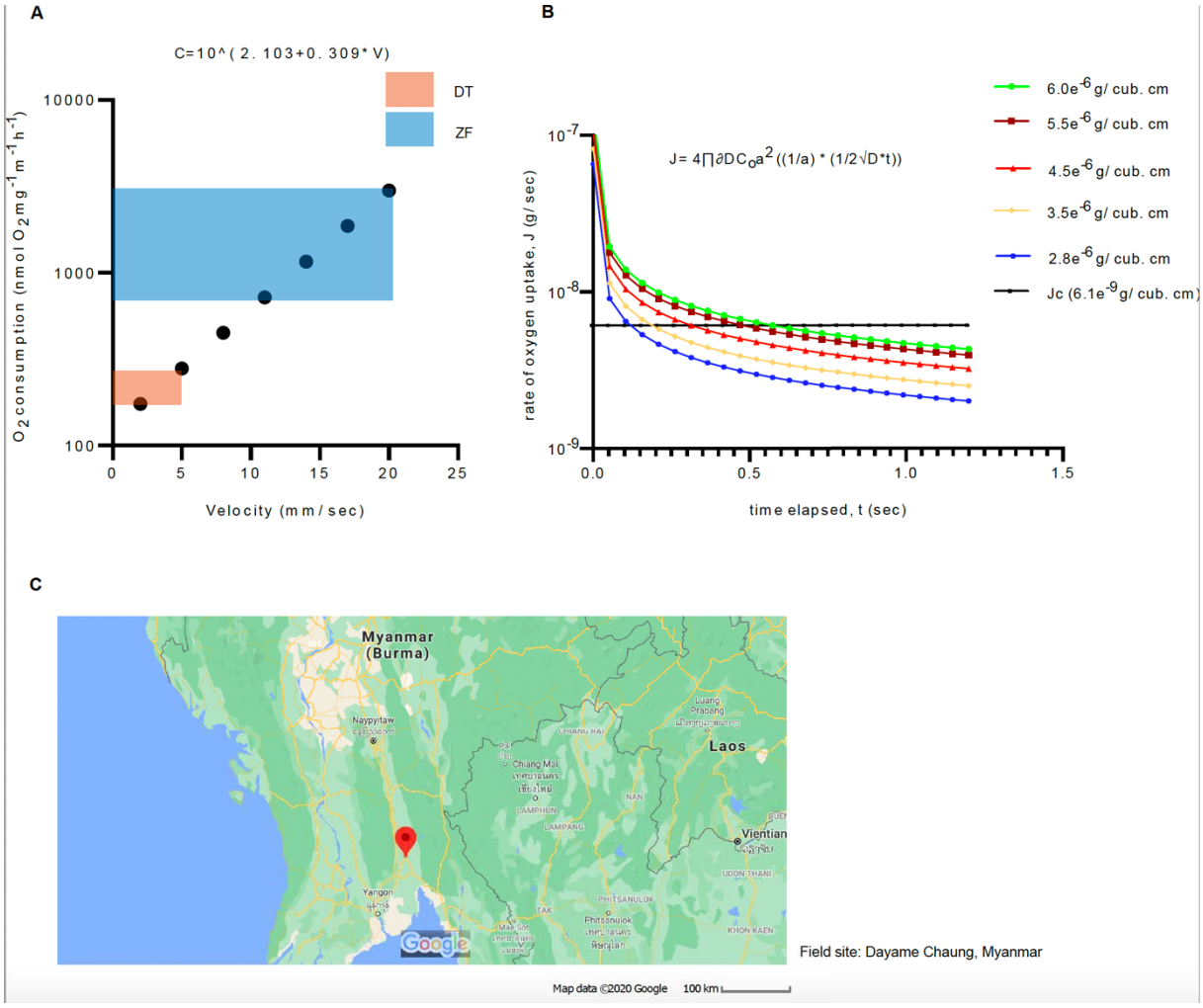

Figure S5: Influence of oxygen availability on swimming pattern

(A) Many studies have looked at the relationship between speed of locomotion and oxygen consumption. Using a relationship derived by Bagatto et al., 2001 in larval ZF between oxygen consumption and swimming speed, here we try to show how the oxygen demand would vary for a ZF-like larva swimming in the range of speeds reported for DT and ZF in our study. Log C = 2.103 + 0.309 x V, where C is a measure of oxygen consumed per mg of the animal per hour and V is the speed.

(B) Analytical model showing lower availability of dissolved oxygen (DO) in the surrounding can lead to a shorter inactivity time between swim events, leading to a more continuous swimming (based on Weihs, 1980). The rate of oxygen uptake (J) over time (t=0, when the animal stops moving) depends on the initial concentration of dissolved oxygen (C_o) in the surrounding water (shown in colored curves). ∂ is density of water: 1 gm/cm^3, D is diffusion constant for dissolved oxygen at 22°C: 2.22E-5 and a is the radius of an equivalent sphere, the surface area of which is equal to the surface area of the larval body. Horizontal line (J_c) indicates the approximation of the critical oxygen uptake rate, beyond which the larvae would have to start to swim again in order to replenish oxygen in its surrounding (calculated based on the inter-bout duration information available on ZF). From the plot: as the C_o decreases, the J

drops rapidly; and this leads to a lower delay to reach the J_c, giving rise to more continuous DT-like swimming with shorter pauses. For simplicity, the range of DO values used is based on the values recorded for DT and ZF in nature (Shukla & Bhat, 2017). (C) Map shows the site of field collection: Dayame Chaung, Myanmar.

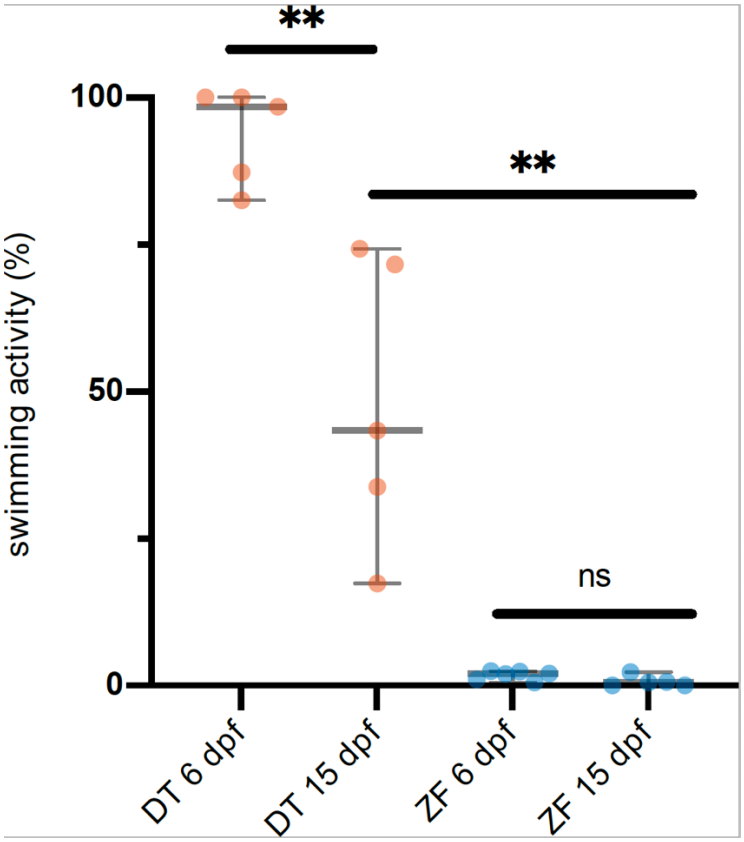

Figure S6: Head-embedded swimming in 1-week old DT larva (without swim bladder) and 2-weeks old (with swim bladder) DT larva.

Percentage of time spent swimming in 2-week old DT with swim bladder (n=5), 1-week old DT without swim bladder (n=5), 1-week old ZF with swim bladder (n=6) and 2 weeks old ZF with swim bladder (** $p<0.01$, Mann-Whitney test). Swimming activity in 2 weeks old DT larva is decreased when compared to 1-week old DT larva. However, this % of swimming activity is still much higher than ZF at 1or 2 week(s).

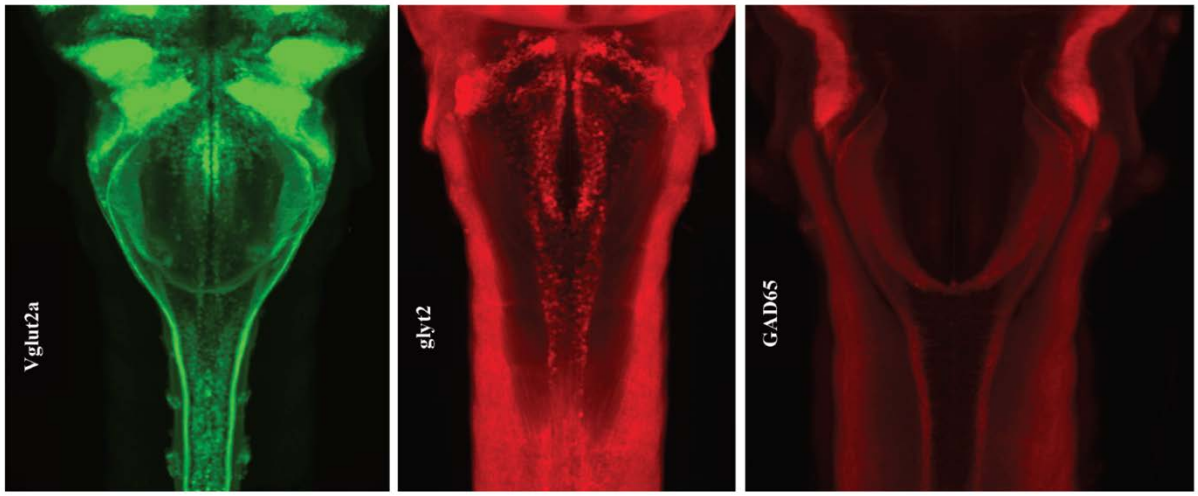

Figure S7: Distribution of glutamatergic, glycinergic and GABAergic neurons in ZF hindbrain.

Distribution of glutamatergic, glycinergic and GABAergic neurons in the hindbrain of ZF obtained from Z-brain atlas (Randlett et al., 2015). Maximum projection of *vglut2a*-GFP (Bae et al., 2009), *glyt2*-GFP (Mclean et al., 2007) and anti-GAD67 (Randlett et al., 2015). The rostrocaudal striped distribution reported in ZF literature is very similar to the results obtained in DT as shown in Fig. 3.

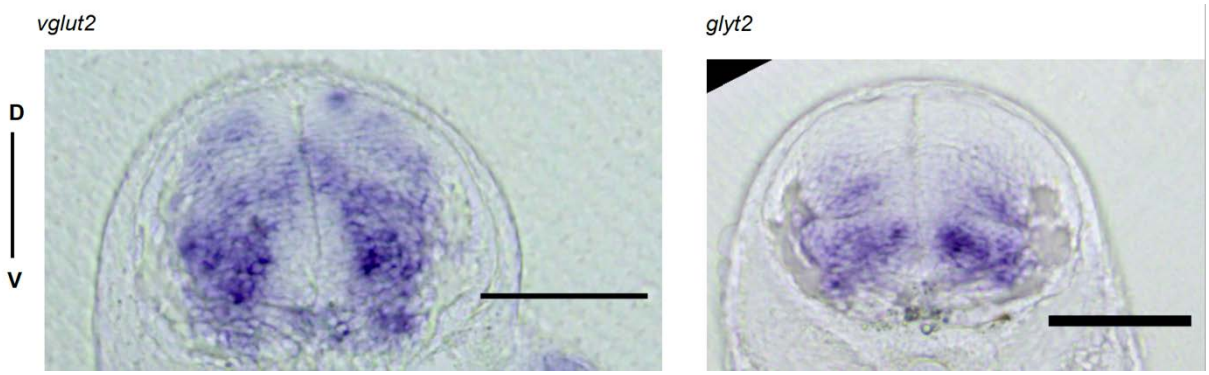

Figure S8: Cross-sectional view of glutamatergic and glycinergic neurons in the hindbrain of DT.

Representation of cross-sectional view of DT hindbrain showing distribution of *vglut2* and *glyt2* markers.

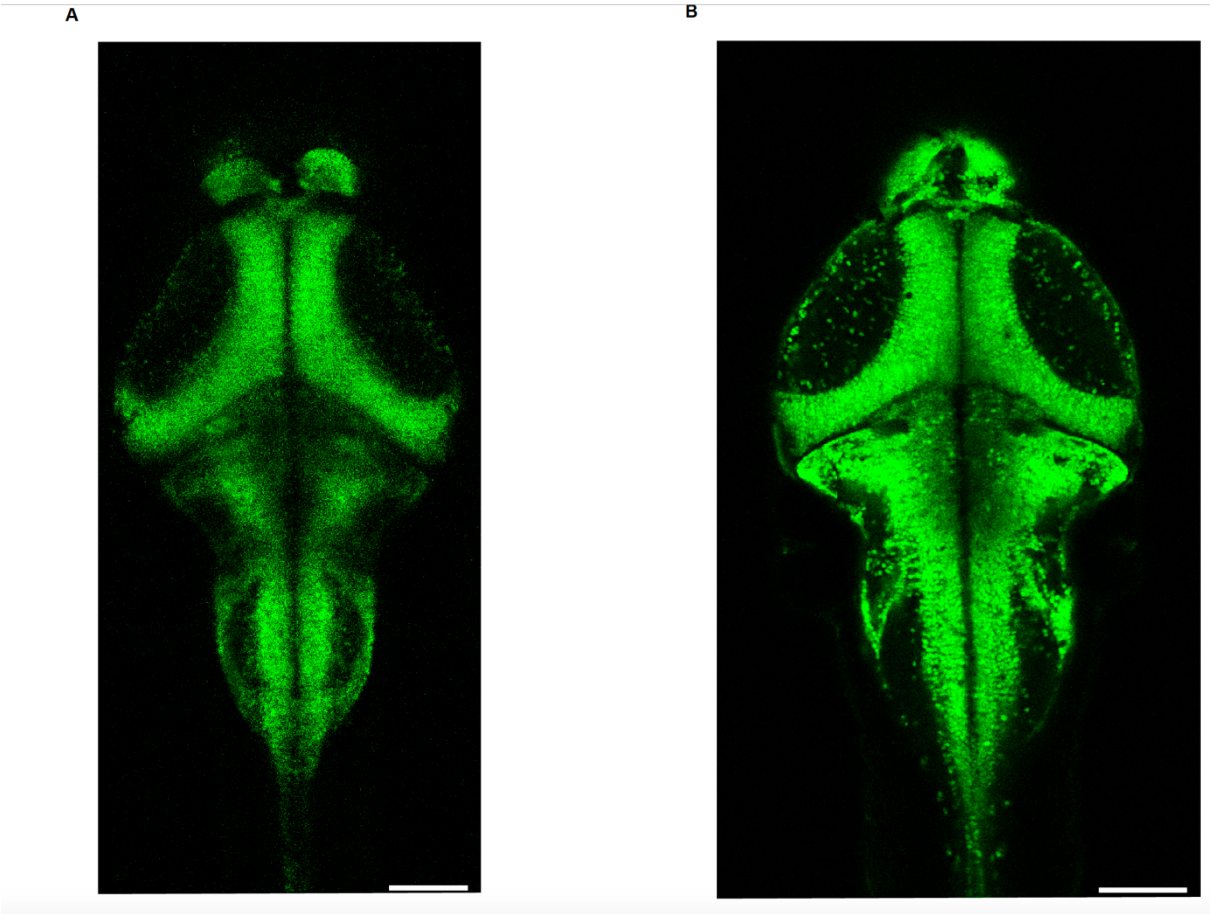

Figure S9: 5 dpf *Tg(HuC:H2B-GCaMP6s)* DT and ZF.

(A) A maximum intensity projection of 5dpf *Tg(HuC:H2B-GCaMP6s)* DT fish. (B) A maximum intensity projection of 5 dpf *Tg(HuC:H2B-GCaMP6s)* ZF. The expression pattern of the GCaMP appears very conserved between the two larvae.

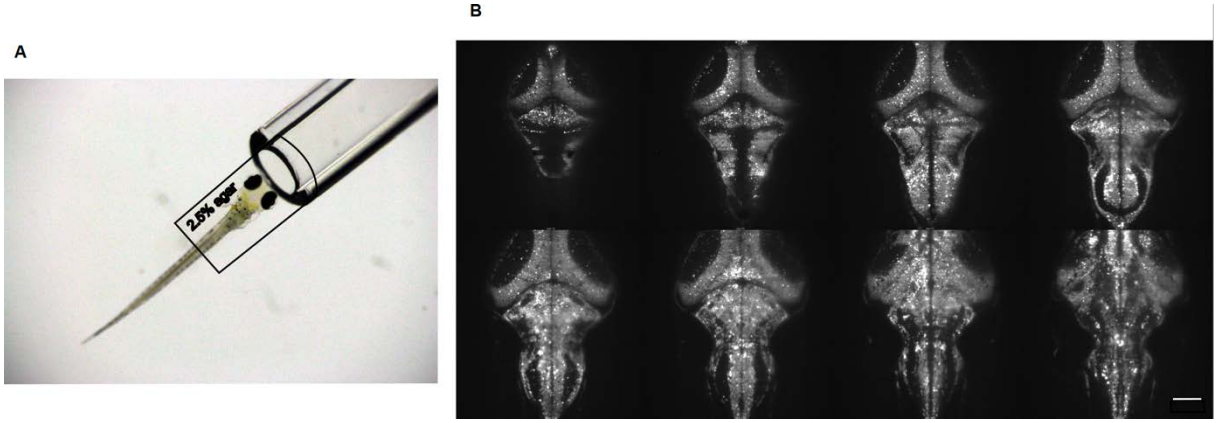

Figure S10: Whole brain imaging using light sheet microscopy.

(A) Holding capillary to immobilize the fish during imaging. 2.5% agar is used to hold the fish in the capillary. 1/3rd of the body (tail-region) is freed from the agar. The tail activity is recorded during the brain imaging and used as readout for the swimming activity.
(B) A 5dpf DT brain at various depths represented by Z (0 µm being most dorsal). Approximately 200 µm of brain (in 8 µm steps) in DT and ZF was acquired at 1 Hz during simultaneous recording of tail activity to identify and compare the activity of neuronal correlates of locomotion in the two species. Scale bar is 100 µm.

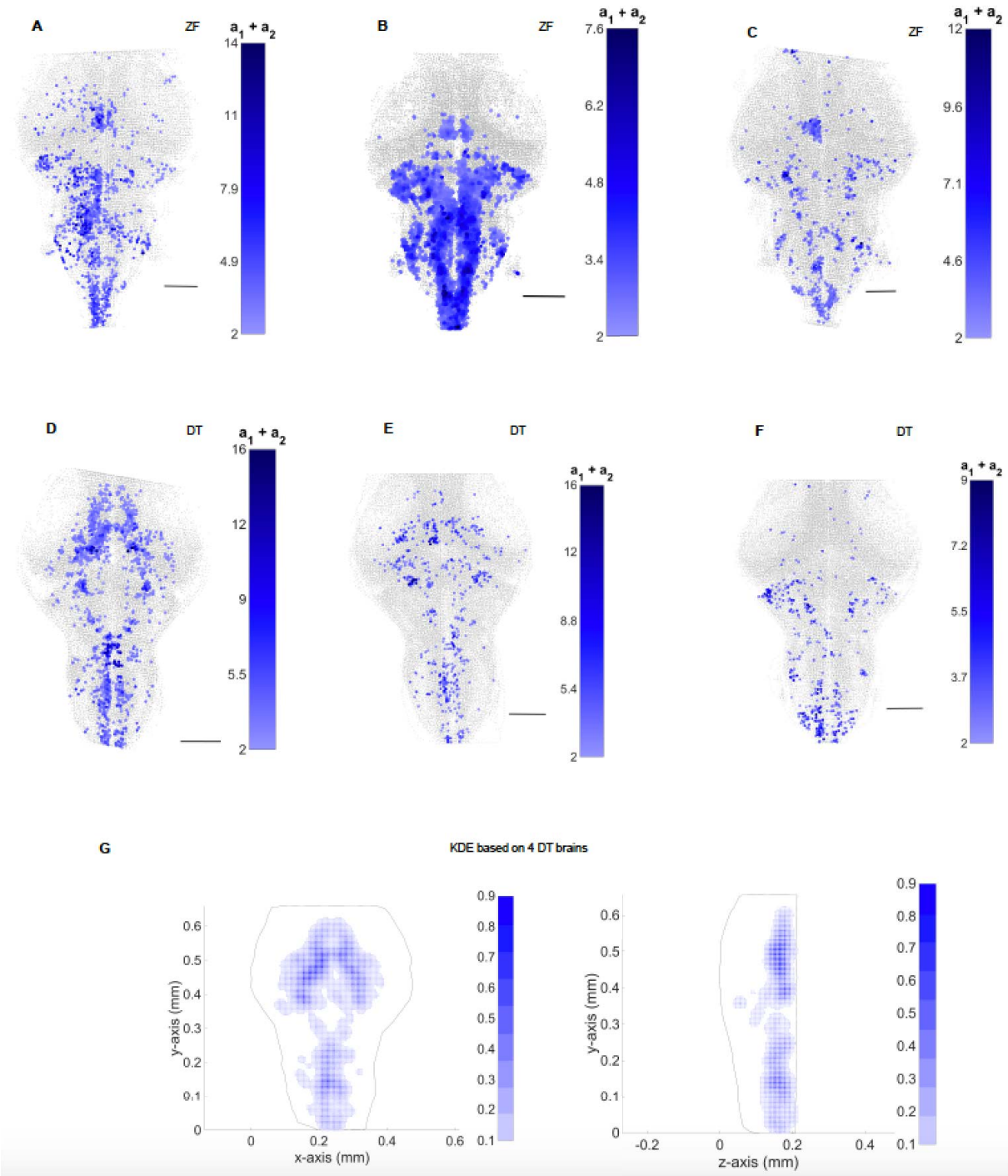

Figure S11: Neuronal correlates of swimming in ZF and DT.

(A), (B) and (C) represent neuronal correlates of swimming in three ZF brains. Highly correlated neurons of ZF are color-coded in blue. The identification is based on the regression coefficient and t-score. See Fig. 4(A) for an illustration of the method. Similarly, (D), (E) and (F) represent neuronal correlates of swimming in three DT brains. The common swimming-associated nuclei in DT and ZF are located in the medial mid-brain, lateral midbrain and hindbrain of DT and ZF. The variability can be partly assigned to the differing number of swim events in each fish (ranging from 2 to 24 events in DT in all our acquisitions). Scale bar is 100 µm. (G) KDE (kernel density estimator) plot shows the

probability of a neuron to be a swim neuron. The KDE is estimated based on regression data from four DT brains.

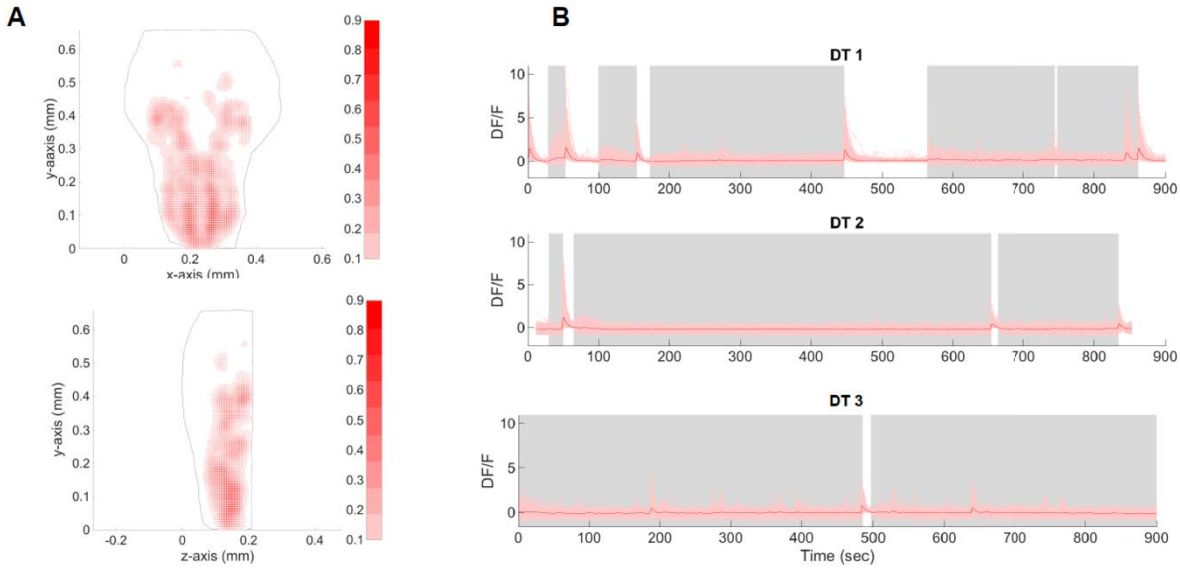

Figure S12: Neuronal correlates of swim offset in DT.

(A) KDE (kernel density estimator) plot shows the probability of a neuron to be an offset neuron. The KDE is estimated based on regression data from three DT brains. (B) This represents the activity of the offset neurons (in red) with respect to swimming activity (in grey) in three DT fish.

Movie 1: Movie of a 6 dpf *Danionella translucida* (DT) exploring its environment.

Movie 2: Movie of a 6 dpf zebrafish (ZF) exploring its environment.

Movie 3: Movie demonstrating the assay used to study the tap-induced escape response.

References

Bae, Y. K., Kani, S., Shimizu, T., Tanabe, K., Nojima, H., Kimura, Y., Higashijima, S. ichi, & Hibi, M. (2009). Anatomy of zebrafish cerebellum and screen for mutations affecting its development. *Developmental Biology*, *330*(2), 406–426. https://doi.org/10.1016/j.ydbio.2009.04.013

Bagatto, B., Pelster, B., & Burggren, W. W. (2001). Growth and metabolism of larval zebrafish:

Effects of swim training. *Journal of Experimental Biology*, *204*(24), 4335–4343.

Budick, S. A., & O'Malley, D. M. (2000). Locomotion of larval zebrafish. *The Journal of Experimental Biology*, *203*, 2565–2579. http://jeb.biologists.org/content/jexbio/203/17/2565.full.pdf

Mclean, D. L., Fan, J., Higashijima, S.-I., Hale, M. E., & Fetcho, J. R. (2007). *LETTERS A topographic map of recruitment in spinal cord. 446*. https://doi.org/10.1038/nature05588

Parichy, D. M. (2015). Advancing biology through a deeper understanding of zebrafish ecology and evolution. *ELife*, *4*. https://doi.org/10.7554/eLife.05635

Randlett, O., Wee, C. L., Naumann, E. A., Nnaemeka, O., Schoppik, D., Fitzgerald, J. E., Portugues, R., Lacoste, A. M. B., Riegler, C., Engert, F., & Schier, A. F. (2015). Whole-brain activity mapping onto a zebrafish brain atlas. *Nature Methods*, *12*(11), 1039–1046. https://doi.org/10.1038/nmeth.3581

Roberts, T. R. (1986). Danionella translucida, a new genus and species of cyprinid fish from Burma, one of the smallest living vertebrates. *Environmental Biology of Fishes*, *16*, 231–241. https://link.springer.com/content/pdf/10.1007%2FBF00842977.pdf

Shukla, R., & Bhat, A. (2017). Morphological divergences and ecological correlates among wild populations of zebrafish (Danio rerio). *Environmental Biology of Fishes*, *100*(3), 251–264. https://doi.org/10.1007/s10641-017-0576-3

Weihs, D. (1980). Energetic significance of changes in swimming modes during growth of larval anchovy Engraulis mordax. *Fishery Bulletin*, *77*(August), 597–604.

Author Contributions

Thesis title: Divergence of exploratory locomotion and the underlying neuronal circuitry in two closely related vertebrate species

Project conception: **GR**, CW and FDB conceived the project.

Chapter 3: **GR** developed all the behavior assays and acquisition systems. **GR** performed all the behavioral experiments and developed all the analysis pipeline. Analysis script for calculation of MSD and R were written by GD. **GR** carried out the husbandry and breeding of *Danionella translucida* with the support of KD and FDB.

Chapter 4: KD performed the staining for *in-situ* hybridization and immunohistochemistry and **GR** performed the confocal imaging and analysis. **GR** and MCT performed the backfill injections, MCT carried out the imaging and **GR** performed the cell-to-cell analysis. **GR** developed the Tg(HuC:H2B-GCaMP6s) line of *Danionella translucida.* **GR** performed all the light sheet acquisitions. JL performed the segmentation and regression analysis with inputs from **GR**.

Manuscript for peer-reviewed publication:
GR and FDB are currently writing a manuscript that incorporates the results from Chapter 3 and Chapter 4.

Supervision: **GR** was supervised by FDB. JL was supervised by GD. MCT was supervised by CW.

Author names:
GR: Gokul Rajan, JL: Julie Lafaye, MCT: Martin-Carbo-Tano, KD: Karine Duroure, GD: Georges Debregeas, CW: Claire Wyart, FDB: Filippo Del Bene

Résumé

Marcher, nager, sauter et ramper sont quelques exemples des diverses formes de locomotion retrouvées dans la nature qui sont adaptées aux contraintes environnementales d'un animal. Au cours de ma thèse, j'ai établi une approche pour comprendre comment les circuits neuronaux sous-jacents à la locomotion divergent en comparant les larves de deux espèces de Danionins étroitement apparentées, occupant des environnements similaires et présentant des nages différentes : l'organisme modèle *Danio rerio* ou poisson-zèbre (ZF) et *Danionella translucida* (DT). J'ai étudié les causes immédiates (cellulaires et physiologiques) et ultimes (au niveau de l'organisme) pouvant expliquer cette divergence dans leurs nages malgré leur proximité phylogénétique et environnementale.

Afin d'étudier le comportement des deux poissons, j'ai développé un système d'imagerie à grande vitesse et un pipeline d'analyse. Les nages sont décomposées en demi-battements de queue pour pouvoir définir des unités comparables de locomotion chez les deux espèces. Ceci a montré qu'en nage spontanée, les larves DT utilisent des fréquences de battement de queue plus basses et des angles de queue inférieurs, exécutant des événements de nage plus lents mais plus longs. En comparaison, les larves ZF effectuent une nage rapide et intermittente par « rafale et glissement ». Cependant, lors des fuites DT peut atteindre des vitesses maximales élevées avec une latence pour atteindre cette vitesse étonnamment inférieure à celle de ZF. En nage spontanée, malgré de grandes différences de vitesses instantanées, le déplacement quadratique moyen s'est révélé comparable entre les deux animaux. Cela est dû à une randomisation plus lente de l'orientation chez DT que chez ZF, ce qui conduit à un régime de nage balistique plus long chez DT. En plus d'une fine caractérisation de la nage et de son influence sur l'exploration, au niveau de l'organisme j'ai proposé deux observations faites chez DT et contribuant au schéma de nage observé : une disponibilité moindre d'oxygène en raison de sa préférence pour les couches inférieures de la colonne d'eau et un retard de l'inflation de la vessie natatoire.

Par hybridation *in situ* et immunohistochimie, une forte similitude de la distribution des neurones excitateurs et inhibiteurs du cerveau postérieur est montrée. De plus, avec des expériences de « backfill », une forte conservation de la distribution des neurones réticulospinaux se projetant du tronc cérébral vers la moelle épinière est observée. Pour étudier les différences physiologiques, j'ai créé une lignée transgénique DT, *Tg (HuC:H2B-GCaMP6s)*,

exprimant l'indicateur de calcium GCaMP6s dans les noyaux de la majorité des neurones. Avec cette lignée et une lignée transgénique ZF équivalente, j'ai effectué de la microscopie à feuillet de lumière sur des larves nageant spontanément. Nous avons ainsi identifié des populations neuronales du cerveau de DT pour lesquelles leur activité est mesurée avec l'augmentation de la nage. Ces régions sont donc des candidats potentiels pour fournir une stimulation excitatrice des neurones en aval afin de maintenir le réseau locomoteur spinal actifs et produire une longue nage continue. De plus, les événements de nage longue de DT ont permis une dissection supplémentaire des neurones corrélés à la nage par rapport aux différentes phases de la nage.

Ce travail fournit une vision unique, à l'échelle comportemental et physiologique, de la capacité de circuits neuronaux similaires à produire des comportements différents. Ces résultats ont été brièvement évalués au niveau de l'organisme. À notre connaissance, une comparaison aussi complète, combinant comportement, anatomie et physiologie, n'a jamais été réalisée directement entre deux vertébrés. Ces travaux donnent les bases de futures études comparatives de vertébrés en neurosciences, en particulier chez les Danionins, afin d'acquérir une compréhension approfondie des circuits neuronaux sous-jacents aux comportements.

RÉSUMÉ

Que ce soit pour explorer son environnement, se nourrir ou échapper à un prédateur, la capacité de se déplacer est essentielle dans le monde animal. Marcher, nager, sauter, ramper sont quelques exemples de la diversité des déplacements mais des différences plus subtiles entre des animaux apparentés peuvent fournir une occasion unique d'étudier les circuits neuronaux sous-jacents aux mouvements et leurs différences. Dans cette étude, j'utilise le poisson-zèbre (ZF) et *Danionella translucida* (DT). DT nage beaucoup plus lentement et en continu que ZF, qui est rapide et intermittent. Une forte conservation de leur anatomie cérébrale est démontrée. Dans ce contexte, il serait intéressant d'élucider comment les différents schémas de nage sont produits si l'anatomie (= matériel) est la même. Il se trouve que la réponse réside dans la physiologie (= logiciel). En effet, Je montre comment certaines populations neuronales du cerveau de DT sont adaptées pour assurer sa longue durée de nage.

MOTS CLÉS

Locomotion, Circuits Neuronaux, Danionins

ABSTRACT

Whether to explore its environment for food or to escape from an approaching predator, the ability to move around in its environment is critical in the animal world. Walking, swimming, hopping, crawling are a few examples of how this is achieved. More subtle differences in the movement pattern of related animals can provide us with a unique opportunity to investigate the neuronal circuits underlying the movements and their differences. In the current study, I use Zebrafish (ZF) and *Danionella translucida* (DT). DT swims much slower and continuously as compared to the fast and intermittent swimming of ZF. A high degree of conservation in their brain anatomy is demonstrated. The interesting question that follows is how is the different swimming pattern produced if the broad anatomy (= hardware) is the same? The answer, as it turns out, lies in the physiology (= software). Here, I show how some of the neuronal populations in the brain of DT are adapted to sustain the long swimming duration of DT.

KEYWORDS

Locomotion, Neuronal Circuits, Danionins